Thèse Présentée pour obtenir le grade de docteur

Université de Lille

GEMTEX : *Laboratoire de Recherche Textile Roubaix*

École doctorale n°72: *Science Pour l'Ingénieur Université Lille Nord-de-France*

Discipline: Chimie des matériaux

Design of double-layered microcapsule shell by electrospraying route for functional coating of fibers and textile

Conception d'une coque de microcapsule à double couche par voie d'électropulvérisation pour le revêtement fonctionnel des fibres et du textile

Présentée par :

Shengchang ZHANG

Soutenue le 19 /01/2021 devant la commission d'examen

Membres du Jury :

M. Dominique ADOLPHE	Professeur des Universités, Université de Haute-Alsace (UHA), Mulhouse	Rapporteur
Mme Isabelle VROMAN	Professeur des Universités, Université de Reims Champagne-Ardenne, Reims	Rapporteur
Mme Corinne JEGAT	Maître de conférences, Université de Saint-Etienne, Saint-Étienne	Examinatrice
Mme Anne BERGERET	Professeur, IMT Mines d'Ales, Alès	Examinatrice
Mme Valérie GAUCHER	Professeur des Universités, Université de Lille, Lille	Examinatrice
M. Fabien SALAUN	Professeur des Universités, Ensait, Roubaix	Directeur
Mme Christine CAMPAGNE	Professeur des Universités, Ensait, Roubaix	Co-directeur

Acknowledgement

In the beginning, I would say thanks to my supervisors Prof. Fabien SALAUN and Prof. Christine CAMPAGNE to guide me well throughout the research work from title's selection to find the results. Their immense knowledge, motivation and patience have given me more power and spirit to excel in the research writing. Conducting the academic study regarding such a difficult topic couldn't be as simple as he made this for me. They are my mentors and better advisors for my doctorate study beyond the imagination.

Apart from my supervisors, I won't forget to express the gratitude to rest of the team: Mme. Sabine CHLEBICKI, Mr. Guillaume LEMORT and Dr. Chan HUI, for giving the encouragement and sharing insightful suggestions. They all have played a major role in polishing my research writing skills. Their endless guidance is hard to forget throughout my life.

I am also pleased to say thank you to Dr. Cheng CHI, Dr. Xin ZHAO and Dr. Kaichen WANG, who made my access simpler to the research facilities and laboratory and gave an opportunity to become part of their team as an intern. It wouldn't have been possible to conduct this research without their precious support. They all really mean a lot to me.

I would always remember my fellow lab-mates too for the fun-time we spent together, sleepless nights that gave us the courage to complete tasks before deadlines and for stimulating the discussions. I would also like to thank my friends from ENSAIT. The man who also supported me well throughout the entire research program is Dr. Xiang YAN. Their immense support actually guided me to rectify numerous things that could create major challenges in the acceptance of my paper.

In the end, I am grateful to my parents, siblings, friends and acquaintances who remembered me in their prayers for the ultimate success. I consider myself nothing without them. They gave me enough moral support, encouragement and motivation to accomplish the personal goals.

Shengchang ZHANG

Table of contents

Liste of Figures

Liste of Tables

Introduction

Phase change materials (PCMs) were inorganic or organic compounds, which can store or release a large amount of latent heat during their phase change transitions induced with the surrounding temperature variations. Due to their high thermal and chemical stability, high latent heat storage capacity and low cost, they are regarded as main candidates for delaying the increase in energy consumption and for satisfying the growing demand for thermal management. When PCMs were encapsulated into shell matrix to form phase change microcapsules (mPCMs), their drawbacks and limitations including the loss behavior during liquid-solid phase transition, low thermal conductivity and flammability characteristics can be further overcome. Therefore, mPCMs can be widely used in space equipment, thermal-regulated textiles, industrial waste heat recovery, energy conservation in buildings and solar energy use.

Electrospraying as a green and high-efficiency electrohydrodynamic atomization technology, was applied to design and fabricate mPCMs. Under cone-jet mode, not only the electrosprayed mPCMs with a desired mean diameter and a mono-dispersed size distribution can be obtained, but also high encapsulation efficiency and high loading content of PCMs in electrosprayed mPCMs can be achieved. Meanwhile, the surface morphology, the core-shell structure and the size of electrosprayed mPCMs can be controlled effectively via adjusting the solution properties, operating parameters and the geometry of nozzle. More interestingly, the functional coating of mPCMs on the surface of textiles to fabricate thermal-regulated textiles can be implemented simultaneously during electrospraying process when target textile was put at collector. The interfacial adhesions between mPCMs and textiles can be further strengthened via introducing the second layer active shell which can form interactions with textiles. Therefore, designing electrosprayed mPCMs with double-layered shells not only improve the stability of mPCMs, but also the durability of mPCMs-coated textiles.

N-hexadecane and n-eicosane as common PCMs, due to their phase transition temperatures (from 18 °C to 35 °C) within the ambient temperature and comfort range of humans' body, are suitable to be applied in thermal-regulated textiles. Combined with the lack of super-cooling phenomenon, little volume changes during phase transition, non-corrosive and nontoxicity, they are selected as core materials to fabricate electrosprayed mPCMs in this thesis. Poly(caprolactone) (PCL) and poly(lactic acid) (PLA) as green, biocompatible and biodegradable

synthetic polyesters, are currently attracting increasing attention as shell matrix for manufacturing environmentally friendly functional microcapsules. They have been widely used in drug control release, tissue engineering, active substance package and food engineering. Therefore, they are selected as shell matrix to encapsulate n-alkanes in our investigation.

This PhD work is funded by China Scholarship Council (CSC), and performed in Laboratoire de Génie et Matériaux Textiles (GEMTEX, ENSAIT, France). The objective is to design and fabricate mPCMs with double-layered shell via coaxial electrospraying and achieve their functional coating on the surface of textiles for obtaining thermal-regulated textiles.

In Chapter I, a literature survey was conducted. Microencapsulation is a preservation or protection technology for active substances via enclosing them into polymeric or inorganic containers. When phase change materials (PCMs) were microencapsulated into shell matrix to form phase change microcapsules (mPCMs), some of their drawbacks and limitations during use are solved effectively. Meanwhile, before coating PCMs on the surface of textile for fabricating thermal-regulated textiles, it is necessary to carry out the microencapsulation of PCMs. Microencapsulation technology and microcapsules are crucial for accelerating the application of PCMs in textile industry. Therefore, the definition, structure, morphology, properties, formation methods and applications in textiles industry of microcapsules were also introduced in details. Among these formation methods of microcapsules, electrospraying technology was regarded as a green, simple and high-effciency method to carry out the formation of mPCMs. Meanwhile, the functional coating of mPCMs on the surface of textiles can also be completed during electrospraying process. Therefore, the running mechanism, experimental devices and applications of electrospraying technology were also presented. Some factors that influences the electrospraying process and the structures, morphologies and properties of electrosprayed particles were also discussed. Finally, some information about polycaprolactone (PCL), poly(lactic acid) (PLA), the applications of PCL or PLA electrosprayed productions and the application of electrospraying technology in the fabrication of mPCMs were also presented.

In order to design n-alkane/PLA/PCL mPCMs with double-layered shells from coaxial nozzle electrospraying, the experimental contents of this thesis can be divided into five chapters:

In the chapter III, electrosprayed PCL microparticles were produced using five solvents (ethyl acetate, acetone, anisole, glacial acetic acid and chloroform) under different PCL concentrations and different operating

parameters. Not only green and appropriate solvent for PCL electrospraying was pointed out, but also the effects of solution properties (surface tension, electrical conductivity, viscosity and vapor pressure) and operating parameters (flow rate, working distance and applied voltage) on the formation of electrosprayed particles were clarified. Meanwhile, the optimal conditions for fabricating desired electrosprayed particles with mono-dispersed size distribution and spherical, non-porous and smooth morphologies were also obtained. In addition, a suitable solvent system for PLA electrospraying was also discussed.

In the chapter IV, two n-alkanes (n-hexadecane and n-eicosane) with three theoretical loading contents (30%, 50%, and 70% by weight) was encapsulated successfully in a PCL matrix via single nozzle electrospraying. Meanwhile, ethyl acetate (EA) and chloroform (Chl) were chosen as solvents to prepare the electrospraying solutions. The objective of this chapter is to clarify the microencapsulation process and mechanism during electro-spraying and to optimize the structures, morphologies and properties of the electro-sprayed mPCMs. The effects of phase state of n-alkanes, n-alkanes additions and used solvents on the electro-microencapsulation process and the structures, morphologies as well as properties of obtained mPCMs were also discussed.

In the chapter V, due to some limitations of PCL shell, for example, poor thermal-mechanical properties and low melting point, it is necessary to seek a substitute to PCL for encapsulating PCMs. Meanwhile, in order to investigate the effects of the shell material on the electro-microencapsulation process as well as the structures, morphologies and properties of obtained mPCMs, PLA as a green, biocompatible and biodegradable polyester, due to its strong physical strength, good barrier effect and satisfactory melting temperature, was selected as shell matrix for achieving the microencapsulation of PCMs. In this chapter, a series of n-hexadecane/PLA mPCMs were fabricated via physical blending method based on a single nozzle electrospraying technology. In order to investigate the effects of PLA concentration and n-hexadecane loading content on the structures and properties of resulted mPCMs, two concentrations of PLA (3 w/v% and 5 w/v%) and three weight ratios between n-hexadecane and PLA (30/70, 50/50 and 70/30 by weight) in chloroform were applied.

In the chapter VI, in order to further improve the encapsulation efficiency of PCMs in electrosprayed microcapsules and design a core-shell structure of electrosprayed microcapsules, a coaxial nozzle was used to prepare n-hexadecane/PCL microparticles. Meanwhile, the effects of the concentration of shell liquid (5 w/v% or 10 w/v% PCL in chloroform) and the different theoretical loading contents of n-hexadecane (30 wt%, 50 wt% and wt70 %) on the formation of mPCMs and their structures, morphologies as well as properties during coaxial nozzle

electrospraying were also investigated. Finally, a comprehensive comparison between single and coaxial nozzle electrospraying in the encapsulation of PCMs, focusing on the structures, morphologies, and thermal properties of the corresponding microcapsules was also discussed.

In the chapter VII, in order to improve the thermal-mechanical properties of electrosprayed mPCMs, the interfacial adhesion between mPCMs and textiles and the encapsulation efficiency of PCMs, double-layered shell microcapsules were fabricated from coaxial nozzle electrospraying. Due to its good viscoelastic, low glass transition temperature and low melting point, PCL is easy to form interfacial adhesion with textiles. Therefore, PCL was selected as outer shell matrix. Meanwhile, owing to relatively high glass transition temperature and melting point, good thermal-mechanical property and enough physical strength, PLA was selected as inner shell matrix to encapsulate n-hexadecane. Furthermore, in order to optimize the structures, morphologies and thermal properties of final n-hexadecane/PLA/PCL microcapsules and better achieve the functional coating of textiles, the effects of different n-hexadecane additions, different weight ratios between PCL and PLA on the structures, morphologies and properties of obtained mPCMs were investigated in details. Electrosprayed microcapsules with double-layered shell not only will offer great potential and advantages for fabricating thermal-regulated textiles, but also offer a new direction for the fields of energy storage and thermal management.

In the research, the physico-chemical properties of electrospraying solutions were characterized from surface tension, electrical conductivity and viscosity. The formation of Taylor cone during electrospraying was captured by high-speed camera. The size, size distribution, and surface morphology of electrosprayed microparticles were observed by optical microscopy (OM) and scanning electron microscopy (SEM). The thermal properties and thermal stability of electrosprayed microparticles were characterized by differential scanning calorimetry (DSC) and thermo gravimetric analysis (TGA). And the chemical strcture of samples was analyzed by Fourier transform infrared spectroscopy (FTIR).

Chapter 1 State of the Art

Microencapsulation is a preservation or protection technology for active substances via enclosing them into polymeric or inorganic containers. Phase change materials (PCMs) as smart materials, due to their relatively higher thermal capacity and storage density, enabling a compact energy storage system at nearly isothermal conditions, high latent heat release or storage, thermal and chemical stability, non-toxicity and low cost, were widely used in the fields of space equipment, thermal-regulate textiles, industrial waste heat recovery, energy conservation in buildings, electric appliances with thermostatic regulator, energy-storage kitchen utensil and solar energy use. Meanwhile, the textiles incorporated with PCMs can broaden the application direction of conventional textile and satisfy the people's demand in thermal comfort in harsh environments (for example, intense sunshine, strong wind and cold rain). When PCMs were prepared into phase change microcapsules (mPCMs), some drawbacks and limitations of PCMs can be further overcome effectively. Therefore, microencapsulation technology can accelerate and develop the applications of PCMs in related fields. The definition, structure, morphology, properties of microcapsules, various methods for achieving the microencapsulation process of PCMs and the related applications of functional microcapsules as well as mPCMs were introduced.

Among these methods, electrospraying as a green, simple and high-efficiency electrohydrodynamic atomization technology, was regarded as a suitable method to fabricate mPCMs with mono-dispersed size distribution, controllable structures as well as morphologies, and high encapsulation efficiency of PCMs. Not only the mechanism, experimental devices and related applications of electrospraying were discussed, but also the effects of solution properties and operating parameters on the formation of electrosprayed particles as well as the properties of obtained particles. Meanwhile, electrospraying technology was also regarded as a feasible and high-efficiency method to achieving the functional coating of textiles by electrosprayed mPCMs for obtaining thermal-regulated textiles.

Finally, polycaprolactone (PCL) and poly(lactic acid) (PLA) as green, non-toxic, biocompatible and biodegradable materials, have attracted the attention of more and more scientific researchers. Therefore, we also paid our attention on the fabrication and applications of electrosprayed PCL and PLA productions.

1.1 Microencapsulation

Microencapsulation is a preservation or protection technology for active substances via enclosing them into polymeric or inorganic containers. This inspiration comes from the imitation of encapsulation examples in nature, for example, a seed in a coat, birds' eggs and cells in membranes, for protecting materials from the surrounding environment (Salaün, 2016). With the development of microencapsulation technology, it also become an effective method to design new structures and create new properties as well new functions. For example, when drug is encapsulated into some polymeric shell, owing to the existence of core-shell structure, not only its release rate can be controlled effectively, but also its life can be further prolonged. Meanwhile, when multi-component functional substances are encapsulated into drug-based microcapsules, the effective delivery of drugs and the tracking function inside the human body were obtained (Sukhorukov et al., 2007). For PCMs, when they are encapsulated into shell matrix, some drawbacks and limitations will be overcome. Firstly, due to the protection shell matrix, the leaching behavior of PCMs during phase transition process was prevented. Meanwhile, shell matrix also protects PCMs from outside environment or mediums (heat source, fire source, mechanical stress, chemical corrosion, etc.). Therefore, the stability and durability of PCMs were improved after encapsulation. Furthermore, the increase in the surface/volume ratio of microencapsulated PCMs (mPCMs) leads to an increase of the contact area with surrounding mediums, which improves their heat transfer efficiency as well as their thermal conductivities depending on the selected polymer shell (Jamekhorshid, Sadrameli, & Farid, 2014). Microencapsulation as a protection and functional modification technology is widely used in various fields, mainly including medical, thermal regulation, clothing, agriculture and food fields (Dubey, Shami, & Bhasker Rao, 2009).

1.1.1 Definition, structure and morphology

Microencapsulation is a process by which individual particles of an active agent was entrapped within a shell, surrounded or coated with a continuous film of polymeric material to produce particles in the micrometre to millimetre range, for protection and/or later release. Particles obtained by this process are called microparticles, microcapsules and microspheres according their morphologies and internal structure. For particles with a size range below 1 mm, the terms 'nanoparticles', 'nanocapsules' and 'nanospheres' are used, respectively. Furthermore, particles larger than 1000 mm are designed as macrocapsules. The nomenclature used to define

different parts of the encapsulated product includes terms for the shell, i.e., ‘wall’, ‘coating’, membrane material’; and for the core material, i.e., ‘active agent’, ‘payload’, ‘some internal active coatings for smart textiles’, respectively. Different kinds of compounds such as dye, protein, fragrance, monomers, catalyst and so on can be encapsulated with different types of wall materials such as natural polymer (gelatine, cellulose, chitosan, etc.), artificial polymers (cellulosic derivatives, etc.) and synthetic polymers (polyamide, polyester, etc.), with a loading content between 5% and 90% of the microparticles in weight (Salaün, 2016).

Microcapsules can exhibit a wide range of geometries and structures (Figure 1-1). Their morphologies depend mainly on the physicochemical characteristics of the core material and the deposition process or formation of the membrane around it. Thus, microparticles may have regular or irregular shapes, and on the basis their morphology several classifications may be done as mononuclear or core/shell structure, multinuclear or polynuclear particles and matrix particle or microsphere. Microspheres consist of a polymeric network structure in which an active substance is distributed homogeneously, whereas microcapsules or core/shell structures exhibit a reservoir structure, i.e., a core substance is surrounded by a distinct polymeric layer (Salaün, Vroman, & Aubry, 2009; Vinogradova, 2004). Furthermore, the numbers of layer or core components are not only limited to a single one, but also double-layered microcapsules shell, multilayer microcapsules or dual-core particle are found in the literature. These different characteristics that endows more functions to targeted microcapsules not only were designed via using different formation processes, but also influenced by the selection of raw materials as well as solvent systems. For example, Gander et al. showed that the morphology of the microparticles depended mainly on the polymer solvent system (Gander et al., 1996). When ethyl acetate, dimethyl carbonate, toluene and nitroethane were used as single solvent system for achieving the microencapsulation of bovine serum albumin (BSB) in poly(D,L-lactic acid) matrix, regularly shaped microspheres with a non-porous surface were fabricated. When water miscible solvents acetone, methylal, tetrahydrofuran and 1,4-dioxane were used, a substantial part of coalesced microspheres with irregular morphology were obtained.

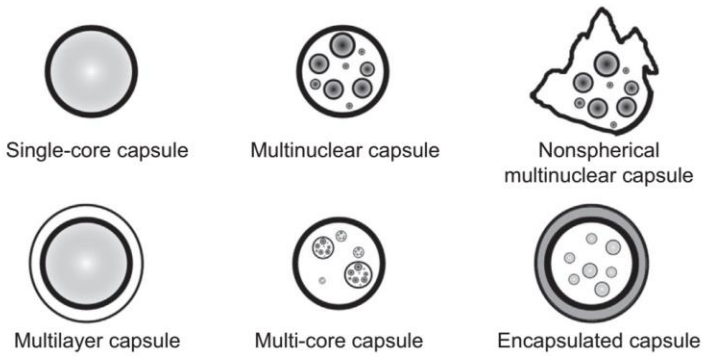

Figure 1-1 Schematic diagrams of possible microcapsule structures (Salaün, 2016).

1.1.2 Microencapsulation in the textile field-applications

In general, the functionalization of textiles was carried out via adding some active substance (or functional materials). The microencapsulation process of active substances is indispensable before their uses in textiles. Firstly, owing to the protection or physical barrier effect of shell matrix, the contacts between active substances and surrounding environments were prevented effectively. Therefore, the processability, stability and durability of active substances were improved obviously after microencapsulation process. For PCMs, their leaching behaviors during phase transition process are prevented effectively when they were encapsulated into shell matrix via microencapsulation technology. Meanwhile, some undesired properties of active substances including toxicity or smell can be depressed during the manufacture and end use owing to the isolation of shell materials. Secondly, the properties offered from the shell materials and core materials which consist of microcapsules can endow additional properties to textiles. For PCMs, their low thermal conductivities are improved obviously via selection the special shell materials that has high thermal conductivity for microencapsualtion process. Thirdly, the design in the surface morphology as well as core-shell structure of microcapsules also provides some ideas and potential to broaden the applications of multi-functions textiles used in energy storage and thermal management.

1.1.2.1 Protection and shelf life enhancement

Some of the active substances used are chemically fragile, volatile when stored or unstable (chemically, thermally or physically), and cannot be used directly without being contained in a capsule. Thus, microencapsulation technology not only protects active substances from the surrounding environment (oxidisation,

heat, acidity, alkalinity, moisture, etc.) to increase the shelf life of the product and its activity, especially for fragrance or cosmetic applications in textiles, but also prevents the interactions with other compounds in the system or other components. The existence of shell matrix also prevents the evaporation of volatile substances. Furthermore, the microcapsules protect both workers and end users from exposure to toxic or hazardous substances, and therefore the active substances are handled more safely in this form before processing. This allows a soluble compound to be transformed in a temporarily insoluble form or to a complex mixture of various components to be placed in a single capsule for a specific application. This process also allows an odour or unpleasant fragrance from active compounds to be masked during manufacture and end use.

1.1.2.2 Controlled release

The use of microencapsulation for controlled release is one of the best ways to increase efficiency and minimise environmental damage. This technology delays the release of an active substance until a stimulus is encountered at a specific rate, time or situation, i.e., heat, moisture, mechanical pressure, etc. Thus, the shell acts as a protective barrier and prevents diffusion and mass loss of the active substance, which allows the compounds (fragrance, dye, drugs, enzymes, cosmetics, etc.) to maintain intact during textile functionalization. For these kinds of active substances, the microcapsules are expected to release the core contents to the wearer under a variety of controlled conditions, which depends mainly on the selection of wall materials, the microencapsulation process used and their specific end uses.

1.1.2.3 Compatibility

The ability to transform a liquid into a pseudo-solid or powder not only prevents the accumulation of liquid but improves the mixing among incompatible compounds. Furthermore, for a textile application, the efficiency of a binder to link microcapsules on a textile surface depends on the compatibility among different products (including microcapsules, binder molecular and textiles) involved in the coating process, and it closely relates to the chemical nature of each component (Salaün et al., 2009a; Salaün et al., 2009b). The compatibility between core materials and binders (or core materials and textiles) will be improved significantly when a shell material that has good affinity to binder (or textiles) is used for encapsulating core materials.

1.1.2.4 Thermal regulation

Phase change materials (PCMs) were inorganic or organic compounds, which can store or release a large amount of latent heat during their phase change transitions induced with the surrounding temperature variations. Due to their high thermal and chemical stability, high latent heat storage capacity and low cost, they are regarded as main candidates for energy storage and thermal regulation fields. Microencapsulation technology also overcomes the drawbacks as well as the limitations of PCMs that hinders their applications and developments in thermal-regulated textiles. On the one hand, the leaching benavior of PCMs was prevented effectively based on the protection effects and physical barrier of shell matrix. On the other hand, the thermal conductivity of PCMs was enhanced obviously when shell materials with high thermal conductivity were used for the microencapsulation of PCMs. And introducing some metals, metal oxides and inorganic particles into shell materials also further improved the thermal conductivity of PCMs. Furthermore, the microencapsulation process also causes a reduction in the size of PCMs. The increase in the surface/volume ratio of microencapsulated PCMs (mPCMs) leads to an increase in the contact area with surrounding mediums, which improves their heat transfer efficiencies. Therefore, microencapsulation technology accelerates the applications and developments of PCMs in the fields thermal regulation textiles.

Microencapsulation technology was utilised in the early 1970s by the US National Aeronautics and Space Administration (NASA) with the aim of managing the thermal barrier properties of garments, in particular for use in space suits. They encapsulated n-alkane with the expection of reducing the impact of extreme variations in temperature encountered by astronauts during their missions in space.

Outlast Technologies Company has introduced mPCMs into textile fibres and fabric coatings, and these mPCMs-incorporated textiles or fabric coatings are now applied to all manner of materials, particularly outdoor wear (parkas, vests, thermals, snowsuits and trousers) and in the house in blankets, duvets, mattresses and pillowcases (Hartmann, & Eyal, 2016; Zuckerman et al., 2001). As well as being designed to fight the cold, textiles containing mPCMs also help to combat overheating, so overall the effect can be described as thermoregulation. In general, the mPCMs used in textile fields have walls less than 1 μm thick and are typically 20-40 μm in diameter, with a PCM loading content of 80-85%. The small capsule size provides a relatively large surface area for heat transfer. Thus, the rate at which the mPCMs react to an external temperature changes is very rapid (Nelson, 2001).

Kahraman et al. microencapsulate coconut oil (PCMs) in melamine formaldehyde and poly (methyl

methacrylate) polymer shells by in situ and suspension polymerization methods, respectively. Then, the fabricated microcapsules were applied on a daily wear stretch denim fabric and a cotton shirting fabric by knife-coating to impart thermo-regulation functionality (Saraç, Öner, & Kahraman, 2019).

1.1.2.5 Fire retardants

The combustibility of fabrics has also become one of the reasons that limit the development and application of textiles in many fields. When some flame retardant microcapsules obtained from microencapsulation technology are used in textiles, the flame retardant properties of the textiles will be greatly improved. For example, the flame-retardant properties of cellulose fibers can be enhanced obviously by incorporation of acid-resistant magnesium-oxide microcapsules. Magnesium oxide (MgO) microcapsules were synthesized via in-situ emulsion polymerization, and obtained microcapsules were incorporated into cellulose fibers by blend wet spinning. Experimental results indicated that the minimal limiting oxygen index (LOI) value obtained for the cellulose-MgO fibers was much higher than that of the unmodified cellulose fibers (Li et al., 2017).

1.1.3 Microencapsulation methods

Until now, there have been more than 200 methods to carry out the microencapsulation process of active substances, mainly dividing into three groups, i.e., physical methods, chemical methods and physicochemical methods. Among these methods, interfacial, *in-situ* and suspension polymerization methods, phase coacervation method, solvent evaporation methods and electrospraying method are most common methods for achiving the microencapsulation process of active substances (Appendix 3). Electrospraying as an electrohydrodynamic atomization technology, is regarded as a green, simple and high-efficiency method to fabricate polymeric microcapsules (Bock, Dargaville, & Woodruff, 2012). Compared to other microencapsulation processes, electrospraying method has been recognized as offering more advantages and potential for producing microcapsules. Firstly, electrospraying as an one-step electrohydrodynamic atomization technology is a method allowing the formation of uniform-sized particles, with simple equipmental device as well as operations and carrying out at atmospheric conditions. Furthermore, the rate of the particle production is mainly governed by adjusting voltage and flow rate. Secondly, the operation of vigorous stirring, the use of surfactants or toxic chemical additives, and a large amount of organic solvent is not necessary in the process of electrospraying.

Furthermore, the optimization of the physico-chemical properties of the solution and the associated operating parameters make it possible to design the desired structure and/or morphologies and to obtain a narrow and monodispersed particle size distribution. The desired morphology also depends on the choice of nozzle geometry. The single nozzle is mainly used to produce core-shell microcapsules and polynuclear microcapsules. The coaxial double and tri-capillary nozzle is used to manufacture yolk-like and double-layered shell microcapsules for improving the encapsulation efficiency of PCMs as well as their durability and stability. The latter is not only critical for achieving improvement in the properties of electrospray particles and diversifying of the structure as well as morphology, but it also promotes the efficiency of the process and broadens the applications of electrospray particles. Besides, when shell materials were used to encapsulate active substance via electrospraying, high encapsulation efficiency of the fragile active substance or PCMs, as well as its protection, and avoiding any particle aggregation attributed to the Coulomb repulsions among charged droplets as well as rapid solvent evaporation during their flight toward the collector. In addition, when targeted textiles were placed directly on the collector, the functional coating of textiles can also be finished during the electro-microencapsulation process (Hwang, Jeong, & Cho, 2008; Kim, & Kim, 2010, 2011; Li, Liu, & Shi, 2018).

1.2 The introduction of electrospraying

Electrospraying, as a rapidly emerging electrohydrodynamic atomization process, has great potential and advantages to prepare nano- or micro- scale particles and capsules. In the process of electrospraying, the polymeric solution is polarized firstly due to the applied electric field, and then charged droplets is stretched and accelerated into the charged jet by the electrostatic force generated on the droplets surface. Next, charged jet breakups into smaller charged droplets via Coulomb repulsion forces. After evaporation of the solvent, micro- or nanoscale particles are collected (Zhang, Campagne, & Salaün, 2019a). According to the different geometries of used nozzles, electrspraying technology is divided into single nozzle electrospraying and coaxial nozzle electrospraying. In single nozzle electrospraying, a solvent able to solubilize both polymer shell and PCMs is used to form the working solution. Then, this solution is pumped out from the electro-sprayed nozzle with an applied voltage to prepare mPCMs. During the evaporation of the solvent, the solvent richest phase diffuses to form a shell, and poor solvent phase stays in the inner part of the microcapsules to form the core, due to the solubility differences between matrix and PCMs in the working solvent (Zhang, Campagne, & Salaün, 2020). In coaxial nozzle electrospraying,

the solutions from the core (PCMs) and polymeric shell flow independently of the inner and outer capillaries, respectively (Bock, Dargaville, & Woodruff, 2012; Hwang, Jeong, & Cho, 2008; Zhang et al., 2012). This configuration allows a short-term limitation of the physico-chemical interactions between the core and shell compounds, which restrain the diffusion of PCMs into shell phase and induce a mono-nuclear morphology. This type of morphology makes it possible to highlight some interesting functional properties of mPCMs, such as their durability, shape, and thermal stabilities. Meanwhile, a higher encapsulation efficiency and a higher loading content of PCMs can be obtained from coaxial electrospraying process (Zhang et al., 2020). Nevertheless, adjustment of the solution properties and working parameters is required for the formation of a stable Taylor cone, and thus to induce a uniform breaking process of the charged jets, which is considered to be more difficult compared to a single-nozzle electrospraying process.

1.2.1 The mechanism of electrospraying

Electrospraying is a method of liquid atomization that achieves the stretching and breakup of polymeric solution to obtain micro- or nanoscale particles via means of electrical forces. Six types of forces govern the electrospraying process, i.e., (i) gravity of polymeric solution, (ii) electrostatic force generated from external electric field between nozzle and collector, (iii) Coulomb repulsion force among adjacent charged carriers on the surface of jet, (iv) viscoelastic force of polymeric solution, (v) surface tension in the interface between air and liquid, and (vi) frictional force between charged jet and surrounding air (Figure 1-2) (Enayati et al., 2011; Hartman at al., 1999). Among these forces, electrostatic force, Coulomb repulsion forces, viscoelastic force, and surface tension affect the stretching as well as atomization of polymeric droplets obviously during the electrospraying process. When polymeric solution flows out of the nozzle, the charge distribution and carried charge quantity on the surface of the polymeric solution will change in varying degrees (some extent) according to its electrical conductivity and dielectric constant because of the polarization effect coming from the external electric field. At the same time, initially, the uncharged liquid becomes charged jet and is further stretched towards the direction of electrostatic attraction. However, compared to gravity and electrostatic force that accelerates the moving and stretching of polymeric solution from the nozzle to the collector, the surface tension and viscoelastic ones prevent this moving and elongation because of their opposite behavior on the electrosprayed solution. When these forces reach a balance at a certain range, the droplets at the tip of the nozzle are stretched from the spherical surface into

conical surface (Collins et al., 2008). In 1964, Taylor proposed, for a perfectly conducting liquid, a first explanation of the conical shape formation, corresponding to a hydrostatic balance between electrostatic forces and surface tension (Taylor, 1964). The presence of the conical surface at the tip of the nozzle during electrospraying is also called Taylor cone. According to Rayleigh's theory, when the charge quantity distributed on the surface of droplets reaches the value range between 50% and 80% of the Rayleigh limit (Equation (1-1)), the breakup and fission of charged droplets will occur due to Coulomb repulsions among charged droplets beyond the binding force coming from surface tension that held the droplets together. The aggregation among electrosprayed particle is depressed during their flight from the nozzle to collector due to Coulomb repulsions, to induce the formation of tiny solid particles after solvent evaporation.

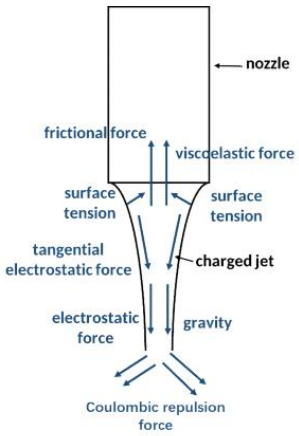

Figure 1-2 Schematic representation of the formation of cone jet as well as the breakup process of charged jet in electrospraying process indicating the controlling forces.

$$q_{\lim}^2 = 8\pi^2 \varepsilon_0 \gamma D_d \qquad \text{Equation (1-1)}$$

Where, q_{lim}, ε_0, γ, and D_d are the charge quantity of Rayleigh limit, the dielectric constant of the medium surrounding the droplets, the surface tension of electrospray liquid, and the diameter of droplets, respectively.

The formation of a Taylor cone and the fission of charged droplets are indispensable for preparing electrosprayed particles with idea structure as well as morphology via electrospraying. On the one hand, the size of the electrosprayed particles were dispersed into micrometer or even nanometer range by the Coulomb repulsions, and the mono-dispersion of particles is obtained under cone-jet mode. On the other hand, the effective design and control of the structure, as well as the morphology of electrosprayed particles and the process

reproducibility is achieved easily under cone-jet mode due to its stability and continuity. The effects of various parameters on the formation of the Taylor cone as well as the breakup of the charged droplets have been the topics of several research projects (Deitzel et al., 2001; Martin et al., 2012; Wan et al., 2012; Yao et al., 2008). The spray mode changes gradually from dripping mode to cone-jet mode with increasing the applied voltage. Then, the spray mode is further transmitted from stable cone-jet to multi-jet mode (unstable cone-jet mode) when the applied voltage beyond a certain range (Jaworek, 2008). Therefore, a suitable applied voltage to reach a balance among electrostatic, viscoelastic forces and surface tension in a droplet at the tip of the nozzle is required for achieving the cone-jet of the electrospraying solution. The value of working distance from nozzle to collector also affects the formation of Taylor cone and the breakup of the charged droplets via changing the strength of electric field. According to Smeets et al., the achievement of a stable cone-jet rises with the use of a lager tip-to-collector distance and smaller flow rate (Smeets, Clasen, & Van den Mooter, 2017). Apart from operating parameters, the success of stable cone-jet and the breakup of droplets are also closely related with the physical properties of electrospraying solution (Almería et al., 2010; Garoz et al., 2007; Wongsasulak et al., 2007). The value of electrical conductivity of electrospraying solution affects the charge quantities on the surface of droplets and further influences the strength of electrostatic force. Several authors have concluded that cone-jet mode was obtained in air only if the electrical conductivity of the liquid was set in a certain range (Barrero et al., 1999; Cloupeau, & Prunet-Foch, 1989). As for the upper limit, Mutoh et al. have found that the jet changes from a permanent to an intermittent jet, when the conductivity of the solution beyond than 10^{-1} μS/cm. For lower limit, estimates generally vary between 10^{-4} and 10^{-6} μS/cm. Besides, the range from the upper and lower limits of conductivity broadens when the solution has low surface tension (Mutoh, Kaieda, & Kamimura, 1979).

When the surface tension is too high, the formation of the Taylor cone at the tip of the nozzle is maintained due to the change in spherical shape of the liquid. Corona discharge results from excessively high surface tension at the tip prevents the electrostatic atomization of charged droplets (Cloupeau, 1994). According to Smith et al., the atomization of charged droplets in cone-jet mode can not be achieved if the surface tension of electrosprayed liquid exceeds 50 mN/m (Smith, 1986). The upper limit of the surface tension of the solutions varies, according to the properties of solute and solvent. Furthermore, the viscosity of the solution needs also to be considered, since it influences the formation of cone-jet. Some researchers concluded that the solution with higher viscosity is efficient to maintain the cone-jet mode during the electrospraying process (Barrero et al., 1998; López-Herrera et

al., 2003).

1.2.2 The effects of solvent systems

During the process of electrospraying, there are lot of interrelated parameters which influence the realization and the outcomes. By controlling these parameters, different structures and morphologies of electrosprayed particles (or droplets) are obtained. According to their inherent characteristics, these parameters are divide into two categories, i.e., (1) solution formation parameters, and (2) operating parameters. Solution formation parameters mainly include solvent systems, polymer concentration, polymer molecular weight, and active substance concentration. These solution formulation parameters mainly determine the physico-chemical properties of electrospraying solution (including solubility parameters, viscosity, surface tension, vapor pressure, dielectric constant, electrical conductivity, and chains entanglement). Process parameters mainly include applied voltage, flow rate, working distance, nozzle gauge and geometry, collection method, environmental temperature, environmental pressure, and environmental humidity. Among these interrelated parameters, the selection of a suitable solvent system as the carrier of matrix material is fundamental and a prerequisite for the optimization of electrospraying and controlling the morphology as well as the structure of electrosprayed particles. These properties influence the process stability and the formation of Taylor cone during the electrospraying, but also the working range values of operating parameters, i.e., the applied voltage, the flow rate, and the working distance. The formation of Taylor cone during the electrospraying is necessary for stabilizing experimental process and achieving the micronization, the nanonization, as well as the homogenization of electrosprayed particles. Secondly, the size, size distribution, and morphology of the electrosprayed particles are also determined by these solution properties and operating parameters. For instance, increasing electrical conductivity of electrospraying solution or applied voltage not only decreases particles size significantly, but also broadens the particle size distribution. The entanglement among polymeric chains and the solution viscosity determine the final morphology of electrospraying object, i.e., fibers or spheres. In general, electrolytically sprayed microspheres are manufactured with a low viscosity and a lower polymer chain entanglement, unlike electrospun fibers, which require the use of a solution with a higher viscosity and a higher entanglement amount. Besides, the phase separations and the solidification processes of electrosprayed droplets play a primary role in the shape on the morphology of the obtained particles. They are also affected by the physico-chemical properties of electrospraying solution and more

especially the system solvent choice used to solubilize the polymer.

Meanwhile, the electrosprayed particles with porous structure are easily obtained when the binary solvent system is used (Gao et al., 2015). The different evaporation rates, as well as compatibility among non-solvent, solvent and polymeric matrix, lead to the phase separation and result in the synthesis of highly porous particles. Furthermore, the formation of a core-shell structure for PCL capsules and the encapsulation efficiency of active substance are also closely related to the selection of solvents systems. According to these above mentioned, investigating these effects coming from different solvent systems and selecting a desirable solvent system for electrospraying are significant for designing and obtaining an ideal structure as well as the morphology of electrosprayed PCL particles. Therefore, when a solvent system was selected for preparing electrospraying solution, three of them are mainly considered, i.e., (i) it needs at least partially solubilize matrix material, (ii) the obtained physico-chemical properties of the solution (surface tension, electric conductivity, viscosity, vapor pressure, boiling point, and dielectric constant) should be suitable to achieve a cone-jet mode; and (iii) the selection of solvent systems should take into account the desired structure and morphology of final electrosprayed particles (Zhang, Campagne, & Salaün, 2019a, 2019b).

1.2.2.1 Solubility parameters and compatibility

Firstly, when considering whether a solvent system is suitable for being used as carrier for polymeric matrix and active substance during electrospraying process, the first step is ensuring the solubility or compatibility among solvent system, polymer and active substance. In general, in order to ensure the stable progress of electrospraying, active substance and polymeric matrix need to be dissolved partially or completely in solvent systems. The Hansen Solubility Parameters (HSPs) methodology is one of the approaches used to select a suitable solvent system for dissolving electrospraying solution (Bock, Dargaville, & Woodruff, 2014). From HSPs, solubility parameters of substances consist of three parts, i.e., (1) a dispersed component (δ_d) derived from London interaction resulting from the existence of induced dipoles as two molecules approach one another (2) a polar component (δ_p) derived from Keesom forces occurring when two permanent dipoles are present and (3) a hydrogen component (δ_h) derived from hydrogen bonding forces. Three Hansen solubility parameters (δ_d, δ_p, δ_h) define a three dimension “solubility space” in which all liquid or solid substances are localized. In the “Hansen space”, solvents in which a given molecule is soluble form a cloud of points corresponding in most cases to a sphere whose center point is the solute

coordinates (Bordes et al., 2010). All solvents and mixtures found in the inner of sphere are good solvents for the studied solute and the solvents outside are non-solvents. The more a solvent is close to the solute in the "Hansen space", the better its affinity for this solute. Meanwhile, a distance (D) between a solvent (S) and the solute (P) in the "solubility space" is calculated by the following equation (1-2):

$$D = (4(\delta_{dS} - \delta_{dP})^2 + (\delta_{pS} - \delta_{pP})^2 + (\delta_{hS} - \delta_{hP})^2)^{1/2} \quad \text{Equation (1-2)}$$

And the radius Rs of the "solubility sphere" of solute is determined by the maximum distance between the good solvent the furthest from the center and the sphere center. When the distance (D) between the location of solvent (δ_{dS}, δ_{pS}, δ_{hS}) and the location of solute (δ_{dP}, δ_{pP}, δ_{hP}) in "Hansen space" is less than Rs, this solvent will be regarded as good solvent for solute. The smaller distance (D) between two substances, in "Hansen space", means that the stronger compatibility and better solubility are obtained between these two substances.

Taking poly(lactic acid) (PLA) and polycaprolactone (PCL) as examples, the Hansen solubility parameters of PCL are 21.2 ± 0.6 (δ_d, $(MPa)^{\frac{1}{2}}$), 3.4 ± 0.9 (δ_p, $(MPa)^{\frac{1}{2}}$) and 5.2 ± 0.8 (δ_h, $(MPa)^{\frac{1}{2}}$,), and the Hansen solubility parameters of PLA are 20.0 ± 0.6 (δ_d, $(MPa)^{\frac{1}{2}}$,), 5.9 ± 0.7 (δ_p, $(MPa)^{\frac{1}{2}}$,) and 7.6 ± 0.9 (δ_h, $(MPa)^{\frac{1}{2}}$,), which was calculated by Adamska et al (Adamska, Voelkel, & Berlińska, 2016). Meanwhile, the Hansen solubility parameters of PCL or PLA are also effected by measurement methods, measurement temperature, measurement concentration and macromolecular weight. Considering from Hansen solubility parameters, toxicity and cost, green and suitable solvents for dissolving PCL are chloroform (18.2 (δ_d), 6.3 (δ_p) and 6.2 (δ_h), unit: $(MPa)^{\frac{1}{2}}$), ethyl acetate (15.8 (δ_d), 5.3 (δ_p) and 7.2 (δ_h), unit: $(MPa)^{\frac{1}{2}}$), anisole (17.8 (δ_d), 4.1 (δ_p) and 6.7 (δ_h), unit: $(MPa)^{\frac{1}{2}}$), acetic acid (14.5 (δ_d), 8.0 (δ_p) and 15.3 (δ_h), unit: $(MPa)^{\frac{1}{2}}$) and acetone (15.7 (δ_d), 5.3 (δ_p) and 11.7 (δ_h), unit: $(MPa)^{\frac{1}{2}}$). For dissolving PLA with low molecular weight, chloroform (18.2 (δ_d), 6.3 (δ_p) and 6.2 (δ_h), unit: $(MPa)^{\frac{1}{2}}$), ethyl acetate (15.8 (δ_d), 5.3 (δ_p) and 7.2 (δ_h), unit: $(MPa)^{\frac{1}{2}}$) and acetone (15.7 (δ_d), 5.3 (δ_p) and 11.7 (δ_h), unit: $(MPa)^{\frac{1}{2}}$) are more suitable. However, for dissolving PLA with high molecular weight, only chloroform (18.2 (δ_d), 6.3 (δ_p) and 6.2 (δ_h), unit: $(MPa)^{\frac{1}{2}}$) was suitable.

When selecting solvent used for preparing microspheres or microcapsules based on electrospraying, the compatibility among shell material, core material and solvent is also crucial. In general, good compatibility

between solvent and polymer results in the formation of beaded structures or spherical particles. Partial compatibility between solvent and polymer results in the formation of fibrous structure. For preparing microcapsules via single nozzle electrospraying, active substance is randomly distributed in polymeric matrix if the compatibility among active substance, matrix and solvent is complete. And active substance tends to locate in the center of matrix when the compatibility between active substance and polymer/solvent system is partial (Bock, Dargaville, &Woodruff, 2012; Valo et al., 2009).

1.2.2.2 Electrical conductivity

The physico-chemical properties of the electrospraying solution depend on the properties of the solvent system, i.e., (i) electrical conductivity, (ii) surface tension, (iii) viscosity, (iv) vapor pressure, and (v) dielectric constant. The control of these characteristics allows the formation of the Taylor cone, which leads to the production of particles having a low mean diameter and narrow particle size distribution.

During electrospraying, due to the electrostatic forces, generated from the applied electric field, the solution is stretched and accelerated into a jet from the tip of the nozzle to the collector. The formation of the Taylor cone occurs at the tip of the nozzle, when a balance among six forces, including gravity, electrostatic force, Coulomb repulsions, viscoelastic and frictional forces, and surface tension, is achieved (Figure 1-3). The strength of the electrostatic force and Coulomb repulsion acting on electrosprayed droplets mainly depend on the amount of polarization charge in droplets and the strength of the applied electric field. The amount of polarized charges on the surface of the droplets is closely related to the range of the electrical conductivity of working solution in the electric field. The surface tension and viscoelastic forces are counteracted by the electrostatic forces under the electric field, leading to the formation of the Taylor cone. If the electrical conductivity of the working solution is too high, the Coulomb repulsions among charged droplets increase, as well as the breakup of charged droplets. All these phenomena contribute to modify the balance among the six forces, and the stable cone-jet change to an unstable jet. On the other hand, an excessively low electrical conductivity leads to insufficient electrostatic forces on the droplets to match with the surface tension and viscoelastic forces of the working solution. Thus, the Taylor cone at the tip of the nozzle is not achieved, nor is the formation of particles.

According to Jaworek and Xie et al., the electrohydrodynamic process is carried out under cone-jet mode when the electrical conductivity of working liquids are in the range of 10^{-7} to 10^{3} μS/cm (Jaworek, 2007; Xie et

al., 2015). It was noticed that it also increases with the increase of surface tension and the viscosity of working solutions. In some cases, if the surface tension and viscosity of the solution are too high, their electrical conductivity of working liquids, exceeding the mentioned range, is required to balance the surface tension and viscoelastic forces to achieve the cone-jet mode.

In the use of a coaxial electrospraying, the formation of cone-jet at the tip of the nozzle is also closely related to the electrical conductivities of inner and outer liquid phases (Chen et al., 2005; López-Herrera et al., 2003). On the one hand, for a higher electrical conductivity of the inner liquid than the outer one, the free charges are located at the interface. In this case, inner liquids regard as the driving component and dominate the formation of the Taylor cone. Then, inner droplets are stretched into the conical shape due to the electrostatic forces acting on their surface, which leads to the transfer of the free charges to the surface of the outer phase. Finally, the formation of the Taylor cone of the outer liquid is done when the electrostatic attractions acting on the surface of outer liquid counteract the viscoelastic forces and surface tension (Figure 1-3 a). On the other hand, a higher the electrical conductivity of the outer phase leads to the distribution of the free charges on its surface. The outer liquid dominates the formation of cone-jet of this configuration. In the first step, it is stretched into the Taylor cone due to the electrical attractions acting on its surface. The Taylor cone formation is only reached when the viscosity of the outer liquid is higher than the inner phase one (Figure 1-3 b). According to Mei and Zhang et al., the cone-jet during coaxial electrospraying is easier to form in the case of inner driving, where the electrical conductivity of the outer liquid is less than that of the inner liquid. This principle is also applied to three-needle or four-needle coaxial electrospraying. To obtain suitable electrical conductivity, some authors reported the addition of metal oxide or high electrical conductivity solvents in the working solutions (Mei, & Chen, 2007; Zhang et al., 2012).

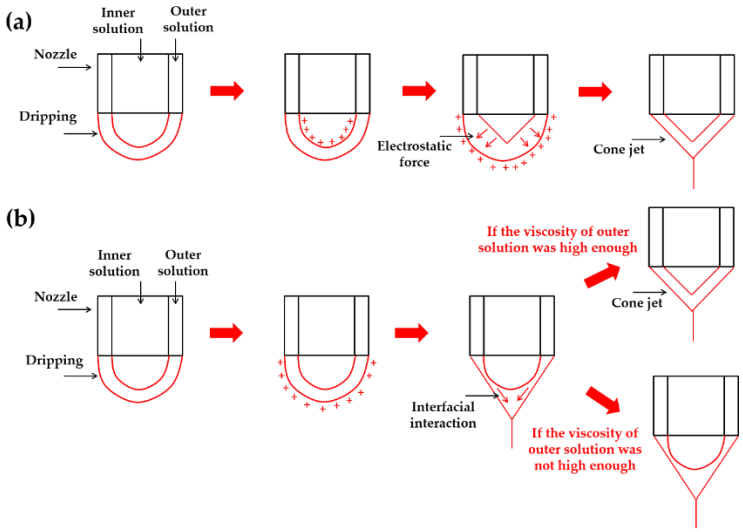

Figure 1-3 The formation process of cone jet in coaxial electrospraying for inner and outer solutions with different electrical conductivities. (a) inner solution has higher electrical conductivity (b) outer solution has higher electrical conductivity.

1.2.2.3 Surface tension

The surface tension of the working solution affects the formation of the Taylor cone at the tip of the nozzle during the electrospraying process. According to Cloupeau and Smith, the value of surface tension of the electrosprayed solution cannot exceed 50 mN/m (Cloupeau, 1994; Smith, 1986), even if some papers report the use of glycerine (63.0 mN/m) or water (72.8 mN/m) (John, 1917; Taylor, 1969). In general, a suitable range of surface tension for achieving Taylor cone and stable electrospraying process was ranging from 22.5 to 32.8 mN/m. Furthermore, liquids with a high surface tension trigger also a corona discharge at the tip of the nozzle, which change the stable cone-jet into an irregular spraying and an asymmetrical mode.

In the coaxial mode, when the surface tension of the inner phase is higher than the outer one, the formation of a stable Taylor cone is possible, which leads to the formation of core-shell particles as described by Loscertales et al (Loscertales et al., 2002). The relations between the surface and interfacial tensions to promote the formation of a cone-jet mode have been studied in details by Mei et al. (Figure 1-4), with the use of the spreading coefficients (S_i) (Equation (1-3)) (Mei, & Chen, 2008).

$$S_i = \gamma_{jk} - (\gamma_{ik} + \gamma_{ij}) \qquad \text{Equation (1-3)}$$

where, 1, 2, and 3 represent core liquid, air, and shell in the liquid state, respectively. γ_{23}, γ_{12} and γ_{13} are the surface tension of shell and core liquid, and γ_{13} the interfacial tension between core liquid and shell liquid phases, respectively.

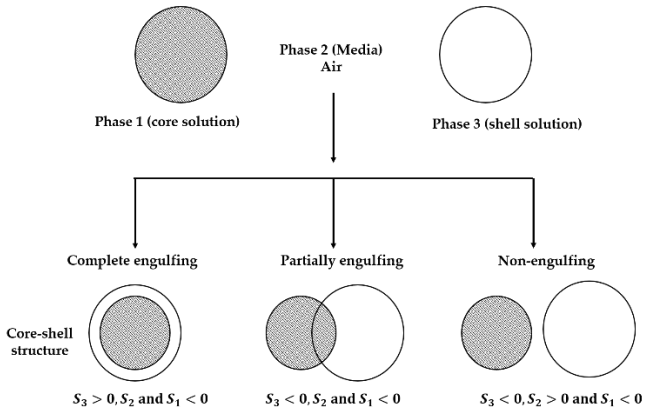

Figure 1-4 Prediction of microencapsulation configuration based on spreading coefficients.

The thermodynamic conditions of the system required for the formation of a complete engulfing are S3 > 0, S1 < 0 and S2 < 0. In other cases, partial or non-engulfing are obtained, due to the presence of unstable cone-jet. Therefore, the core substance or inner phase needs to have a high surface tension value to promote the formation of cone-jet, and after that, a core-shell structure via a coaxial electrospraying process (Ahmad et al., 2008; Pareta & Edirisinghe, 2006; Xu & Hanna, 2008). To succeed in the design of the electrospraying methods with three-needle or four-needle coaxial, the authors preconize the choice of solvents having similar surface tensions, or close to the dispersed active substance one (Kim, & Kim, 2010, 2011; Labbaf et al., 2014). Surfactants or protective colloid may also be added to the various phases until to reach the desired surface properties of the working solutions (Farook, Stride, & Edirisinghe, 2009).

1.2.2.4 Viscosity

The viscosities of the electrosprayed solutions influence the formation of a stable Taylor cone, where the direction of the viscoelastic force is opposite to those of gravity and electrostatic attraction ones. On the one hand, the combined viscoelastic force and surface tension are too weak to counteract the gravity and electrostatic attraction ones in a low viscosity medium, leading to a dripping mode rather than a cone-jet one. On the other hand, the use of high viscosity working solutions prevents the formation of stable Taylor cone. The drying of the polymeric particles with the solvent evaporation during the process occludes the tip of the capillary; and therefore limiting the stability of the Taylor cone (Jaworek, & Krupa, 1999; Jayasinghe & Townsend-Nicholson, 2006). Thus, there is an appropriate range in viscosity of solution for achieving cone-jet mode during the electrospraying process. It ranges from 1.5 to 5500 mPa·s (Smeets, Clasen, & Van den Mooter, 2017). An increase of the solution viscosity leads a decrease to the distance from the exit of the nozzle to the apex of the cone. In general, a long

distance from the tip of the nozzle to the apex of the cone induces an increase in jetting diameter at the tip of the cone and may lead to dripping mode or spindle mode. An increase in the solution viscosity allows obtaining a cone angle close to the theoretical value of Taylor cone (about 98.6°), which reduces the mean diameter of the obtained particles and narrows its size distribution (Cloupeau, & Prunet-Foch, 1994). For a coaxial process, the formation of the Taylor cone is favored, when the viscosity of the outer phase is higher than the inner one. In this case, its formation for the inner phase is driving by the interfacial interactions and related viscosities diffusion.

1.2.2.5 Boiling point

The formation of Taylor cone during electrospraying is also affected by the boiling point of working solution. The solvent evaporation in jetting occurs at the same time that the formation of Taylor cone at the tip of the nozzle. A too low boiling point or high vapor pressure value modifies the shape of the cone-jet to change it in an unstable mode. Furthermore, it leads to the drying of the polymeric particles inside the tube or at the tip of the nozzle, until to stop the process. Therefore, the Taylor cone formation is promoted with high boiling point solvent, and is especially useful for high PCL concentrations. However, a too high boiling point or low vapor pressure also reduces the evaporation rate of solvent during the flight process of electrosprayed droplets, which will result in a large amount of solvent remaining in the final electrospray product. The residual solvent will cause the electrosprayed particles to agglomerate and finally get the electrosprayed film.

1.2.2.6 Dielectric constant

To date, few papers have studied the effect of dielectric constant on the process and outcomes of the electrospraying method. The effects of the dielectric constant on the cone-jet are similar to the electrical conductivity ones. Too high or too low dielectric constant is not conducive to achieving the cone-jet during PCL electrospraying process. Some research works published about the electrospinning of polystyrene noticed that the yield of productivity was correlated to the dipole moment and the dielectric constant of the working solutions (Jarusuwannapoom et al., 2005; Pham, Sharma, & Mikos, 2006). Thus, based on the use of 18 solvents to prepare the working solution, it was concluded that the formation of the cone-jet was related to the use of solvent solution having high electrical conductivity and dielectric constant, moderate viscosity, surface tension, and boiling point.

1.2.3 The effects of operating parameters

As a multi-physical process, the process and results of electrospraying, Taylor cone formation, and particle morphology are determined not only by the properties of the starting solution, but also by the setting of the machine parameters, i.e., (i) the applied voltage, (ii) the working distance, (iii) the liquid flow, (iv) the nozzle type and (v) experimental temperature and humidity. The adjustment of the various working parameters, to obtain a conical jet during the electrospray process, is mainly governed by the physico-chemical properties of the solutions. The study of the relationships between the conical jet working range and the related properties of the solutions provides a better understanding of the importance of choosing appropriate solvent systems and theoretical knowledge for future system optimization.

1.2.3.1 Applied voltage

The value of the voltage applied between the nozzle and the collector is one of the parameters to be controlled for process optimization since it influences the stretching of the jet and then the formation of a Taylor cone at the end of the nozzle. Its increase leads to a gradual increase in electrostatic forces acting on the surface of the charged droplets. The spray mode gradually changes from drip to multi-jet mode, including micro-drop, pulsed cone-jet, and stable cone-jet modes as the applied voltage increases (Smeets, Clasen, & Van den Mooter, 2017; Xie et al., 2008). Drop-to-drop mode is obtained for low voltage values when the electrostatic forces acting on the surface of the spray droplets are not sufficiently strong to exceed that of the surface and viscoelastic tension, and it leads to the production of films. In the dripping regime, drops of electrified liquid form at the end of the capillary until the combined effect of gravitational and electrical forces exceeds their surface tension. The droplet break-up occurs at a relatively low frequency, and their spherical morphology is maintained as long as gravitational and surface forces play primary roles. As the voltage increases, the shape of the ejected liquid is affected by its wetting properties. The use of this regime allows obtaining particles of high average diameter with broad size distribution. By further increasing the tension, a pulsating cone jet appears. For higher voltages, the spray mode switches to stable conical jet mode, since the electrostatic force is strong enough to overcome surface tension and viscoelastic force and achieve a balance between different forces. In this regime, particles of small mean diameter and with a narrow size distribution are obtained. Beyond this tension, the multi-jet is observed, and then if the applied

potential increases further, the jet disintegrates.

Thus, depending on the inherent characteristics of the solutions used (electrical conductivity, surface tension, and viscosity), there is an appropriate voltage range for obtaining a stable cone-jet regime. In general, the conical jet window of the voltage applied in the electrospray process is between several kilovolts and a dozen kilovolts. These differences are mainly related to variations in the molecular weight as well as physical properties of the polymers used, the concentration, and the solvent selected, which modify the electrical conductivity, viscosity and surface tension of the prepared solutions. As the concentration of the polymer solution increases, surface tension and viscosity increase, while electrical conductivity decreases. Thus, a stronger electrostatic force is required to form the stable jet cone for a solution with a higher polymer concentration. In most cases, an increase in concentration leads to a widening of the voltage range and/or an increase in it. This increase is also correlated with a variation in the electrical conductivity of the solutions. The applied electric field required forming a cone on the tip of the nozzle decreases with increasing conductivity. In general, in cone-jet mode, the mean diameter of electrosprayed particles decreases with the increasing of applied voltage. The particle diameters range from several hundred nanometers up to several hundred micrometers. According to Zhou et al., the mean diameters of the PCL particles decreases from 27.6, through 23.8, to 21.9 μm in increasing the applied voltage from 6.5 to 8.5 kV (Zhou et al., 2016).

In the case of the use of a coaxial tip, the applied voltage affects the ratio between the thickness of the polymeric shell and the radius of the core component (T/R). Thus, the T/R value increases with the applied voltage, when the electrical conductivity of the core solution is higher than the shell one, and for a higher viscosity of the shell solution than the core one (Gao et al., 2016).

1.2.3.2 Working distance

The working distance, between the top of the tip and the collector, is adjusted to adapt the intensity of the electric field in order to ensure the formation of the Taylor cone, i.e., at a constant voltage, shorter distance is privileged to generate a higher electric field strength leading to the formation of smaller particles. Nevertheless, insufficient time to allow solvent evaporation may induce coalescence and aggregation of the particles at the surface of the collector. On the other hand, a longer working distance requires the use of higher applied voltage to compensate the lower electric field strength (Zhang et al., 2012). In this context, this distance may lead to lower

yield due to material loss to the surrounding environment with the presence of turbulence during the droplet flight. Nevertheless, a long working distance is required to obtain denser polymer particles, since it allows the complete solvent evaporation and diffusion before reaching the collector surface.

Furthermore, it is usually smaller for the low conductive solution and increases when the electrical conductivity increases to improve the stability of the cone-jet mode. In most cases, the working distance range applied for polymeric particle production is set between several centimeters up to 20 cm, and more especially from 3 to 15 cm. 3 cm is the lower limit allowing the creation of the electrical discharge in the system (Zhang et al., 2012). For working distance higher than 15 cm, the intensity of the electric field weakens, and the forces generated are too low to compensate the surface tension and viscoelastic force. Therefore, a long working distance is preconized for high conductivity, and low vapor saturated pressure solutions. Also, the formation of the cone-jet mode for high surface tension or high viscous solutions requires small working distance in the electrospraying process.

Besides, the working distance between the nozzle tip and the collector also affects the structure and morphology of the particles. Thus, high working distance leads to a decrease in the electric field, which increases the mean diameter of the particles. One the other hand, there is a trend to achieve smaller particles under low working distance based on an increase of the voltage. However, an incomplete solvent removal during the flying process leads to an increase of the particles size as well as a widening distribution. Thus, the swelled particles may be deformed and coalesce at the surface of the collector. As the working distance increases, the particle size distribution becomes narrow with a monomodal distribution induced by the complete evaporation of the solvent and the homogeneous break-up of the charged droplets, and the particles are spherical (Gao et al., 2016; Zhou et al., 2016). However, for higher working distance value, more than 30 cm, the number of particles at the surface of the collector decreases, since the charged particles tend to be attracted to the nearest ground object during long-distance flights. Besides, in the coaxial electrospraying process, the thickness of the shell decreases with increasing working distance due to complete evaporation of the solvent, and the macromolecular chains aggregation to form the condense polymeric shell (Gao et al., 2016). For a working distance less than 10 cm, the residual solvent molecules swell the recovered polymeric particles, even if a strong electric field is applied. The control of the solvent system and operating parameters during the electrospraying process allows tailoring design, physico-chemical properties, and morphology of particles to respond to a specific end-use application.

1.2.3.3 Flow rate

The flow rate of the electrospray solution as it passes through the nozzle is also an essential factor in the formation of the Taylor cone. The optimization of the setting of this parameter depends on the intrinsic characteristics of the prepared solutions, i.e., (i) saturated vapor pressure of the solvent, (ii) and the electrical conductivity of the solutions. In most cases, there are usually a lower and an upper flow rate limits allowing a stable jet formation.

A Taylor cone is preferred for low flow rates since the uncharged liquid at the tip of the nozzle requires sufficient time to be polarized, and then polarized charges are generated on the droplet surface to promote Taylor cone formation. For higher flows, the reduction of the polarization time induces a continuous dripping of droplets due to gravity. Thus, in most cases, depending on the choice of matrix materials and solvent used, the flow rate values vary from several µL/min to 50 µL/min to obtain a stable conical jet. The use of a solvent with a high saturation vapor pressure requires a higher setting than other solvents to avoid clogging the nozzle when the solvent evaporates. On the other hand, a lower flow rate must be used for solutions prepared from solvents with a low saturated vapor pressure to ensure complete evaporation of the solvent during the solidification process.

The conductivity value of the solutions influences the droplet polarization time, and therefore the adjustment of an adequate flow rate. Indeed, the polarization time of the droplets is longer to obtain when using solutions with low conductivity, which requires working at low flow rates. The adjustment range is widened, and the values increase for solutions with higher conductivity. On the other hand, in this case, an excessively high flow rate causes an accumulation of charges to accumulate at the end of the nozzle, and the stable conical jet breaks and turns into a multiple jet mode due to the too strong Coulomb repulsions of the charged droplets. In addition, the mean diameter of electrosprayed particles increases with the increasing of flow rate, and related size distribution also broadens gradually.

In the case of coaxial electrodeposition, the flow rates of the internal and external liquids also affect the formation of the Taylor cone. In general, the Taylor cone is more easily obtained if the flow rate of the external liquid is higher than that of the internal (Jayasinghe, & Townsend-Nicholson, 2006). For example, Hwang et al. concluded that the PS/PCL microcapsules with an incomplete core-shell structure as well as irregular morphology were obtained when the flow rate of outer liquid was the same than the inner one. The increase of the flow rate ratio (outer/inner liquids) from 1:1 to 4:1 allowed to prepared complete core-shell structure with a smooth

morphology (Hwang, Jeong, & Cho, 2008). Otherwise, the conical jet is challenging to form, and an incomplete encapsulation of the system with an irregular morphology is obtained. Chen et al. also found that the working range of the voltage applied to the stable cone-jet mode can be extended by increasing the flow rate of the internal liquid and decreasing that of the external by considering it as a driving fluid (Chen et al., 2005).

1.2.3.4 Humidity, temperature, and atmospheric pressure

Also, the morphology of electrosprayed particles also depends on environmental parameters (humidity, temperature, and atmospheric pressure) (Case et al., 2004; Sill & von Recum, 2008; Wu, Kennedy, & Clark, 2009). In general, the increase in relative humidity (humid atmosphere) leads to an increase in the number, diameter, shape, and distribution of pores on the surface of particles. Besides, the boiling point of the solvent and its evaporation rate are also correlated with atmospheric pressure. The increase in atmospheric pressure leads to an increase in the boiling point of the solvent and a decrease in its evaporation rate. Therefore, electrosprayed particles with a smooth and non-porous structure can be obtained with increasing atmospheric pressure. On the contrary, with the decrease in atmospheric pressure, the morphology of atomized particles becomes irregular and porous.

1.2.4 The design of the structure and morphology of electrosprayed particles

The fission and solidification processes of electrosprayed droplets are also closely related to the physical and chemical properties of the working solutions as well as the related operating parameters. Therefore, the morphology, size, and size distribution of obtained particles from electrospraying are affected and determined by the properties of the working solution as well as operating parameters. Thus, understanding of the relationships among the solution properties, operating parameters and the structure, morphology of the electrosprayed makes it possible to obtain desired production from electrospraying process.

1.2.4.1 Droplets or fibers

Electrohydrodynamic methods are divided into two categories having the same processes and mechanisms but differ in the obtained morphologies (spherical and fibrous materials), i.e., electrospinning and electrospraying processes. The generation of materials with different shape mainly depends on the fission process of the charged

droplet, and more especially on the strength of the intermolecular interactions between macromolecular polymeric chains. Fiber shape is obtained with strong interactions since they stabilize the charged jet and match the Coulomb repulsions of the charged droplets. The polymeric solution is further stretched, and the solvent evaporation induces to the formation of ultrathin fibers (Costa, Bretas, & Gregorio, 2010). The formation of tiny particles is promoted by the presence of low interactions and strong Coulomb repulsions. Thus, the extent of intermolecular entanglement among polymeric chains in working solution is one of the main factors governing the resulted shape. Limited polymeric chain entanglements in the system represent a key parameter to achieve particle morphology by electrospraying according to Shenoy et al. (2005). The degree of entanglement per chain in the electrosprayed solution ($(n_e)_{sol}$) is obtained from Equation (1-4).

$$(n_e)_{sol} = \frac{\varphi M_w}{M_e} \qquad \text{Equation (1-4)}$$

Where, φ is the polymer volume fraction in the electrosprayed solution, M_w and M_e are the average molecular weight of polymer and entanglement molecular weight, respectively.

The number of entanglement per chain, ($(n_e)_{sol}$), and the critical chain overlap concentration, C_{ov}, corresponding to the crossover concentration between the dilute and the semi-dilute concentration regimes or the concentration inside the radius of gyration of every single macromolecular chain, influence the obtained morphology of the final material. Thus, for ($(n_e)_{sol}$) ~ 2.5 (1 entanglement per chain), or a polymer concentration less than $3C_{ov}$, the process leads to the formation of spherical particles. The increase of ($(n_e)_{sol}$) up to 3.5 or the use of a polymer concentration >$3C_{ov}$ allow having the entangled regime and therefore obtained in the first step a beaded-fiber structure, which evolves in fiber shape morphology. The entanglement is also related to the molecular weight of the polymer used (Zhou et al., 2016) (Figure 1-5). Thus, the use of PCL with a molecular weight between 10,000 and 45,000 g/mol and a concentration of 9 to 30% by weight leads to the formation of spherical particles. At higher molecular weights, fibrous morphology is preferred, and when it reaches 80,000 g/mol, even working at a relative low concentration, from 0.5% to 10% by weight, ultrafine fibers are also obtained.

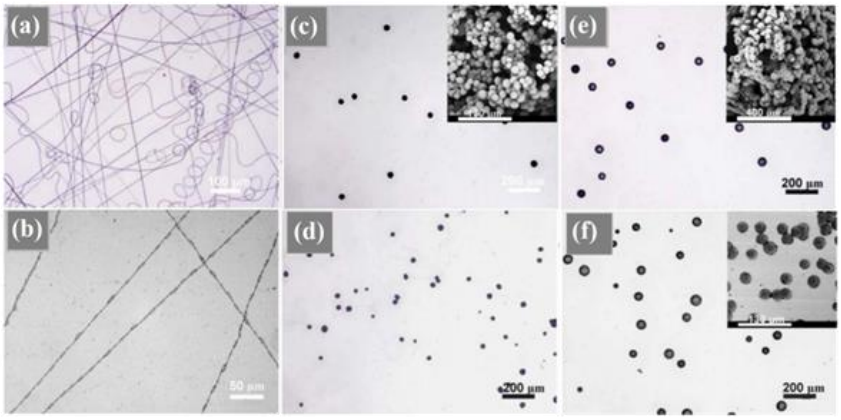

Figure 1-5 The effects of polymer molecular weight and solution concentration on the results of PCL electrospraying (a) smooth fibers from PCL with 80,000 g/mol, 10 wt.%; (b) beaded fibers from PCL with 80,000 g/mol, 0.5 wt.%; (c) particles from PCL with 45,000 g/mol, 9 wt.%; (d) particles from PCL with 45,000 g/mol, 11 wt.%; (e) particles with fibrils from PCL with 45,000 g/mol, 30 wt.%; (f) particles from PCL with 10,000 g/mol, 30 wt.% (Zhou et al., 2016).

Besides, the degree of entanglement of the polymer chains of the electrosprayed solution is also related to the nature of the solvents used. Thus, intermolecular tangles are of two kinds, i.e., (i) interactions between solvents and molecular solutes, and (ii) intermolecular tangles between macromolecular chains. The calculation of the parameter (D) is used to guide the approach, since a low value illustrates a good solubility of the polymer in the solvent and a low degree of entanglement among macromolecular chains, while the latter increases with the increase in D. Therefore, spherical particles may be obtained by selecting a polymer/solvent system with a low value of D, while matrix or fibrillar structures resulting from a higher entanglement and therefore a higher value of D or a partial solubility of the polymer in the system. According to Qin and Luo et al., with a fixed PCL concentration, the use of solvents such as 1-methyl-2-pyrrolidone, formic acid and N, N-dimethylformamide, in which the solubility of PCL is partial, results in smooth and uniform fibers (Luo, Stride, & Edirisinghe, 2012; Qin & Wu, 2012). On the other hand, the use of solvents that perfectly solubilize PCL such as toluene, chloroform, dichloromethane, and tetrahydrofuran leads to the formation of beaded structures or spherical particles.

1.2.4.2 Particles size and size distribution

Mean diameter of electrosprayed particles increases with increasing polymer concentration and/or polymer molecular weight, related to an increase in the solution viscosity, and a decrease in conductivity. It was also expected that at low polymer concentration, the changes in concentration have more variation in viscosity compared with conductivity. At high concentration, the viscoelastic forces in the droplets are opposed to those of

Coulomb repulsion to prevent droplet break-up, resulting in the formation of bigger particles. For example, the increase in PCL concentration from 0.5 to 6 (wt.%) induces an increase in particle size according to Xie, Marijnissen & Wang (2006). When PCL concentration increases further, to 9.6%, PCL particle size decreases as observed by Bock et al. (Figure 1-6) (2012). In their work, Ghanbar et al. studied the effect of the variation in the molecular weight of PCL (from 10,000 to 45,000 g/mol) at various concentrations in toluene (Ghanbar et al., 2013). They found that changes in formulation parameters leading to an increase in the viscosity of the solution also lead to an increase in size. Some researchers have also reported that working with very low polymer concentrations, weak viscosity makes the process unstable and therefore particle size increase. Besides, at higher concentration, the observed decrease in conductivity leads to an unstable cone jet and therefore an increase in size particle distribution. Besides, the increase in viscosity also results in a decrease in jet diameter (Jayasinghe, & Edirisinghe, 2002), which can be correlated with a lower mean droplet diameter during the rupture process according to Cloupeau et al. and Ganan-Calvo et al. (Cloupeau, 1994; Cloupeau, & Prunet-Foch, 1989; Gañán-Calvo et al., 2016; Gañán-Calvo, 1994).

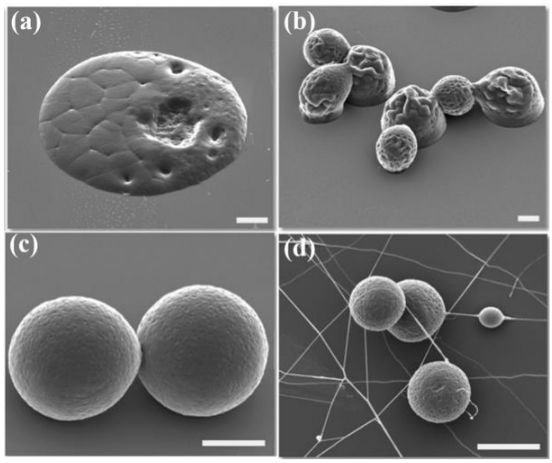

Figure 1-6 Scanning electron micrographs of dried PCL microparticles. PCL concentration in chloroform is: (a) 5%, (b) 7.4%, (c) 8.7%, (d) 9.6% (w/v). Electrospraying conditions are 26 G for needle gauge, 20–25 cm for tip-to-collector distance, 0.5 mL/h for flow rate, and 10 kV for voltage. The molecular weight of PCL on average is 130 kg/mol with a polydispersity index of 1.45. Scale bar is 10 μm (Bock et al., 2012).

The surface tension of the electrospray solution influences the breakage of the charged droplets and thus the final particle size. Indeed, the particle size increases with decreasing surface tension (Bock et al., 2011). According to Midhun et al., the use of higher concentrations of PCL produces larger particles due to increased surface tension (Midhun et al., 2011). However, during the electrospraying process, due to the viscosity changes and evaporation of the solvent, it is difficult to determine the value of the variation of the surface tension at equilibrium at the time

scale of the phenomenon. Therefore, the relationship between particle size and surface tension is not always correlated or interpreted as such.

During the solidification of the droplets, the size is influenced by the polymer–polymer interactions that take place during the evaporation of the solvent to obtain solid particles. Thus, a high vapor saturation pressure value of the solvent induces its evaporation when passing from the nozzle to the collector. For low values, the evaporation rate is low, and the residual solvent limits the condensation of the macromolecular chains and causes the particles to aggregate on the collector. Besides, the ability of the solvent to evaporate during the process is also related to the concentration of the solutions. An increase in the latter due to a higher rate of entanglement allows complete evaporation during flight time and promotes the aggregation of macromolecular chains.

The use of the electrospraying process allows obtaining mono-modal and narrow particle size distribution, which promotes a controlled release behavior of the drug. Its release rate, as well the shell erosion phenomena, is enhanced for particles with a low mean diameter and a narrow size distribution. These kinds of particles are mainly used in biomedical engineering and medical treatment. Nevertheless, even if the cone-jet mode is a prerequisite to obtain a monodispersed size distribution of electrosprayed particles, the ejection of offspring secondary and satellite droplets from primary split ones can lead to an inhomogeneous particle size distribution. The case happens for high electrical solution conductivity with a low viscosity value (Bock, Dargaville, & Woodruff, 2012). Different evaporation process of electrosprayed droplets also results in the different size distribution of final particles. Thus, under lower vapor pressure and viscosity, the quicker evaporation of the solvent and the instability of droplets shape lead to the deformation of electrosprayed droplets during the solidification process, which introduces a non-homogeneous particle size distribution. The choice of the solvent system, with medium vapor pressure and medium viscosity, limits the droplet deformation and reduces the evaporation rate until obtained a narrow particle size. Besides, higher vapor pressure and viscosity lead to a change in the obtained morphology, i.e., beaded fibers when the concentration of the solution or the molecular weight of the polymer used is too high, and particle agglomeration when the evaporation rate is too low are commonly reported. Meanwhile, the use of a co-solvent in the formulation leads to the same phenomena since it induces some modification during the evaporation step (Chul, & Jonghwi, 2009; Xie et al., 2006). Therefore, the monodispersed particle size distribution is achieved if the solution has low electrical conductivity, moderate boiling point, and medium viscosity values. Also, when the mean diameter of electrosprayed particles exceeds 100 μm, it is difficult to recover these particles.

Thus, due to the decreasing of the specific surface area resulted from the increase of mean diameter, the evaporation of the solvent in electrosprayed droplets becomes slow. The presence of residual solvent results in the aggregation and deformation of electrosprayed droplets or polymeric films.

In addition, with the decreasing of flow rate, the mean diameter of electrosprayed particles decreases, and mono-dispersed size distribution can also be obtained. For the effects of working distance on the size and size distribution of electrosprayed particles, too short working distance will result a strong and unstable electrical field and less flight time for the evaporation of solvent. Therefore, poly-dispersed size distribution can be obtained from too short working distance. However, too long working distance will lead to a reduction of electrical field and a long flight time for electrosprayed particles from nozzle to collector. The former will lead to an increasing of mean diameter of electrosprayed particles, the later will cause a reduction of the number or mass of obtained electrosprayed particles. Therefore, a moderate working distance is better for prepare electrosprayed particles with desired mean diameter as well as mono-dispersed size distribution. Furthermore, in the cone-jet mode, the mean diameter of electrosprayed particles decreases with the increasing of applied voltage (Zhang, Campagne, & Salaün, 2019b).

1.2.4.3 Morphology

The electrospraying process makes it possible to obtain various morphologies depending on the properties of the solutions used and the settings of the equipment. Morphological control is an important criterion to consider given their specific properties. These morphologies, whether porous, hollow, pleated, cup-shaped, semi-spherical, oval, or polygonal, are mainly related to the mechanisms of solidification of droplets, and in particular to the phenomena governing the change of state or the evaporation of solvents used according to environmental conditions. The transition from a liquid phase to a solid polymer phase is related to the vitrification of a rubber phase to an amorphous or glassy state of the polymer when the solvent evaporates. Bodnár et al. identified that particle morphology varied according to the dynamic regime of the fluid at which polymer vitrification occurs, and for reduced polymer concentrations, i.e., (i) incomplete jet failure, (ii) complete jet failure without Coulomb instabilities, (iii) Coulomb instabilities without progeny droplets emission, and (iv) Coulomb instability of main droplets with progeny droplets emission (coulomb fission) (Bodnár, Grifoll, & Rosell-Llompart, 2018). The first regime leads to the production of main particles surrounded by thin nanofibers, which have a secondary bead, the

second to globular particles, the third to particles with one or two different filaments, or having elongated shapes, and the last to particle residues from droplets of progeny from Coulomb droplet fissions. The molecular weight of the polymer used and its concentration favors a particular structure. Thus, low concentrations and/or low molecular weight of the polymer lead to the first morphology. The increase in molecular weights and concentrations allows globular particles to be obtained first, then in a second phase at pearled structures. A relatively high concentration of polymer correlated with higher molecular weights allows maintaining a sufficient macromolecular chain entanglement rate to lead to a spherical morphology by promoting its precipitation during the evaporation of the solvent.

The characteristics of the solvent, such as its saturation vapor pressure or evaporation rate, also influence morphologies. Thus, the use of a low-volatility solvent produces spherical particles with a smooth surface, but which tend to deform when they reach the collection in semi-spherical particles. On the contrary, a solution containing a more volatile solvent leads to the creation of hollow, porous and irregular particles, linked to an excessive evaporation rate and the precipitation of macromolecular chains (Gao et al., 2015). Also, the number and size of pores on the surface of PCL microspheres also decrease with the increase in PCL concentration from 2 to 4% by weight.

This porosity can be also controlled by adding a non-solvent to the initial solution (Gao et al., 2014). Due to differences in solubility and compatibility between two solvents and the polymer, the polymer tends to diffuse from the low-affinity solvent to the one where it is most soluble, leading to phase separation. Thus, concerning differences in evaporation rate, the polymer-rich phase allows the formation of matrix particles, and the poor one to more porous structures. This non-solvent can also be used in a bath to collect particles and leads to porous and non-homogeneous structures (Gao et al., 2015; Wu, & Clark, 2007). Due to the concentration gradient between the droplets and the collection medium, the solvent present in the electrosprayed droplets tends to diffuse into the bath, causing phase separation and solidification of the particles. Also, with the extraction of the solvent and the solidification of the droplets in the bath, part of the non-solvent is also encapsulated in a polymer matrix. After drying, the non-solvent evaporates to form pores. Besides, when different non-solvents with different physico-chemical properties (surface tension, viscosity, and vapor pressure) are used as the collection medium, the morphology of the collected particles is different governed by droplet deformation, their solidification, and the solvent diffusion (Gao et al., 2015).

For example, Gao et al. (2015) have observed that PCL particles with ellipsoidal macroporous (methanol), continuous and dense pores (ethanol), flower-shaped surface (propanediol-1,2), uniform spherical pores (tetraethyl orthosilicate) and pod-shaped (n-butanol) can be produced in sequence when these different non-solvents are used as collection medium (Figure 1-7). Also, as the surface tension of the collection liquid increases and the evaporation rate decreases, the shape of the droplets sprayed in the bath changes from spherical to flat.

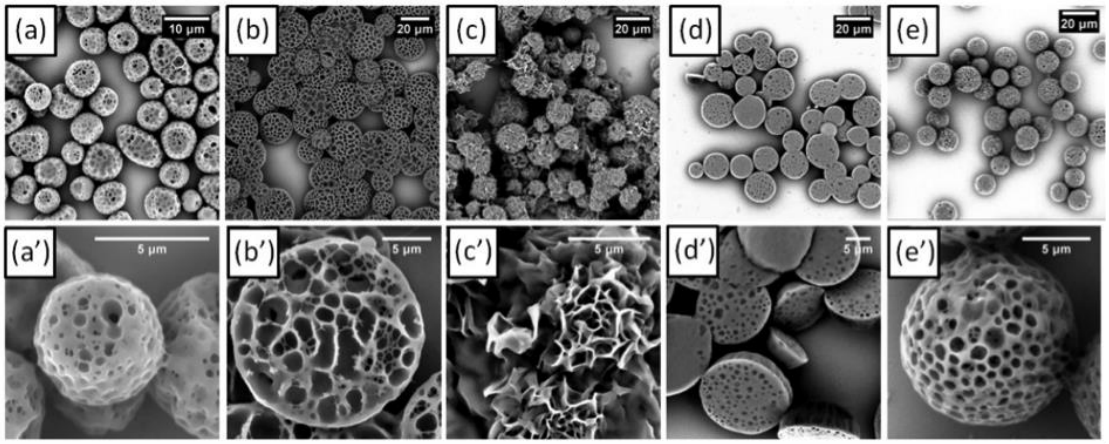

Figure 1-7 SEM images of PCL-dichloromethane (DCM) microparticles (MPs) collected in the different organic solvents (non-solvents): (a) methanol; (b) ethanol; (c) 1,2-propanediol; (d) n-butanol; (e) tetraethyl orthosilicate. (a'–e') High-magnification images showing the surface detail of the same porous MPs from (a–e), respectively (Gao et al., 2015).

Besides, PCL thin films with different morphologies and textures are also obtained from electrospray coating, mainly when non-solvent systems were used to dissolve PCL (Boda, Li, & Xie, 2018; Bodnár et al., 2018). Thus, the use of 2-ethoxyethyl acetate (2EEA), a nonsolvent at room temperature, and which partially solubilizes PCL at 30 °C lead to the obtaining of electrospun fibers with electrosprayed relics (PCL thin films with texture) (Luo et al., 2012).

Bock et al. characterized the particle morphologies prepared by different electrosprayed solutions of PCL in chloroform (Bock et al., 2011). Depending on the polymer concentration, microsphere or flattened particles were obtained in the case of higher and lower polymer concentration, respectively. The polymer concentration affects the solvent evaporation rate and chain polymer entanglement during the droplet flying process. Thus, a low polymer concentration leads to incomplete solvent evaporation, and recovered particles are still wet, or the PCL macromolecular chains are partially dissolved at the collector surface. The drying stage induces the formation of heterogeneous, semisolid, and flattened particles. They also denoted that this morphology was a consequence of fewer entanglement possibilities for polymer chains in the concentration range from 5 to 7.5 wt.%.

1.2.4.4 Core-shell structures

During the electrospraying process, the core-shell structure of electrosprayed microcapsules can be designed and controlled via using different electrosprayed nozzles with different geometries (Figure 1-8) (Chen et al., 2008; Kim, & Kim, 2010, 2011; Labbaf et al., 2014). Poly-nuclear microcapsules can be fabricated via using single nozzle. And the distribution of active substance in shell matrix mainly depends on the compatibility among solvent, active substance and shell material in electrospraying solution. Good compatibility among solvent, active substance and shell matrix will lead to a random distribution of active substance in shell matrix. On the contrary, if the compatibility between shell matrix and solvent is better than the compatibility between solvent and active substance, active substance will tend to locate in the center of shell matrix (Valo et al., 2009). When coaxial nozzle was applied in electrospraying, microcapsules with core-shell structure can be obtained. Meanwhile, according to the differences in the number of coaxial capillary, yolk-like, double-layered shell and triple-layered shell microcapsules can be prepared respectively. In addition, Lei et al also applied parallel-capillary nozzle, which consists of some parallel inner capillaries and an outer capillary, to prepare a single microcapsule with multiple active substances embedded. They achieved that each component in microcapsule is inhibited into individual compartments free of contact with others.

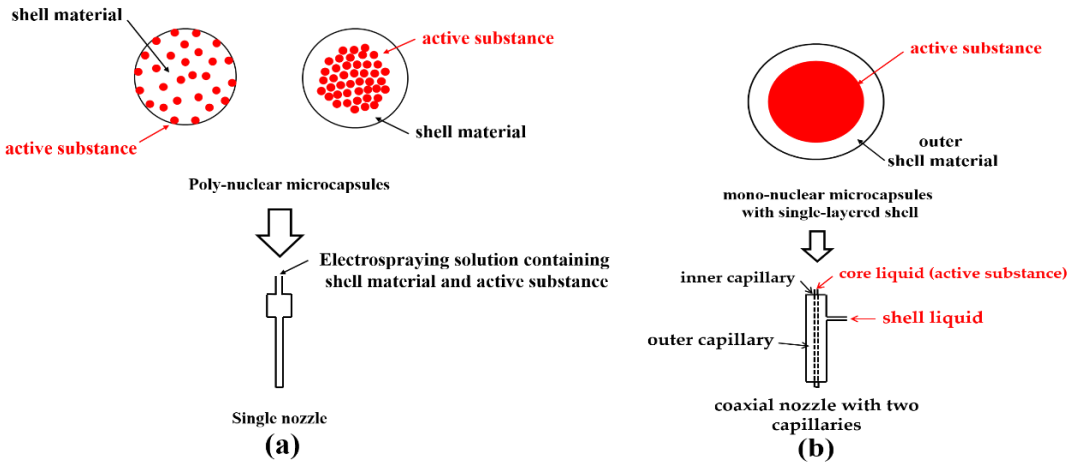

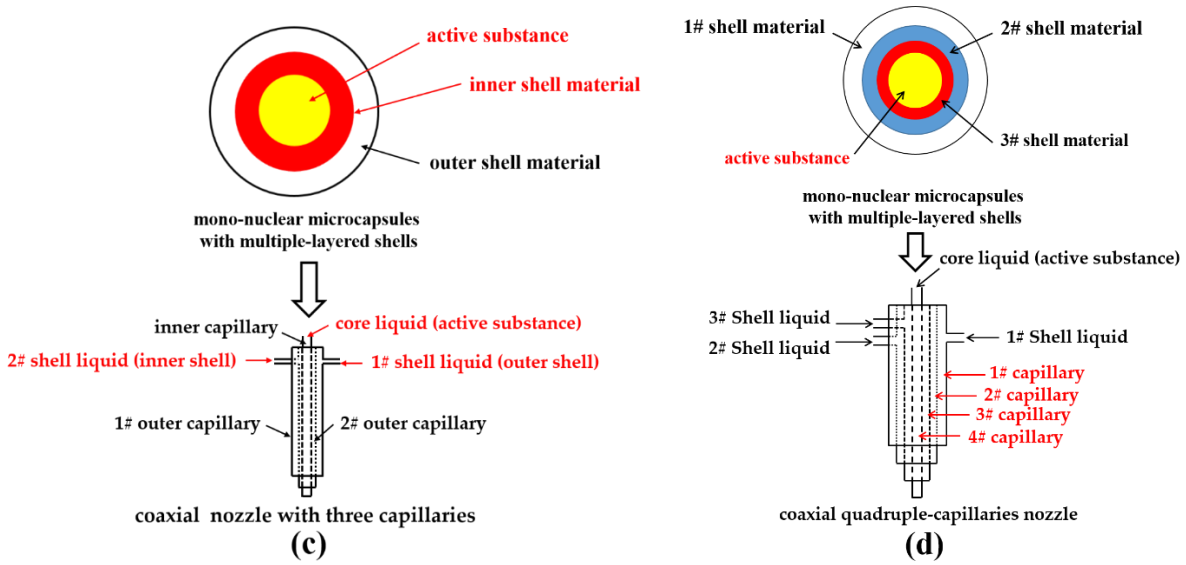

Figure 1-8 Fabricating different core-shell structures from different nozzle geometries.

1.2.5 The electrospraying apparatus

In general, the setup of electrospraying mainly composes by syringe, syringe pump, nozzle, high-voltage generator, and collector (Figure 1-9 a). In order to facilitate observation and analysis, light source and high-resolution camera connected with a computer are also often used in the process of electrospraying (Zhang et al., 2012). At first, electrospraying solution is added into a syringe and further transported to the nozzle under an adjustable flow rate via syringe pump. The nozzle is linked with one end of the high-voltage generator (mostly positive), and the other end of the high-voltage generator is connected to the collector (often grounded or more rarely negatively charged). The distance between the tip of the nozzle and collector usually range from a few centimeters to several tens of centimeters. Due to the strong electric field between nozzle and collector and the Coulomb repulsions, the electrospraying solution will be stretched and further dispersed into smaller droplets, which are ejected from the tip of Taylor cone. During the flight of droplets to the collector, solvents in these droplets will evaporate, and solid particles can be obtained in collector finally. Further, if needed, these particles could be placed into a vacuum oven to remove the residual solvent. Sometimes, in order to further stabilize the process of electrospraying and cone-jet, a ring-shaped electrode is placed between the nozzle and the collector (Ciach, 2006; Wu, Kennedy, & Clark, 2009; Wu et al., 2009). The strength of electric field between the nozzle and ring-shaped electrode and the strength of electric field between ring-shaped and collector can be effectively

adjusted via controlling the distance among them. Meanwhile, the size and distribution of electrosprayed particles will change obviously with the changing of the electric field among nozzle, ring-shaped electrode, and collector.

With increasing demands for diversified structures of polymeric particles in the biomedical field, there are some changes and innovations in the setup of electrospraying to prepare polymeric particles with novel structure and morphology for satisfying these demands. Major innovations and changes focused on the structure of nozzle and collection method. According to the position of the capillary in the nozzle, the nozzles used in electrospraying divide into two categories, coaxial-capillary nozzle, and parallel-capillary nozzle. Common coaxial-capillary nozzles include two or three capillaries coaxial nozzle (Figure 1-9 b, c). Single-shell capsules and double-shell capsules can be fabricated by using these nozzles in electrospraying. The core material is added into the inner capillary and shell material is added into the outer capillary. A separate syringe pump controls the flow rate of liquid in each capillary. As for parallel-capillary nozzle, it consists of some parallel inner capillaries and an outer capillary (Figure 1-9 d). Jiang et al. first time adopted these nozzles to prepare a single microcapsule with multiple active substances embedded (Chen et al., 2008). They found that each component in microcapsule is inhibited into individual compartments free of contact with others. If two active substances in microcapsules need to be mixed, the nozzle with static micromixer (Figure 1-9 e) can be used during electrospraying. Wu et al. have used this nozzle to fabricate QD605/Cy5-G3139-loaded lipoplexes with high compatibility, high encapsulation efficiency, highly uniform and fine size (Wu et al., 2012). Besides, in order to improve the throughputs and productivity of electrospraying, some special nozzles (Figure 1-9 f, g) are also used in electrospraying to achieve the stable multi-jet (Almería et al., 2010; Kim, & Kim, 2010, 2011). Using grooved inner nozzle can not only strengthen the electric field at the groove but also promote the formation of Taylor cone at each groove. Therefore, the stable multi-jet that ensures the desired size and uniform dispersion of electrosprayed particles can be successfully achieved, and the throughputs, as well as the productivity of electrospraying, also enhance significantly. Meanwhile, the interactions between inner and outer liquids and its interference in the formation of cone-jet can be optimized and minimized when the inner capillary is extended some distance out from the outer capillary. Similar results are also obtained using multiplexed electrospray device with several electrospraying sources operating in parallel and an extractor. The extractor not only minimizes interference between sources but also localizes the electric field.

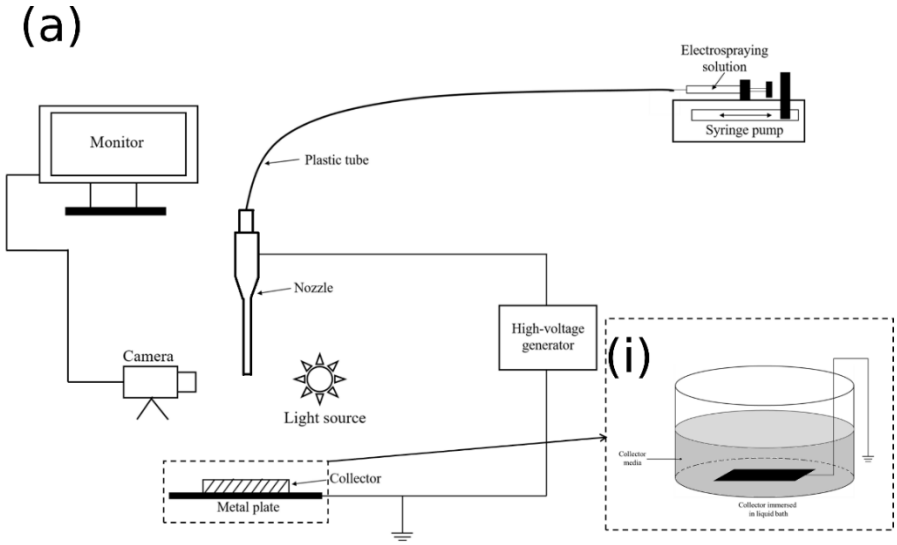
(a)
Electrospraying solution
Syringe pump
Monitor
Plastic tube
Nozzle
High-voltage generator
Camera
Light source
(i)
Collector media
Collector immersed in liquid bath
Collector
Metal plate

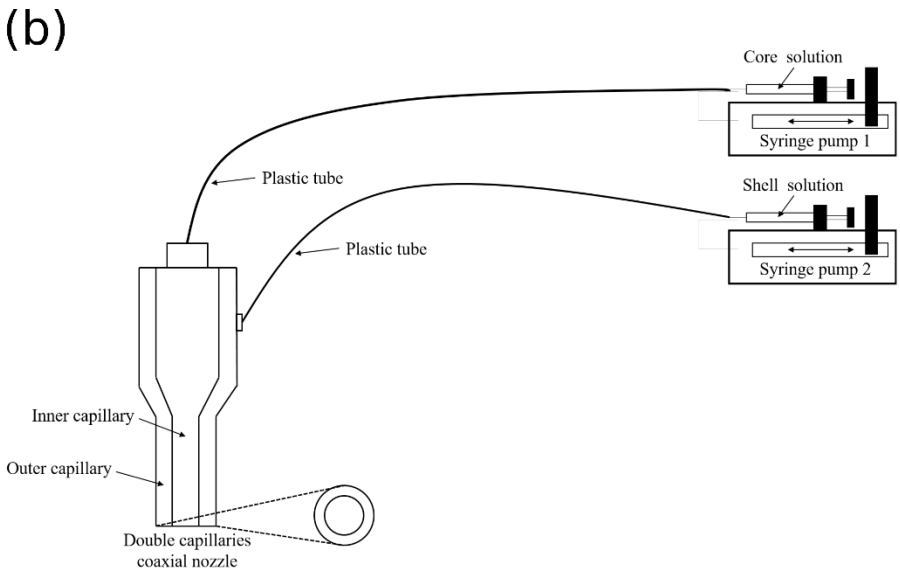
(b)
Core solution
Syringe pump 1
Plastic tube
Shell solution
Plastic tube
Syringe pump 2
Inner capillary
Outer capillary
Double capillaries coaxial nozzle

(c)

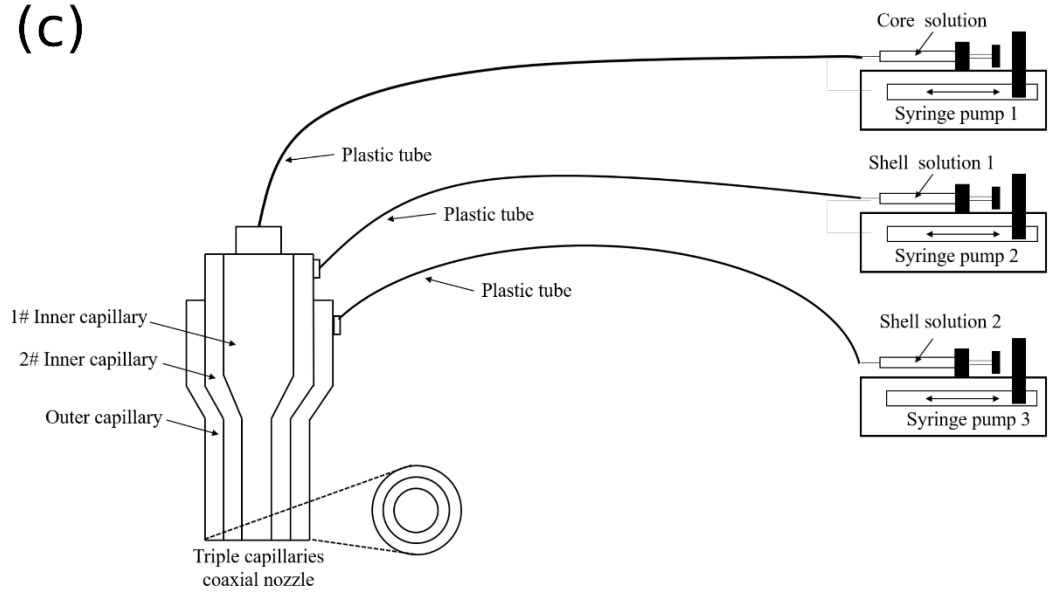
Core solution
Syringe pump 1
Plastic tube
Shell solution 1
Plastic tube
Syringe pump 2
Plastic tube
Shell solution 2
1# Inner capillary
2# Inner capillary
Outer capillary
Syringe pump 3
Triple capillaries
coaxial nozzle

(d)

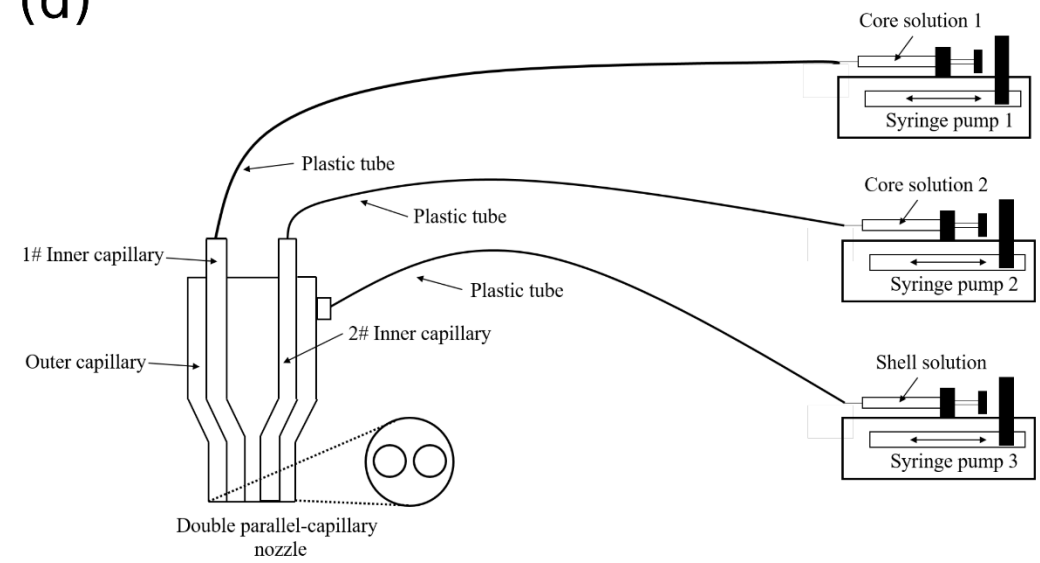
Core solution 1
Syringe pump 1
Plastic tube
Plastic tube
Core solution 2
Syringe pump 2
1# Inner capillary
Plastic tube
2# Inner capillary
Outer capillary
Shell solution
Syringe pump 3
Double parallel-capillary
nozzle

(e)

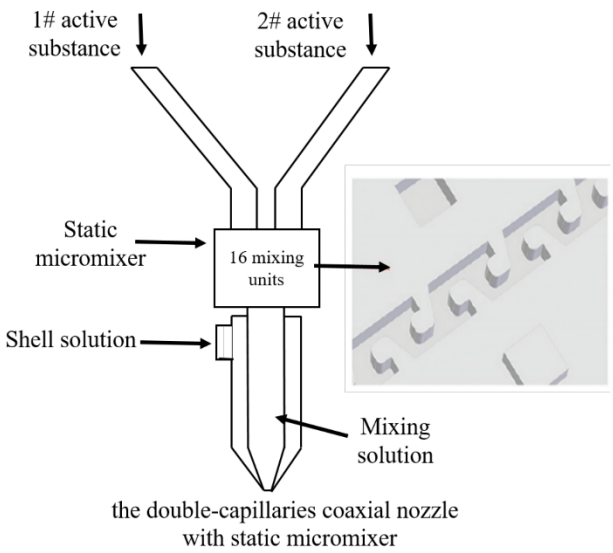

the double-capillaries coaxial nozzle with static micromixer

(f)

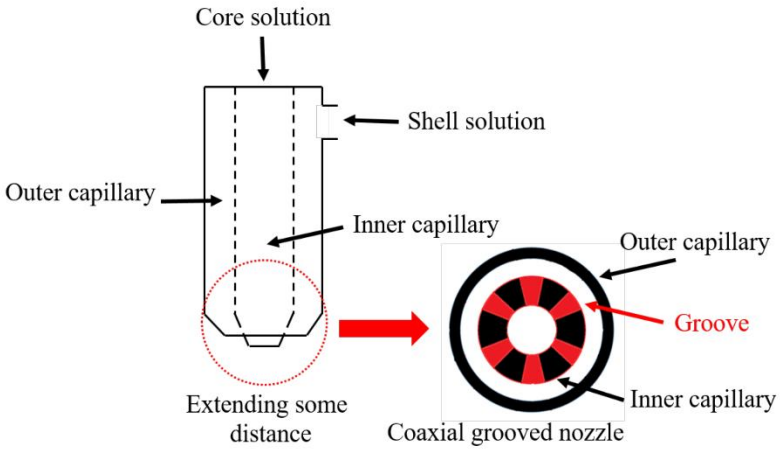

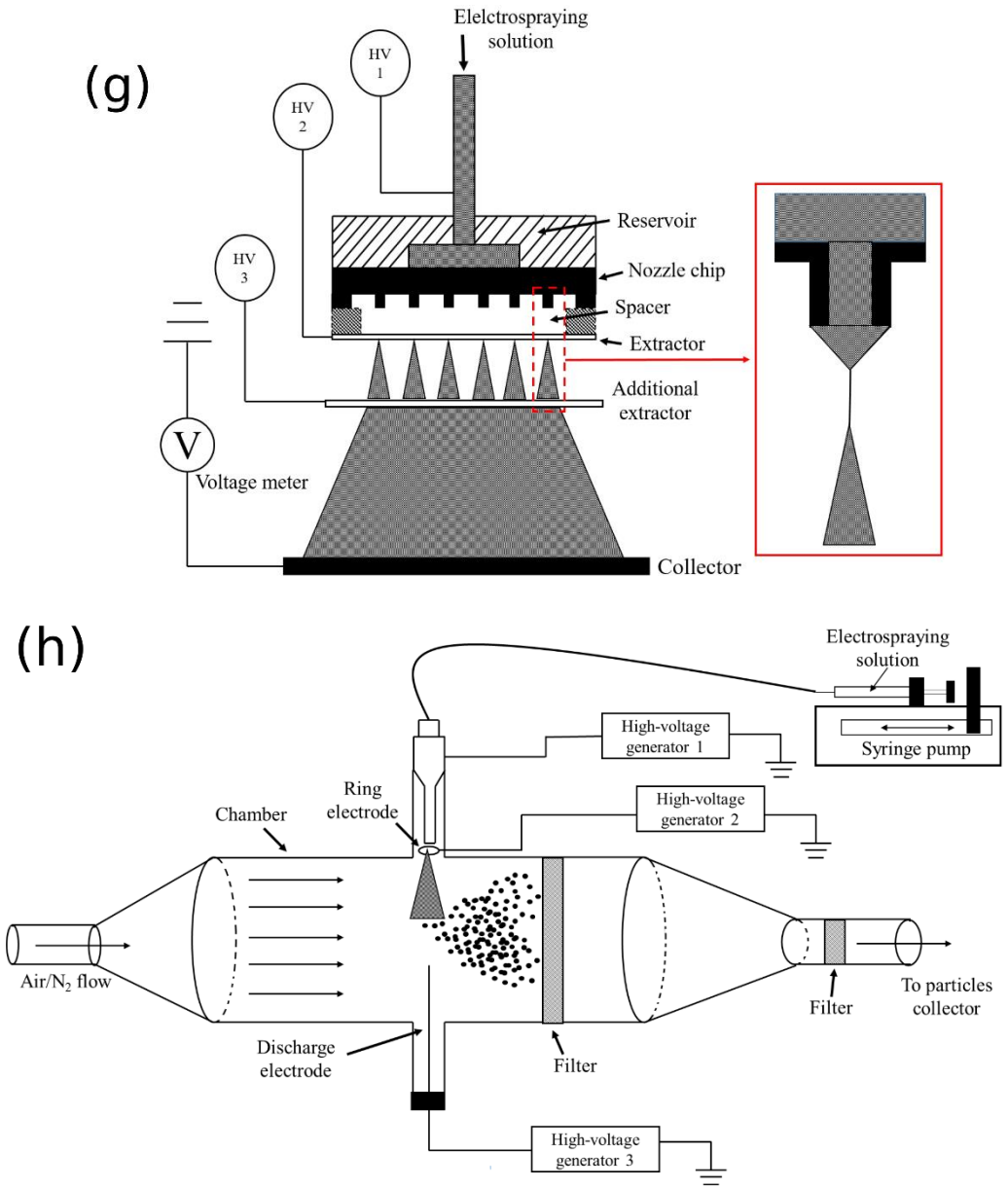

Figure 1-9 Common examples of electrospraying apparatus, (a) single-capillary electrospraying, (b) double-capillaries coaxial nozzle, (c) triple-capillaries coaxial nozzle, (d) double parallel-capillaries coaxial nozzle, (e) double parallel-capillaries coaxial nozzle with static micromixer, (f) double-capillaries coaxial nozzle with grooved structure, (g) multiplexed electrospraying setup with several electrospray sources operating in parallel and an extractor, (h) electrospraying via a nozzle-ring setup inside a glass chamber under air flow, and (i) electrospraying device with liquid bath collector (modified from (Almería et al., 2010; Bock et al., 2011; Chen et al., 2008; Ding, Lee, & Wang, 2005; Kim, & Kim, 2011; Lee, Bai, & Chen, 2011; Moghaddam, Mortazavi, & Khayamian, 2015; Park, Kim, & Kim, 2011; Wu et al., 2012)).

A grounded metal plate (usually an aluminum foil) is mainly used to collect electrosprayed particles, and sometimes a glass slide is also placed on the metal plate. Although these collection methods are

convenient and straightforward, there are still some drawbacks. For example, the solvent with a high boiling point is challenging to be removed out when droplets reach the surface of the collector. These particles with residual solvents trace tend to aggregate together to form large droplets. Meanwhile, the collection efficiency of metal plate or glass slide is relatively low due to the airflow and long flight distance. The majority of the electrosprayed particles is carried away by the airflow and cannot reach the surface of the collector, then finally deposited on the other place of working cupboard. In order to prevent the aggregation among electrosprayed particles and improve the collection efficiency, a grounded bath containing liquid media (Figure 1-9 i) and an enclosed chamber with air/nitrogen flow and filters (Figure 1-9 h) are applied to collect electrosprayed particles. The selection of collection liquid media mainly depends on its chemical interactions with the particles (including core and shell material), compatibility to solvent systems in electrospraying solution, and surface tension (Bock, Dargaville, & Woodruff, 2012).

Thus, this system requires a poor chemical affinity between the liquid media to the polymeric shell and core substance, to achieve complete entrapment of it under microsphere or microcapsule form. The compatibility between collection media and solvent system in electrospraying solutions need to be higher than that between polymeric matrix and solvent system. The residual solvent in particles diffuses into collection media and is effectively removed from particles due to the existence of a concentration gradient. The aggregation of electrosprayed particles can be further prevented with the use of a low surface tension collection solution. The main disadvantages of this collection method are that (1) the drug or active substance absorbed on the surface of particles may diffuse into the collection media, and (2) these collected particles tend to form a film at the surface, which hampers their further dispersion. In addition, some researchers also put some aqueous solution containing a polyelectrolyte into the bath (Fukui et al., 2010; Yunoki et al., 2014). The use of air/nitrogen flow with vacuum aspiration as well as filters in a chamber allows to increase the collection yield and to obtain particles with a smooth surface state and low mean diameter, due to sufficient evaporation time of solvent (Ding et al., 2005). In some cases, ring-shaped grounded copper wire was also applied to collect the electrosprayed particles, having a uniform size and a smooth surface. This method has a higher collection efficiency compared with other collection methods (Zhou et al., 2016).

1.2.6 The applications of electrospraying

Electrospraying (electrohydrodynamic spraying) as a method of liquid atomization by means of electrical forces, its advantages include that (1) micro- or nano- scale particles (or droplets) with mono-dispersed size distribution can be fabricated successfully under cone-jet mode (2) the structure and morphology of electrosprayed particles (or droplets) can be designed and controlled via adjusting the physico-chemical properties of electrospraying solution as well as operating parameters (3) particles (or droplets) with multi-layered shells or multi-component cores can be designed via using different electrospraying nozzles (different geometries). Due to its properties and advantages, electrospraying is considered as an effective route for achieving the production of micro- or nano thin film, the design of self-assembled micro- or nano- structures, the generation of in micro- or nano- particles, the formation of micro- or nano- capsules and the functional coating or printing.

1.2.6.1 Micro- and nano-thin-film deposition

Recently, many researchers have tested the electrospraying deposition technique of liquid-phase materials on various substrates. Electrospraying deposition (Figure 1-10 a), is a process in which droplets produced by electrospraying from a solution or suspension of a material to be deposited are targeted to a substrate to form a tight surface layer. A solid layer is obtained after solvent evaporation. Evaporation can be sped-up by heating the substrate. To improve mechanical properties, the layer may be sintered at higher temperatures, if applicable. Usually, the material to be deposited is sprayed directly onto the substrate, but the layer can also be formed from a precursor. The precursor is a compound which is decomposed at high temperature or converted to another substance in chemical reactions with other compound sprayed simultaneously or delivered in the gaseous phase. The reactions usually take place on the substrate, and a new product is obtained (Figure 1-10 b). Furthermore, with the increasing of deposition rate of electrospraying solution, the thickness of obtained films also increases gradually.

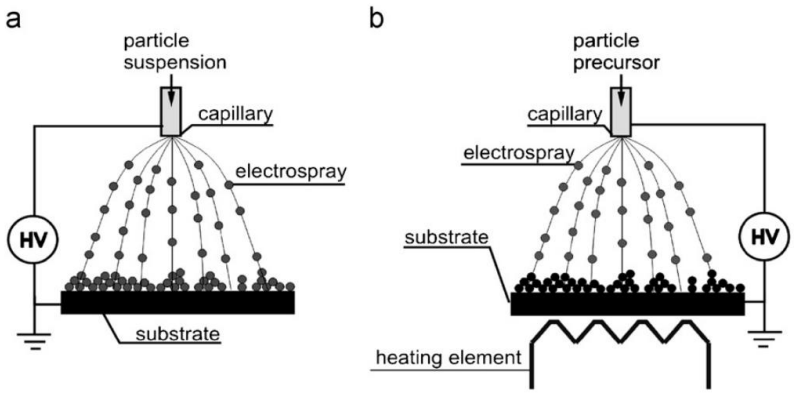

Figure 1-10 Scheme of electrospraying deposition of micro- and nano- thin film: (a) from a solution or suspension of particles to be deposited and (b) from a precursor thermally decomposed on the substrate (A. Jaworek, 2007).

In general, electrospraying was used to produce thin layers of radioactive materials, such as α- or β-particle sources or neutron emitters (e.g. obtained from U233, Pu238, Am241 or Cm242 nitrates) or targets prepared for activation in particle accelerators or nuclear reactors (Bruninx, & Rudstam, 1961; Michelson, & Richardson, 1963; Shorey, & Michelson, 1970). Nowadays, CdS, CdSe, SnO_2, or TiO_2 are deposited on substrate for fabricating solar cells thin films (Chandrasekhar, & Choy, 2001; Chen et al., 1996); fuel cells thin films are obtained from depositing La(Sr)MnO_3 on Zr substrate, YO_x on Ni-ZrO_2, and ZrO_2:Y_2O_3, Gd_xCe_1-xO_2, La_1-xSr_xCo1-yFe_yO_3, or ZrO_2:Y_2O_3 deposited on $Ni_{72}Cr_{16}Fe_8$ substrate; thin cathode layers of lithium batteries are made of $LiMn_2O_4$, $LiNiO_2$, $LiCoO_2$, $LiCo_xMn_2$-xO_4, $LiCo_{0.5}Ni_{0.5}O_2$, $LiAl_{0.25}Ni_{0.75}O_2$, and V_2O_5; anodes made of SnO_2; and some metal-oxide layers used as dielectric for micro- and nano- electronic devices are prepared from electrospraying deposition (Jaworek, & Sobczyk, 2008).

1.2.6.2 Micro- and nano- particles production

Fine particles of size smaller than 10 μm are, for example, applied for ceramic coatings, paints, or emulsion production, as powder in the cosmetic or pharmaceutical industries, or as toner in electro reprographic systems. Nanoparticles may also be deposited to create thin solid films. Electrospraying was also successfully tested as a tool for fine particle production (Deotare, & Kameoka, 2006; Lenggoro et al., 2000; Lenggoro et al., 2002). A diagram of the steps involved in micro- and nano- particles production from electrospraying is shown in Figure 1-11. The solvent from the electrosprayed droplets evaporates, and the remaining solid material forms a fine powder. The particles are produced from a solution or suspension of a solid material. For the solution-based

droplets, the remaining substance crystallizes forming solid particles. When a suspension is used for powder production, the nanosized particles suspended in the solvent form a tight cluster after the droplets dry. The size of such particles can be controlled by changing the concentration of the dissolved or suspended substance. Electrospraying allows the generation of particles of small size, down to 1-10 nm, and of high mono-dispersed size distribution (Chen, Pui, & Kaufman, 1995; Dudout, Marijnissen, & Scarlett, 1999). The common materials (precursor), solvent, obtained particles (droplets) size, flow rate used as well as the size of capillary for preparing particles from electrospraying are also summarized by Jaworek et al (Jaworek, & Sobczyk, 2008).

In general, fine particles with mono-dispersed size distribution can be obtained under cone-jet mode. The formation of cone-jet mode is achieved by special applied voltage range, special flow rate range and special solution properties (mainly including surface tension, electrical conductivity and viscosity). Any change in these operating parameters as well as solution properties will result in a change of jet mode from cone-jet mode to other unstable modes. Correspondingly, the mean diameter and size distribution of the droplets and particles can also undergo unacceptable change. The size of the particles (or droplets) can be controlled by changing operating parameters or solution properties. For example, the size of final production decreases with the increasing of applied voltage, and increases with the increasing of flow rate.

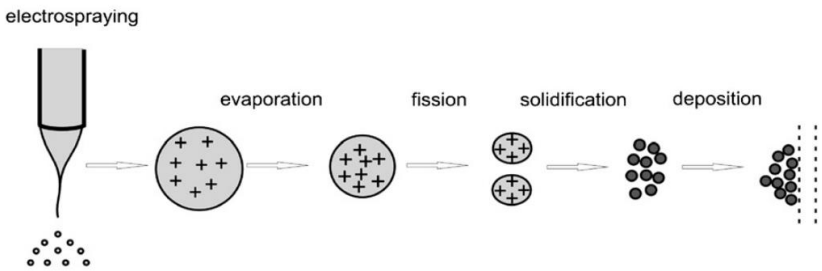

Figure 1-11 Steps of micro- and nano- particles production via electrospraying (Anatol Jaworek, 2008).

1.2.6.3 Electro-microencapsulation

Encapsulation is a process for capturing solid particles, liquid droplets, or a gaseous bubble as a core material in a solid or liquid envelope (shell) made of another material. Encapsulation can be regarded as the conversion of liquid phase to powder particles having the physical and chemical properties of the shell for easier transport and processing of the core material. Under certain conditions (heating, diffusion, or shell dissolution), the core material can be released from the shell.

Electrospraying method has been recognized as offering more advantages and potential for producing

microcapsules compared to other microencapsulation processes. Firstly, electrospraying as an one-step electrohydrodynamic atomization technology is a green and high-efficiency method allowing the formation of uniform-sized particles, with inexpensive equipment, simple operation and carrying out at atmospheric conditions. Furthermore, the rate of the particle production is mainly governed by adjusting voltage, working distance and flow rate. Secondly, the electrospraying method does not require the use of surfactants or toxic chemical additives, and the volume of organic solvent is limited. Furthermore, the optimization of the physico-chemical properties of the solution and the associated operating parameters make it possible to design the desired structure and/or morphologies and to obtain a narrow and mono-dispersed particle size distribution. The desired morphology also depends on the choice of nozzle geometry. The single nozzle is mainly used to produce core-shell microcapsules and polynuclear microcapsules. The coaxial double and tri-capillary nozzle is used to manufacture yolk-like and double-layered shell microcapsules for improving the encapsulation efficiency of PCMs as well as their durability and stability. In addition, when targeted textiles were placed directly on the collector, the functional coating of textiles can also be finished during the electro-microencapsulation process.

There are several methods or devices to achieve the microencapsulation process based on electrohydrodynamic atomization (Figure 1-12). The first one is the impacting of two oppositely charged droplets (Figure 1-12 a) (Langer, & Yamate, 1969). Core liquid and shell liquid are emitted from two separated capillary nozzles maintained at opposite potentials, one of the capillaries at positive, and the other at negative. After the break-up process of charged droplets, these fine droplets with opposite charges will collide together during their flight process from nozzle to collector due to Coulomb attraction, forming a capsule via submerging the droplet of higher surface tension within that of smaller surface tension. The second one is the evaporation of electrosprayed colloidal suspension (Figure 1-12 b) (Ding et al., 2005; Xie, Lim, et al., 2006; Xie, Marijnissen, & Wang, 2006). The suspension consisted of core material, shell matrix and solvent is electrosprayed and next the shell matrix is solidified by solvent evaporation for achieving the encapsulation of core materials. The surplus solvent of the solution evaporates, forming a hardened envelope. Electro-encapsulation via spraying of colloidal suspension requires low concentration of the active substance in order to generate droplets with only one active substance inside. The third one is the gelatinization of electrosprayed colloidal suspension (Figure 1-12 c) (Sato, Kato, & Saito, 1996). A polyanionic or polycationic aqueous solution blended with core material is electrosprayed into a bath with an aqueous solution containing a polyelectrolyte with the opposite charge. The formation of wall

materials is achieved by the electrostatic interaction between polyelectrolyte with the opposite charges. The forth one is preparation microcapsules with core-shell structure via coaxial nozzle electrospraying (Figure 1-12 d) (Marín et al., 2007). The process is a simultaneous spraying of two different liquids from two coaxial capillaries. In this case, the capillaries are at the same potential. The core liquid flows from the central capillary, and the shell liquid flows through the annular nozzle between the capillaries. Coaxial electrospraying allows the formation of microcapsules with high encapsulation efficiency as well as high loading content of core materials. Meanwhile, core-shell structure (Figure 1-12 e) is easier to obtain when core liquid has higher electrical conductivity than shell liquid; the surface tension of core liquid is higher than that of shell liquid; and the viscosity of shell liquid is higher than that of core liquid.

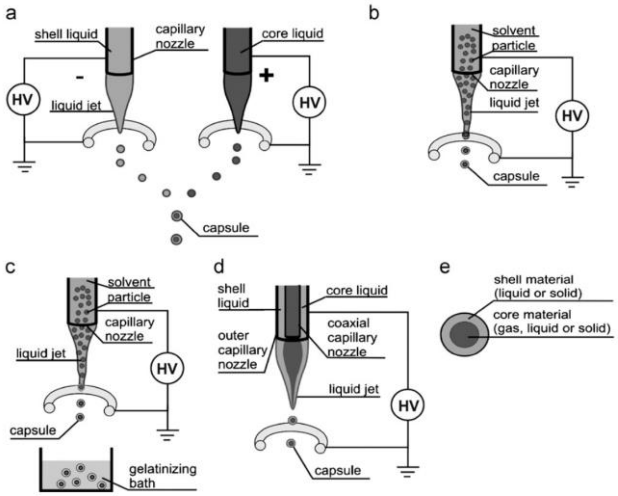

Figure 1-12 Schematics of various electro-encapsulation processes: (a) impacting of two oppositely charged droplets; (b) electrospraying/evaporation of colloidal suspension; (c) electrospraying/gelatinization of colloidal suspension; (d) coaxial electrospraying; and (e) structure of microcapsule (Jaworek, & Sobczyk, 2008).

Until now, the common core materials used in electrospraying for achieving their encapsulation mainly include drugs, cultures, vitamins, flavours, dyes, enzymes, salts, sweeteners, acidulates, nutrients, or preservatives. And common shell materials may consist of starch, gums, fats, waxes, oils, dextran, polysaccharides, proteins, or glucoses, bio-compatible and bio-degradable polymers. For their properties, micro- and nano-capsules are applied in pharmaceutical, cosmetic, food industries, agrochemistry used to control insecticides and textile industry for functional coating.

1.2.6.4 Electrospray forming and direct writing

Electrospray forming is a process of layer-by-layer deposition of electrosprayed droplets of a solution or a colloidal suspension which are continuously dried or solidified to form a thick coating or bulk product. In conventional spray forming systems, 40-50% of the material is oversprayed, but in the electrospray forming process the efficiency can exceed 80% (Schneider et al., 2004).

In electrospray forming, the particles are of the same size, and have similar thermodynamic states. This feature offers significant advantages in reduction of the number and size of voids and cracks in the bulk product. Simultaneous, layer-by-layer or drop-by-drop deposition of solutions of materials of different properties allows composite bulk materials having novel and unique properties to be formed.

Direct writing is a maskless process of drop-by-drop deposition of a material in a liquid or semi-solid phase to draw a pattern on a substrate. The pattern can be directly printed under computer control by moving the substrate on an x–y table. The electrospray technique seems to be ideal tool for this goal, because it is a low-cost, flexible, and high-speed process which, additionally, can trace patterns of higher resolution compared to ink-jet printing or conventional lithography. In contrast to traditional inkjet printing techniques, in which the droplet size is about twice of the nozzle diameter, the electrospray process can produce droplets at least an order of magnitude smaller than the nozzle size. Thus, using coarser nozzles prevents them from clogging, but at the same time, the droplets can be of micrometer size.

1.2.6.5 Biotechnology

Recently, electrospraying technology has presented great advantages and potential to be used in medical field, food packaging fields and cosmetic industry as a biotechnology. For example, bio-compatible and bio-degradable polymers were used as shell materials to encapsulate active proteins or drugs for achieving control release and drug delivery in medical field (Zhang, Campagne, & Salaün, 2019a). And the poly(lactic acid) (PLA), polycaprolactone (PCL) nanofibers or active scaffolds loaded with active drug-loaded microcapsules fabricated from the combination of electrospinning process and electrosprayinng process can be used for organ repair and wound regeneration in tissue engineering (Bock, Dargaville, & Woodruff, 2012). In food industry, on the one hand, some food additives (including flavoring agents, sweeteners, colors, nutrients, essential oils and anti-oxidants agents) are encapsulated into polymeric microspheres to achieving their controlling release and prolong their shelf

life. On the other hand, some phase change materials are also encapsulated by the polymeric shell to obtain some temperature-controlled microspheres. Using these temperature-controlled microspheres in the storage and transportation of food can prolong the activity and storage life of food (Tapia-Hernández et al., 2015).

1.2.6.6 Coating

Some functional substances can be also electrosprayed onto the surface of matrix for modifying the surface properties and morphologies of matrix materials (Li, Wang, & Li, 2019b; Wang, Li, & Li, 2018a, 2018b). Meanwhile, some new properties can be also endowed to matrix materials by introducing a functional coating prepared by electrospraying. For example, Wang et al. published that a durable superamphiphobic fluorinated nano-silica/epoxy composite coating with good environment resistant was successfully fabricated from coaxial electrospraying based on fluorinated nano-silica as shell material and epoxy solution as core material. Compared with raw epoxy coating, fluorinated nanosilica/epoxy composite coating has higher modulus and hardness. Meanwhile, durability of the superamphiphobic coating was assessed by performing harsh chemical environments immersion and scotch tape test (Wang et al., 2018).

1.2.7 The electrospraying of poly(caprolactone) and poly (lactic acid)

In the past ten years, degradeble polyesters have aroused great interest among scientific researchers and industrial producers owing to the growing environmental interest and the new regulations, including less damage to human, less toxicity and less pollution. Poly(caprolactone) (PCL) and poly(lactic acid) (PLA) as most common bio-based polymers, due to their biocompatibility, biodegradation, non-toxic and harmless final degradation products (CO_2 and H_2O), have been widely used in many fields, particularly in medical fields, food packaging industry and functional coating (Bajpai, Singh, & Madaan, 2014; Mohamed, & Yusoh, 2015). Until now, electrosprayed PCL or PLA microcapsules (or microspheres) and electrospun PCL or PLA fibers have been widely used as drug carrier for achieving controlled release and delivery, biological scaffolds and bones in tissue engineering, medical instruments for recovery treatment and food packaging (Cipitria et al., 2011; Toncheva et al., 2014; Zhao et al., 2020). In addition, in order to make up for the shortcomings of PLA and PCL, PLA and PCL are often made into composite materials to be used various fields (Fortelny et al., 2019).

1.2.7.1 Polycaprolactone

Polycaprolactone (PCL), a semi-crystalline polyester, is prepared from ring-opening polymerization of ε-caprolactone monomer under the catalysis of metal anion complex catalyst (Labet, & Thielemans, 2009). Due to its relatively low melting temperature (Tm = 60 °C) and glass transition temperature (Tg = -60 °C), PCL has excellent viscoelastic properties, softness, ductility and processability. Moreover, PCL is regarded as a green environmental and non-toxic polymer material due to its prominent biocompatibility and biodegradation. Thus, PCL is widely used in medical tissue engineering, drug delivery, and control release systems, food packaging industry, antibacterial study, protective clothing fabrication, and biosensors (Mochane et al., 2019). Particularly, micro- or nanoscale PCL particles with a wide specific surface area, a small pore size, high encapsulation efficiency, and a high porosity are considered to be the main candidates in these fields. For instance, the release profiles of active drug encapsulated in polymer microsphere are controlled by the size, distribution, and porous structure of microcapsules. Meanwhile, the drug-loaded nanoparticles with small size and narrow distribution have an enhanced ability to reach their target. The degradation process of these particles with a huge surface to volume ratio also occurs at a relatively faster rate. Apart from the chemical and physical nature of particles, the properties and applications of polymeric particles are mainly determined by their structure and morphology. However, if we consider the practical requirements of packaging engineering and medical systems, PCL also has two disadvantages: (i) low physical strength and mechanical properties (ii) low thermal stability (low melting point limits the application scope of PCL) (Siracusa et al., 2008).

1.2.7.2 Poly (lactic acid)

Poly (lactic acid) (PLA) is frequently reported as one of the most promising biodegradable, biocompatibility synthetic polyester synthesized from the direct condensation polymerization of L-lactic acid and D-lactic acid or the ring-opening polymerization of L-dilactide, D-dilactide and meso-dilactide. PLA was approved by the US Food and Drug Administration as far back as in the 1970s and has since been widely utilized in sutures, clips, plates and screws, in drug delivery devices, in tissue engineering and bone fixation devices and in food packaging applications due to its well documented biocompatibility, full biodegradability, and high stiffness (Garlotta, 2001). Being similar as PCL, micro- or nanoscale PLA particles (or capsules) and fibers have great potential and advantages in these fields. More importantly, PLA has higher glass transition temperature (Tg =55-60 °C) and

higher melting point (Tm =160-165 °C) compared with PCL. Therefore, PLA has better thermal stability and better mechanical properties compared with PCL (Ahmed, & Varshney, 2011). However, when PLA is actually put into use in various fields, there are still some disadvantages that limit its application and development. Firstly, due to its high glass transition temperature as well as high melting point, the processability of PLA is not very good, and it puts forward higher requirements for processing equipment and processing temperature. Meanwhile, PLA also presents the shortcomings of brittle fracture. Secondly, the interfacial adhesion or compatibility between PLA and other plastics, textiles or matrix is worse than the situation from PCL owing to the rigidity of PLA chains. Finally, the degradation rate of PLA cannot meet a wide range of application specific requirements; and there are no cell recognition sites that are important for tissue compatibility on the surface of PLA application on tissue engineering (Ahmed, & Varshney, 2011). Until now, there are mainly two methods to overcome these disadvantages of PLA. On the one hand, the properties of PLA depend on the chemical components, compositions, morphological structure of PLA. Therefore, the properties of PLA can be improved via introducing the second monomer (flexible chain segments or hydrophilic groups including other lactone-type monomers, a hydrophilic macromonomers (polyethylene glycol (PEG)), or other monomers with functional groups (such as amino and carboxylic groups, etc.)) during the polymerization of lactide. These flexible chain segments or hydrophilic groups not only can further enhance the interfacial compatibility or adhesion of PLA with other materials as well as the degradation rate of PLA, but also improve the brittleness of PLA and the processability of PLA. On the other hand, the toughness of brittle PLA can be improved via blending with a soft, ductile component. PCL is regarded as a suitable component to couple with PLA to enhancing the flexibility of PLA, the compatibility of PLA with other materials and interfacial activity of PLA matrix and the processability of PLA. More importantly, PLA also a suitable component to overcome the shortcomings of PCL. When introducing PLA into PCL, the thermal stability and the mechanical properties of PCL can be also improved obviously. For example, according to Patrício et al., the melting point and thermal degradation temperature of PCL matrix can be further increased via adding some PLA component. When the weight ratio between PCL and PLA is 70/30, the melting point and the thermal degradation temperature of PCL increases by about 14 °C and 1.2 °C, respectively compared with neat PCL matrix (Patrício, & Bártolo, 2013). And Fortelny et al. also published that a high toughness or even “super-toughness” of PLA/PCL blends without a compatibilizer can be achieved for blends with the proper size of PCL particles. Available literature data suggest that the optimal composition for PLA/PCL blends is around 80/20 (w/w). The

PLA/PCL (80/20) blends keep high stiffness of PLA matrix and the concentration of PCL particles is sufficient to achieve high toughness (Ostafinska et al., 2015).

1.2.7.3 Drug control release

In the PCL matrix, the slow controlled release behavior, compared to other biodegradable polymers, allows vectorizing the drug to the suitable cells. Furthermore, this polymer shows a high selective permeability towards small drug molecules, and drug degradation in an acidic medium may be prevented. Thus, PCL electrosprayed particles are suitable for long-term delivery extending throughout more than one year (Aishwarya, Mahalakshmi, & Sehgal, 2008), especially in the biomedical field for parenteral and oral drug deliveries, in which anti-hypertensive, antibiotic, anti-inflammatory drugs are entrapped (Cao et al., 2014; Ding et al., 2005; Midhun et al., 2011; Nguyen, Clasen, & Van den Mooter, 2016). The applications of electrospraying particles in the field of biomedical engineering depend in part on their morphology. Thus, interactions between cells and biomaterials are promoted when particles have a gully-shaped surface with wrinkles (Wang et al., 2009). Semi-spherical particles with a porous structure are used in multi-stage biological and drug delivery scaffolding (Gao et al., 2015). Also, their high specific surface area coupled with low density allows them to be used for pulmonary drug delivery. In addition, Mai et al. (2017) prepared successfully curcumin/PLA microcapsules with high loading content as well as encapsulation efficiency of curcumin (more than 95 %) via electrospraying. Meanwhile, the mean diameter of curcumin/PLA microcapsules can be controlled from 3.8 μm to 4.4 μm via adjusting solvent systems, flow rates, polymer and drug concentrations. Hydrophilic and hydrophobic drugs were also encapsulated into PLA matrix respectively by Valo et al. (2009) based on an electrohydrodynamic atomization. They also published that the location of drugs in PLA matrix was related with the compatibility between drugs and PLA matrix. For hydrophilic drug, it is randomly distributed in the PLA matrix owing to its bad compatibility with PLA (hydrophobic macromolecular). For hydrophilic drug, it tends to locate in the center of PLA matrix due to its good compatibility with PLA matrix.

There are two main methods to encapsulate the drug via the electrospraying route, according to their solubility and the desired morphology and final used end, i.e., (i) dispersion of the active substance in the polymer solution to obtain microspheres, and (ii) the use of a coaxial system for the production of core/shell structure. The release behavior depends on the particle size, core-shell structure as well as the surface area/volume ratio, to allow

the drug diffusion (Bock et al., 2012; A. Jaworek, 2007), and burst release is reached from tinier particles (Ding et al., 2005). Meanwhile, the early burst release of drug from microcapsules can be prevented based on a core-shell structure. The release rate significantly increases for thin layer shell or porous membrane as well as the wrinkled surface structure and is homogeneous for a monodispersed particle size. The polymer degradation rate depends on the structure and morphology of the particles (Bock, Dargaville, & Woodruff, 2012; Guarino et al., 2010; Kalpna et al., 2007). Thus, it increases with decreasing the size of microcapsules, and wrinkled and porous morphology induce its degradation (Rezwan et al., 2006), and a high specific contact area improves interactions between particles and cells (Gaumet et al., 2008).

1.2.7.4 Tissue engineering

As a three-dimensional and degradable material, electrosprayed PCL or PLA microspheres (or microcapsules and fibers) are also used in the tissue engineering field as biologically active and temporary devices to achieve repairing and regenerating of tissue, supporting and reinforceme (Dash, & Konkimalla, 2012). In order to promote tissue growth, the microspheres scaffolds with porous morphology is one the best candidates. On the one hand, the contacting area as well as interactions between microsphere scaffolds and cells increases with increasing the specific surface area of microsphere scaffolds. On the other hand, due to the presence of porous structure, cells can penetrate the pores, which must be interconnected to improve nutrient and waste exchanges by cells (Bock et al., 2012). The degradation rate of polymer microsphere scaffolds is also a crucial factor to influence their applications in tissue engineering, and it is controlled effectively by designing the structure and morphology of polymer microspheres. At the same time, the size and shape of electrosprayed microparticles can be designed carefully according to a specific application. Also, to further improve the ability of cell adhesion as well as degradation properties, gelatin or collagen is blended with PCL or PLA to prepare scaffolds or supporting materials used in the biomedical field (Dulnik et al., 2016; Ghasemi-Mobarakeh et al., 2008; Sell et al., 2010). Collagen and gelatin contain Arg-Gly-Asp (RGD) amino acid sequences. Then, integrins (cell binding proteins) recognize those sequences and promote cell adhesion. This biopolymer addition increases cell attachment and spreading to the surface of a material.

Furthermore, electrosprayed drug-PCL microcapsules are also coated on the surface of degradable electrospun fibers to be used in tissue engineering, particularly in bone and cartilage tissue engineering (Bock,

Dargaville, & Woodruff, 2012). During the process of cells regeneration in scaffolds, the controlling release of active drug from microcapsules provides a sustained and suitable environment to improve the activity and growth of cells (Dash, & Konkimalla, 2012). In 2009, Wang et al. (2009) firstly fabricated a soft tissue engineered construct (TEC) with anisotropic structure via combining coaxial electrospraying and electrospinning. The release of insulin-like growth factor from microcapsules coating on the surface of scaffolds can deliver growth factors for the survival of cells, which are often subjected to hypoxia and a nutrient starvation microenvironment in the context of TECs.

1.2.7.5 Functional coating

Functional coating can endow some new properties to target matrix, which can improve the value of target material as well as the range of application. Until now, the most common functional coating process is that coating some polymeric microspheres or microcapsules with special functions on the surface of the textiles for achieving the corresponding modification. During the electrospraying process, the functional coating of matrix material can be carried out directly when target was placed on the surface of collector. Meanwhile, in order to further enhance the interfacial adhesion between textile and electrosprayed microparticles, an active outer shell which can form interaction with textiles for prolonging the durability of coating can be designed in the electrospraying process based on a coaxial nozzle. A honeycomb-like hierarchical structure microspheres of PCL-b-PTFOA(4h) was prepared based on electrohydrodynamic atomization technology by Li et al., then a superhydrophobic coatings and robust superhydrophobic-coated cotton woven fabric surfaces were prepared by using PCL-b-PTFOA(4h) microspheres with hierarchical structure and low surface energy. The contact angle (CA) and sliding angle (SA) of PCL-b-PTFOA(4h) microspheres-coated cotton woven fabric surfaces reached 164.4 ± 5.5° and 6.8 ± 0.5°, respectively, which allows for self-cleaning (Li, Wang, & Li, 2019a). In order to improve water resistance and barrier properties of paperboard, Archaviboonyobul et al. introduces PLA microspheres on the surface of paperboard via electrospraying. The results showed that water and oil contact angles of paperboard were significantly increased after electrospraying PLA microspheres (Archaviboonyobul et al., 2014). Water and oil absorption was significantly reduced, especially when using PLA concentration of 1%. On the basis of electrospraying technique, the amount of coat materials or functional particles can be significantly reduced to achieve results comparable to other common coating methods.

1.2.7.6 Food packaging

Biodegradable polymeric microspheres or microcapsules also show some applications in the field of food packaging (Desai, Liu, & Park, 2006). On the one hand, some food additives (including flavoring agents, sweeteners, colors, nutrients, essential oils and anti-oxidants agents) are encapsulated into polymeric microspheres to achieving their controlling release. It helps to overcome both the inefficient utilization and the loss of food additives during the processing steps (Pothakamury, & Barbosa-Cánovas, 1995). The polymeric shell, as an active barrier, plays a role in isolation and protection. On the other hand, some phase change materials are also encapsulated by the polymeric shell to obtain some temperature-controlled microspheres (Durán, & Marcato, 2013). Using these temperature-controlled microspheres in the storage and transportation of food can prolong the activity and storage life of food. Also, adding some anti-oxidant agents into the polymeric shell and using this shell to encapsulate food improve the antioxidant capacity of food and extend the shelf life of food (Beltrán et al., 2014).

1.2.8 Preparing phase change microcapsules via electrospraying

Although electrospraying technology has been widely used for preparing functional microspheres in the fields of controlled drug release, tissue engineering, functional coating and food packaging industry, the use of electrospraying for PCM (phase change material) microencapsulation, even if some authors recognize it as a suitable method, is seldom described in the scientific literature. Most scientific researchers tended to apply the coaxial electrospinning method to prepare phase change nanofibers with core-sheath structure. Moghaddam et al. prepared n-nonadecane/sodium alginate mPCM, using melting coaxial electrospraying (Moghaddam & Mortazavi, 2015; Moghaddam, Mortazavi, & Khayamian, 2015a, 2015b). The formation of the shell was carried out via the cross-linking solidification reaction between alginate solution (outer liquid) and calcium chloride in collecting bath. The investigation of the alginate solution concentration and the optimization of the process parameters, controlling the mean diameter of the particles, allowed them to reach an encapsulation efficiency of about 59%, a phase change enthalpy of their capsules about 88 J/g, and a mean diameter between 200 to 700 μm. N-octadecane was successfully entrapped in a polyamic acid shell via a coaxial electrospraying process (Yuan et al., 2015). The authors observed that the core feed rate affected the surface morphology as well as the mean diameter of the capsules. Furthermore, microcapsules with a mean diameter between 1 to 2 μm, with narrow size distribution and

a loading content of 60%, were obtained.

1.3 Conclusions

Through the literature review, it can find that the importance of phase change materials (PCMs) in the fields of energy storage and thermal management, particularly in the fabrication of thermal-regulated textiles. Textiles incorporated with PCMs can be used in many fields, for example space, wearing clothes, bedding and accessories, medical application and shoes and accessories. Among various PCMs, organic paraffin waxes are regarded as the most suitable PCMs to fabricate thermal-regulated textiles. When PCMs are applied into the fabrication of thermal-regulated textiles, two steps are usually required. The first step is the microencapsulation process of PCMs. When PCMs are encapsulated into shell matrix to form phase change microcapsules (mPCMs), the durability, stability, processability and thermal conductivity of PCMs can be improved significantly. Meanwhile, the interfacial interactions between textiles and mPCMs can be further improved via designing a second active shell for mPCMs. The second step is functional coating process.

Electrospraying as a green and high-efficiency electrohydrodynamic atomization technology, is widely used to fabricate polymeric micro- (or nano-) particles (or capsules). Compared with conventional methods for achieving the microencapsulation process of PCMs, electrospraying technology can offer more advantages and potential. Firstly, the experimental device as well as operational steps of electrospraying are simple, and the formation of electrosprayed microcapsules can be finished in seconds. Secondly, the use of a large amount of organic solvent, toxic or corrosive chemical reagents, surfactant and some additives can be avoided in electrospraying process. Thirdly, under stable cone-jet mode, not only the mono-dispersed size distribution can be obtained, but also the adjustment of the size, structure and surface morphology of targeted microcapsules via controlling the physico-chemical properties of electrospraying solutions and the operating parameters. Fourthly, different core-shell structures or multi-shell structures of electrosprayed microcapsules can be designed easily when different nozzles were used in electrospraying. Fifthly, when coaxial nozzle was applied for fabricating mPCMs, high loading content and high encapsulation efficiency of PCMs can be achieved. Finally, the functional coating process of textiles can be also completed during electrospraying process when textiles were placed on the surface of collector. Meanwhile, the use of binder can be avoided when electrospraying process was used to carry out the functional coating of textiles, and the original structures and properties (including softness, breathability

and mechanical properties) of textiles can be retained to the greatest extent. Therefore, electrospraying process is not only regarded as a feasible and high-efficiency method to prepare n-alkanes-based mPCMs, but also a convenient and advantageous method for achieving the functional coating of textiles by electrosprayed mPCMs.

During the electrospraying process, the selection of solvent system as the carrier of shell matrix and core material is very crucial. Firstly, the physico-chemical properties of electrospraying solution will determine the formation of stable Taylor cone. Carrying out the electrospraying process under stable cone-jet mode is the precondition to obtain the electrosprayed microparticles with mono-dispersed size distribution and achieve the design of the size, surface morphology and structure of obtained microparticles via changing the solution properties and operating parameters. Secondly, the working window of operating parameters for achieving the formation of Taylor cone are also effected by the physico-chemical properties of electrospraying solution. Thirdly, the physico-chemical properties of electrospraying solution and operating parameters also influenced the size, structure and surface morphology of electrosprayed microparticles.

In addition, the solution properties, phase state of PCMs, the addition of PCMs and shell materials also influenced the microencapsulation process of PCMs during electrospraying process. Therefore, electrosprayed mPCMs with different size, size distribution, surface morphology, loading content of PCMs and encapsulation efficiency of PCMs can be obtained when different solvent, different PCMs and different shell materials were applied in electrospraying. Meanwhile, different nozzles with different geometries also influenced the microencapsulation process of PCMs during electrospraying process. Furthermore, different core-shell structures and multi-shell structures of electrosprayed mPCMs can be designed when different nozzles with different geometries were applied in electrospraying.

Electrosprayed mPCMs with double-layered shell can present more properties, functions and advantages. For example, physical strength and thermal-mechanical properties can be offered from the inner shell material, and stronger interfacial adhesion between electrosprayed mPCMs and textiles can be achieved via forming the active interactions between outer shell material and textiles. Meanwhile, high loading content and high encapsulation efficiency of PCMs in electrosprayed microcapsules can be expected when double-layered shell was designed. In addition, the weight fractions between inner shell material and outer shell material and the addition of PCMs not only influenced the microencapsulation process of PCMs, but also the structures and properties of final microcapsules.

Even though electrospraying technology had presented much potential and advantages in preparation of mPCMs as well as the functional coating of textiles, only few people recognized the values of electrospraying and published some limited progress. Most people tended to applied the coaxial electrospinning technology to prepare phase change nanofibers with core-sheath structure. Meanwhile, until now, most mPCMs are still fabricated from conventional methods, including interfacial polymerization, in-situ polymerization, suspension polymerization, phase coaversion and solvent evaporation methods, which not only does not meet the current requirements for green, non-toxic and pollution-free experimental production processes, but also is still an inefficient way to realize the preparation of mPCMs. Therefore, it is necessary to accelerate the application of electrospraying technology in the preparation of mPCMs. In this thesis, how to achieve the microencapsulation process of PCMs during electrospraying process was investigated in details. And all the factors (mainly including solvent systems, solution properties, operating paramters, the phase state of PCMs, the addition of PCMs, nozzle geometries and multi-shell structure) that influenced the electrospraying microencapsulation process and the final structures and properties of obtained electrosprayed mPCMs were also studied. Meanwhile, until now, common shell materials for the microencapsulation of PCMs mainly includes urea-formaldehyde resins, melamine-formaldehyde resins, urea-melamine-formaldehyde resins, polyurethane, poly (methyl methacrylate), polystyrene. However, considering the toxicity, environmental and health problems, some natural polymers (e.g. agar, arabic gum and gelatine), green synthetic polymers (e.g. poly(caprolactone) (PCL) and poly (lactic acid) (PLA)) and inorganic materials (e.g. silicon, calcium carbonate and metal oxide) have gradually become the substitutes for conventional shell materials. Due to their biocompatibility, biodegradability, green, non-toxic, thermal-mechanical properties and interfacial adhesion, PCL and PLA were used as shell matrix in this thesis to prepare single-layered shell mPCMs and double-layered shell mPCMs during electrospraying process. Finally, a green, non-toxic and high efficiency method to design mPCMs with desired structure and properties can be obtained and developed based on electrospraying technology. And it also offers a new direction to achieving the functional coating of textiles by electrosprayed mPCMs.

References

Adamska, K., Voelkel, A., & Berlińska, A. (2016). The solubility parameter for biomedical polymers—Application of inverse gas chromatography. *Journal of Pharmaceutical and Biomedical Analysis, 127,* 202–206. https://doi.org/10.1016/j.jpba.2016.04.014

Ahmad, Z., Zhang, H. B., Farook, U., Edirisinghe, M., Stride, E., & Colombo, P. (2008). Generation of multilayered structures for biomedical applications using a novel tri-needle coaxial device and electrohydrodynamic flow. *Journal of the Royal Society Interface*, *5*(27), 1255–1261. https://doi.org/10.1098/rsif.2008.0247

Ahmed, J., & Varshney, S. K. (2011). Polylactides-chemistry, properties and green packaging technology: A review. *International Journal of Food Properties*, *14*(1), 37–58. https://doi.org/10.1080/10942910903125284

Aishwarya, S., Mahalakshmi, S., & Sehgal, P. K. (2008). Collagen-coated polycaprolactone microparticles as a controlled drug delivery system. *Journal of Microencapsulation*, *25*(5), 298–306. https://doi.org/10.1080/02652040801972004

Almería, B., Deng, W., Fahmy, T. M., & Gomez, A. (2010). Controlling the morphology of electrospray-generated PLGA microparticles for drug delivery. *Journal of Colloid and Interface Science*, *343*(1), 125–133. https://doi.org/10.1016/j.jcis.2009.10.002

Archaviboonyobul, T., Jinkarn, T., Sane, S., Chariyachotilert, S., & Kongcharoenkiat, S. (2014). Water Resistance and Barrier Properties Improvement of Paperboard by Poly(Lactic Acid) Electrospraying. Packaging and Technology and Science, 27, 341–352. https://doi.org/10.1002/pts

Bajpai, P. K., Singh, I., & Madaan, J. (2014). Development and characterization of PLA-based green composites: A review. *Journal of Thermoplastic Composite Materials*, *27*(1), 52–81. https://doi.org/10.1177/0892705712439571

Barrero, A., Gañán-Calvo, A. M., Dávila, J., Palacio, A., & Gómez-González, E. (1998). Low and high Reynolds number flows inside Taylor cones. *Physical Review E - Statistical Physics, Plasmas, Fluids, and Related Interdisciplinary Topics*, *58*(6), 7309–7314. https://doi.org/10.1103/PhysRevE.58.7309

Barrero, A., Gañán-Calvo, A. M., Dávila, J., Palacios, A., & Gómez-González, E. (1999). The role of the electrical conductivity and viscosity on the motions inside Taylor cones. *Journal of Electrostatics*, *47*(1–2), 13–26. https://doi.org/10.1016/S0304-3886(99)00021-2

Beltrán, A., Valente, A. J. M., Jiménez, A., & Garrigós, M. C. (2014). Characterization of poly(ε-caprolactone)-based nanocomposites containing hydroxytyrosol for active food packaging. *Journal of Agricultural and Food Chemistry*, *62*(10), 2244–2252. https://doi.org/10.1021/jf405111a

Bock, N., Dargaville, T. R., & Woodruff, M. A. (2012). Electrospraying of polymers with therapeutic molecules: State of the art. *Progress in Polymer Science*, *37*(11), 1510–1551. https://doi.org/10.1016/j.progpolymsci.2012.03.002

Bock, N., Dargaville, T. R., & Woodruff, M. A. (2014). Controlling microencapsulation and release of micronized proteins using poly(ethylene glycol) and electrospraying. *European Journal of Pharmaceutics and Biopharmaceutics*, *87*(2), 366–377. https://doi.org/10.1016/j.ejpb.2014.03.008

Bock, N., Woodruff, M. A., Hutmacher, D. W., & Dargaville, T. R. (2011). Electrospraying, a reproducible method for production of polymeric microspheres for biomedical applications. *Polymers*, *3*(1), 131–149. https://doi.org/10.3390/polym3010131

Boda, S. K., Li, X., & Xie, J. (2018). Electrospraying an enabling technology for pharmaceutical and biomedical applications: A review. *Journal of Aerosol Science*, *125*, 164–181. https://doi.org/10.1016/j.jaerosci.2018.04.002

Bodnár, E., Grifoll, J., & Rosell-Llompart, J. (2018). Polymer solution electrospraying: A tool for engineering particles and films with controlled morphology. *Journal of Aerosol Science*, *125*, 93–118. https://doi.org/10.1016/j.jaerosci.2018.04.012

Bordes, C., Fréville, V., Ruffin, E., Marote, P., Gauvrit, J. Y., Briançon, S., & Lantéri, P. (2010). Determination of poly(ε-caprolactone) solubility parameters: Application to solvent substitution in a microencapsulation process. *International Journal of Pharmaceutics*, *383*(1–2), 236–243. https://doi.org/10.1016/j.ijpharm.2009.09.023

Bruninx, E., & Rudstam, G. (1961). Electro-spraying: A method of making samples for β counting allowing accurate correction for self-scattering and self-absorption. *Nuclear Instruments and Methods*, *13*(C), 131–140. https://doi.org/10.1016/0029-554X(61)90181-1

Cao, Y., Wang, B., Wang, Y., & Lou, D. (2014). Dual drug release from core-shell nanoparticles with distinct release profiles. *Journal of Pharmaceutical Sciences*, *103*(10), 3205–3216. https://doi.org/10.1002/jps.24116

Casper, C. L., Stephens, J. S., Tassi, N. G., Chase, D. B., & Rabolt, J. F. (2004). Controlling surface morphology of electrospun polystyrene fibers: Effect of humidity and molecular weight in the electrospinning process. *Macromolecules*, *37*(2), 573–578. https://doi.org/10.1021/ma0351975

Chandrasekhar, R., & Choy, K. L. (2001). Electrostatic spray assisted vapour deposition of fluorine doped tin oxide. *Journal of Crystal Growth*, *231*(1–2), 215–221. https://doi.org/10.1016/S0022-0248(01)01477-4

Chen, C. H., Kelder, E. M., Jak, M. J. G., & Schoonman, J. (1996). Electrostatic spray deposition of thin layers of cathode materials for lithium battery. *Solid State Ionics*, *86–88*(PART 2), 1301–1306. https://doi.org/10.1016/0167-2738(96)00305-0

Chen, D. R., Pui, D. Y. H., & Kaufman, S. L. (1995). Electrospraying of conducting liquids for monodisperse aerosol generation in the 4 nm to 1.8 μm diameter range. *Journal of Aerosol Science*, *26*(6), 963–977. https://doi.org/10.1016/0021-8502(95)00027-A

Chen, H., Zhao, Y., Song, Y., & Jiang, L. (2008). One-step multicomponent encapsulation by compound-fluidic electrospray. *Journal of the American Chemical Society*, *130*(25), 7800–7801. https://doi.org/10.1021/ja801803x

Chen, X., Jia, L., Yin, X., Cheng, J., & Lu, J. (2005). Spraying modes in coaxial jet electrospray with outer driving liquid. *Physics of Fluids*, *17*(3), 1–8. https://doi.org/10.1063/1.1850691

Chul, H. P., & Jonghwi, L. (2009). Electrosprayed Polymer Particles: Effect of the Solvent Properties Chul. *Journal of Applied Polymer Science*, *114*, 430–437. https://doi.org/10.1002/app

Ciach, T. (2006). Microencapsulation of drugs by electro-hydro-dynamic atomization. *International Journal of Pharmaceutics*, *324*(1), 51–55. https://doi.org/10.1016/j.ijpharm.2006.06.035

Cipitria, A., Skelton, A., Dargaville, T. R., Dalton, P. D., & Hutmacher, D. W. (2011). Design, fabrication and characterization of PCL electrospun scaffolds - A review. *Journal of Materials Chemistry*, *21*(26), 9419–9453. https://doi.org/10.1039/c0jm04502k

Cloupeau, M. (1994). Recipes for use of EHD spraying in cone-jet mode and notes on corona discharge effects. *Journal of Aerosol Science*, *25*(6), 1143–1157. https://doi.org/10.1016/0021-8502(94)90206-2

Cloupeau, M., & Prunet-Foch, B. (1989). Electrostatic spraying of liquids in cone-jet mode. *Journal of Electrostatics*, *22*(2), 135–159. https://doi.org/10.1016/0304-3886(89)90081-8

Cloupeau, M., & Prunet-Foch, B. (1994). Electrohydrodynamic spraying functioning modes: a critical review. *Journal of Aerosol Science*, *25*(6), 1021–1036. https://doi.org/10.1016/0021-8502(94)90199-6

Collins, R. T., Jones, J. J., Harris, M. T., & Basaran, O. A. (2008). Electrohydrodynamic tip streaming and emission of charged drops from liquidcones. *Nature Physics*, *4*(2), 149–154.

https://doi.org/10.1038/nphys807

Costa, L. M. M., Bretas, R. E. S., & Gregorio, R. (2010). Effect of Solution Concentration on the Electrospray/Electrospinning Transition and on the Crystalline Phase of PVDF. *Materials Sciences and Applications*, *01*(04), 247–252. https://doi.org/10.4236/msa.2010.14036

Dash, T. K., & Konkimalla, V. B. (2012). Poly-ε-caprolactone based formulations for drug delivery and tissue engineering: A review. *Journal of Controlled Release*, *158*(1), 15–33. https://doi.org/10.1016/j.jconrel.2011.09.064

Deitzel, J. M., Kleinmeyer, J., Harris, D., & Beck Tan, N. C. (2001). The effect of processing variables on the morphology of electrospun nanofibers and textiles. Polymer, 42, 261–272. https://doi.org/10.1016/S0032-3861(00)00250-0

Deotare, P. B., & Kameoka, J. (2006). Fabrication of silica nanocomposite-cups using electrospraying. *Nanotechnology*, *17*(5), 1380–1383. https://doi.org/10.1088/0957-4484/17/5/036

Desai, K. G., Liu, C., & Park, H. J. (2006). Characteristics of vitamin C encapsulated tripolyphosphate-chitosan microspheres as affected by chitosan molecular weight. *Journal of Microencapsulation*, *23*(1), 79–90. https://doi.org/10.1080/02652040500435360

Ding, L., Lee, T., & Wang, C. H. (2005). Fabrication of monodispersed Taxol-loaded particles using electrohydrodynamic atomization. *Journal of Controlled Release*, *102*(2), 395–413. https://doi.org/10.1016/j.jconrel.2004.10.011

Dubey, R., Shami, T.C., & Bhasker Rao, K.U. (2009). Microencapsulation Technology and Applications. *Defense Science Journal*, *59*(1), 82-95. http://dx.doi.org/10.14429/dsj.59.1489

Dudout, B., Marijnissen, J. C. M., & Scarlett, B. (1999). Use of EHDA for the production of nanoparticles. *Journal of Aerosol Science*, *30*(Suppl. 1), 1999–2000. https://doi.org/10.1016/S0021-8502(99)80354-1

Dulnik, J., Denis, P., Sajkiewicz, P., Kołbuk, D., & Choińska, E. (2016). Biodegradation of bicomponent PCL/gelatin and PCL/collagen nanofibers electrospun from alternative solvent system. *Polymer Degradation and Stability*, *130*, 10–21. https://doi.org/10.1016/j.polymdegradstab.2016.05.022

Durán, N., & Marcato, P. D. (2013). Nanobiotechnology perspectives. Role of nanotechnology in the food industry: A review. *International Journal of Food Science and Technology*, *48*(6), 1127–1134. https://doi.org/10.1111/ijfs.12027

Enayati, M., Chang, M. W., Bragman, F., Edirisinghe, M., & Stride, E. (2011). Electrohydrodynamic preparation of particles, capsules and bubbles for biomedical engineering applications. *Colloids and Surfaces A: Physicochemical and Engineering Aspects*, *382*(1–3), 154–164. https://doi.org/10.1016/j.colsurfa.2010.11.038

Farook, U., Stride, E., & Edirisinghe, M. J. (2009). Stability of microbubbles prepared by co-axial electrohydrodynamic atomisation. *European Biophysics Journal*, *38*(5), 713–718. https://doi.org/10.1007/s00249-008-0391-z

Fortelny, I., Ujcic, A., Fambri, L., & Slouf, M. (2019). Phase Structure, Compatibility, and Toughness of PLA/PCL Blends: A Review. *Frontiers in Materials*, *6*(August), 1–13. https://doi.org/10.3389/fmats.2019.00206

Fukui, Y., Maruyama, T., Iwamatsu, Y., Fujii, A., Tanaka, T., Ohmukai, Y., & Matsuyama, H. (2010). Preparation of monodispersed polyelectrolyte microcapsules with high encapsulation efficiency by an electrospray technique. *Colloids and Surfaces A: Physicochemical and Engineering Aspects*, *370*(1–3), 28–34. https://doi.org/10.1016/j.colsurfa.2010.08.039

Gañán-Calvo, A. M., López-Herrera, J. M., Rebollo-Muñoz, N., & Montanero, J. M. (2016). The onset of electrospray: The universal scaling laws of the first ejection. *Scientific Reports*, *6*(September), 1–9. https://doi.org/10.1038/srep32357

Gañán-Calvo, A. M. (1994). the Size and Charge of Droplets in the Electrospraying of Polar liquids in cone-jet mode, and the minimum droplet size. *Journal of Aerosol Science*, *25*(X), 309–310.

Gander, B., Johansen, P., Nam-Trân, H., & Merkle, H. P. (1996). Thermodynamic approach to protein microencapsulation into poly(D,L-lactide) by spray drying. *International Journal of Pharmaceutics*, *129*(1–2), 51–61. https://doi.org/10.1016/0378-5173(95)04240-7

Gao, J., Li, W., Wong, J. S. P., Hu, M., & Li, R. K. Y. (2014). Controllable morphology and wettability of polymer microspheres prepared by nonsolvent assisted electrospraying. *Polymer*, *55*(12), 2913–2920. https://doi.org/10.1016/j.polymer.2014.04.033

Gao, Y., Bai, Y., Zhao, D., Chang, M. W., Ahmad, Z., & Li, J. S. (2015). Tuning microparticle porosity during single needle electrospraying synthesis via a non-solvent-based physicochemical approach. *Polymers*, *7*(12), 2701–2710. https://doi.org/10.3390/polym7121531

Gao, Y., Zhao, D., Chang, M. W., Ahmad, Z., & Li, J. S. (2016). Optimising the shell thickness-to-radius ratio for the fabrication of oil-encapsulated polymeric microspheres. *Chemical Engineering Journal*, *284*, 963–971. https://doi.org/10.1016/j.cej.2015.09.054

Garlotta, D. (2001). A literature review of poly(lactic acid). *Journal of Polymers and the Environment*, *9*(2), 63–84. https://doi.org/10.1023/A:1020200822435

Garoz, D., Bueno, C., Larriba, C., Castro, S., Romero-Sanz, I., De La Mora, J. F., Yoshida, Y., & Saito, G. (2007). Taylor cones of ionic liquids from capillary tubes as sources of pure ions: The role of surface tension and electrical conductivity. *Journal of Applied Physics*, *102*(6). https://doi.org/10.1063/1.2783769

Gaumet, M., Vargas, A., Gurny, R., & Delie, F. (2008). Nanoparticles for drug delivery: The need for precision in reporting particle size parameters. *European Journal of Pharmaceutics and Biopharmaceutics*, *69*(1), 1–9. https://doi.org/10.1016/j.ejpb.2007.08.001

Ghanbar, H., Luo, C. J., Bakhshi, P., Day, R., & Edirisinghe, M. (2013). Preparation of porous microsphere-scaffolds by electrohydrodynamic forming and thermally induced phase separation. *Materials Science and Engineering C*, *33*(5), 2488–2498. https://doi.org/10.1016/j.msec.2012.12.098

Ghasemi-Mobarakeh, L., Prabhakaran, M. P., Morshed, M., Nasr-Esfahani, M. H., & Ramakrishna, S. (2008). Electrospun poly(ε-caprolactone)/gelatin nanofibrous scaffolds for nerve tissue engineering. *Biomaterials*, *29*(34), 4532–4539. https://doi.org/10.1016/j.biomaterials.2008.08.007

Guarino, V., Lewandowska, M., Bil, M., Polak, B., & Ambrosio, L. (2010). Morphology and degradation properties of PCL/HYAFF11® composite scaffolds with multi-scale degradation rate. *Composites Science and Technology*, *70*(13), 1826–1837. https://doi.org/10.1016/j.compscitech.2010.06.015

Hartman, R. P. A., Brunner, D. J., Camelot, D. M. A., Marijnissen, J. C. M., & Scarlett, B. (1999). Electrohydrodynamic atomization in the cone-jet mode physical modeling of the liquid cone and jet. *Journal of Aerosol Science*, *30*(7), 823–849. https://doi.org/10.1016/S0021-8502(99)00033-6

Hartmann, M. & Eyal, A. (2016). Articles containing functinal polymeric phase change materials and methods of manufacturing the same. *United States Patent, Patent No:US9234059B2*

Hwang, Y. K., Jeong, U., & Cho, E. C. (2008). Production of Uniform-Sized Polymer Core−Shell Microcapsules by Coaxial Electrospraying. *Langmuir*, *24*(6), 2446–2451. https://doi.org/10.1021/la703546f

Jamekhorshid, A., Sadrameli, S. M., & Farid, M. (2014). A review of microencapsulation methods of phase change materials (PCMs) as a thermal energy storage (TES) medium. *Renewable and Sustainable Energy Reviews*, *31*, 531–542. https://doi.org/10.1016/j.rser.2013.12.033

Jarusuwannapoom, T., Hongrojjanawiwat, W., Jitjaicham, S., Wannatong, L., Nithitanakul, M., Pattamaprom, C., Koombhongse, P., Rangkupan, R., & Supaphol, P. (2005). Effect of solvents on electro-spinnability of polystyrene solutions and morphological appearance of resulting electrospun polystyrene fibers. *European Polymer Journal*, *41*(3), 409–421. https://doi.org/10.1016/j.eurpolymj.2004.10.010

Jaworek, A. (2007). Micro- and nanoparticle production by electrospraying. *Powder Technology*, *176*(1), 18–35. https://doi.org/10.1016/j.powtec.2007.01.035

Jaworek, A., & Krupa, A. (1999). Classification of the modes of EHD spraying. *Journal of Aerosol Science*, *30*(7), 873–893. https://doi.org/10.1016/S0021-8502(98)00787-3

Jaworek, A., & Sobczyk, A. T. (2008). Electrospraying route to nanotechnology: An overview. *Journal of Electrostatics*, *66*(3–4), 197–219. https://doi.org/10.1016/j.elstat.2007.10.001

Jaworek, A. (2008). Electrostatic micro- and nanoencapsulation and electroemulsification: A brief review. *Journal of Microencapsulation*, *25*(7), 443–468. https://doi.org/10.1080/02652040802049109

Jayasinghe, S. N., & Edirisinghe, M. J. (2002). Effect of viscosity on the size of relics produced by electrostatic atomization. *Journal of Aerosol Science*, *33*(10), 1379–1388. https://doi.org/10.1016/S0021-8502(02)00088-5

Jayasinghe, S. N., & Townsend-Nicholson, A. (2006). Stable electric-field driven cone-jetting of concentrated biosuspensions. *Lab on a Chip*, *6*(8), 1086–1090. https://doi.org/10.1039/b606508m

John, Z. (1917). Instability of liquid surfaces. *Physical Review*, *10*, 1–6. https://doi.org/10.1103/PhysRev.10.1

Kalpna, G., Shalini, V., Jonnalagadda, S., & Neeraj, K. (2007). Fast Degradable Poly(L-lactide-co-e-caprolactone) Microspheres for Tissue Engineering: Synthesis, Characterization, and Degradation Behavior. *Journal of Polymer Science: Part A: Polymer Chemistry*, *45*(April), 2755–2764. https://doi.org/10.1002/pola

K. Moghaddam, M., & Mortazavi, S. M. (2015). Preparation, characterisation and thermal properties of calcium alginate/n-nonadecane microcapsules fabricated by electro-coextrusion for thermo-regulating textiles.

Journal of Microencapsulation, *32*(8), 737–744. https://doi.org/10.3109/02652048.2015.1073388

Kim, W., & Kim, S. S. (2010). Multishell encapsulation using a triple coaxial electrospray system. *Analytical Chemistry*, *82*(11), 4644–4647. https://doi.org/10.1021/ac100278c

Kim, W., & Kim, S. S. (2011). Synthesis of biodegradable triple-layered capsules using a triaxial electrospray method. *Polymer*, *52*(15), 3325–3336. https://doi.org/10.1016/j.polymer.2011.05.033

Labbaf, S., Ghanbar, H., Stride, E., & Edirisinghe, M. (2014). Preparation of multilayered polymeric structures using a novel four-needle coaxial electrohydrodynamic device. *Macromolecular Rapid Communications*, *35*(6), 618–623. https://doi.org/10.1002/marc.201300777

Labet, M., & Thielemans, W. (2009). Synthesis of polycaprolactone: A review. *Chemical Society Reviews*, *38*(12), 3484–3504. https://doi.org/10.1039/b820162p

Langer, G., & Yamate, G. (1969). Encapsulation of liquid and solid aerosol particles to form dry powders. *Journal of Colloid And Interface Science*, *29*(3), 450–455. https://doi.org/10.1016/0021-9797(69)90125-8

Lee, Y. H., Bai, M. Y., & Chen, D. R. (2011). Multidrug encapsulation by coaxial tri-capillary electrospray. *Colloids and Surfaces B: Biointerfaces*, *82*(1), 104–110. https://doi.org/10.1016/j.colsurfb.2010.08.022

Lenggoro, I. W., Okuyama, K., De La Mora, J. F., & Tohge, N. (2000). Preparation of ZnS nanoparticles by electrospray pyrolysis. *Journal of Aerosol Science*, *31*(1), 121–136. https://doi.org/10.1016/S0021-8502(99)00534-0

Lenggoro, I. W., Xia, B., Okuyama, K., & De la Mora, J. F. (2002). Sizing of colloidal nanoparticles by electrospray and differential mobility analyzer methods. *Langmuir*, *18*(12), 4584–4591. https://doi.org/10.1021/la015667t

Li, M., Liu, J., & Shi, J. (2018). Synthesis and properties of phase change microcapsule with SiO2-TiO2 hybrid shell. *Solar Energy*, *167*(March), 158–164. https://doi.org/10.1016/j.solener.2018.04.016

Li, W., Wang, H., & Li, Z. (2019a). Hierarchical structure microspheres of PCL block copolymers via electrospraying as coatings for fabric with mechanical durability and self-cleaning ability. *Polymers for Advanced Technologies*, *30*(9), 2321–2330. https://doi.org/10.1002/pat.4660

Li, W., Wang, H., & Li, Z. (2019b). Preparation of golf ball-shaped microspheres with fluorinated polycaprolactone via single-solvent electrospraying for superhydrophobic coatings. *Progress in Organic Coatings*, *131*(199), 276–284. https://doi.org/10.1016/j.porgcoat.2019.02.039

Li, X., Zhang, K., Shi, R., Ma, X., Tan, L., Ji, Q., & Xia, Y. (2017). Enhanced flame-retardant properties of cellulose fibers by incorporation of acid-resistant magnesium-oxide microcapsules. *Carbohydrate Polymers*, *176*(April), 246–256. https://doi.org/10.1016/j.carbpol.2017.08.096

López-Herrera, J. M., Barrero, A., López, A., Loscertales, I. G., & Márquez, M. (2003). Coaxial jets generated from electrified Taylor cones. Scaling laws. *Journal of Aerosol Science*, *34*(5), 535–552. https://doi.org/10.1016/S0021-8502(03)00021-1

Loscertales, I. G., Barrero, A., Guerrero, I., Cortijo, R., Marquez, M., & Gañán-Calvo, A. M. (2002). Micro/nano encapsulation via electrified coaxial liquid jets. *Science*, *295*(5560), 1695–1698. https://doi.org/10.1126/science.1067595

Luo, C. J., Stride, E., & Edirisinghe, M. (2012). Mapping the influence of solubility and dielectric constant on electrospinning polycaprolactone solutions. *Macromolecules*, *45*(11), 4669–4680. https://doi.org/10.1021/ma300656u

Mai, Z., Chen, J., He, T., Hu, Y., Dong, X., Zhang, H., Huang, W., Ko, F., & Zhou, W. (2017). Electrospray biodegradable microcapsules loaded with curcumin for drug delivery systems with high bioactivity. *RSC Advances*, *7*(3), 1724–1734. https://doi.org/10.1039/c6ra25314h

Marín, Á. G., Loscertales, I. G., Márquez, M., & Barrero, A. (2007). Simple and double emulsions via coaxial jet electrosprays. *Physical Review Letters*, *98*(1), 1–4. https://doi.org/10.1103/PhysRevLett.98.014502

Martin, S., Perea, A., Garcia-Ybarra, P. L., & Castillo, J. L. (2012). Effect of the collector voltage on the stability of the cone-jet mode in electrohydrodynamic spraying. *Journal of Aerosol Science*, *46*, 53–63. https://doi.org/10.1016/j.jaerosci.2011.11.003

Mei, F., & Chen, D. R. (2007). Investigation of compound jet electrospray: Particle encapsulation. *Physics of Fluids*, *19*(10). https://doi.org/10.1063/1.2775976

Mei, F., & Chen, D. R. (2008). Operational modes of dual-capillary electrospraying and the formation of the stable compound cone-jet mod. *Aerosol and Air Quality Research*, *8*(2), 218–232. https://doi.org/10.4209/aaqr.2008.01.0003

Michelson, D., & Richardson, H. O. W. (1963). A note on making thin β-ray sources by electrostatic spraying. *Nuclear Instruments and Methods*, *21*(C), 355. https://doi.org/10.1016/0029-554X(63)90141-1

Midhun, B. T., Shalumon, K. T., Manzoor, K., Jayakumar, R., Nair, S. V., & Deepthy, M. (2011). Preparation

of budesonide-loaded polycaprolactone nanobeads by electrospraying for controlled drug release. *Journal of Biomaterials Science, Polymer Edition*, *22*(18), 2431–2444. https://doi.org/10.1163/092050610X540486

Mochane, M. J., Motsoeneng, T. S., Sadiku, E. R., Mokhena, T. C., & Sefadi, J. S. (2019). Morphology and properties of electrospun PCL and its composites for medical applications: A mini review. *Applied Sciences (Switzerland)*, *9*(11), 1–17. https://doi.org/10.3390/app9112205

Moghaddam, M. K., Mortazavi, S. M., & Khayamian, T. (2015a). Preparation of calcium alginate microcapsules containing n-nonadecane by a melt coaxial electrospray method. *Journal of Electrostatics*, *73*, 56–64. https://doi.org/10.1016/j.elstat.2014.10.013

Moghaddam, M. K., Mortazavi, S. M., & Khaymian, T. (2015b). Micro/nano-encapsulation of a phase change material by coaxial electrospray method. *Iranian Polymer Journal (English Edition)*, *24*(9), 759–774. https://doi.org/10.1007/s13726-015-0364-x

Mohamed, R. M., & Yusoh, K. (2015). A Review on the Recent Research of Polycaprolactone (PCL). *Advanced Materials Research*, *1134*, 249–255. https://doi.org/10.4028/www.scientific.net/amr.1134.249

Mutoh, M., Kaieda, S., & Kamimura, K. (1979). Convergence and disintegration of liquid jets induced by an electrostatic field. *Journal of Applied Physics*, *50*(5), 3174–3179. https://doi.org/10.1063/1.326352

Nelson, G. (2001). Microencapsulation in textile finishing. *Review of Progress in Coloration and Related Topics*, *32*, 57–64. https://doi.org/10.1111/j.1478-4408.2001.tb00138.x

Nguyen, D. N., Clasen, C., & Van den Mooter, G. (2016). Pharmaceutical Applications of Electrospraying. *Journal of Pharmaceutical Sciences*, *105*(9), 2601–2620. https://doi.org/10.1016/j.xphs.2016.04.024

Ostafinska, A., Fortelny, I., Nevoralova, M., Hodan, J., Kredatusova, J., & Slouf, M. (2015). Synergistic effects in mechanical properties of PLA/PCL blends with optimized composition, processing, and morphology. *RSC Advances*, *5*(120), 98971–98982. https://doi.org/10.1039/c5ra21178f

Pareta, R., & Edirisinghe, M. J. (2006). A novel method for the preparation of biodegradable microspheres for protein drug delivery. *Journal of the Royal Society Interface*, *3*(9), 573–582. https://doi.org/10.1098/rsif.2006.0120

Park, I., Kim, W., & Kim, S. S. (2011). Multi-jet mode electrospray for non-conducting fluids using two fluids and a coaxial grooved nozzle. *Aerosol Science and Technology*, *45*(5), 629–634.

https://doi.org/10.1080/02786826.2010.551148

Patrício, T., & Bártolo, P. (2013). Thermal stability of PCL/PLA blends produced by physical blending process. *Procedia Engineering*, *59*, 292–297. https://doi.org/10.1016/j.proeng.2013.05.124

Pham, Q. P., Sharma, U., & Mikos, A. G. (2006). Electrospinning of Polymeric Nanofibers for Tissue Engineering Applications: A Review. *Tissue Engineering*, *12*(5), 1197–1211.

Pothakamury, U. R., & Barbosa-Cánovas, G. V. (1995). Fundamental aspects of controlled release in foods. *Trends in Food Science and Technology*, *6*(12), 397–406. https://doi.org/10.1016/S0924-2244(00)89218-3

Qin, X., & Wu, D. (2012). Effect of different solvents on poly(caprolactone)(PCL) electrospun nonwoven membranes. *Journal of Thermal Analysis and Calorimetry*, *107*(3), 1007–1013. https://doi.org/10.1007/s10973-011-1640-4

Rezwan, K., Chen, Q. Z., Blaker, J. J., & Boccaccini, A. R. (2006). Biodegradable and bioactive porous polymer/inorganic composite scaffolds for bone tissue engineering. *Biomaterials*, *27*(18), 3413–3431. https://doi.org/10.1016/j.biomaterials.2006.01.039

Salaün, F. (2016). Microencapsulation technology for smart textile coatings. In *Active Coatings for Smart Textiles*. https://doi.org/10.1016/B978-0-08-100263-6.00009-5

Salaün, F., Devaux, E., Bourbigot, S., & Rumeau, P. (2009a). Influence of process parameters on microcapsules loaded with n-hexadecane prepared by in situ polymerization. *Chemical Engineering Journal*, *155*(1–2), 457–465. https://doi.org/10.1016/j.cej.2009.07.018

Salaün, F., Devaux, E., Bourbigot, S., & Rumeau, P. (2009b). Application of Contact Angle Measurement to the Manufacture of Textiles Containing Microcapsules. *Textile Research Journal*, *79*(13), 1202–1212. https://doi.org/10.1177/0040517508100724

Salaün, F., Vroman, I., & Aubry, C. (2009). Preparation of double layered shell microparticles containing an acid dye by a melt dispersion-coacervation technique. *Powder Technology*, *192*(3), 375–383. https://doi.org/10.1016/j.powtec.2009.01.018

Saraç, E. G., Öner, E., & Kahraman, M. V. (2019). Microencapsulated organic coconut oil as a natural phase change material for thermo-regulating cellulosic fabrics. *Cellulose*, *26*(16), 8939–8950. https://doi.org/10.1007/s10570-019-02701-9

Sato, M., Kato, S., & Saito, M. (1996). Production of oil/water type uniformly sized droplets using a convergent

AC electric field. *IEEE Transactions on Industry Applications*, *32*(1), 138–145. https://doi.org/10.1109/28.485825

Schneider, A., Uhlenwinkel, V., Harig, H., & Bauckhage, K. (2004). Overspray injection in spray forming of CuSn13.5 billets. *Materials Science and Engineering A*, *383*(1 SPEC. ISS.), 114–121. https://doi.org/10.1016/j.msea.2004.02.038

Sell, S. A., Wolfe, P. S., Garg, K., McCool, J. M., Rodriguez, I. A., & Bowlin, G. L. (2010). The use of natural polymers in tissue engineering: A focus on electrospun extracellular matrix analogues. *Polymers*, *2*(4), 522–553. https://doi.org/10.3390/polym2040522

Shenoy, S. L., Bates, W. D., Frisch, H. L., & Wnek, G. E. (2005). Role of chain entanglements on fiber formation during electrospinning of polymer solutions: Good solvent, non-specific polymer-polymer interaction limit. *Polymer*, *46*(10), 3372–3384. https://doi.org/10.1016/j.polymer.2005.03.011

Shorey, J. D., & Michelson, D. (1970). On the mechanism of electrospraying. *Nuclear Instruments and Methods*, *82*(C), 295–296. https://doi.org/10.1016/0029-554X(70)90368-X

Sill, T. J., & von Recum, H. A. (2008). Electrospinning: Applications in drug delivery and tissue engineering. *Biomaterials*, *29*(13), 1989–2006. https://doi.org/10.1016/j.biomaterials.2008.01.011

Siracusa, V., Rocculi, P., Romani, S., & Rosa, M. D. (2008). Biodegradable polymers for food packaging: a review. *Trends in Food Science and Technology*, *19*(12), 634–643. https://doi.org/10.1016/j.tifs.2008.07.003

Smeets, A., Clasen, C., & Van den Mooter, G. (2017). Electrospraying of polymer solutions: Study of formulation and process parameters. *European Journal of Pharmaceutics and Biopharmaceutics*, *119*, 114–124. https://doi.org/10.1016/j.ejpb.2017.06.010

Smith, D. P. H. (1986). The Electrohydrodynamic Atomization of Liquids. *IEEE Transactions on Industry Applications*, *IA-22*(3), 527–535. https://doi.org/10.1109/TIA.1986.4504754

Sukhorukov, G. B., Rogach, A. L., Garstka, M., Springer, S., Parak, W. J., Muñoz-Javier, A., Kreft, O., Skirtach, A. G., Susha, A. S., Ramaye, Y., Palankar, R., & Winterhalter, M. (2007). Multifunctionalized polymer microcapsules: Novel tools for biological and pharmacological applications. *Small*, *3*(6), 944–955. https://doi.org/10.1002/smll.200600622

Tapia-Hernández, J. A., Torres-Chávez, P. I., Ramírez-Wong, B., Rascón-Chu, A., Plascencia-Jatomea, M.,

Barreras-Urbina, C. G., Rangel-Vázquez, N. A, & Rodríguez-Félix, F. (2015). Micro- and Nanoparticles by Electrospray: Advances and Applications in Foods. *Journal of Agricultural and Food Chemistry*, *63*(19), 4699–4707. https://doi.org/10.1021/acs.jafc.5b01403

Taylor, I. G. (1964). Disintegration of water drops in an electric field. *Proceedings of the Royal Society of London. Series A. Mathematical and Physical Sciences*, *280*(1382), 383–397. https://doi.org/10.1098/rspa.1964.0151

Taylor, I. G. (1969). Electrically driven jets. *Proceedings of the Royal Society of London. A. Mathematical and Physical Sciences*, *313*(1515), 453–475. https://doi.org/10.1098/rspa.1969.0205

Toncheva, A., Spasova, M., Paneva, D., Manolova, N., & Rashkov, I. (2014). Polylactide (PLA)-based electrospun fibrous materials containing ionic drugs as wound dressing materials: A review. *International Journal of Polymeric Materials and Polymeric Biomaterials*, *63*(13), 657–671. https://doi.org/10.1080/00914037.2013.854240

Valo, H., Peltonen, L., Vehviläinen, S., Karjalainen, M., Kostiainen, R., Laaksonen, T., & Hirvonen, J. (2009). Electrospray encapsulation of hydrophilic and hydrophobic drugs in poly(L-lactic acid) nanoparticles. *Small*, *5*(15), 1791–1798. https://doi.org/10.1002/smll.200801907

Vinogradova, O. I. (2004). Mechanical properties of polyelectrolyte multilayer microcapsules. *Journal of Physics Condensed Matter*, *16*(32). https://doi.org/10.1088/0953-8984/16/32/R01

Wang, H., Li, W., & Li, Z. (2018a). A Facile Strategy for Preparing PCL/PEG Block Copolymer Microspheres via Electrospraying as Coatings for Cotton Fabrics. *Macromolecular Materials and Engineering*, *303*(8), 1–12. https://doi.org/10.1002/mame.201800164

Wang, H., Li, W., & Li, Z. (2018b). Preparation of fluorinated PCL porous microspheres and a super-hydrophobic coating on fabrics: Via electrospraying. *Nanoscale*, *10*(39), 18857–18868. https://doi.org/10.1039/c8nr05793a

Wang, K., Wen, H. F., Yu, D. G., Yang, Y., & Zhang, D. F. (2018). Electrosprayed hydrophilic nanocomposites coated with shellac for colon-specific delayed drug delivery. *Materials and Design*, *143*, 248–255. https://doi.org/10.1016/j.matdes.2018.02.016

Wang, Y., Shi, X., Ren, L., Wang, C., & Wang, D. A. (2009). Porous poly (lactic-co-glycolide) microsphere sintered scaffolds for tissue repair applications. *Materials Science and Engineering C*, *29*(8), 2502–2507.

https://doi.org/10.1016/j.msec.2009.07.018

Wang, Y., Tan, M. K., Go, D. B., & Chang, H. C. (2012). Electrospray cone-jet breakup and droplet production for electrolyte solutions (Europhysics Letters (EPL) (2012) 99 (64003)). *Epl*, *100*(2), 2–3. https://doi.org/10.1209/0295-5075/100/29901

Wongsasulak, S., Kit, K. M., McClements, D. J., Yoovidhya, T., & Weiss, J. (2007). The effect of solution properties on the morphology of ultrafine electrospun egg albumen-PEO composite fibers. *Polymer*, *48*(2), 448–457. https://doi.org/10.1016/j.polymer.2006.11.025

Wu, Y. Q., & Clark, R. L. (2007). Controllable porous polymer particles generated by electrospraying. *Journal of Colloid and Interface Science*, *310*(2), 529–535. https://doi.org/10.1016/j.jcis.2007.02.023

Wu, Y., Kennedy, S. J., & Clark, R. L. (2009). Polymeric particle formation through electrospraying at low atmospheric pressure. *Journal of Biomedical Materials Research - Part B Applied Biomaterials*, *90 B*(1), 381–387. https://doi.org/10.1002/jbm.b.31296

Wu, Y., Mackay, J. A., Mcdaniel, J. R., Chilkoti, A., & Clark, R. L. (2009). Fabrication of elastin-like polypeptide nanoparticles for drug delivery by electrospraying. *Biomacromolecules*, *10*(1), 19–24. https://doi.org/10.1021/bm801033f

Wu, Y., Li, L., Mao, Y., & Lee, L. J. (2012). Static micromixer-coaxial electrospray synthesis of theranostic lipoplexes. *ACS Nano*, *6*(3), 2245–2252. https://doi.org/10.1021/nn204300s

Xie, J., Jiang, J., Davoodi, P., Srinivasan, M. P., & Wang, C. H. (2015). Electrohydrodynamic atomization: A two-decade effort to produce and process micro-/nanoparticulate materials. *Chemical Engineering Science*, *125*, 32–57. https://doi.org/10.1016/j.ces.2014.08.061

Xie, J., Lim, L. K., Phua, Y., Hua, J., & Wang, C. H. (2006). Electrohydrodynamic atomization for biodegradable polymeric particle production. *Journal of Colloid and Interface Science*, *302*(1), 103–112. https://doi.org/10.1016/j.jcis.2006.06.037

Xie, J., Marijnissen, J. C. M., & Wang, C. H. (2006). Microparticles developed by electrohydrodynamic atomization for the local delivery of anticancer drug to treat C6 glioma in vitro. *Biomaterials*, *27*(17), 3321–3332. https://doi.org/10.1016/j.biomaterials.2006.01.034

Xie, J., Ng, W. J., Lee, L. Y., & Wang, C. H. (2008). Encapsulation of protein drugs in biodegradable microparticles by co-axial electrospray. *Journal of Colloid and Interface Science*, *317*(2), 469–476.

https://doi.org/10.1016/j.jcis.2007.09.082

Xu, Y., & Hanna, M. A. (2008). Morphological and structural properties of two-phase coaxial jet electrosprayed BSA-PLA capsules. *Journal of Microencapsulation*, *25*(7), 469–477. https://doi.org/10.1080/02652040802049513

Yao, J., Kuang Lim, L., Xie, J., Hua, J., & Wang, C. H. (2008). Characterization of electrospraying process for polymeric particle fabrication. *Journal of Aerosol Science*, *39*(11), 987–1002. https://doi.org/10.1016/j.jaerosci.2008.07.003

Yuan, W. J., Wang, Y. P., Li, W., Wang, J. P., Zhang, X. X., & Zhang, Y. K. (2015). Microencapsulation and characterization of polyamic acid microcapsules containing n-octadecane via electrospraying method. *Materials Express*, *5*(6), 480–488. https://doi.org/10.1166/mex.2015.1268

Yunoki, A., Tsuchiya, E., Fukui, Y., Fujii, A., & Maruyama, T. (2014). Preparation of inorganic/organic polymer hybrid microcapsules with high encapsulation efficiency by an electrospray technique. *ACS Applied Materials and Interfaces*, *6*(15), 11973–11979. https://doi.org/10.1021/am503030c

Zhang, L., Huang, J., Si, T., & Xu, R. X. (2012). Coaxial electrospray of microparticles and nanoparticles for biomedical applications. *Expert Review of Medical Devices*, *9*(6), 595–612. https://doi.org/10.1586/erd.12.58

Zhang, S., Campagne, C., & Salaün, F. (2019a). Influence of solvent selection in the electrospraying process of polycaprolactone. *Applied Sciences (Switzerland)*, *9*(3). https://doi.org/10.3390/app9030402

Zhang, S., Campagne, C., & Salaün, F. (2019b). Preparation of Electrosprayed Poly(caprolactone) Microparticles Based on Green Solvents and Related Investigations on the Effects of Solution Properties as Well as Operating Parameters. *Coatings*, *9*(2), 84. https://doi.org/10.3390/coatings9020084

Zhang, S., Campagne, C., & Salaün, F. (2020). Preparation of n -Alkane / Polycaprolactone Phase-Change Microcapsules via Single Nozzle Electro-Spraying : Characterization on Their Formation , Structures and Properties. *Applied Sciences*, *10*(2), 561-580. http://dx.doi.org/10.3390/app10020561

Zhang, S., Chen, Y., Campagne, C., & Salaün, F. (2020). Influence of a Coaxial Electrospraying System on the n-Hexadecane / Polycaprolactone Phase Change Microcapsules Properties. *Materials*, *13*(9), 2205-2221. http://dx.doi.org/10.3390/ma13092205

Zhao, L., Duan, G., Zhang, G., Yang, H., Jiang, S., & He, S. (2020). Electrospun functional materials toward

food packaging applications: A review. *Nanomaterials*, *10*(1), 1–31. https://doi.org/10.3390/nano10010150

Zhou, F., Cristinacce, P. L. H., Eichhorn, S. J., & Paker, G. J. M. (2016). Preparation and characterization of polycaprolactone microspheres by electrospraying. *Aerosol Sci. Technol.*, *370*, 28–34.

Zuckerman, J. L., Pushaw, R. J., Perry, B. T., & Wyner, D. M. (2001). Fabric coating composition containing energy absorbing phase change material. *United States Patent, Patent No: US20010000517A1*

Chapter 2 Materials and Experimental Method

In this chapter, the raw materials including the shell materials (PCL and PLA), core materials (n-alkanes) and solvents are described. Meanwhile, the electrospraying device and the related preparation process of microspheres (PCL and PLA) and microcapsules (n-alkanes/PCL, n-alkane/PLA and n-alkane/PLA/PCL with double-layered shells) are also presented. In addition, all methods used in this study for characterizing and analyzing the structures, morphologies and thermal properties of all samples are also introduced in detail.

2.1 Raw materials

2.1.1 Shell materials

Polycaprolactone (PCL) (CapaTM 6400, number average molecular weight: 37,000 g/mol) was purchased from Perstorp (Skåne County, Sweden). Poly(lactic acid) (PLA) (INGEO 6202D, number average molecular weight: 58300 g/mol, D-Isomer: 1.3 %) was purchased from Cargill-Dow (Midland, MI, United States).

2.1.2 Core materials

n-hexadecane (C16-parafol 16-97), and n-eicosane (C20-parafol 20z) used as phase change materials were obtained from Sasol Germany Gmbh (Hamburg, Germany). The melting range of raw n-hexadecane is from 17.9 to 23.7 °C with a latent heat of 199.4 ± 2.2 J/g, and the freezing range of raw n-hexadecane is from 16.2 to 13.0 °C with a latent heat of 195.9 ± 4.7 J/g. The melting range of raw n-eicosane is from 34.3 to 39.2 °C with a latent heat of 205.3 ± 1.7 J/g, and the freezing range of raw n-hexadecane is from 35.7 to 28.7 °C with a latent heat of 204.2 ± 1.9 J/g.

2.1.3 Solvent systems

Chloroform (analytical reagent, surface tension: 27.1 mN/m, electrical conductivity: <1x10-6 μS/cm, viscosity: 0.563 mPa·s, boiling point: 61.3 °C), ethyl acetate (analytical reagent, surface tension: 23.5 mN/m, electrical conductivity: 3.0x10-5 μS/cm, viscosity: 0.441 mPa·s, boiling point: 77.2 °C), anisole (analytical

reagent surface tension:35.0 mN/m, electrical conductivity: 8.6x10-5 μS/cm, viscosity: 0.778 mPa·s (30°C), boiling point: 154.0 °C), acetone (analytical reagent surface tension: 23.7 mN/m, electrical conductivity: 5.8x10-4 μS/cm, viscosity: 0.316 mPa·s, boiling point: 56.5 °C) and glacial acetic acid (analytical reagent, surface tension: 31.9 mN/m, electrical conductivity: 6.0x10-5 μS/cm, viscosity: 1.040 mPa·s (30°C), boiling point: 118.1 °C) were purchased from Sigma Aldrich (Lyon, France). All solution properties were measured under 25 °C. All reagents were used as received without any further treatment.

2.2 Electrospraying device

The experimental set-up of electrospraying (CAT000002, Electrospraying Instrument Kit Instruction Manual, Spraybase®, AVECATS, Kildare, Ireland) used to produce a series of microparticles. It consists of two syringe pumps connected with computer and controlled via software, a voltage generator, a stainless steel nozzle linked to voltage generator, a high-speed camera (Chameleon CMLN-13S2M-CS USB camera, FLIR Integrated Imaging Solutions GmbH, Ludwigsburg, Germany) connected with computer, a light source and a grounded collector. In general, working solution is pumped into plastic syringe, then squeezed into the plastic tube, and finally to the nozzle. The flow rate of working solution is controlled by syringe pumps and the working distance between nozzle and collector is adjusted via movable support. Two stainless steel single nozzles (28 gauge, outer diameter: 360 μm, internal diameter: 180 μm; 26 gauge, outer diameter: 460 μm, inner diameter: 260 μm) were used for single nozzle electrospraying. A stainless steel coaxial nozzle with two capillaries (inner capillary: 28 gauge, inner and outer diameters of 180 and 360 μm, respectively; outer capillary: 20 gauge, inner and outer diameters of 600 and 910 μm, respectively) was used for coaxial nozzle electrospraying.

2.3 Sample preparation

2.3.1 Preparation of PCL electrospraying solutions based different solvents

In order to seek a green and suitable solvent system as the carrier of electrospraying PCL and investigate the effect of solution properties (surface tension, electrical conductivity, viscosity and vapor pressure) and operating parameters (flow rate, working distance and applied voltage) on the formation of electrosprayed particles (including the formation of stable Taylor cone, the mean diameter, size distribution and surface morphology), four

green solvents (anisole, acetone, ethyl acetate and acetic acid) and chloroform are used for dissolving PCL to obtain a series of electrospraying solutions.

Table 2-1 The formation operating parameters of a series of PCL solutions with different PCL concentrations based on different solvent systems.

Sample label	Solvent system	PCL concentration (wt%)	Applied voltage (kV)	Dripping time for one single droplet (s)	Working distance (cm)
1 wt%-chlorofrom	chloroform	0.1 g in 10 g chloroform	3.75	5	17
3 wt%-chlorofrom	chloroform	0.3 g in 10 g chloroform	3.75	5	17
5 wt%-chlorofrom	chloroform	0.5 g in 10 g chloroform	2~7	118, 9, 5, 4, 3	9, 13, 17, 21, 25
7 wt%-chlorofrom	chloroform	0.7 g in 10 g chloroform	3.75	5	
10 wt%-chlorofrom	chloroform	1.0 g in 10 g chloroform	3.75	5	
1 wt%-ethyl acetate	ethyl acetate	0.1 g in 10 g ethyl acetate	3.75	5	
3 wt%-ethyl acetate	ethyl acetate	0.3 g in 10 g ethyl acetate	3.75	5	
5 wt%-ethyl acetate	ethyl acetate	0.5 g in 10 g ethyl acetate	2~7	115, 9, 5, 4, 3	9, 13, 17, 21, 25
7 wt%-ethyl acetate	ethyl acetate	0.7 g in 10 g ethyl acetate	3.75	5	
10 wt%-ethyl acetate	ethyl acetate	1.0 g in 10 g ethyl acetate	3.75	5	
1 wt%-acetic acid	acetic acid	0.1 g in 10 g acetic acid	5.25	5	
3 wt%-acetic acid	acetic acid	0.3 g in 10 g acetic acid	5.25	5	
5 wt%-acetic acid	acetic acid	0.5 g in 10 g acetic acid	2~7	104, 9, 5, 4, 3	9, 13, 17, 21, 25
7 wt%-acetic acid	acetic acid	0.7 g in 10 g acetic acid	5.25	5	
10 wt%-acetic acid	acetic acid	1.0 g in 10 g acetic acid	5.25	5	
1 wt%-acetone	acetone	0.1 g in 10 g acetone	4.75	5	
3 wt%-acetone	acetone	0.3 g in 10 g acetone	4.75	5	
5 wt%-acetone	acetone	0.5 g in 10 g acetone	2~7	62, 9, 5, 4, 3	9, 13, 17, 21, 25
7 wt%-acetone	acetone	0.7 g in 10 g acetone	4.75	5	
10 wt%-acetone	acetone	1.0 g in 10 g acetone	4.75	5	
1 wt%-anisole	anisole	0.1 g in 10 g anisole	3.75	93	
3 wt%-anisole	anisole	0.3 g in 10 g anisole	3.75	93	
5 wt%-anisole	anisole	0.5 g in 10 g anisole	2~7	129, 104, 93, 67, 45	9, 13, 17, 21, 25
7 wt%-anisole	anisole	0.7 g in 10 g anisole	3.75	93	
10 wt%-anisole	anisole	1.0 g in 10 g anisole	3.75	93	

A series PCL electrospraying solutions were prepared by dissolving appropriate quantities of PCL pellets in each of five solvents (chloroform, ethyl acetate, anisole, acetone, and acetic acid) at 40 ◦C with stirring for 1 h to

allow complete dissolution. For each solvent, five PCL concentrations (1, 3, 5, 7 and 10 wt%) were prepared. Before electrospraying, each solution was cooled to room temperature (25 ◦C). The formation of all PCL electrospraying solutions with different concentrations based on different solvent systems is listed in Table 2-1.

2.3.2 Preparation of paraffin wax/PCL electrospaying solutions

n-hexadecane, in liquid state, and n-eicosane, in solid state, at room temperature are selected as PCMs. A series of n-hexadecane/PCL or n-eicosane/PCL electrospraying solutions with different weight ratios, PCMs to PCL, were prepared from the solubilization of PCL in ethyl acetate (EA) or chloroform (Chl) (10 w/v%) at 40 ◦C under vigorous magnetic stirring during 1 h. The required weight of n-hexadecane or n-eicosane was subsequently added to achieve final PCMs/PCL weight ratios of 0/100, 30/70, 50/50, and 70/30, under continuous agitation during 2 h. The formation of a series of n-alkane/PCL solutions is listed in Table 2-2

Table 2-2 The formation of a series of n-alkanes/PCL solutions with different PCMs and different PCMs/PCL weight ratios based on different solvent systems.

Sample label	Solvent system	PCL concentration (w/v%)	n-alkane addition (g)
n-hexadecane/PCL (00/100)-Chl	Chloroform	1.0 g in 10 mL chloroform	0.0
n-hexadecane/PCL (30/70)-Chl	Chloroform	1.0 g in 10 mL chloroform	0.43
n-hexadecane/PCL (50/50)-Chl	Chloroform	1.0 g in 10 mL chloroform	1.0
n-hexadecane/PCL (70/30)-Chl	Chloroform	1.0 g in 10 mL chloroform	2.33
n-hexadecane/PCL (00/100)-EA	Ethyl acetate	1.0 g in 10 mL ethyl acetate	0.0
n-hexadecane/PCL (30/70)-EA	Ethyl acetate	1.0 g in 10 mL ethyl acetate	0.43
n-hexadecane/PCL (50/50)-EA	Ethyl acetate	1.0 g in 10 mL ethyl acetate	1.0
n-hexadecane/PCL (70/30)-EA	Ethyl acetate	1.0 g in 10 mL ethyl acetate	2.33
n-eicosane/PCL (30/70)-Chl	Chloroform	1.0 g in 10 mL chloroform	0.43
n-eicosane/PCL (50/50)-Chl	Chloroform	1.0 g in 10 mL chloroform	1.0
n-eicosane/PCL (70/30)-Chl	Chloroform	1.0 g in 10 mL chloroform	2.33
n-eicosane/PCL (30/70)-EA	Ethyl acetate	1.0 g in 10 mL ethyl acetate	0.43
n-eicosane/PCL (50/50)-EA	Ethyl acetate	1.0 g in 10 mL ethyl acetate	1.0
n-eicosane/PCL (70/30)-EA	Ethyl acetate	1.0 g in 10 mL ethyl acetate	2.33

2.3.3 Preparation of n-hexadecane/PLA electrospraying solutions

PLA solutions with two concentrations (3 w/v% and 5 w/v%) were prepared from the solubilization of special weight PLA in chloroform at 40°C under magnetic stirring (1000 rpm), equipped with a water-jacketed reflux condenser during 1 hour. Then, the required weight of n-hexadecane was subsequently added to achieve final PCMs/PLA weight ratios of 0/100, 30/70, 50/50, and 70/30, under continuous agitation during 2 h to obtain a homogenous solution. The formation of a series of n-hexadecane/PLA solutions is listed in Table 2-3.

Table 2-3 The formation of a series of n-alkanes/PLA solutions with different PCMs/PLA weight ratios based on different PLA concentrations.

Sample label	PLA concentration (w/v%)	n-hexadecane addition (g)
n-hexadecane00-PLA100-3 w/v%	0.3 g in 10 mL chloroform	0.0
n-hexadecane30-PLA70-3 w/v%	0.3 g in 10 mL chloroform	0.13
n-hexadecane50-PLA50-3 w/v%	0.3 g in 10 mL chloroform	0.30
n-hexadecane70-PLA30-3 w/v%	0.3 g in 10 mL chloroform	0.70
n-hexadecane00-PLA100-5 w/v%	0.5 g in 10 mL chloroform	0.0
n-hexadecane30-PLA70-5 w/v%	0.5 g in 10 mL chloroform	0.21
n-hexadecane50-PLA50-5 w/v%	0.5 g in 10 mL chloroform	0.50
n-hexadecane70-PLA30-5 w/v%	0.5 g in 10 mL chloroform	1.17

When preparing n-hexadecane/PLA/PCL microcapsules with different n-hexadecane additions, neat PCL/chloroform solution was used as outer liquid and a series of n-hexadecane/PLA/chloroform were used as inner liquids. Not only the concentration of PCL or PLA in chloroform was kept at 5 w/v%, but also the weight fraction of PLA component was equal to that of PCL component. Then, the required weight of n-hexadecane was subsequently added in PLA solution to achieve four PCL/PLA/PCMs weight ratios, including 50/50/0, 35/35/30, 25/25/50, 15/15/70, under continuous agitation during 2 h to obtain a homogenous solution. The solution formations used for a series of n-hexadecane/PLA/PCL microcapsules with different n-hexadecane addtions are listed in Table 2-4.

Table 2-4 The solution formations used for a series of n-hexadecane/PLA/PCL microcapsules with different n-hexadecane addtions.

Sample label	PCL concentration in outer liquid (w/v%)	PLA concentration in inner liquid (w/v%)	n-hexadecane addition in inner liquid (g)
PLA50/PCL50	0.5g in 10 mL chloroform	0.5g in 10 mL chloroform	0.0
n-hexadecane30-PLA35-PCL35	0.5g in 10 mL chloroform	0.5g in 10 mL chloroform	0.43
n-hexadecane50-PLA25-PCL25	0.5g in 10 mL chloroform	0.5g in 10 mL chloroform	1.0
n-hexadecane70-PLA15-PCL15	0.5g in 10 mL chloroform	0.5g in 10 mL chloroform	2.33

2.3.4 The single nozzle electrospraying process of a series of electrospraying solutions

During electrospraying, temperature and relative humidity were maintained at 25 ◦C and 45%, respectively. For the methods for controlling the flow rate of working solution, air pressure was used for facricating neat PCL micorparticles based different solvents as well as different operating parameters, syringe pump connected with computer was used for preparing a series of n-alkanes/PCL, n-alkanes/PLA and n-alkanes/PLA/PCL microcapsules. In order to investigate the effects of operating parameters on the formation of electrosprayed particles (including the formation of stable Taylor cone, the mean diameter, size distribution and surface morphology), different operating parameters (including applied voltage, flow rate and working distance) were set to prepare neat PCL microparticles based on different solvent systems as listed in Table 2-1. Firstly, a series of PCL solutions were added into an electrospraying pressure vessel, and a plastic tube was used to link a stainless steel nozzle (28 gauge, outer diameter: 360 μm, internal diameter: 180 μm) and pressure vessel. Then, the liquid was pumped from vessel to nozzle by air pressure. Meanwhile, the flow rate of electrospraying solutions was characterized by the dripping time for one single droplet from nozzle. The same dripping time for one single droplet from the nozzle indicates that the flow rate of PCL solutions is consistent. In most cases, for PCL/chloroform, PCL/glacial acetic acid, PCL/ethyl acetate and PCL/acetone, the dripping time for one single droplet was fixed at 5 s; for PCL/anisole, the dripping time for one single droplet was fixed at 93 s. Different dripping times for one single droplet can be obtained via adjusting the air pressure. The working distance from nozzle to collector was set to 9, 13, 17, 21 or 25 cm. After setting dripping time and working distance, high voltage generated from a high-voltage generator was applied between the nozzle and collector ranging from 2 to 7 kV.

The electrosprayed microparticles were collected onto glass slides for optical microscopy observation and aluminum foil for scanning electron microscopy analysis, with a collecting time of 3 and 10 min, respectively.

For fabricating n-alkanes/PCL and n-alkanes/PLA microcapsules from single nozzle electrospraying, firstly, the working solutions listed in Table 2-2 and Table 2-3 were added into 10 mL plastic syringe, and then were pumped with a digitally controlled syringe pump at a flow-rate of 1 mL/h through a single stainless steel nozzle (26 gauge, single nozzle, outer diameter: 460 μm, inner diameter: 260 μm). Then, the applied voltage between nozzle and collector was set at 4.0 kV for n-alkanes/PCL working solutions and at 7.25 kV for n-alkane/PLA working solutions. The working distance between the tip of nozzle and collector was set as 17 cm. Samples were collected on a grounded copper plate covered with aluminum foil for SEM analyses, with glass slides for OM analyses and metal dish for the other characterizations, with a collecting time of 10, 3, and 300 min, respectively.

2.3.5 The coaxial nozzle electrospraying process of a series of electrospraying solutions

In order to further improve the encapsulation efficiency as well as loading content of n-alkane in PCL matrix during electrospraying, coaxial nozzle electrospraying was used to fabricate a series of n-hexadecane/PCL microcapsules. Meanwhile, the effects of nozzle geometries (single nozzle or coaxial nozzle) on the structure, morphologies and properties of final n-hexadecane/PCL microcapsules were studied via comparing the results obtained from coaxial nozzle electrospraying with the results obtained from single nozzle electrospraying.

Raw n-hexadecane liquid was used as the core liquid. A series of PCL electrospraying solutions at different concentrations (5 and 10 w/v %) as shell liquid, were prepared using chloroform at 40 ◦C under vigorous magnetic stirring equipped with a water-jacketed reflux condenser for 1 h. Before their uses, they were cooled to room temperature. A stainless-steel coaxial nozzle with two capillaries (inner capillary: 28 gauge, inner and outer diameters of 180 and 360 μm, respectively; outer capillary: 20 gauge, inner and outer diameters of 600 and 910 μm, respectively) was used. Raw n-hexadecane liquid and PCL/chloroform solutions with different concentrations were injected into the inner and outer capillaries, respectively. The flow rates of the core or shell solutions were controlled by the syringe pump connected to a computer, and different theoretical weight ratios between n-hexadecane and PCL (00/100, 30/70, 50/50, and 70/30 by weight) were achieved by changing the feed ratio between the core and shell liquids (Table 2-5). The applied voltage between the nozzle and collector was set at 8.25 kV. Samples were collected on a grounded copper plate covered with glass slides and an aluminum foil for

OM and SEM analyses, respectively, and with a metal dish for the other characterization. The collection times were adjusted to 3, 10, and 300 min, respectively. All the containers were placed at 17 cm from the tip of the nozzle, and during the various experiments, temperature and relative humidity were kept constant at 25 °C and 45%, respectively.

Table 2-5 Solutions and process flow rates used for a series of n-hexadecane/PCL mPCMs synthesis.

Sample label	PCL concentration (w/v%)	Shell flow rate (mL/h)	Core flow rate (mL/h)
n-hexadecane$_{00}$-PCL$_{100}$-5	5	1.00	0.00
n-hexadecane$_{30}$-PCL$_{70}$-5	5	1.00	0.03
n-hexadecane$_{50}$-PCL$_{50}$-5	5	1.00	0.07
n-hexadecane$_{70}$-PCL$_{30}$-5	5	1.00	0.17
n-hexadecane$_{00}$-PCL$_{100}$-10	10	1.00	0.00
n-hexadecane$_{30}$-PCL$_{70}$-10	10	1.00	0.06
n-hexadecane$_{50}$-PCL$_{50}$-10	10	1.00	0.14
n-hexadecane$_{70}$-PCL$_{30}$-10	10	1.00	0.33

For fabricating a series of n-hexadecane/PLA/PCL with different n-hexadecane additions (30 wt%, 50 wt% and 70 wt%), 5 w/v% PCL/chloroform solution was used as outer liquid, and a series n-hexadecane/PLA/chloroform solutions with different n-hexadecane additions were used as inner liquid (Table 1-4). The flow rates of core liquid and shell liquid were fixed at 0.5 mL/h. Meanwhile, for preparing a series of n-hexadecane/PLA/PCL microcapsules with different weight fractions between PLA component and PCL component, the addition of n-hexadecane was fixed at 50 wt%. And n-hexadecane/PLA/PCL microcapsules with different weight fractions between PLA component and PCL component can be obtained via adjusting the flow rate of inner liquid as well as outer liquid and the addition of n-hexadecane (Table 2-6). The applied voltage between the nozzle and collector was set at 9.25 kV, and the working distance between the tip of nozzle and collector was set as 17 cm. Samples were collected on a grounded copper plate covered with aluminum foil for SEM analyses, with glass slides for OM analyses and metal dish for the other characterizations, with a collecting time of 10, 3, and 300 min, respectively.

Table 2-6 Solutions and process flow rates used for the n-hexadecane/PLA/PCL mPCMs with different weight fractions between PLA component and PCL component synthesis.

Sample lable[a]	PCL concentration (w/v%)	PLA concentration (w/v%)	n-hexadecane (g)	Flow rate of inner liquid (mL/h)	Flow rate of outer liquid (mL/h)
n-hexadecane50-PLA40-PCL10	0.5 g in 10 mL chloroform	0.5 g in 10 mL chloroform	0.625	0.8	0.2
n-hexadecane50-PLA30-PCL20	0.5 g in 10 mL chloroform	0.5 g in 10 mL chloroform	0.833	0.6	0.4
n-hexadecane50-PLA25-PCL25	0.5 g in 10 mL chloroform	0.5 g in 10 mL chloroform	1.0	0.5	0.5
n-hexadecane50-PLA20-PCL30	0.5 g in 10 mL chloroform	0.5 g in 10 mL chloroform	1.25	0.4	0.6
n-hexadecane50-PLA10-PCL40	0.5 g in 10 mL chloroform	0.5 g in 10 mL chloroform	2.50	0.2	0.8

2.4 Characterization methods

2.4.1 Solution properties of electrospraying solutions

2.4.1.1 Surface tension

The surface tension (γ, mN/m) of working solutions were measured by Standard Wilhelmy's plate method based on a tensiometer from GBX Instruments (France). The temperature and humidity of measurement were maintained at 25 ºC and 45 %, respectively. The vessel was washed with detergent, placed in chromosulfuric acid overnight, washed with distilled water, and briefly flamed with a Bunsen burner prior to use. The platinum plate was rinsed in acetone and distilled water, and flamed before use. The accuracy of measurement was ±0.1 mN/m. The measurements were taken five times for each sample, and the mean values were considered for analysis.

2.4.1.2 Electrical conductivity

The electrical conductivities (K, unit: μS/cm) of electrospraying solutions were measured with a

conductimeter type CDRV 62 (Tacussel electronique Instruments, Lyon, France). For each working solution, electrical conductivity measurements were repeated 5 times per sample and each sample was prepared in triplicate. The average values and standard deviations were calculated. The temperature and humidity of measurement were maintained at 25 °C and 45%, respectively.

2.4.1.3 Kinematic viscosity

The kinematic viscosity (ν, unit: mm2/s) of electrospraying electrospraying solutions were measured by Ubbelohde viscometer (SI Analytics, Mainz, Germany). For each sample, the flow time (t) in seconds was recorded, and kinematic viscosity was calculated from Equation (2-1):

$$\nu = \alpha \times t \quad (2\text{-}1)$$

where, t is the time in s, and α the instrument constant related with the type of capillary. Two Ubbelohde viscometers with different capillaries were used according to the viscosity range of the solutions. For 0.84 mm capillary, α is 0.03; for 0.47 mm capillary, α is 0.003. For each working solution, kinematic viscosity measurements were repeated 5 times per sample and each sample was prepared in triplicate. The average values and standard deviations were calculated. The temperature of measurement was controlled at 25.0 ◦C by a thermostatic water-circulator bath.

2.4.2 Characterization of mean diameter, size distribution, surface morphologies of electrosprayed microarticles

2.4.2.1 optical microscopy (OM)

The size and size distribution of electrosprayed microparticles were observed via optical microscopy (Motic BA410, Barcelona, Spain) linking with a Moticam 5 Digital Camera (Barcelona, Spain). The software Motic image plus 3.0 was used to capture the images, and the image analysis software (Image J, version 1.52j) was used to determine the mean diameter and sizes distribution. In order to obtain accurate results, 100–500 random electrosprayed microparticles were selected to be measured and analyzed.

2.4.2.2 scanning electron microscopy (SEM)

Scanning electron microscopy was conducted on an Inspect F50 (FEI Company, Hillsboro, OR, USA) at an

accelerating voltage of 20 kV. The accelerated voltage was 20 KV. The surfaces of PCL microparticles were coated with gold before analysis. The SEM images are also analyzed by image analysis software (Image J, version 1.52j) to determine the mean diameter as well as the particle size distribution

2.4.3 Thermal properties of electrosprayed microparticles and raw paraffin waxes

2.4.3.1 Differential scanning calorimetry (DSC)

The thermal behavior of all the samples was studied via DSC with TGA/DSC 3 + (Mettler Toledo, USA), piloted on PC with STARe software, under constant nitrogen flow (50ml/min). 3-8 mg of each sample was placed in a hermetically sealed aluminum pan, and the heating or cooling rate was set about 10 °C/min. The sample space was purged with nitrogen flow during the experiments. The thermal scanning procedure was adjusted according to the type of sample tested. For raw n-hexadecane, raw n-eicosane, neat PCL microparticles and a series of n-alkanes/PCL microcapsules, in order to erase any previous thermal history of these substance, the scanning procedure involved initial heating from -30 to 70 °C, followed by an isothermal step at 70 °C for 10min. The sample was then cooled to -30 °C, before repeating the temperature scan in the heating and cooling range between -30 °C and 70 °C as the second cycle, in which the onset temperatures of solid-liquid and liquid-solid transitions (T_{onset}), end temperatures of phase transitions (T_{end}), and maximum temperatures of melting (T_m) and crystallization (T_c), as well as melting (ΔH_m) and crystallization (ΔH_C) enthalpies of each transitions were determined. Each test was conducted twice, and carried out with a least three independent experiments.

The crystallinity indexes (X_c) of the PCL matrix in the electrosprayed n-alkane/PCL mPCMs (including measured ($X_{c(m)}$) and theoretical ($X_{c(th)}$)) were obtained from Equations (2-2) and (2-3),

$$X_{c(m)} = \frac{\Delta H_{m\ (PCL\ phase\ in\ mPCMs)}}{\Delta H^0_{m(PCL)}(1 - w_{m\ (m)-PCMs})} \times 100 \quad (2\text{-}2)$$

$$X_{c(th)} = \frac{\Delta H_{m\ (PCL\ phase\ in\ mPCMs)}}{\Delta H^0_{m(PCL)}(1 - w_{m\ (th)-PCMs})} \times 100 \quad (2\text{-}3)$$

Where, the indices m and th represent the measured and theoretical weight, ΔHm is the specific melting heat, $\Delta H^0_{m(PCL)}$ is the theoretical specific heat of 100% crystalline PCL, which was taken as 139.5 J/g (Zhang, Campagne, & Salaün, 2020), and $w_{m(m)\text{-}PCMs}$ was the weight fraction of PCMs in the samples and $w_{m(th)\text{-}PCMs}$ was the theoretical addition of PCMs in the samples

For neat PLA, n-hexadecane/PLA, PLA/PCL and n-hexadecane/PLA/PCL electrosprayed particles, the

thermal behavior was recorded during three cycles. The first one was conducted up to 70 °C to erase the thermal history of the PCMs sample (n-hexadecane), and after an isothermal step during 10 min, cooled to -30°C to study the crystallization behavior of n-hexadecane (ΔH_c, T_{onset}, T_c and T_{end}). The second one was conducted up to 120 °C to investigate the melting behavior of n-hexadecane (ΔH_m, T_{onset}, T_m and T_{end}), the melting of PCL shell (ΔH_m, T_{onset}, T_m and T_{end}) as well as the PLA glass transition (T_g) and cold crystallization ($T_{cc\text{-}onset}$, $T_{cc\text{-}max}$ and $T_{cc\text{-}end}$). After cooled the system to -30°C to investigate the crystallization behavior of PCL shell (ΔH_c, T_{onset}, T_c and T_{end}), the third one was realized up to 200°C, and after an isothermal step during 10 min, cooled to -30°C to study the PLA shell melting (T_{onset}, T_m, T_{end} and ΔH_m) and crystallization behaviors (T_{onset}, T_c, Tend and ΔH_c).

For n-hexadecane/PLA electrosprayed particles, the theoretical crystallinity degree ($X_{c(th)}$) and measured crystallinity degree ($X_{c(m)}$) of the PLA matrix were obtained from Equation (2-4) and Equation (2-5) respectively.

$$X_{c(th)} = \frac{\Delta H_{m(PLA\ phase\ in\ mPCMs)}}{\Delta H^0_{m(PLA)} \times (1 - w_{m(th)-\mathrm{PCMs}})} \times 100 \quad (2\text{-}4)$$

$$X_{c(m)} = \frac{\Delta H_{m(PLA\ phase\ in\ mPCMs)}}{\Delta H^0_{m(PLA)} \times (1 - w_{m(m)-\mathrm{PCMs}})} \times 100 \quad (2\text{-}5)$$

Where, $\Delta H_{m(PLA\ phase\ in\ mPCMs)}$ is the melting enthalpy of PLA, $\Delta H^0_{m(PLA)}$ is the melting enthalpy of 100% crystalline PLA, which was taken as 93.6 J/g (Xiong et al., 2013) and $w_{m(m)\text{-}PCMs}$ was the measured weight fraction of n-hexadecane in mPCMs, and $w_{m(th)\text{-}PCMs}$ was the theoretical addition of n-hexadecane in samples.

The relative cold crystallization enthalpy ($\Delta H_{cc(r)}$) of PLA matrix in n-hexadecane/PLA microcapsules was calculated from Equation (2-6)

$$\Delta H_{cc(r)} = \frac{\Delta H_{cc}}{(1 - w_{m(m)-\mathrm{PCMs}})} \quad (2\text{-}6)$$

Where, (ΔH_{cc}) (J/g) was the measured cold crystallization enthalpy of PLA matrix, and $w_{m(m)\text{-}PCMs}$ was the measured weight fraction of n-hexadecane in n-hexadecane/PLA microparticles.

For PLA/PCL and n-hexadecane/PLA/PCL electrosprated microparticles, the theoretical crystallinity index ($X_{c(th)\text{-}PCL}$) and measured crystallinity index ($X_{c(m)\text{-}PCL}$) of the PCL component in the final samples were obtained from Equations (2-7) and (2-8)

$$X_{c(th)-PCL} = \frac{\Delta H_{m(PCL\ phase\ in\ mPCMs)}}{\Delta H^0_{m(PCL)}(1 - w_{m(th)-PCMs}) \times \theta_{PCL}} \times 100 \quad (2\text{-}7)$$

$$X_{c(m)-PCL} = \frac{\Delta H_{m(PCL\ phase\ in\ mPCMs)}}{\Delta H^0_{m(PCL)}(1 - w_{m(m)-PCMs}) \times \theta_{PCL}} \times 100 \quad (2\text{-}8)$$

Where $w_{m(th)\text{-}PCMs}$ was the theoretical weight fraction of n-hexadecane in mPCMs, $w_{m(m)\text{-}PCMs}$ was the measured weight fraction of n-hexadecane in mPCMs and θ_{PCL} was the theoretical weight fraction of PCL

component in PLA and PCL mixture.

The theoretical crystallinity index ($X_{c(th)\text{-}PLA}$) and measured crystallinity index ($X_{c(m)\text{-}PLA}$) of the PLA component in the final mPCMs were obtained from Equations (2-9) and (2-10)

$$X_{c(th)-PLA} = \frac{\Delta H_{m(PCL\ phase\ in\ mPCMs)}}{\Delta H^{0}_{m(PCL)}(1-w_{m(th)-PCMs})\times\theta_{PLA}} \times 100 \quad (2\text{-}9)$$

$$X_{c(m)-PLA} = \frac{\Delta H_{m(PCL\ phase\ in\ mPCMs)}}{\Delta H^{0}_{m(PCL)}(1-w_{m(m)-PCMs})\times\theta_{PLA}} \times 100 \quad (2\text{-}10)$$

Where, θ_{PLA} was the theoretical weight fraction of PLA component in PLA and PCL mixture.

The theoretical relative cold crystallization enthalpy ($\Delta H_{cc(r)\text{-}th}$) of PLA matrix in n-hexadecane/PLA/PCL microcapsules was calculated from Equation (2-11)

$$\Delta H_{cc(r)-\mathrm{th}} = \frac{\Delta H_{cc}}{w_{m(th)-\mathrm{PLA}}} \quad (2\text{-}11)$$

Where, $w_{m(th)\text{-}PLA}$ was the theoretical addition of PLA component in n-hexadecane/PLA/PCL systems.

Based on the phase transitions enthalpies of encapsulated PCMs, the loading content (LC) of PCMs as well as the encapsulation efficiency (EE) of PCMs in electrosprayed mPCMs were calculated from the Equations (2-12) and (2-13) (Roy et al., 2018),

$$LC = \frac{\Delta H_{m(PCMs\ in\ mPCMs)}}{\Delta H_{PCMs}} \quad (2\text{-}12)$$

$$EE = \frac{LC}{LC_{th}} \quad (2\text{-}13)$$

where, $\Delta H_{m(PCMs\ in\ mPCMs)}$ and ΔH_{PCMs} are the melting enthalpies of encapsulated PCMs in microcapsules, and raw n-alkanes (n-hexadecane ~ 199 J/g, and n-eicosane ~ 205 J/g) (Zhang et al., 2020), respectively. LC_{th} is the theoretical loading content of PCMs in mPCMs.

2.4.3.2 Thermogravimetric analysis (TGA)

The thermal stability of n-alkanes (n-hexadecane and n-eicosane), neat PCL microparticles, neat PLA microparticles, PCL/PLA microparticles, n-alkanes/PCL mPCMs, n-hexadecane/PLA mPCMs and n-hexadecane/PLA/PCL mPCMs were assessed by thermogravimetric analysis, carried out on a TGA 3+ (Mettler Toledo, Columbus, OH, USA) under inert atmosphere at a purge rate of 50 mL·min^{-1}. A heating rate of 10 °C·min^{-1} was applied, and the temperature raised from 20 to 700 °C. For each experiment, 3 to 8 mg was used in the TGA test. In addition to the percentage weight (TG) curves, the derivative weight loss percentage (DTG) was calculated for each sample.

2.4.4 The formation of Taylor cone

During electrospraying, the formation and shape of Taylor cone was observed and analysed via high-speed images captured by camera (Chameleon CMLN-13S2M-CS USB camera, FLIR Integrated Imaging Solutions GmbH, Ludwigsburg, Germany).

2.4.5 Fourier Transform Infrared (FT-IR) Analysis of the Samples

The chemical structure of electro-sprayed raw materials and obtained electrosprayed particles was analyzed by Fourier transform infrared spectroscopy (Nexus-560 spectrometer, Nicolet, Madison, WI, USA). The powdery electro-sprayed materials, n-hexadecane liquid and n-eicosane solid were dispersed in spectroscopic grade potassium bromide (KBr), and analyzed in absorbance mode. All spectra were acquired in the wavenumber range of 400-4000 cm^{-1}, by averaging 256 scans at 2 cm^{-1} resolutions.

2.5 Characterizations of raw materials

2.5.1 Characterizations of n-alkanes

The chemical structure, phase transition behavior and thermal stability of raw n-alkanes were characterized by FT-IR, DSC and TGA.

2.5.1.1 Chemical structure of n-alkanes

In Figure 2-1, n-alkanes spectra exhibit a strong absorption band at 2920–2852 cm^{-1} associated with the aliphatic C–H stretching vibrations of the n-hexadecane or n-eicosane. The in-plane rocking vibration of the CH_2 groups is observed at 717 cm^{-1}, and C–H bending vibration in CH_2 is found at 1470 and 1370 cm^{-1} (Fang et al., 2010; Rezvanpour, et al., 2018).

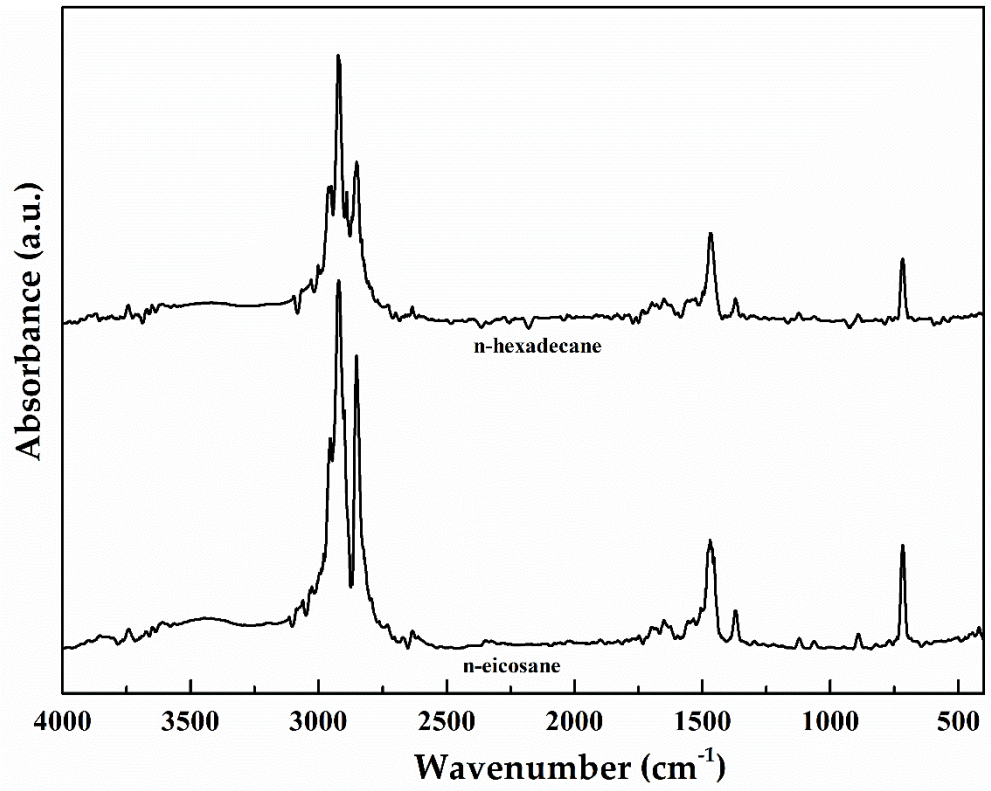

Figure 2-1 The FT-IR spectra of raw n-hexadecane and raw n-eicosane.

2.5.1.2 Phase transition behavior of raw n-alkanes

The phase change temperatures and the latent heats of melting and crystallization of raw n-alkanes were obtained using differential scanning calorimeter (Figure 2-2). On the one hand, the latent heats of fusion of raw n-hexadecane and n-eicosane are 199, and 205 $J \cdot g^{-1}$, respectively. Their melting and crystallization onset temperatures are found at 17.9 °C, 16.2 °C, 34.3 °C, and 35.7 °C.

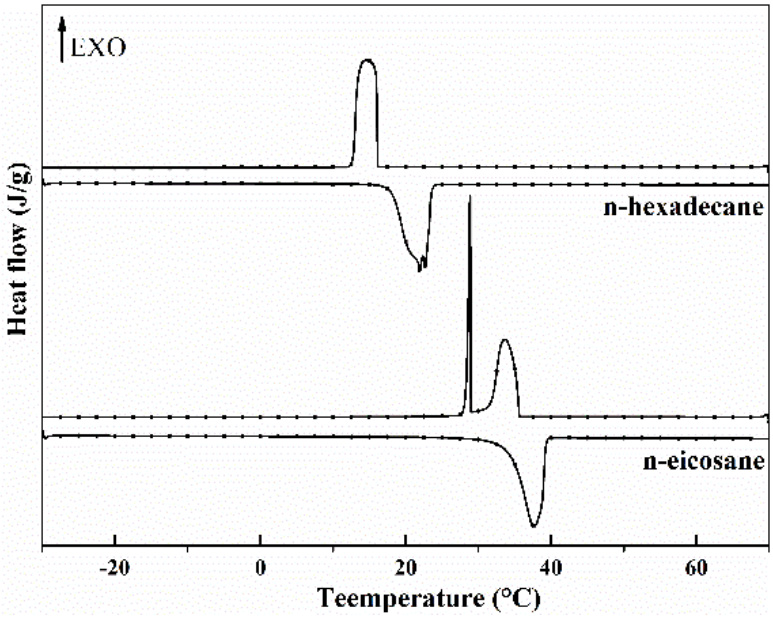

Figure 2-2 The DSC curves of raw n-hexadecane and raw n-eicosane

2.5.1.3 Thermal stability of raw n-alkanes

The thermal stability of raw n-alkanes was analyzed by TGA. TG and DTG curves n-hexadecane and n-eicosane are shown in Figure 2-3. The thermal behavior of n-hexadecane and n-eicosane displays single step degradation under N_2 atmosphere. The decomposition of n-alkanes, characterized by the onset temperature at 5% weight loss, starts at 151.6 and 178.8 °C for n-hexadecane, and n-eicosane, respectively. The main decomposition peaks of n-hexadecane and n-eicosane corresponding to the n-alkanes backbone decomposition take place at 246 °C and 269 °C, and the maximum rates of decomposition are about 2.2, and 2.6 %·°C^{-1}, respectively. Furthermore, there is no residue for these compounds at 300 °C.

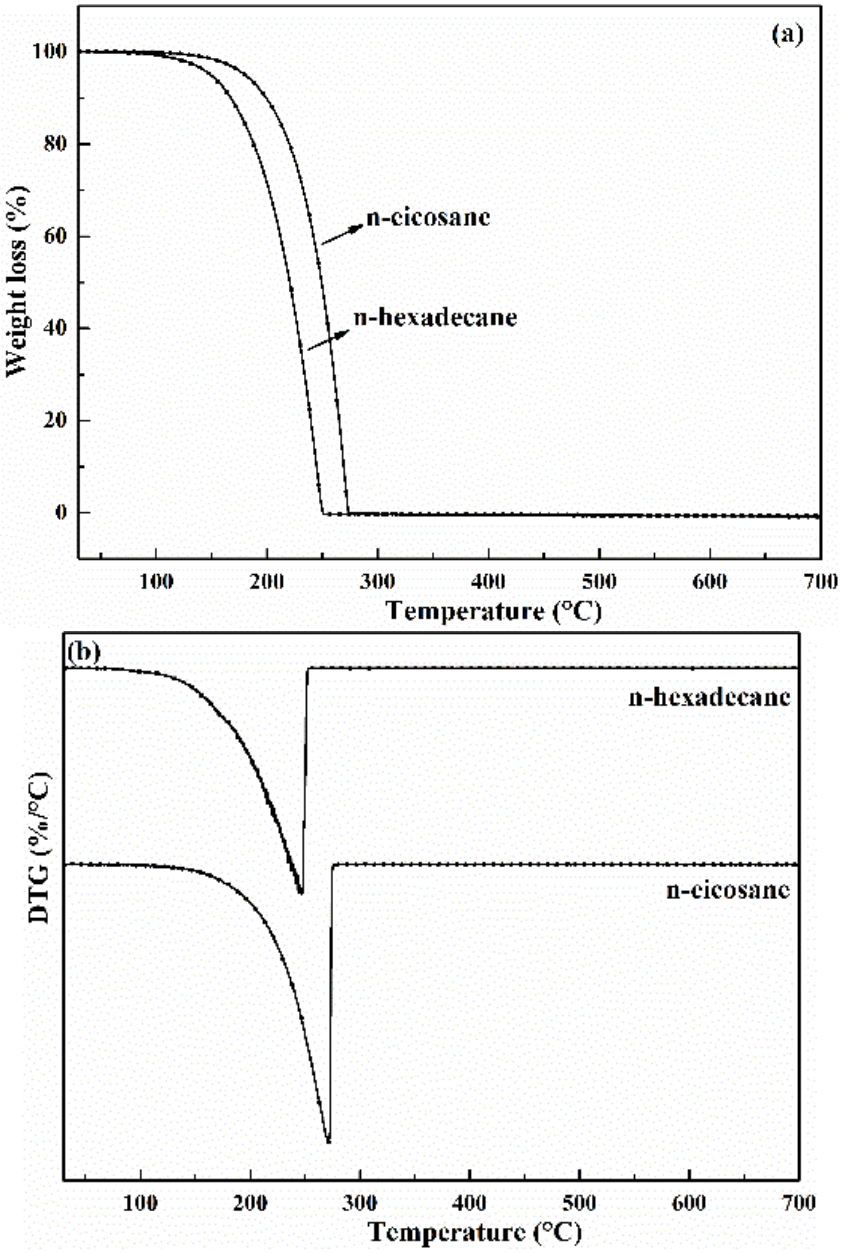

Figure 2-3 The TGA (a) and DTG (b) curves of raw n-hexadecane and raw n-eicosane.

2.5.2 Characterizations of neat PCL electrosprayed microspheres

The phase transition behavior and thermal stability of neat PCL were characterized by DSC and TGA.

2.5.2.1 Phase transition behavior of neat PCL electrosprayed microspheres

Form DSC results (Figure 2-4), the onset of melting and crystallization temperatures of raw PCL are determined at 55.6 and 41.5 °C. And the melting enthalpy of neat PCL is 59.6 J/g, and corresponding

crystallization degree of neat PCL is 42.7 %.

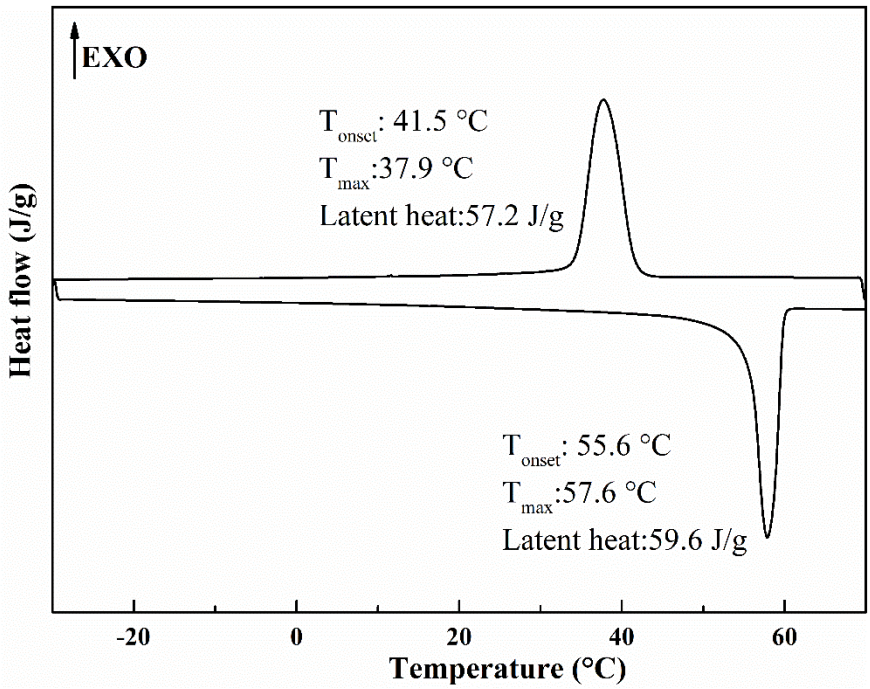

Figure 2-4 The DSC curves of neat PCL electrosprayed micropheres.

2.5.2.2 Thermal stability of neat PCL electrosprayed microspheres

Form the TGA results (Figure 2-5), raw PCL display a single step degradation between 350 to 500 °C, corresponding to polymer pyrolysis with a maximum of degradation temperature at 413.4 °C under an inert atmosphere as well as the corresponding maximum thermal degradation rate at 2.3 %·°C^{-1}. The initial degradation temperature was found to occur at 369 °C.

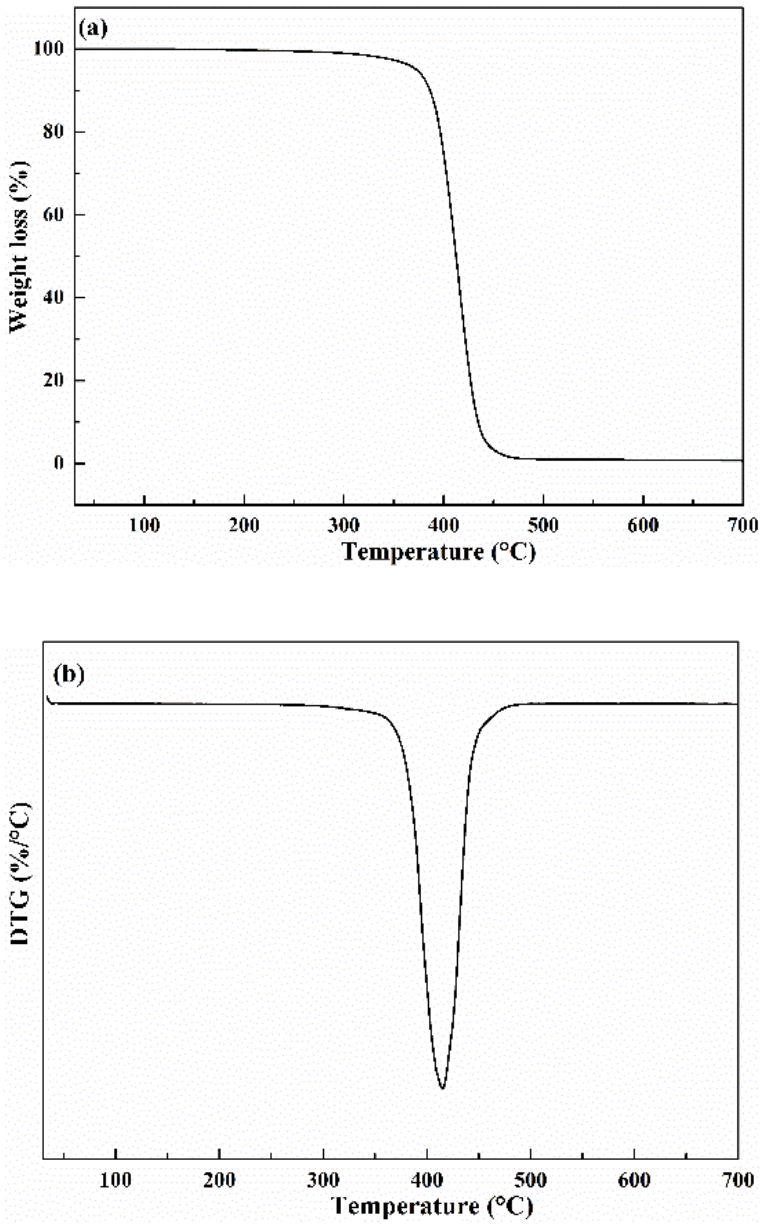

Figure 2-5 The TGA (a) and DTG (b) curves of neat PCL electrosprayed microspheres.

2.5.3 Characterizations of neat PLA electrosprayed microspheres

The phase transition behavior and thermal stability of neat PLA were characterized by DSC and TGA.

2.5.3.1 Phase transition behavior of neat PLA electrosprayed microspheres

DSC was used for analyzing the phase transition behavior of neat PLA. Due to the cooling rate used in DSC measurement is too quick to carry out the crystallization of neat PLA, so there is no crystal peak in the cooling

process of PLA. The second heating process from -30-120 °C (Figure 2-6a) and the third heating process from -30-200 °C (Figure 2-6b) were applied for investigating the glass transition temperature, cold crystallization and melting of neat PLA. The glass transition temperature of neat PLA is 58.2 °C, the onset temperature of PLA cold crystallization is 82.4 °C with a cold crystallization of 224.2 J/g. The onset temperature of PLA melting is 157 °C with a melting enthalpy of 40 J/g. And the crystallization degree of neat PLA is 43 %.

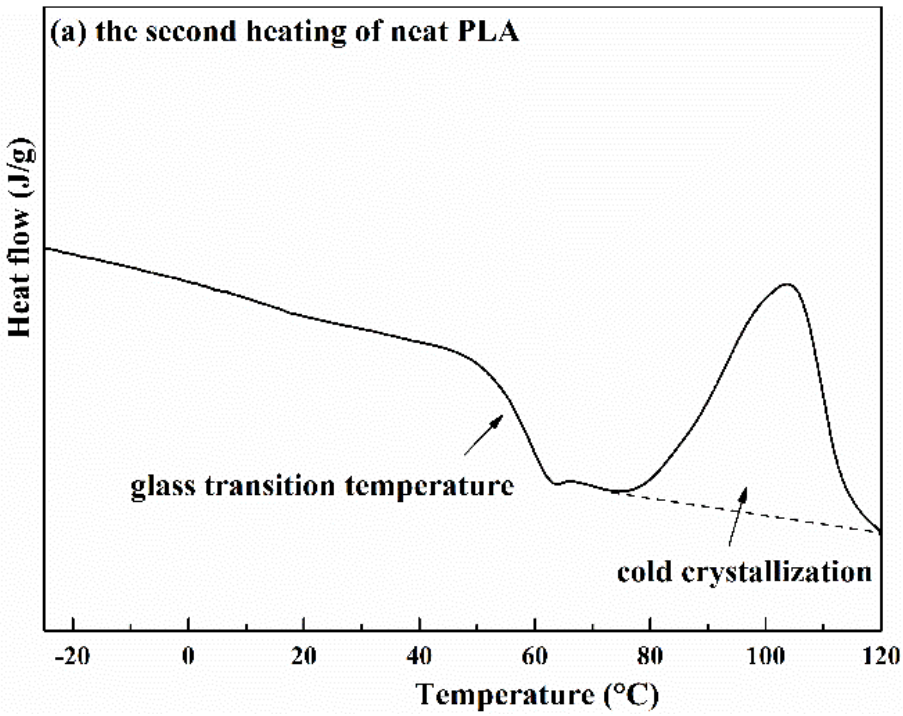

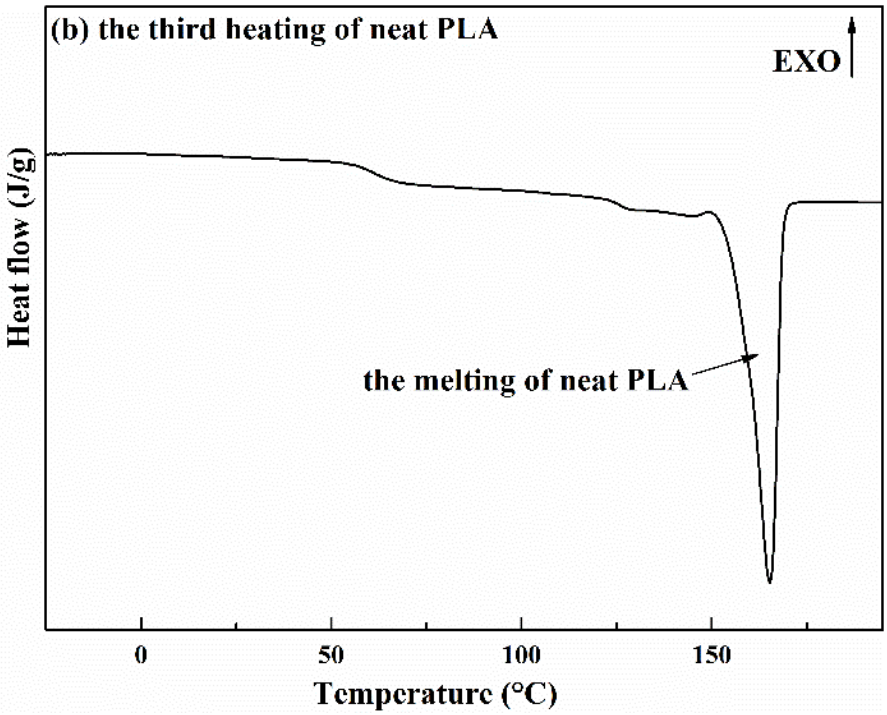

Figure 2-6 The DSC curves of neat PLA electrosprayed microspheres (a) the second heating process and (b) the third heating process.

2.5.3.2 Thermal stability of neat PLA electrosprayed microspheres

The thermal degradation process of neat PLA was analyzed via TGA (Figure 2-7a), and the related DTG curve was also obtained (Figure 2-7b). For neat PLA, a single step degradation was also observed from 300 °C to 400 °C. The initial degradation temperature of neat PLA was 309.7 °C. And the related maximum degradation temperature for neat PLA was370.3 °C with a maximum degradation rate of 2.8 %/°C.

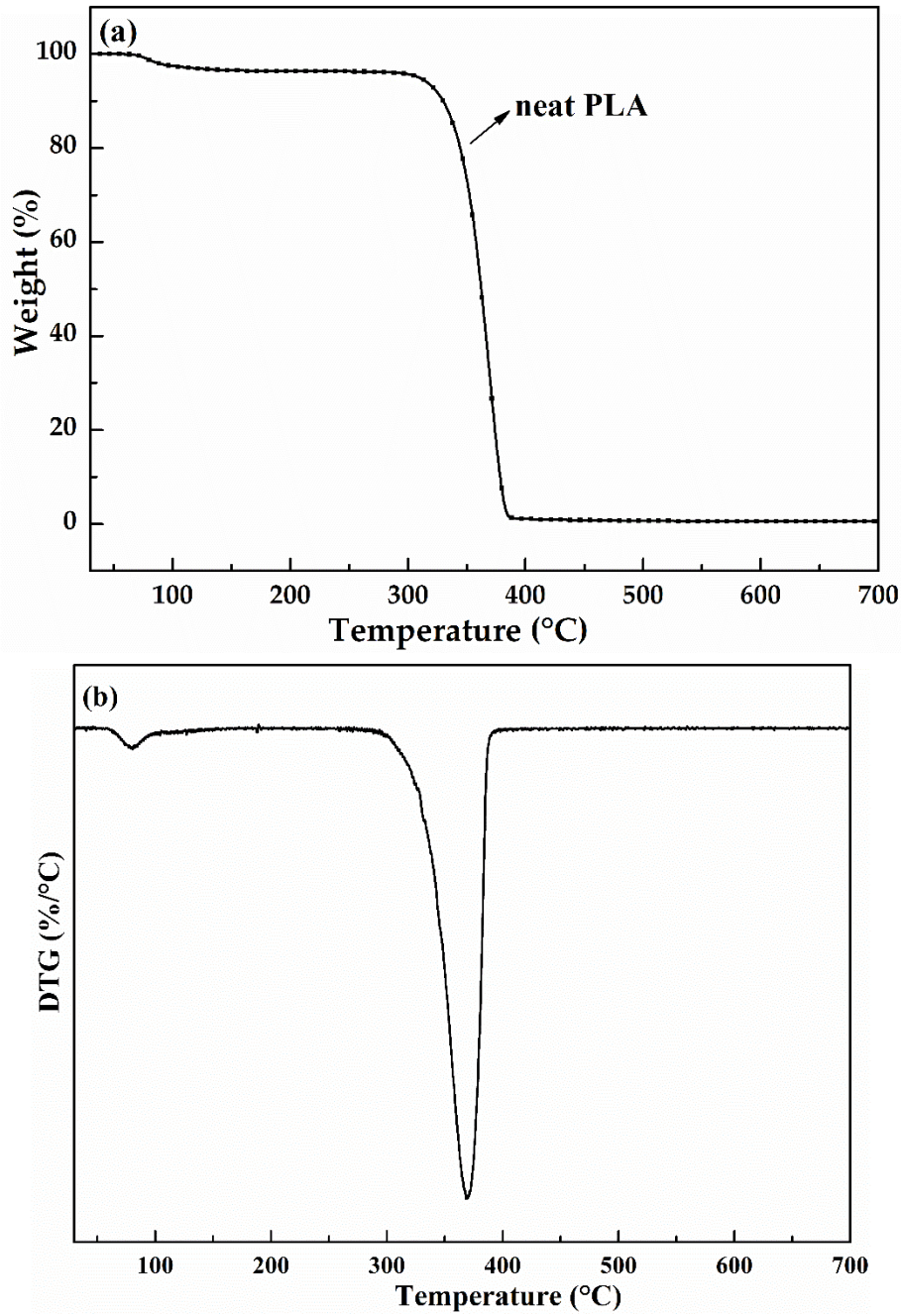

Figure 2-7 The TGA (a) and DTG (b) curves of neat PLA electrosprayed micropheres.

2.5.4 Characterization of neat PCL/PLA double-layered electrosprayed particles

The phase transition behavior and thermal stability of PCL/PLA double-layered particles were characterized by DSC and TGA.

2.5.4.1 Phase transition behavior of PCL/PLA double-layered electrosprayed particles

The phase transition behavior of PCL/PLA double-layered particle was investigated via DSC (Figure 2-8). The theoretical addition of PCL in this double-layered particles is 50 wt%, and the theoretical content of PLA in this double-layered particles is also 50 wt%. The PCL phase melted at 52.7 °C with a melting enthalpy of 28.7 J/g, and crystallized at 34.1 °C with a crystallization enthalpy of 26.9 J/g. Based on the theoretical content of PCL in particles, the theoretical crystallization degree of PCL phase is 41.1 %. Compared with neat PCL, the melting point and crystalline point of PCL phase in this double-layered particles both decrease. It is mainly related with the thermal conductivity of PLA phase, which enhances the heat exchange between PCL phase and temperature control medium.

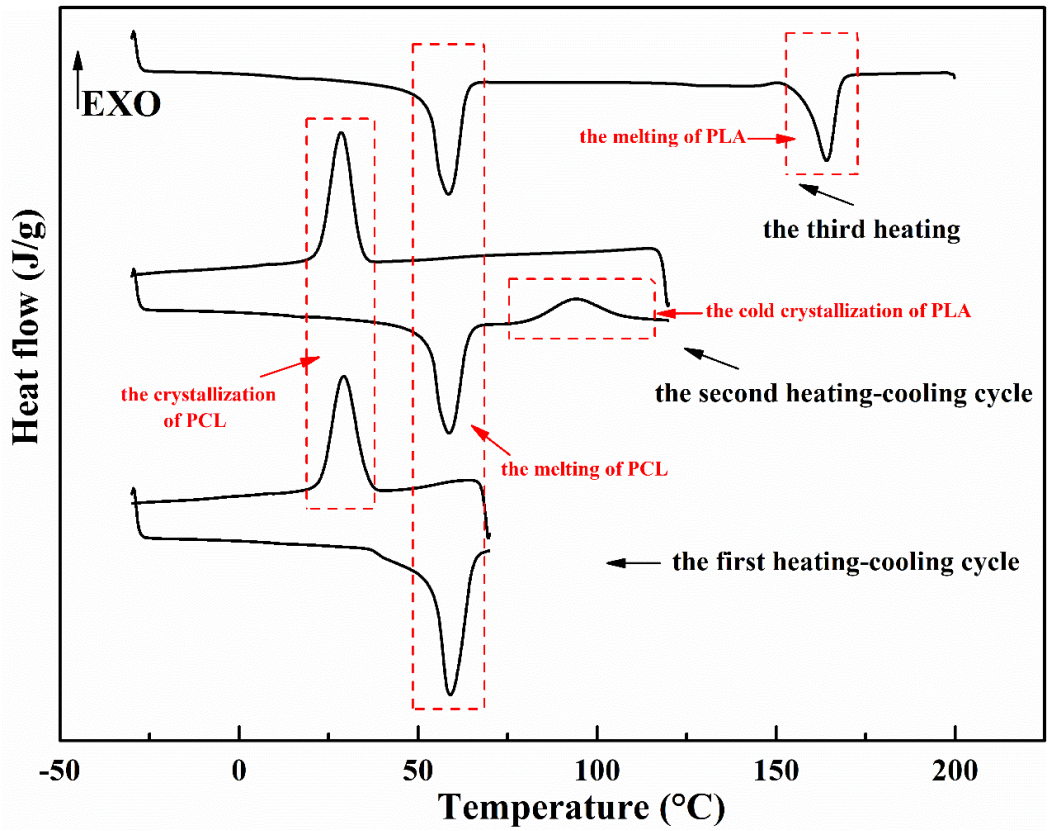

Figure 2-8 The DSC curves of PCL/PLA double-layered particles.

For PLA phase, the cold crystallization occurs at 80.8 °C with a crystallization enthalpy of 11.8 J/g. It also melts at 157.3 °C with a melting enthalpy of 16.9 J/g. Based on the theoretical content of PLA in particles, the theoretical crystallization degree of PLA phase is 36.3 %.

2.5.4.2 Thermal stability of PCL/PLA double layered electrosprayed particles

The thermal degradation process of neat PCL/PLA double layered electrosprayed particles was analyzed via TGA (Figure 2-9a), and the related DTG curve was also obtained (Figure 2-9b). The thermal degradation process of this particle is divided into two steps. The first step is from 300 to 378 °C, which is attributed to the degradation of the most PLA component and a small amount of PCL component; and the second step ranges from 378 to 500 °C, which is attributed to the degradation of a small amount of PLA component and the most of PCL component. The initial thermal degradation temperature of this particle is 323.0 °C. The maximum thermal degradation temperature in first step is at 358.7 °C with a degradation rate of 1.4 %/°C. The related weight loss in this step is 48 %. The maximum thermal degradation temperature in second step is at 418.3 °C with a degradation rate of 1.1 %/°C. The related weight loss in this step is 47.1 %. Compared with neat PLA, the initial thermal degradation temperature of PCL/PLA particle increases by about 15 °C. Thus, PCL matrix as shell material, can prevent or delay the degradation of PLA matrix by its physical barrier effect.

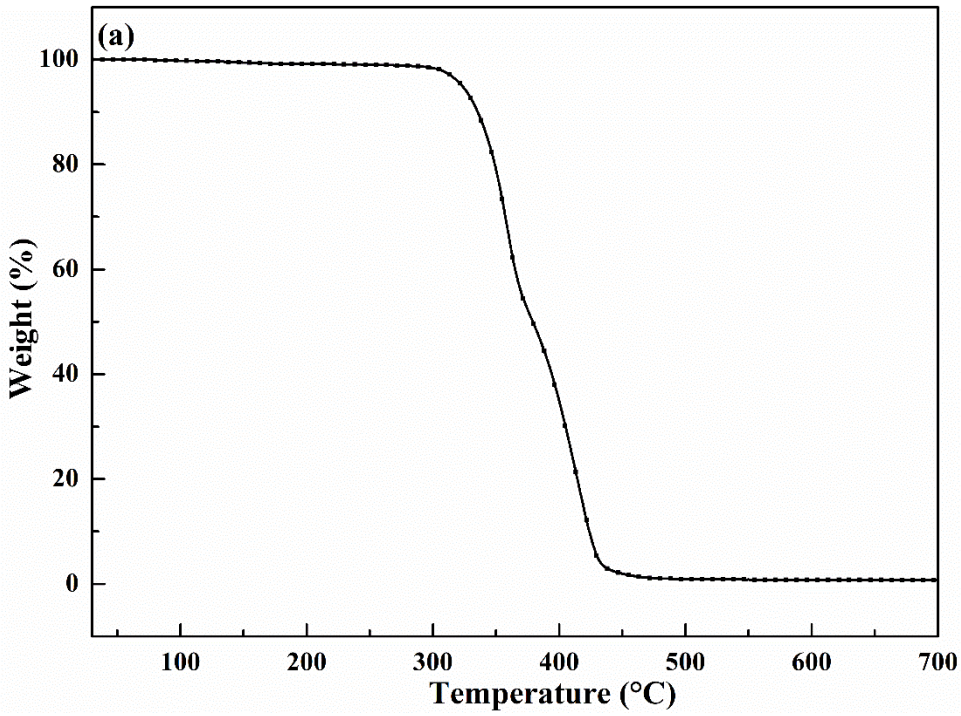

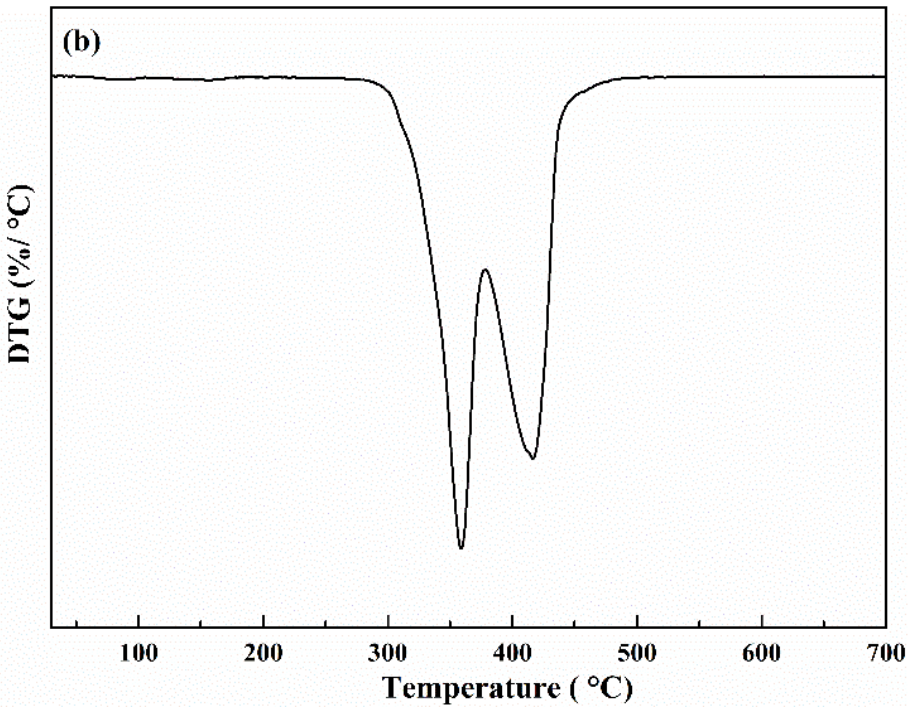

Figure 2-9 The TGA curve (a) and DTG curve (b) of PCL/PLA electrosprayed particles (the theoretical content of PCL is 50 wt% and the theoretical content of PLA is also 50 wt%).

References

Fang, G., Li, H., Chen, Z., & Liu, X. (2010). Preparation and characterization of flame retardant n-hexadecane/silicon dioxide composites as thermal energy storage materials. J*ournal of Hazardous Materials*, 181(1–3), 1004–1009. https://doi.org/10.1016/j.jhazmat.2010.05.114

Rezvanpour, M., Hasanzadeh, M., Azizi, D., Rezvanpour, A., & Alizadeh, M. (2018). Synthesis and characterization of micro-nanoencapsulated n-eicosane with PMMA shell as novel phase change materials for thermal energy storage. *Materials Chemistry and Physics*, 215(3), 299–304. https://doi.org/10.1016/j.matchemphys.2018.05.044

Roy, J. C., Giraud, S., Ferri, A., Mossotti, R., Guan, J., & Salaün, F. (2018). Influence of process parameters on microcapsule formation from chitosan—Type B gelatin complex coacervates. *Carbohydrate Polymers*, *198*(6), 281–293. https://doi.org/10.1016/j.carbpol.2018.06.087

Xiong, Z., Zhang, L., Ma, S., Yang, Y., Zhang, C., Tang, Z., & Zhu, J. (2013). Effect of castor oil enrichment layer produced by reaction on the properties of PLA/HDI-g-starch blends. *Carbohydrate Polymers*, *94*(1), 235–243. https://doi.org/10.1016/j.carbpol.2013.01.038

Zhang, S., Campagne, C., & Salaün, F. (2020). Preparation of n -Alkane / Polycaprolactone Phase-Change

Microcapsules via Single Nozzle Electro-Spraying : Characterization on Their Formation , Structures and Properties. *Applied Sciences, 10*(2), 561-580. http://doi:10.3390/app10020561

Chapter 3 The Selection of Solvent Systems Used in Polycaprolactone Electrospraying as well as the Operating Parameters

The selection of solvent system is important for carrying out the electrospraying of polymer. The solution properties (mainly including the surface tension, viscosity and electrical conductivity) determine the formation of Taylor cone, which is a precondition to obtain particles with a mono-dispersed size distribution, adjustable mean diameter and desired morphology. The operating parameters (applied voltage, flow rate and working distance) used for achieving stable elctrospraying process are also influenced by solution properties. The structure, morphologies and properties of electrosprayed microparticles are also influenced by solution properties and operating parameters.

In order to investigate the effects of solution properties and operating parameters on the formation of the electrosprayed particles, seek a green and suitable solvent for fabricating electrosprayed PCL particles and obtain optimized conditions for fabricating the electrosprayed particles with desired structure, morphology and properties, five solvents (chloroform, ethyl acetate, acetone, acetic acid and anisole), different operating parameters are used in PCL electrospraying (Bordes et al., 2010). Then, the effects of solution properties on the working range of applied voltage, the shape of Taylor cone and the structure and morphology of electrosprayed particles are clarified. Furthermore, the effects of operating parameters on the characteristics of the electrosprayed particles are also investigated. In addition, a suitable solvent for PLA electrospraying is also discussed.

3.1 Physico-chemical properties of a series of PCL electrospraying solutions

In Table 3-1, the Hansen solubility parameters of the solvents used as well as their solubility characteristics to PCL were given. The Hansen solubility parameters of all solvents used in our experiment are close to that of PCL (the δ_d, δ_p and δ_h of PCL is 17.0, 8.3 and 4.8 $(MPa)^{\frac{1}{2}}$, respectively). Meanwhile, for most of them, their distances (Ds) to PCL in "Hansen space" were smaller than the radius of solubility sphere of PCL (Rs ranges from 5.0 to 7.1) (Bordes et al., 2010). It indicates that all of them are suitable for dissolving PCL during electrospraying.

For glacial acetic acid, anisole, and chloroform, the complete dissolution of PCL in these solvents is held for a long time, even if at high PCL concentration. For ethyl acetate and acetone, at relatively high concentrations (7 wt% and 10 wt%), there are some PCL solids precipitated from PCL solution after one week and four days, respectively. Therefore, glacial acetic acid, chloroform, and anisole are regarded as good solvents for dissolving PCL; and acetone and ethyl acetate are regarded as partial solvent for dissolving PCL.

Table 3-1 Hansen solubility parameters of different solvents and physico-chemical properties of electrospraying solutions obtained from different solvents as well as PCL concentrations.

Property	**PCL concentration (wt%)**	**Chloroform**	**Ethyl acetate**	**Acetic acid**	**Acetone**	**Anisole**
δ^a_D $((MPs)^{\frac{1}{2}})$		18.2	15.8	14.5	15.7	17.8
δ^a_H $((MPs)^{\frac{1}{2}})$		6.2	7.2	13.5	11.7	6.7
δ^a_P $((MPs)^{\frac{1}{2}})$		6.3	5.3	8.0	5.3	4.1
D^b_S		1.9	4.0	8.4	5.7	2.4
PCL solubility		good	partial	good	partial	good
Vapor pressure at 25 ºC (kPa)		26.2	12.4	2.09	30.7	0.47
Surface tension ($mN \cdot m^{-1}$)	1	20.8±0.6	22.8±0.5	23.7±0.8	21.6±0.3	31.1±1.4
	3	22.4±0.2	21.8±0.4	24.5±0.5	21.0±0.6	32.9±0.3
	5	21.5±0.5	22.4±0.6	24.7±1.1	21.5±0.3	33.9±0.5
	7	22.6±0.9	22.1±0.6	24.3±0.2	20.9±0.3	32.4±0.7
	10	24.1±0.9	21.5±0.5	24.3±0.7	20.2±1.0	34.7±0.5
Electrical conductivity ($\mu S \cdot cm^{-1}$)	1	<0.037	<0.037	0.251±0.032	0.576±0.006	<0.037
	3	<0.039	<0.038	0.245±0.028	0.481±0.058	<0.039
	5	<0.038	<0.039	0.235±0.026	0.428±0.005	<0.038
	7	<0.040	<0.037	0.218±0.019	0.323±0.001	<0.040
	10	<0.039	<0.039	0.202±0.016	0.302±0.014	<0.039
Viscosity ($mm^2 \cdot s^{-1}$)	1	1.09±0.06	0.73±0.05	1.85±0.13	0.53±0.03	1.65±0.10
	3	4.00±0.07	1.56±0.01	4.28±0.001	0.95±0.05	3.77±0.01
	5	8.40±0.14	3.21±0.01	8.34±0.03	2.06±0.12	7.68±0.06
	7	17.00±0.14	6.13±0.01	16.67±0.05	3.47±0.01	14.77±0.01
	10	38.78±0.47	16.61±0.02	41.30±1.40	11.15±0.05	30.99±0.68

Where, a. δd, δh and δp are disperse part of Hansen solubility parameter, hydrogen part of Hansen solubility parameter and polar part of Hansen solubility parameter, respectively (unit: $(MPa)^{1/2}$)

b. Ds is a distance between solvent (S) and solute (PCL) in the "solubility space"

During electrospraying, the formation and shape of Taylor cone, the break-up of charged droplets and the evaporation of solvent were governed by the physico-chemical properties of the solutions (mainly including, surface tension, electrical conductivity, viscosity, and vapor pressure) and operating parameters. Table 3-1 also

presents the effects of different solvents and different PCL concentrations on the physico-chemical properties of electrospraying solutions. In the cases of PCL/ethyl acetate, PCL/glacial acetic acid and PCL/acetone, the surface tension of solutions do not change significantly with the increasing of PCL concentration. For the couples of PCL/anisole and PCL/chloroform, the surface tension of solutions increases with the increasing of PCL concentration. Furthermore, PCL/anisole solutions have the higher surface tension compared with other solutions. The surface tensions of PCL/glacial acetic acid solutions are slightly higher than those of PCL/ethyl acetate, PCL/chloroform, and PCL/acetone solutions, which are close to each other.

Among five solvents, chloroform, anisole and ethyl acetate belong to low electrical conductivity solvents. Therefore, the electrical conductivities of PCL/chloroform, PCL/anisole, and PCL/ethyl acetate solutions are low (Table 3-1). In cases of PCL/glacial acetic acid and PCL/acetone solutions, their electrical conductivities are relatively higher because of the high electrical conductivity of the pure solvents. Besides, it decreases with the increasing of PCL concentration. With the increasing of PCL concentration, the kinematic viscosity of PCL solutions increases gradually for each solvent and also depends on the kind of solvent used for the solubilization. Thus, kinematic viscosity of the solutions follows the order: PCL/glacial acetic acid > PCL/chloroform > PCL/anisole > PCL/ethyl acetate > PCL/acetone.

3.2 Cone-jet range of applied voltage

Carrying out electrospraying under cone-jet mode is the prerequisite for preparing PCL electrosprayed particles with low mean diameter and narrow particles size distribution. The active control and design on the size, as well as the morphology of electrosprayed microparticles, is achieved only under the cone-jet mode. The main factor for determining the spraying mode during electrospraying is the applied voltage. With increasing it, the spraying mode changes from dripping mode to rapid dripping mode, then to unstable cone-jet mode, next to cone-jet mode, finally to multi-jet mode (Xie et al., 2008). Therefore, it exists a range of applied voltage for achieving cone-jet during electrospraying. In generally, the cone-jet range of applied voltage is influenced by solution properties as well as operating parameters. In Table 3-2, the relationships among the cone-jet range of th applied voltage, the various solvents, the different PCL concentration and the different operating parameters are given. The electrical conductivity of the PCL solutions is the main parameters affecting the cone-jet ranges of the applied voltage. For low electrical conductive solutions, like PCL/chloroform, PCL/ethyl acetate, and PCL/anisole, their

cone-jet ranges of the applied voltage are similar (approximately from 3.25 to 4.5 kV), while for PCL/glacial acetic acid and PCL/acetone, their cone-jet ranges of the applied voltage are higher than that of the other three solvents. It indicates that higher electrical conductivity of the solutions leads to a higher cone-jet range of the applied voltage.

Furthermore, this range also correlates with the surface tension and the kinematic viscosity of the PCL solutions. Thus, for the solutions having the higher surface tension (PCL/glacial acetic acid), the cone-jet range of applied voltage is higher too. In Table 3-2, for PCL/chloroform, PCL/glacial acetic acid and PCL/anisole solutions, the lower limit as well as the upper limit of the applied voltage increase with the increase of PCL concentration, due to higher electrostatic forces required to overcome the viscoelastic one or high surface tension to guarantee the formation of Taylor cone. However, for PCL/ethyl acetate solutions, the upper limit of applied voltage decreases slightly with the increase of PCL concentration. For high concentrations, cone-jet mode tends to change into asymmetrical and slanted with increase the applied voltage. For PCL/acetone solutions, due to their too high electrical conductivities and too low viscosities, the lower and the upper limits of the applied voltage decrease with the increase of PCL concentration. The moderate viscosity is the prerequisite to maintain cone-jet. Due to the too low viscosity, keeping cone-jet mode stable at the low PCL concentration requires a higher applied voltage. Meanwhile, the charge density in electrosprayed jet increases with the increase of the applied voltage. At high PCL concentration, due to the thin charged jet and the accumulation of charges, the charge density in jet becomes too high, and then the cone-jet changes into the multi-jet mode (unstable jet mode) under strong Coulomb repulsions.

Table 3-2 Cone-jet range of applied voltage of PCL electrosprayed solutions under different solvents, different PCL concentration and different operating parameters

Experimental variables		chloroform (kV)	ethyl acetate (kV)	glacial acetic acid (kV)	acetone (kV)	anisole (kV)
PCL concentration [a]	1wt%	3.25-4.25	3.25-4.75	4.00-5.75	5.10-5.50	3.30-4.25
	3wt%	3.32-4.25	3.20-4.40	4.20-5.90	4.75-5.25	3.40-4.50
	5wt%	3.50-4.40	3.20-4.30	4.25-6.15	4.25-5.40	3.40-4.25
	7wt%	3.60-4.40	3.20-4.40	4.25-6.40	4.25-5.30	3.50-4.80
	10wt%	3.70-4.50	3.20-4.40	4.25-6.40	4.00-5.30	3.50-4.80
Working distance [b]	9 cm	3.50-4.20	3.14-4.15	3.87-5.25	3.75-4.75	3.30-4.10
	13 cm	3.60-4.25	3.17-4.25	4.00-5.75	4.00-5.00	3.50-4.20
	17 cm	3.50-4.40	3.20-4.50	4.25-6.15	4.25-5.40	3.40-4.25
	21 cm	3.50-4.30	3.00-4.30	4.30-6.30	4.25-5.60	3.50-4.25
	25 cm	3.70-4.40	3.00-4.30	4.40-6.40	4.25-5.60	3.50-4.50
Dripping time for one single droplet [c]	9 (104) s	3.60-4.40	3.15-4.00	4.00-6.00	4.00-5.40	3.50-4.25
	5 (93) s	3.50-4.40	3.20-4.50	4.25-6.15	4.25-5.40	3.40-4.25
	4 (67) s	3.80-4.60	3.60-4.60	4.25-6.30	4.25-5.25	3.50-4.25
	3 (45) s	3.75-4.60	3.60-4.60	4.40-6.50	4.25-5.00	3.50-4.25

Where, a. Other experimental conditions were fixed as follows: working distance: 17 cm, dripping time: 5s (PCL/anisole: 93 s);

b. Other experimental conditions were fixed as follows: PCL concentration: 5 wt%, dripping time: 5s (PCL/anisole: 93 s);

c. The values in parentheses were the dripping time of PCL/anisole solution, other experimental conditions were fixed as follows: PCL concentration: 5 wt%, working distance: 17 cm.

Apart from solution properties, the cone-jet range of the applied voltage also depends on the operating parameters. In Table 3-2, the lower and upper limits of cone-jet applied voltage increase with augmenting the working distance. Thus, it results in a decrease of the electric field strength, and need to be adjusted to guarantee the formation of the Taylor cone. The increasing trend of applied voltage in PCL/acetone and PCL/glacial acetic acid solutions are more significant compared with low electrical conductivity liquids, such as PCL/chloroform, PCL/ethyl acetate, and PCL/anisole. For high electrical conductivity liquids, they are more sensitive to the change in the strength of the electric field. The relationships between the cone-jet applied voltage and the flow rate of the electrospraying liquid are also given in Table 3-2. Apart from PCL/acetone and PCL/anisole solutions, the lower and upper limits of applied voltage both increase with the accelerating of dripping time. It is due to the liquid gravity that results in dripping mode is stronger under a higher flow rate of the liquid. Therefore, a stronger applied voltage and electrostatic force are required to overcome stronger gravity and guarantee the formation of Taylor

cone. For PCL/acetone solutions, due to the accumulation of excessive charges and drastic coulomb repulsion, the cone-jet mode becomes unstable under higher flow rate. Therefore, their upper limits of applied voltage decrease gradually with the accelerating of the dripping time.

3.3 The shape of Taylor cone

Under cone-jet mode, the shape of the Taylor cone affects the size as well as the distribution of electrosprayed microparticles. The diameter of the charged jet and the distance between the nozzle and the tip of the Taylor cone characterize the shape of the Taylor cone. The size, as well as the size distribution of electrosprayed microparticles, are smaller and more homogeneous when electrospraying is carried out under the thinner charged jet (Gañán-Calvo et a., 1997; Yao et al., 2008). Meanwhile, the jet diameter also decreases with the decrease of the distance between the nozzle and the tip of the Taylor cone (Jaworek, & Krupa, 1999; Jayasinghe, & Edirisinghe, 2002). Different shapes of the Taylor cone obtained from different solvents and different PCL concentrations are shown in Figure 3-1. For PCL/chloroform and PCL/ethyl acetate, the ideal Taylor cone with the small distance from nozzle to the tip of Taylor cone and thin jet diameter is easy to form under various PCL concentrations. For PCL/glacial acetic acid, the shape of Taylor cone is non-ideal at 1 wt% PCL (long distance between the nozzle and the tip of the Taylor cone and thick charged jet). It might be related to the relatively higher surface tension and insufficient viscosity. With the increasing of PCL concentration, the distance from the nozzle to the tip of the Taylor cone decreases gradually, and the shape of the Taylor cone becomes suitable for the electrospraying process. For PCL/acetone, at 1 wt% PCL, a rapid dripping mode with thick charged jet and long distance between the nozzle and the tip of Taylor cone is obtained due to the low viscosity of the solution. With the increase of PCL concentration, the distance and the diameter of charged jet both decrease, and spray mode changes from rapid dripping mode to ideal cone-jet mode. For PCL/anisole solutions, due to a high surface tension and a low vapor pressure, their Taylor cone shapes are always non-ideal. Furthermore, the diameter of charged jet in PCL/anisole decreases gradually with the increase of PCL concentration.

Based on these images (Figure 3-1), medium viscosity and low surface tension values are prerequisites for the formation of Taylor cone with the adequate shape. With the increase of the viscosity, the distance from the nozzle to the tip of the Taylor cone and the jet diameter both decrease gradually, to promote the formation of a suitable cone-jet.

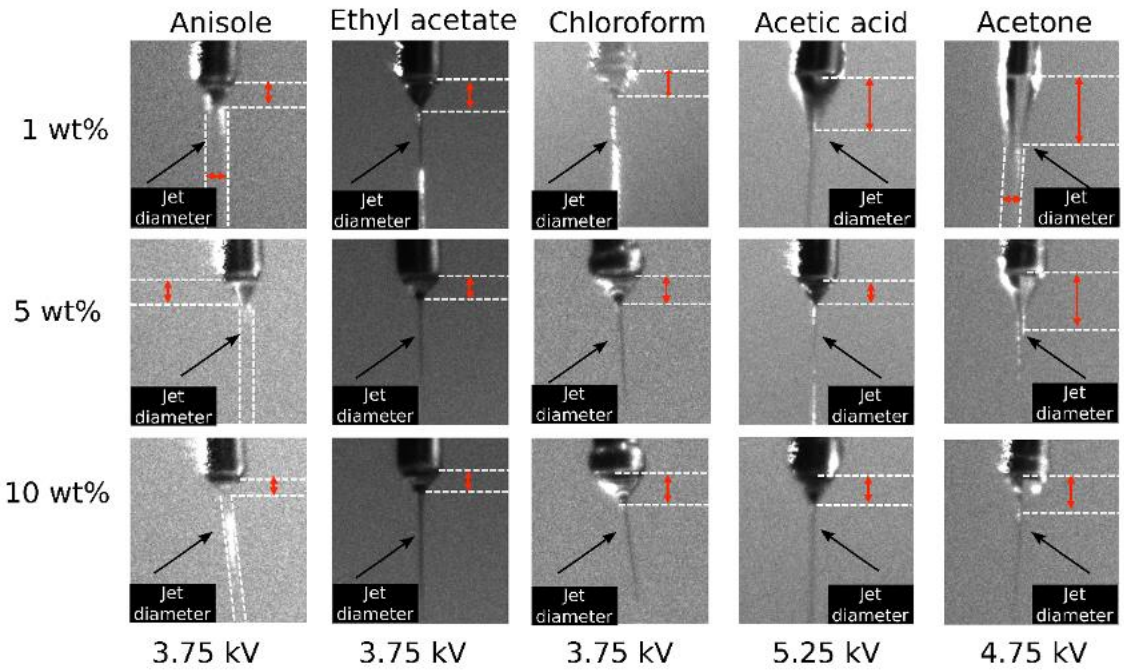

Figure 3-1 Images of Taylor cone obtained with anisole, ethyl acetate, chloroform, acetic acid and acetone at three PCL concentrations (1, 5 and 10 wt%) (working parameters: working distance 17 cm, dripping time: 5 s (excepted for anisole: 93 s)).

The shape of the Taylor cone also correlates with the operating parameters. In Figure 3-2, the distance from the nozzle to the tip of the Taylor cone and jet diameter both increase gradually with the increase of working distance. For PCL/acetone solutions, due to the reduction in the electric field and the electrostatic forces, and the shape as well as the stability are difficult to obtain. High viscosity is a main factor to keep the shape of Taylor cone stable, therefore, the changes in the shape of Taylor cone with the increase of working distance among PCL/anisole, PCL/glacial acetic acid, PCL/ethyl acetate and PCL/chloroform solutions are lower than those of PCL/acetone solutions ones.

The flow rate of electrosprayed liquids also influences the shape of the Taylor cone. In Figure 3-3, with the accelerating of dripping time for one single droplet, the distance from the nozzle to the tip of the Taylor cone as well as jet diameter both increase. It was closely related to the shortening of polarization time of droplets and the enhancing of droplet gravity during the formation of Taylor cone. Due to the lower viscosity in PCL/acetone solutions, their Taylor cone stabilities are reduced. Therefore, the change in shape of the Taylor cone with the accelerating of dripping time is more significant for the PCL/acetone solution.

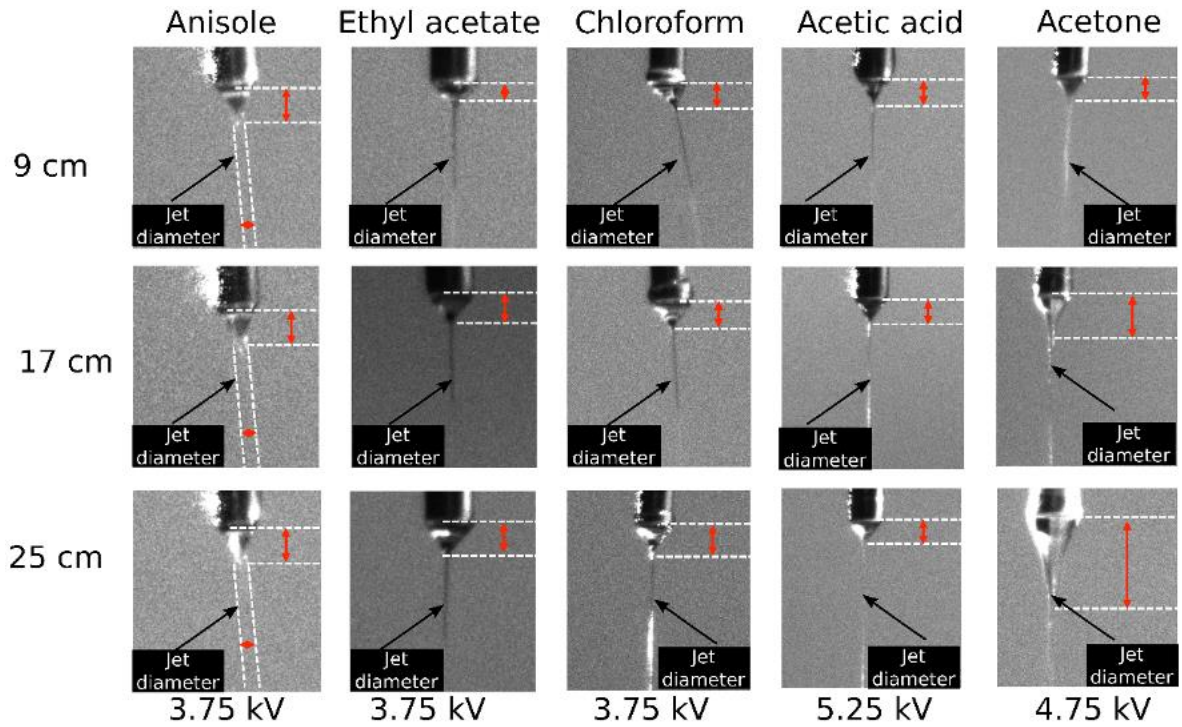

Figure 3-2 Images of Taylor cone obtained with anisole, ethyl acetate, chloroform, acetic acid and acetone at three working distances (9, 17 and 23 cm) at 5 wt% PCL concentrations for a dripping time of 5 s excepted for anisole (93 s).

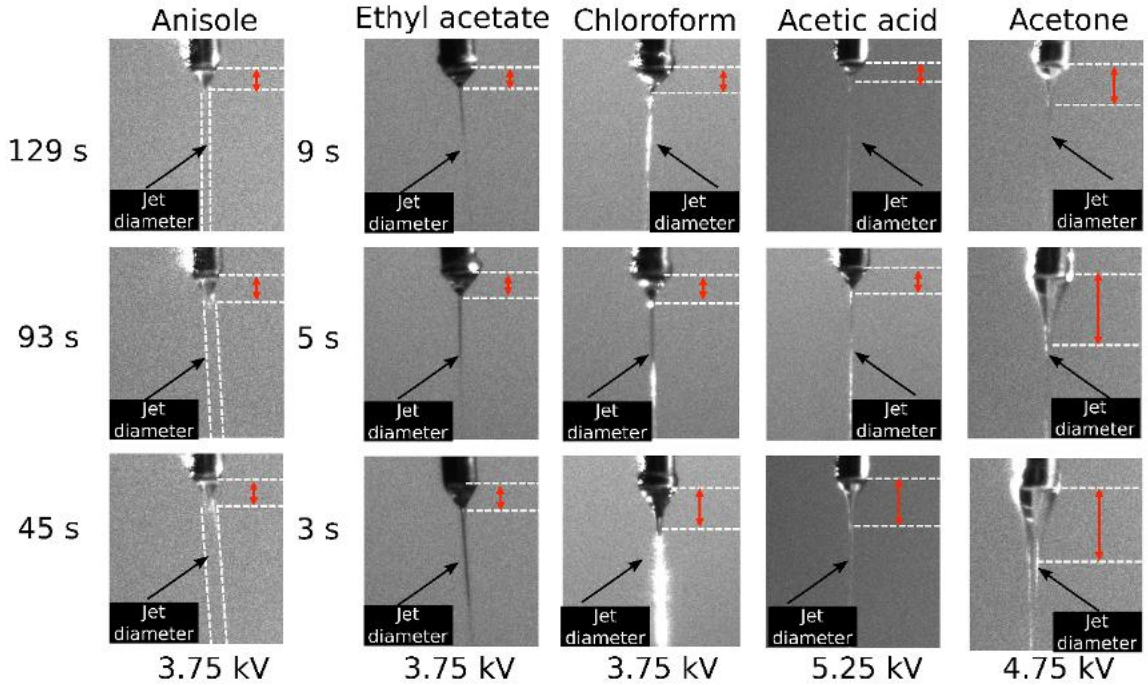

Figure 3-3 Images of Taylor cone obtained with anisole, ethyl acetate, chloroform, acetic acid and acetone at three dripping times (129, 93, and 45 s) at 5 wt% PCL concentrations and a fixed working distance of 17 cm.

3.4 Size and distribution of PCL microparticles

Preparing micro- or nanoscale particles with a narrow distribution is one of the main advantages of the electrospraying method. The size of electrosprayed microparticles mainly depends on the solution properties and operating parameters. Furthermore, the shape of the Taylor cone influences the mean diameter and the particle size distribution of electrosprayed microparticles. Different mean diameters and different size distributions of PCL microparticles depend on the solvent choice as well as PCL concentration (Figure 3-4). For PCL/chloroform and PCL/ethyl acetate solutions, small (mean diameter: 7-8 μm) and mono-dispersed distribution microparticles are obtained for 1 wt% PCL concentration, related on the moderate viscosities, the ability of solvent evaporation, the low surface tensions, and the low electrical conductivities. Thus, for the solutions having low surface tension and moderate viscosity, adequate cone-jet is easy to form, and jet diameter is narrow. The break-up process of thin charged jet is stable and uniform based on low electrical conductivity, when the solvents have a relatively high vapor pressure for complete evaporation, to lead to the formation of tiny microparticles. With the increasing of PCL concentration in these solvents, the mean diameter of microparticles increases gradually from 8 to 28 μm and their size distributions become broaden. It is related to the increasing of solids content in droplets and the enhancing entanglements among PCL chains under high PCL concentration. In this case, combining with their low electrical conductivities, the fine break-up of the charged jet is suppressed. For PCL/glacial acetic acid and PCL/acetone solutions, the size distribution of PCL microparticles is poly-dispersed at low PCL concentration. Because of their higher electrical conductivities and thicker charged jet, the break-up process of the charged jet is drastic and unstable. The subsequent break-up of charged droplets also occurs during their flight to the collector. Therefore, the size distribution under this situation is polydispersed. With the increasing of PCL concentration in glacial acetic acid, the mean diameter of small microparticles increases (from 4.58 μm to 7.63 μm), while this of large microparticles decreases (from 24.17 μm to 19.19 μm). Finally, bimodal-dispersed distribution turns into mono-dispersed distribution at 10 wt% PCL, and the mean diameter of PCL microparticles is about 15 μm. The situation in PCL/acetone solutions is similar to PCL/glacial acetic acid solutions, related to the stability of the break-up process of the charged jet. In addition, some PCL microparticles with too large size (diameter: 97 μm) were prepared from 3 wt% PCL/acetone, due to unstable break-up of charged jet and quickness of the acetone evaporation. There is not enough time for PCL chains to condense together completely before the solidification

of PCL/acetone droplets.

On the one hand, with the increase of PCL concentration in glacial acetic acid or acetone, the electrical conductivities of solutions decrease, while their viscosities increase significantly. Then, the break-up process of the charged jet becomes stable and homogeneous. On the other hand, with the increasing of PCL concentration, the thickness of the charged jet obtained for solutions prepared from acetone or glacial acetic acid decreases, to promote the formation of electrosprayed particles with tiny size and mono-dispersed size distribution. For PCL/anisole solutions, the mean diameter of microparticles is higher than those obtained with the other solvents. It is closely related to the diameter of charged jet and the slow evaporation of the solvent. Due to the high surface tension and low vapor pressure, the diameter of the charged jet is broad. Combining with low electrical conductivity, the fine break-up process of the charged jet is challenging to carry out. Meanwhile, due to the residual solvent, the microparticles tend to swell or aggregate together at the collector surface, which leads to a large size and poly-dispersed distribution. The increase of the PCL concentration in the solutions allows the decrease of the mean diameter, which is related to the thinned charged jet and the reduction of the solvent in droplets.

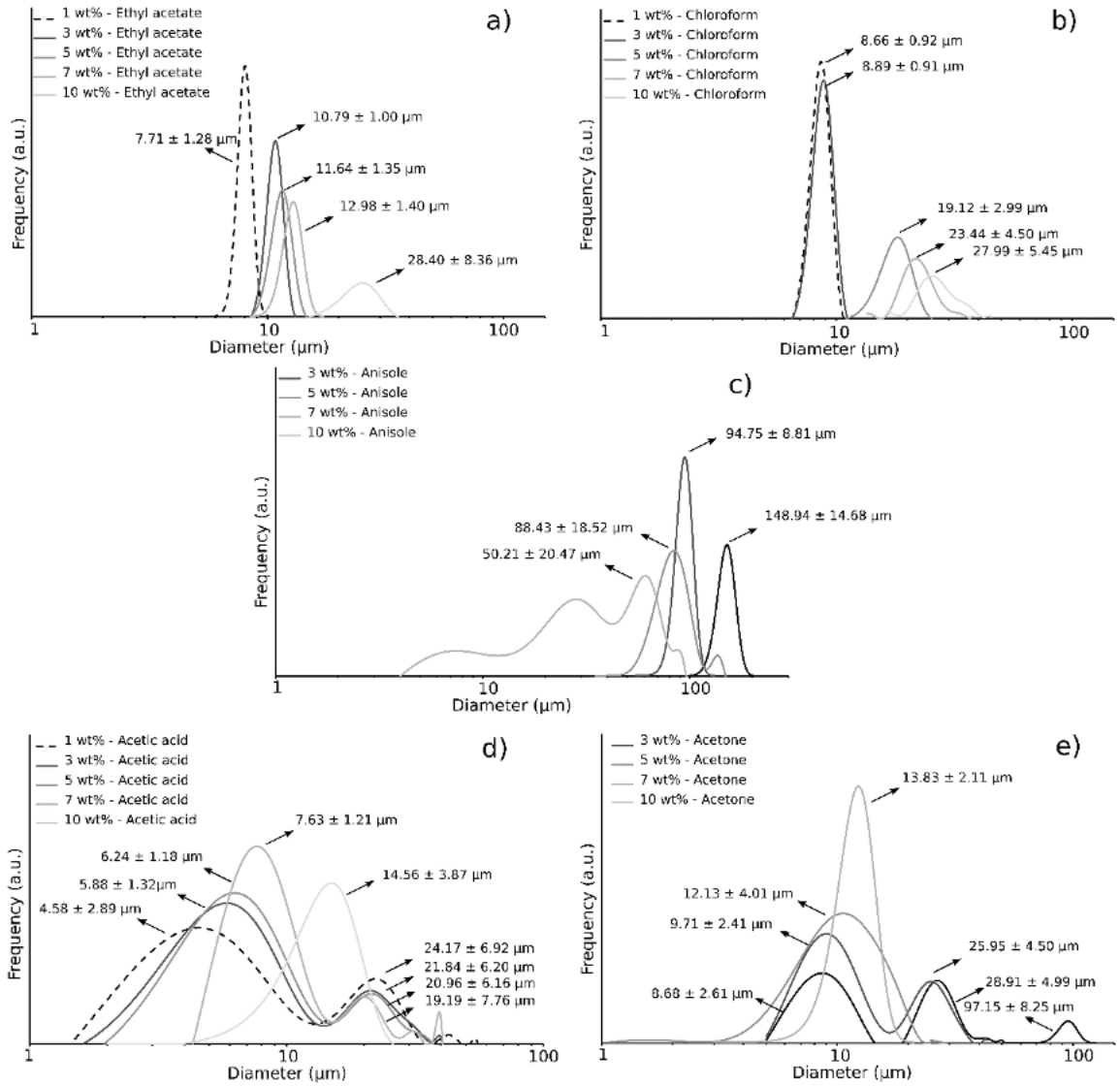

Figure 3-4 Mean diameter and size distribution of PCL electrosprayed microparticles obtained from ethyl acetate (a)), chloroform (b)), anisole (c)), acetic acid (e)), and acetone (f) for a working distance of 17 cm, an applied voltage of 3.75 kV (excepted for acetone: 4.75 kV, and glacial acetic acid: 5.25 kV), and a dripping time of 5 s (excepted for anisole, 93 s)).

The mean diameter and size distribution of PCL electrosprayed microparticles prepared from different working distances with different solvents are presented in Figure 3-5. There are two opposite effects influencing on the mean diameter of the electrosprayed particles (Zhou et al., 2016). The strength of the electric field between the nozzle and the collector weakens gradually with the increase of the working distance. In this configuration, the formation of Taylor cone and the charged droplets break-up process are both suppressed, and then larger PCL microparticles are obtained under longer working distance. However, with the increasing of working distance,

there is longer time to carry out the complete evaporation of the solvent during the flight of droplets to the collector. With the evaporation of solvent, PCL chains tend to condense and the size of electrosprayed microparticles decreases gradually (Arya et al., 2009). In addition, due to the reduction of electric field, the break-up process also becomes more uniform and stable under a higher working distance. The size distributions of electrosprayed particles obtained from all solvents narrow gradually with the increasing of the working distance, and mono-dispersed distributions are finally obtained.

For PCL/ethyl acetate solution, when the working distance increases from 9 to 13 cm, the mean diameter of the PCL microparticles decreases from 19 to 11 μm. Thus, there is more solvent evaporating from droplets with the increase of flight distance. However, when the working distance further increases, the mean diameter of microparticles does not change significantly. Thus, there is a trade-off between the two opposite effects on electrosprayed particles size introduced by the increasing of working distance. For PCL/chloroform solution, due to a higher vapor pressure, the effect of solvent evaporation on particle size is stronger than that of the changing of electric field on particle size. Therefore, the mean diameter of microparticles decreases gradually with the increasing of working distance. For PCL/anisole solution, due to the low vapor pressure of anisole, the evaporation of the solvent is difficult to carry out even under long working distance. Therefore, the effect of the changing of electric field on particle size is more important than that of the solvent evaporation on the particle size (Ghayempour & Mortazavi, 2013). The mean diameter of electrosprayed particles increases gradually with the increasing of the working distance.

For PCL/acetone solution, due to the stronger vapor pressure of acetone, the hardening of electrosprayed droplets during their flight to collector is very quick. Therefore, there is not enough time for the condensation of PCL chains during the solidification of electrosprayed particles. Under strong electric field at a short working distance (9 cm), due to the unstable break-up process of the charged and quick hardening of electrosprayed droplets, tiny (mean diameter ~ 6 μm) and large particles (mean diameter ~ 118 μm) are obtained. With the increasing of working distance, due to the reduction of the electric field, the mean size of the electrosprayed droplets increases gradually. Then, after quick solidification, the mean diameter of solid particles also increases with the increase of the working distance. For PCL/anisole and PCL acetone, the increase of the mean diameter of electrosprayed particles with the increase of working distance also correlates with the increase of the charged jet diameter. For PCL/glacial acetic acid solution, the mean diameter of the electrosprayed particles does not

change significantly with the increase of working distance. Thus, the effect of the changing of electric field on particle size is offset by the effect of solvent evaporation on particle size. In addition, based on the stable break-up process, sufficient solvent evaporation and condensation of PCL chains at 25 cm, mono-dispersed and small microparticles are prepared from glacial acetic acid.

The flow rate of the PCL solutions, related to the dripping time in this work, influences the granulometry of the obtained microparticles (Figure 3-6). For PCL/chloroform and PCL/ethyl acetate solutions with low electrical conductivity, the mean diameter, as well as the size distribution of the PCL microparticles, is small and mono-dispersed under slow dripping time for one single droplet. With accelerating the dripping time, the mean diameter of PCL microparticles increases gradually, and the size distribution of PCL microparticles broadens (Zhang et al., 2012), due to the obtention of the thicker charged jet. For PCL/acetone and PCL/glacial acetic acid solutions with high electrical conductivity, small and mono-dispersed PCL microparticles are obtained under slow dripping time due to thinner charged jet and a fine mist with the break-up of droplets. With accelerating dripping time, the diameter of charged jet increases gradually, and the break-up of charged droplets becomes unstable. Thus, the mean diameter of PCL microparticles increases and size distribution changes into bimodal-dispersed distribution. For PCL/anisole solutions, the mean diameter of PCL microparticles also increases with accelerating the dripping time.

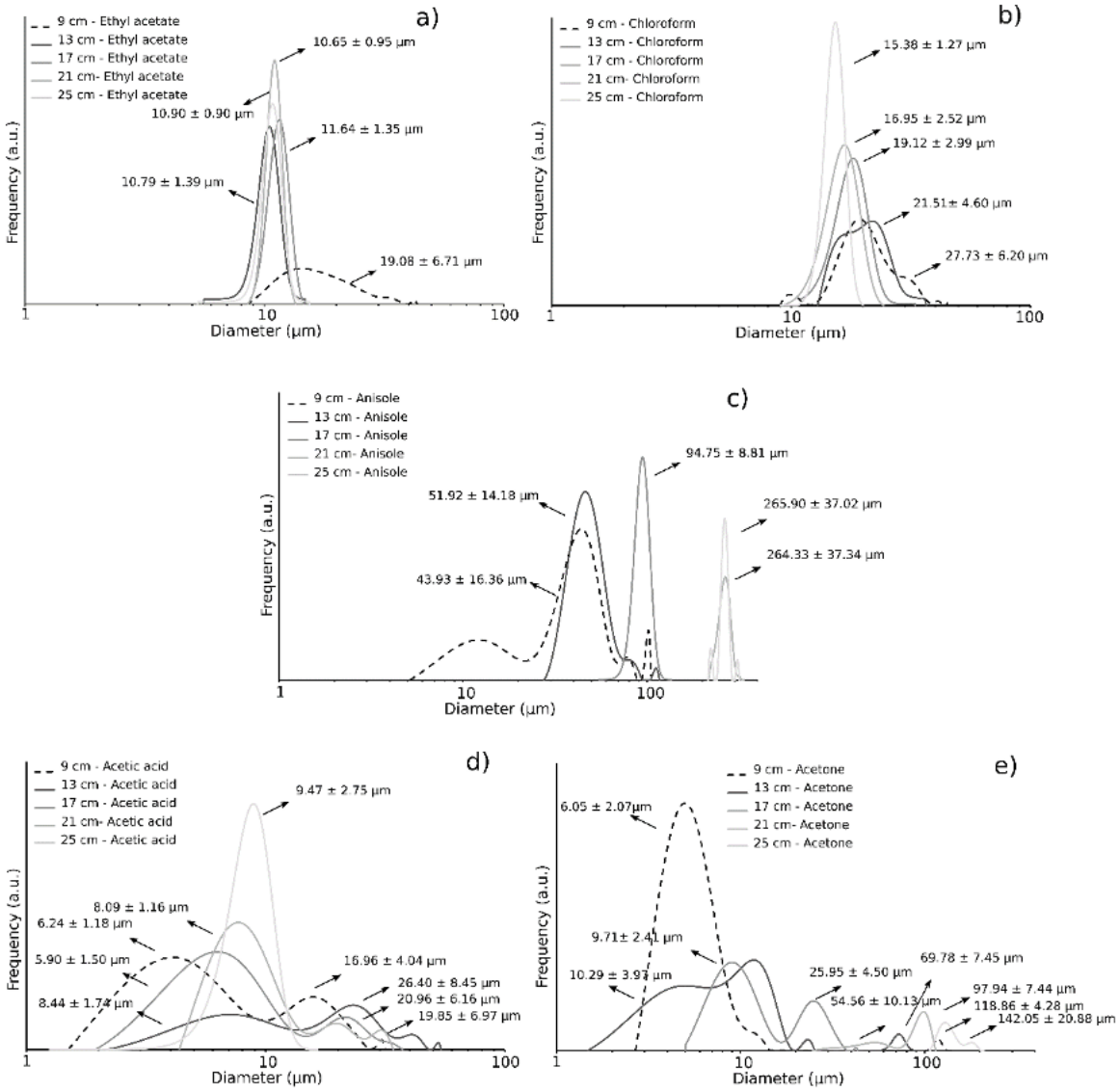

Figure 3-5 Mean diameter and size distribution of PCL electrosprayed microparticles obtained from ethyl acetate (a)), chloroform (b)), anisole (c)), acetic acid (e)), and acetone (f) for various working distances (9, 13, 17, 21; and 25 cm), at 5 wt% PCL concentration for an applied voltage of 3.75 kV (excepted for acetone: 4.75 kV, and glacial acetic acid: 5.25 kV), and a dripping time of 5 s (excepted for anisole, 93 s)).

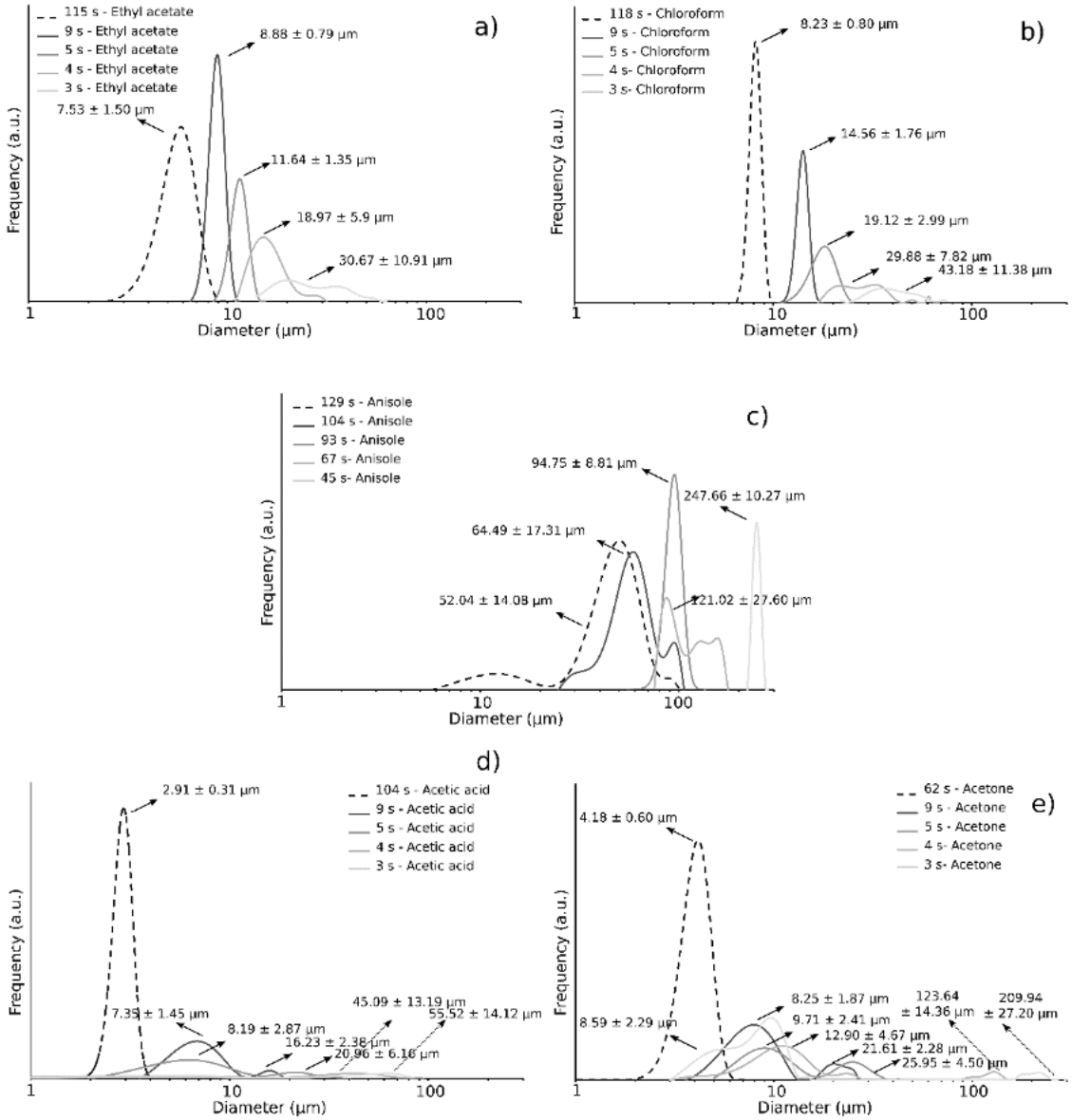

Figure 3-6 Mean diameter and size distribution of PCL electrosprayed microparticles obtained from ethyl acetate (a)), chloroform (b)), anisole (c)), acetic acid (e)), and acetone (f) for various dripping times, at 5 wt% PCL concentration for an applied voltage of 3.75 kV (excepted for acetone: 4.75 kV, and glacial acetic acid: 5.25 kV), and a working distance of 17 cm.

Under cone-jet mode, the spray mode of the electrospraying solutions changes from non-ideal cone-jet mode to ideal cone-jet mode with the increasing of the applied voltage (Chang, Stride, & Edirisinghe, 2010). Moreover, it influences the granulometry of the resulted microparticles (Figure 3-7). With the increase of the applied voltage, the mean diameter of PCL microparticles decreases and its distribution becomes narrow, due to the existence of stronger Coulomb repulsions among charged droplets, as observed in the cases of PCL/ethyl acetate and

PCL/chloroform solutions. Therefore, mono-dispersed PCL microparticles with a mean diameter of about 11-15 µm are obtained at higher applied voltage. For PCL/anisole solution, with the increasing of applied voltage from 3.75 kV to 4.0 kV, there is a phenomenon occurring that the mean diameter of microparticles increases from 69 µm to 97 µm. It might correlate with the aggregation among PCL microparticles resulted from the residual solvent (anisole) in PCL microparticles. In the cases of PCL/glacial acetic acid and PCL/acetone solutions, the increase of the applied voltage allows to decrease the particle size distribution, from poly-dispersed to bimodal or mono-dispersed distribution, and the mean diameters too.

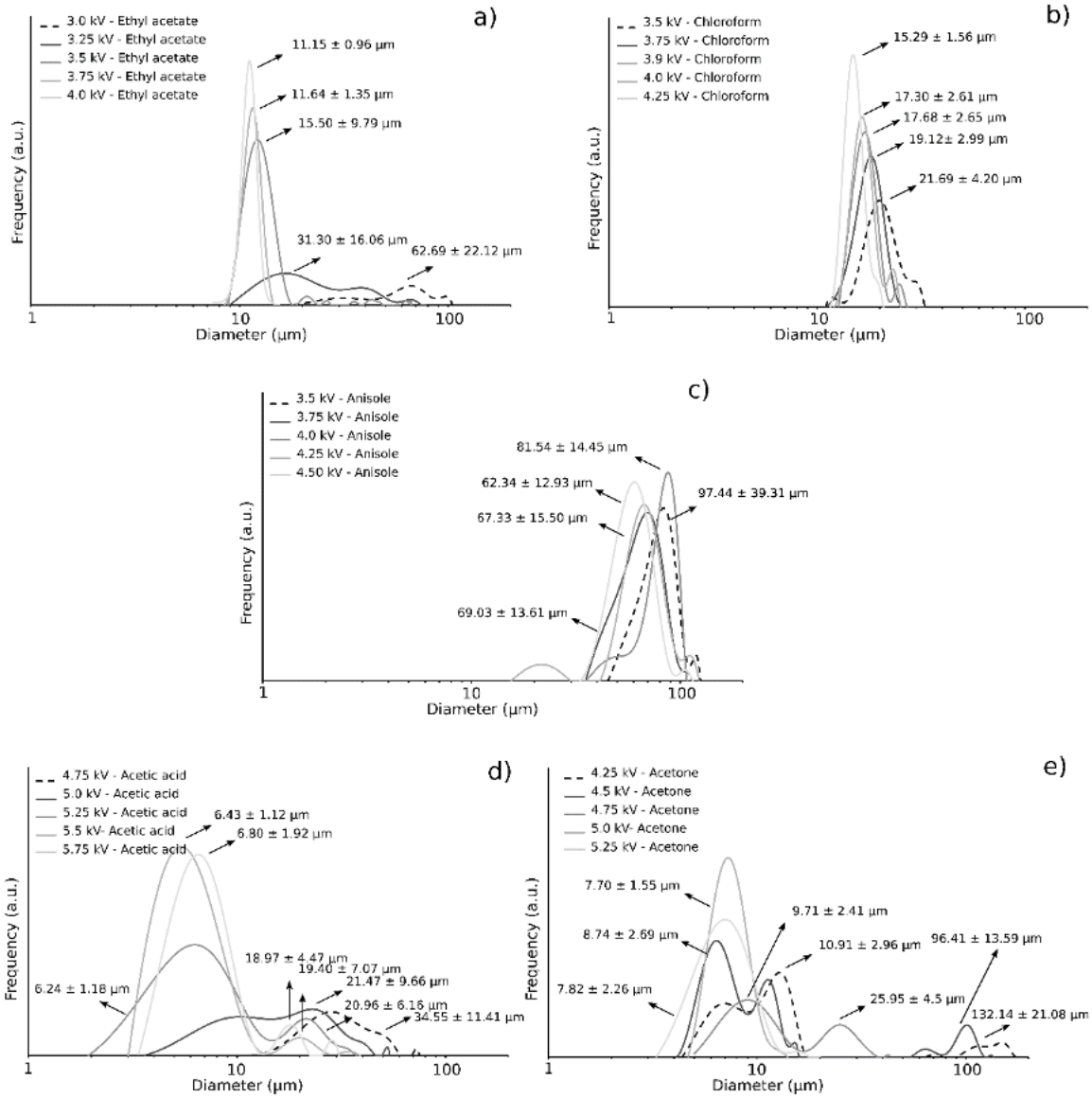

Figure 3-7 Mean diameter and size distribution of PCL electrosprayed microparticles obtained from ethyl acetate (a)), chloroform (b)), anisole (c)), acetic acid (e)), and acetone (f) for a dripping time of 5 s (excepted for anisole, 93 s), at various applied voltages, and a working distance of 17 cm.

3.5 Morphology of PCL microparticles

The morphology of electrosprayed PCL microparticles mainly depends on the phase separation between solvent and PCL as well as the solvent evaporation (Chul, & Jonghwi, 2009; Huang et al., 2017; Lee et al., 2015; Wu, & Clark, 2007), and therefore is affected by the solvent choice and the operating parameters. In general, for low vapor pressure solvents, their evaporations during the electrospraying process are slow. Then, there is enough time for the condensation of polymer chains and phase separation between solvent and PCL matrix before the solidification of electrosprayed droplets. Therefore, nonporous and smooth microparticles (Figure 3-8 (d1-d3)) are obtained from glacial acetic acid (2.09 kPa at 25 ºC). However, some residual solvent in microparticles after reaching collector is also caused by the slowness of solvent evaporation. Due to the residual solvent, microparticles tend to swell and further aggregate together to form blocks or films. Under low working distance, quick dripping time and high PCL concentration, due to the further reduction of solvent evaporation time, this phenomenon is more obvious (Figure 8 (d2 and d3)). For PCL/anisole (0.47 kPa at 25 ºC), due to lower vapor pressure, the evaporation rate of solvent during electrospraying is slower. Therefore, there is more solvent remaining in collected microparticles. After the swelling and aggregation among them, only PCL films are obtained (Figure 3-8 (e)).

For high vapor pressure solvents, their evaporations during electrospraying are quick. Before complete phase separation between solvent and PCL as well as sufficient condensation among PCL chains, solvent had volatilized quickly from electrosprayed droplets and left some pores, gaps and collapses on solid particles. Therefore, porous PCL microparticles are obtained with chloroform and ethyl acetate. Due to the differences between their vapor pressures, cherry-like PCL microparticles with a single pore are observed from a 5 wt% PCL/ethyl acetate solution (Figure 3-8 (a1)). At the same concentration range in chloroform, wrinkle and porous structures are obtained (Figure 3-8 (c1)). With the increasing of PCL concentration, due to the reduction of vapor pressure and the increasing of solid content in electrosprayed droplets, porous morphology tends to convert into nonporous morphology (Figure 3-8 (a2 and c2)). With the decreasing of working distance, the evaporation of chloroform or ethyl acetate becomes incomplete. Therefore, PCL microparticles tend to aggregate together due to residual solvent in microparticles, and some PCL blocks or films with irregular shape and pores can be prepared eventually (Figure 3-8 (a3 and c3)). Meanwhile, with the accelerating of dripping time, the porous structure on PCL

microparticles obtained from ethyl acetate or chloroform becomes more obvious (Figure 3-8 (a4 and c4)).

For PCL/acetone solution, although it has higher vapor pressure (30.7 kPa at 25 ◦C), nonporous and smooth particle surface can be fabricated (Figure 3-8 (b1)). Thus, partial solubility of PCL in acetone leads to complete phase separation before the evaporation of acetone. Meanwhile, combining complete phase separation with quicker solvent evaporation, the morphology of PCL microparticles prepared from acetone keeps unchanged with the evolution of PCL concentration, working distance or dripping time. In addition, due to too high vapor pressure, some microparticles with irregular shape can be fabricated from acetone.

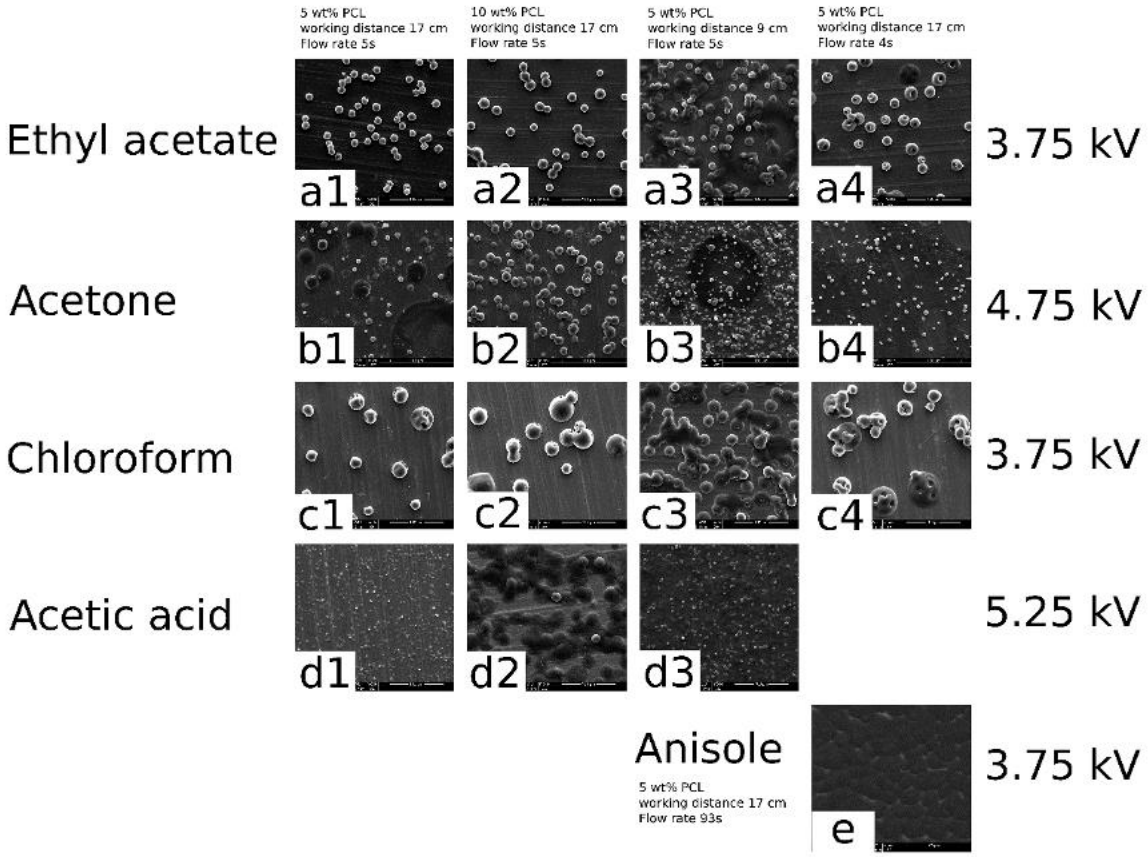

Figure 3-8 SEM images of PCL microparticles obtained from different solvent and different operating parameters (the caption in each figure presents the experimental conditions. For example, ethyl acetate-5wt%-17cm-5s presents that the solvent system is ethyl acetate; PCL concentration is 5wt%; working distance is 17cm; dripping time for one droplet is 5s. For figures a1-a4, c1-c4 and e, the applied voltage is 3.75 kV. For figure b1-b4, the applied voltage is 4.75 kV. For figure d1-d3, the applied voltage is 5.25kv. Scale bar: 100 μm).

3.6 Suitable solvent system for PLA electrospraying

Until now, the common solvent systems used to carry the electrospraying or electrospinning of PLA mainly divide into two groups, i.e., single solvent system and binary solvent system. In previous investigations, when binary solvent systems were used to prepare PLA microparticles, due to the different evaporation rates of the two solvents as well as the phase separation among different solvent phases and PLA phase, the porous structure and irregular morphology are obtained after the unstable evaporation of solvents (Bock, Dargaville, & Woodruff, 2012; Lu et al., 2015; Xu, Skotak, & Hanna, 2006). In general, when single solvent was used to fabricate PLA electrosprayed particles, spherical microspheres or nanofibers with smooth morphology are obtained. The common single solvent systems for PLA electrospraying mainly include 1,2-dichloroethane, chloroform, dichloromethane, acetone, tetrahydrofuran, dimethylformamide and dimethylacetamide. The residual solvent also results in the aggregation of the electrosprayed particles, and a film is finally obtained. Therefore, too fast or too slow evaporation of solvent are both not conductive to the fabrication of electrosprayed particles with desired structure and morphology. Therefore, acetone, dichloromethane, dimethylformamide and dimethylacetamide are not suitable for PLA electrospraying. Considering the toxicity, 1,2-dichloroethane and tetrahydrofuran are also not suitable. Therefore, chloroform is the suitable for PLA electrospraying to obtained PLA electrosprayed particles with desired structure and morphology.

3.7 Conclusions

The effects of solution properties and operating parameters on the formation of electrosprayed PCL microparticles had been clarified. The applied voltage range for cone-jet mainly depends on the electrical conductivity of the electrospraying solution. Solution with higher electrical conductivity needs higher applied voltage to achieve cone-jet during electrospraying. Meanwhile, ideal cone-jet mode is easier to obtain under high viscosity and low surface tension. With the increasing of viscosity, the stability of ideal Taylor cone also improved gradually. Furthermore, the shape of Taylor cone also influences the size and distribution of PCL electrosprayed microparticles. In generally, under low distance from the nozzle to the tip of Taylor cone and thin charged jet, small and homogeneous microparticles are prepared.

For electrospraying liquids with mild electrical conductivity, mono-dispersed microparticles are fabricated.

Their sizes closely correlate to their surface tensions and viscosities. For chloroform and ethyl acetate, small mean diameter about several microns can be obtained from 1 wt% PCL concentration, and particle size increases with the increasing of PCL concentration. For anisole, higher mean diameter about hundreds microns are obtained from 1 wt% PCL concentration, and particle size decreases with the increasing of the the PCL concentration. For electrospraying liquid with a high electrical conductivity, microparticles with poly-dispersed distribution are obtained at low PCL concentration. With the increasing of PCL concentration, the size distribution of microparticles narrows gradually. At 10 wt% PCL, mono-dispersed microparticles with about 15 μm mean diameter are prepared from glacial acetic acid or acetone. Furthermore, for all electrospraying liquids, mono-dispersed microparticles are easier to fabricate under long working distance. During the solidification of electrosprayed droplets, insufficient condensation of polymer chains or remaining solvent in collected particles both introduce large mean diameter. Only the sufficient condensation of polymer chains and the complete evaporation of the solvent carry out simultaneously, tiny electrosprayed particles are fabricated. In addition, the mean diameter of all the PCL microparticles decreases with the increasing of applied voltage or dripping time. Meanwhile, their size distributions also narrow gradually. For the morphology of the electrosprayed PCL microparticles, the slowness of solvent evaporation or complete phase separation between the solvent and the PCL is suitable for obtaining nonporous and smooth morphology. When the evaporation rate of solvent is faster than the rate of phase separation, particles with porous and wrinkle morphology can be obtained. Finally, among four green solvents, ethyl acetate is better substitution of chloroform for preparing PCL microparticles via electrospraying. In addition, chloroform was found to be a suitable solvent to carry out the electrospraying process of PLA.

References

Arya, N., Chakraborty, S., Dube, N., & Katti, D. S. (2009). Electrospraying: A facile technique for synthesis of chitosan-based micro/nanospheres for drug delivery applications. *Journal of Biomedical Materials Research - Part B Applied Biomaterials*, *88*(1), 17–31. https://doi.org/10.1002/jbm.b.31085

Bock, N., Dargaville, T. R., & Woodruff, M. A. (2012). Electrospraying of polymers with therapeutic molecules: State of the art. *Progress in Polymer Science*, *37*(11), 1510–1551. https://doi.org/10.1016/j.progpolymsci.2012.03.002

Bordes, C., Fréville, V., Ruffin, E., Marote, P., Gauvrit, J. Y., Briançon, S., & Lantéri, P. (2010). Determination

of poly(ε-caprolactone) solubility parameters: Application to solvent substitution in a microencapsulation process. *International Journal of Pharmaceutics*, *383*(1–2), 236–243. https://doi.org/10.1016/j.ijpharm.2009.09.023

Chang, M. W., Stride, E., & Edirisinghe, M. (2010). Controlling the thickness of hollow polymeric microspheres prepared by electrohydrodynamic atomization. *Journal of the Royal Society Interface*, *7*(SUPPL. 4). https://doi.org/10.1098/rsif.2010.0092.focus

Chul H. P., & Jonghwi L. (2009). Electrosprayed Polymer Particles: Effect of the Solvent Properties Chul. *Journal of Applied Polymer Science*, *114*, 430–437. https://doi.org/10.1002/app

Gañán-Calvo, A. M., Dávila, J., & Barrero, A. (1997). Current and droplet size in the electrospraying of liquids. Scaling laws. *Journal of Aerosol Science*, *28*(2), 249–275. https://doi.org/10.1016/S0021-8502(96)00433-8

Ghayempour, S., & Mortazavi, S. M. (2013). Fabrication of micro-nanocapsules by a new electrospraying method using coaxial jets and examination of effective parameters on their production. *Journal of Electrostatics*, *71*(4), 717–727. https://doi.org/10.1016/j.elstat.2013.04.001

Huang, X., Gao, J., Li, W., Xue, H., Li, R. K. Y., & Mai, Y. W. (2017). Preparation of poly(ε-caprolactone) microspheres and fibers with controllable surface morphology. *Materials and Design*, *117*, 298–304. https://doi.org/10.1016/j.matdes.2016.12.096

Jaworek, A., & Krupa, A. (1999). Classification of the modes of EHD spraying. *Journal of Aerosol Science*, *30*(7), 873–893. https://doi.org/10.1016/S0021-8502(98)00787-3

Jayasinghe, S. N., & Edirisinghe, M. J. (2002). Effect of viscosity on the size of relics produced by electrostatic atomization. *Journal of Aerosol Science*, *33*(10), 1379–1388. https://doi.org/10.1016/S0021-8502(02)00088-5

Lee, H., Paik, D. H., Jeong, K. Y., Gang, R. H., Lee, J., & Choi, S. W. (2015). Fabrication of poly(methyl methacrylate) and TiO2 composite microspheres with controlled morphologies and porous structures by electrospraying. *Journal of Materials Science*, *50*(19), 6531–6538. https://doi.org/10.1007/s10853-015-9216-5

Lu, J., Hou, R., Yang, Z., & Tang, Z. (2015). Development and characterization of drug-loaded biodegradable PLA microcarriers prepared by the electrospraying technique. *International Journal of Molecular*

Medicine, *36*(1), 249–254. https://doi.org/10.3892/ijmm.2015.2201

Wu, Y. Q., & Clark, R. L. (2007). Controllable porous polymer particles generated by electrospraying. *Journal of Colloid and Interface Science*, *310*(2), 529–535. https://doi.org/10.1016/j.jcis.2007.02.023

Xie, J., Ng, W. J., Lee, L. Y., & Wang, C. H. (2008). Encapsulation of protein drugs in biodegradable microparticles by co-axial electrospray. *Journal of Colloid and Interface Science*, *317*(2), 469–476. https://doi.org/10.1016/j.jcis.2007.09.082

Xu, Y., Skotak, M., & Hanna, M. (2006). Electrospray encapsulation of water-soluble protein with polylactide. I. Effects of formulations and process on morphology and particle size. *Journal of Microencapsulation*, *23*(1), 69–78. https://doi.org/10.1080/02652040500435048

Yao, J., Kuang Lim, L., Xie, J., Hua, J., & Wang, C. H. (2008). Characterization of electrospraying process for polymeric particle fabrication. *Journal of Aerosol Science*, *39*(11), 987–1002. https://doi.org/10.1016/j.jaerosci.2008.07.003

Zhang, L., Huang, J., Si, T., & Xu, R. X. (2012). Coaxial electrospray of microparticles and nanoparticles for biomedical applications. *Expert Review of Medical Devices*, *9*(6), 595–612. https://doi.org/10.1586/erd.12.58

Zhou, F., Cristinacce, P. L. H., Eichhorn, S. J., & Paker, G. J. M. (2016). Preparation and characterization of polycaprolactone microspheres by electrospraying. Aerosol Sci. Technol., 370, 28–34. https://doi.org/10.1080/02786826.2016.1234707

Chapter 4 Preparation of n-Alkanes/Polycaprolactone Microparticles via Single Nozzle Electrospraying and Related Characterizations

Based on the results from chapter III, the effects of solution properties and operating parameters on the formation of electrosprayed particles have been clarified. In this chapter, single electrospraying technology was applied for preparing phase change microcapsules (mPCMs).

In single nozzle electrospraying, a solvent able to solubilize both polymer shell and PCM is used to form the working solution. Then, this solution is pumped out from the electro-sprayed nozzle with an applied voltage to prepare mPCM. During the evaporation of the solvent, the solvent richest phase diffuses to form a shell, and poor solvent phase stays in the inner part of the microcapsules to form the core, due to the solubility differences between matrix and PCM in the working solvent. The cone-jet mode is challenging to reach when compounds with low electrical conductivity, such as PCM, are used. Therefore, the use of a suitable solvent is required to improve the electro-sprayability. Thus, the formation and the final properties of electrosprayed mPCM particles are not only determined by the feed ratio between the polymeric shell and core, but also by the breakup of electrosprayed droplets, the evaporation of solvent, the diffusion of PCM and the phase separation, to lead the formation of the shell around the PCM during the electrospraying process.

In order to clarify the microencapsulation process during electro-spraying and to optimize the structure and properties of the electrosprayed mPCMs, PCL is used as shell matrix, two n-alkanes with different phase state at room temperature (*n*-hexadecane and *n*-eicosane) are used as core materials. Meanwhile, three weight ratios between n-alkanes/PCL in electrospraying solution (30/70, 50/50 and 70/50) are also used to investigate the effects of n-alkanes addition on the formation of the electrosprayed mPCMs. Ethyl acetate (EA) and chloroform (Chl) as suitable carriers for PCL electrospraying have been selected to study the effects of solvent systems on the formation of the electrosprayed mPCMs. The optimization operating parameters obtained from Chapter III are fixed in this Chapter. The structures, morphologies, and thermal properties of the mPCM are characterized by optical microscopy (OM), scanning electron microscopy (SEM), differential scanning calorimeter (DSC), thermogravimetric analysis (TGA), and Fourier transform infrared spectroscopy (FT-IR).

4.1 Size and Morphology of Electro-Sprayed n-alkanes/PCL mPCMs

The size, the surface state, and the morphology of electro-sprayed mPCM were characterized by SEM and OM observations (Figure 4-1). They are mainly influenced by the PCMs content, the phase change temperature of the PCMs used during the process, and also the choice of the solvents. Blank PCL particles present a spherical shape, whatever the solvent selected, i.e., chloroform or ethyl acetate (Figure 4-1 (n1, n2)). The use of chloroform allows the particles to have a smooth surface state. In contrast, the solubilization in ethyl acetate solution leads to the formation of a single-pore morphology as previously described by Zhang et al. (Zhang, Campagne, & Salaün, 2019). Adding PCMs in the working solution does not have a substantial effect on the obtained morphology, since the obtained particles are also spherical. Nevertheless, the increase of n-alkanes in the solution leads to an increase in the mean diameter and the particle size distribution. Furthermore, in the case of the use of EA as the solvent, single-pore morphology turns to a non-porous morphology for PCMs/PCL blends.

The use of n-hexadecane and n-eicosane does not lead to the same granulometric properties. n-hexadecane is in its liquid state at room temperature, while n-eicosane is in its solid state. Under the action of Coulombic repulsions, the break-up process of n-eicosane/PCL charged droplets is different from that of n-hexadecane/PCL one. During the flying process, from the nozzle to the collector, droplets containing n-eicosane start their solidification at the earliest stages due to the evaporation of the solvent, which induces an enhancement of n-eicosane chain interactions and, therefore, their crystallization. Therefore, it leads to a higher specific surface to volume ratio, which prevents the further break-up process of the electro-sprayed droplets, unlike n-hexadecane, which is in a liquid state throughout the process. Furthermore, the crystallization being an exothermic phenomenon increases the local temperature in the inner core of the droplets, which leads to a growth of the solvent evaporation rate. Therefore, the use of n-eicosane leads to the formation of particles having a higher mean diameter and particle size distribution than with n-hexadecane one. Since solid particles are obtained in the earliest stages of the flying process, in the last steps, the solvent release results in the obtaining of the rough and wrinkled surface state of the particles, which is more pronounced with the increase of n-eicosane content. Thus, the black color observed in OM micrographs of n-eicosane/PCL particles belonged to n-eicosane laying on the surface of the PCL matrix (Figure 4-1 (b3, d3)). At low content in n-eicosane, the core compound is completely entrapped by the PCL shell. But when it further increased due to the thermodynamical phenomena and solvent evaporation,

excesive n-eicosane can't be captured completely by limited PCL matrix, and it diffuses on the surface of the particles.

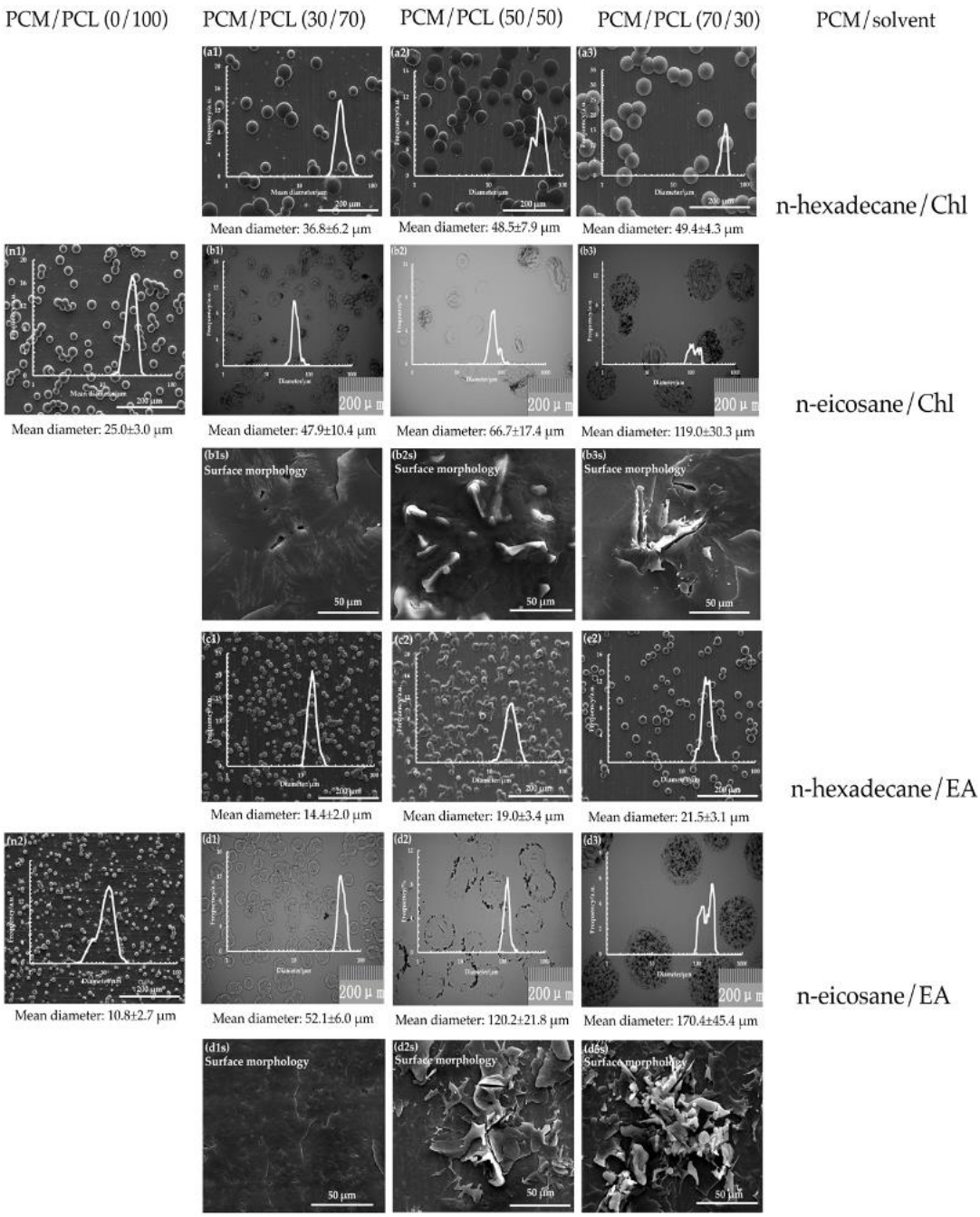

Figure 4-1 Scanning electron microscopy (SEM) and optical microscopy (OM) graphs of neat poly(caprolactone) (PCL) microspheres and mPCM obtained from different conditions (n1) neat PCL microspheres obtained from chloroform (n2) neat PCL microspheres obtained from ethyl acetate (a1–a3) n-hexadecane/PCL/chloroform microcapsules (b1–b3) n-eicosane/PCL/chloroform microcapsules (b1s–b3s: Their

surface morphologies) (c1–c3) n-hexadecane/PCL/ethyl acetate microcapsules (d1–d3) n-eicosane/PCL/ethyl acetate microcapsules (d1s–d3s: their surface morphologies) (scale bar: 200 µm) (b1s–b3s and d1s–d3s) the magnification SEM images of related sample surface morphology (scale bar: 50 µm).

The granulometric properties of the electro-sprayed particles, as well as their morphology, are also affected by the solvent choice, that is used to solubilize the polymer and the n-alkane. Thus, in the presence of ethyl acetate (Figure 4-1 (c1–c3)), the obtained particles with n-hexadecane have a lower mean diameter and a narrower size distribution than with chloroform (Figure 4-1 (a1–a3)). This is related to the higher vapor pressure solution and viscosity of the chloroform based solution (Zhang et al., 2019). During the earliest stages of the flying process, chloroform evaporates quicker in the surrounding medium compared with ethyl acetate solution, and in the absence or at low solvent content, the process break-up stops before to reach the collector. Furthermore, high viscosity also depresses the break-up process of the charged droplets, resulting in a higher size of the electro-sprayed particles (Xie, Marijnissen, & Wang, 2006).

On the other hand, the mean diameter and the particle size distribution of the electro-sprayed n-eicosane particles are determined in the earliest stage of the process due to core compound crystallization, which allows solid particles to be obtained. Then, in the presence of chloroform (Figure 4-1 (b1–b3)), the process break-up coupled to the solvent evaporation allows the formation of tinier particles than with ethyl acetate (Figure 4-1 (d1–d3)).

Also, the crystallization of n-eicosane plays a primary role in the obtained morphology. Thus, n-eicosane/PCL microcapsules, obtained from ethyl acetate, are rougher and more wrinkled than those obtained from chloroform (Figure 4-1 (b1s–b3s) and Figure 4-1 (d1s–d3s)). During the solidification of the n-alkane, ethyl acetate gradually is released from these particles until reaching the collector, which allows the diffusion of the n-alkanes chains to the surface of the particles. Whereas, in the presence of chloroform, due to its quick evaporation, n-eicosane is located in the inner core of the particles.

4.2 Chemical structure of Electro-Sprayed n-alkanes/PCL mPCMs

FT-IR spectra of PCL microparticles, n-hexadecane/PCL microparticles in EA, n-hexadecane/PCL microparticles in Chl, and n-eicosane/PCL microparticles in Chl are depicted in Figure 4-2. PCL microparticles spectrum shows a strong absorption band at 1750 cm^{-1} corresponding to the stretching vibration of carbonyl group,

and characteristic bands at 2915 to 2860 cm^{-1} associated with the aliphatic C–H stretching vibrations. The characteristic bands at 1475 cm^{-1}, 1397 cm^{-1}, and 1361 cm^{-1} are attributed to the bending vibration of the alkyl group, and those located at 1230 cm^{-1}, 1107 cm^{-1}, and 1042 cm^{-1} corresponding to the stretching vibration of –CO-C– group. Stretching vibrations of -C-C- and -CO- are found at 1290, and 1160 cm^{-1}, respectively (Entekhabi et al., 2016). PCMs spectra exhibit a strong absorption band at 2920–2852 cm^{-1} associated with the aliphatic C–H stretching vibrations of the n-hexadecane or n-eicosane. The in-plane rocking vibration of the CH_2 groups is observed at 717 cm^{-1}, and C–H bending vibration in CH_2 is found at 1470 and 1370 cm^{-1}. All of the characteristic peaks for n-hexadecane, or n-eicosane, and PCL, are clearly distinguished in the spectra of the FT-IR spectra of the electro-sprayed micro-particle samples, which verifies that n-alkane are successfully entrapped by PCL.

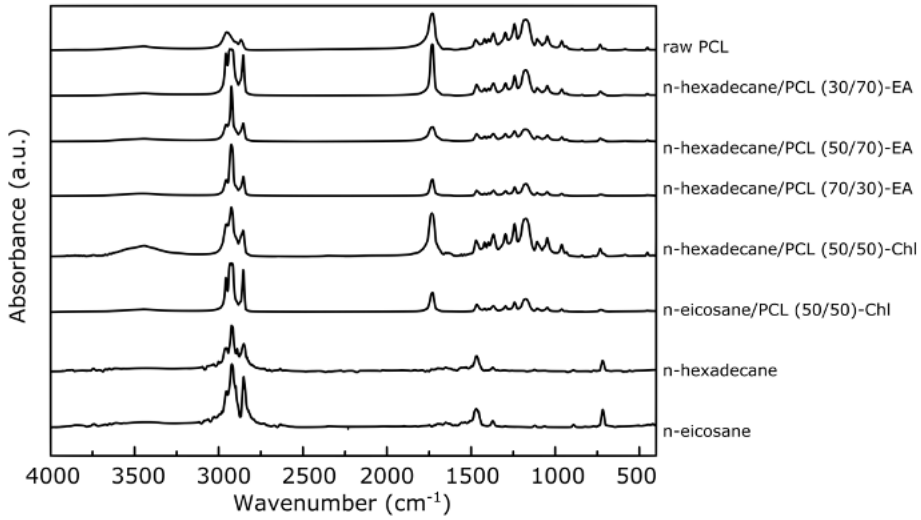

Figure 4-2 The Fourier transform infrared spectroscopy (FT-IR) spectra of n-eicosane, n-hexadecane, neat PCL microsphere and a series of mPCM obtained from different conditions.

4.3 Phase change properties of electro-sprayed n-alkanes/PCL mPCMs

The phase change temperatures and the latent heats of melting and crystallization of raw n-alkanes, neat PCL microspheres, and mPCMs were obtained using differential scanning calorimeter. They are presented in Figures 4-3 and 4-4, and gathered in Tables 4-1 and 4-2. On the one hand, the latent heats of fusion of raw n-hexadecane and n-eicosane are 199, and 205 $J \cdot g^{-1}$, respectively. Their melting and crystallization temperatures are found at 17.9 °C, 16.2 °C, 34.3 °C, and 35.7 °C. On the other hand, the onset of melting and crystallization temperatures of PCL microspheres are determined at 54.9 and 41.2 °C, when they have been prepared from ethyl acetate

solution, and 55.6 and 41.5 °C from chloroform. The solvent used modifies to a limited extent the crystallinity since it is about 40.8% and 42.7% for the samples prepared from EA, and Chl, respectively. DSC thermograms of microencapsulated PCM have both the thermal transitions of the n-alkanes used and PCL.

The increase of n-hexadecane to PCL from 30 to 70 wt.% in the EA working solution results in the increase of the melting (and crystallization) enthalpy from 52 to 113 $J \cdot g^{-1}$, corresponding to an increase of the loading content from 26 to 56%, which is a quite lower than the theoretical content. On the other hand, the encapsulation efficiency reaches a maximum of 89% for 50 wt.%, then decreases to 81% for 70 wt.%. The loading content does not have a significant effect on the phase change transition temperatures, which are close to the raw n-hexadecane one. The mPCMs obtained from chloroform solution have lower melting enthalpy than those with ethyl acetate. The encapsulation efficiency is slightly lower too. Furthermore, the melting and crystallization temperatures for low loading content are found relatively lower compared to the other content. The loss of n-hexadecane during electrospray microencapsulation results from the evaporation of the solvent in flight, which promotes phase separation between n-hexadecane and PCL, and sometimes the presence of pure tiny droplets of n-hexadecane. The solidification of the PCL hindrances this phenomenon. n-hexadecane is highly soluble in chloroform than in ethyl acetate, and therefore, has a better compatibility (Bordes et al., 2010; Pereira, & Vebber, 2019). Thus, the use of the chloroform working solution induces a higher loss in n-hexadecane during its evaporation. The use of ethyl acetate may prevent this phenomenon, and therefore, higher loading contents in PCMs in the microcapsules, are obtained.

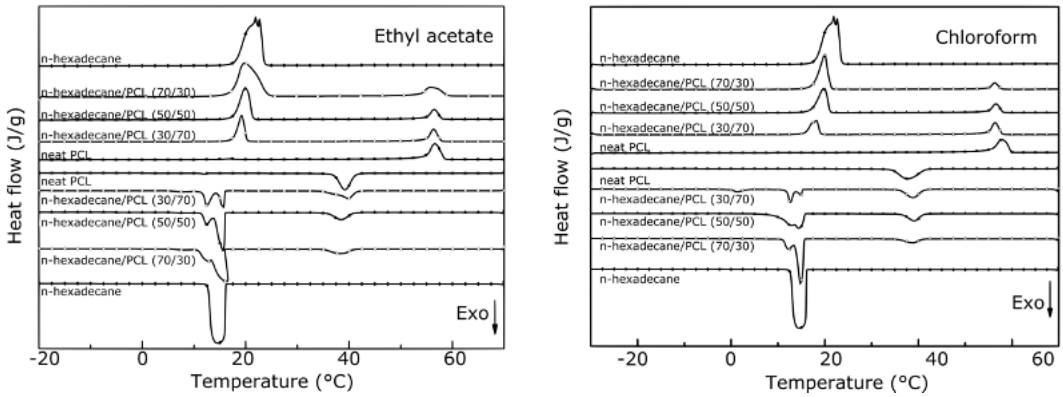

Figure 4-3 DSC curves of n-hexadecane, neat PCL microspheres and a series of n-hexadecane/PCL microcapsules obtained from different solvents with different mass ratios between n-hexadecane and PCL.

Apart from n-hexadecane/PCL microcapsules, the thermal properties of n-eicosane-based mPCMs, obtained

from different solvents and various weight ratios between the n-alkane and PCL, are also presented in Figure 4-4 and Table 4-2. On the one hand, the presence of the PCL and the choice of the solvent used for the working solution does not affect the phase temperatures, which are quite similar to the raw n-hexadecane one. On the other hand, the use of chloroform allows entrapping higher content of n-eicosane (more than 10%) compared to the use of ethyl acetate. These results are the opposite of those obtained in the case of n-hexadecane, highlighting the influence or importance of the phase change that takes place during the flying process. Thus, the solvent evaporation, which occurs in the early stages of the electro-spraying process, induces a quick phase separation and further the PCMs crystallization, which also promotes the stiffening of the PCL. In this context, the more volatile the solvent of the working solution, the more PCMs is entrapped in the microparticles. Furthermore, the calculated loading content of n-eicosane when working with chloroform is quite the same as those obtained with n-hexadecane and ethyl acetate. Higher encapsulation efficiencies are obtained.

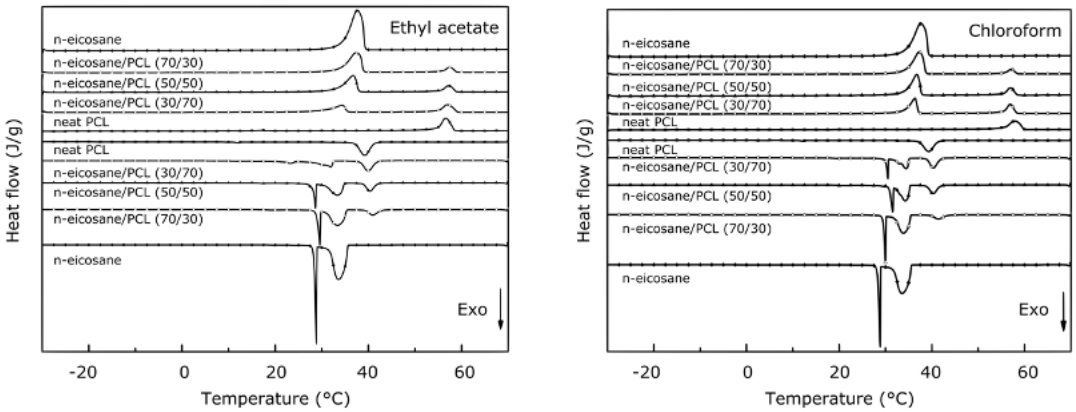

Figure 4-4 Differential scanning calorimeter (DSC) cuves of n-eicosane, neat PCL microspheres and a series of n-eicosane/PCL microcapsules obtained from different solvents with different mass ratios between n-eicosane and PCL.

Table 4-1 Thermal properties of *n*-hexadecane, neat poly(caprolactone) (PCL) microspheres and a series of *n*-hexadecane/PCL microcapsules obtained from ethyl acetate and chloroform solutions at three weight ratios between *n*-hexadecane and PCL.

Sample Label		Latent Heat ($J \cdot g^{-1}$)		T_{onset} (°C)		T_c or T_m (°C)		T_{end} (°C)		*LC* (%)	*EE* (%)	$X_{c(th)}$ (%)	$X_{c(m)}$ (%)
n-hexadecane (C_{16})	heating	199.4 ± 2.2		17.9		20.7		23.7					
	cooling	195.9 ± 4.7		16.2		16.0		13.0					
Neat-PCL-EA	heating		57.0 ± 1.1		54.9		56.4		58.5				
	cooling		54.7 ± 1.3		41.2		39.5		37.2				
C_{16}/PCL-30/70-EA	heating	52.1 ± 7.3	32.5 ± 1.5	17.7	55.0	19.9	56.2	20.2	57.7	26.1 ± 3.7	87.1 ± 12.2	33.3 ± 1.5	31.5 ± 1.5
	cooling	51.7 ± 6.6	33.6 ± 3.9	16.0	41.5	15.9	39.9	14.7	37.1				
C_{16}/PCL-50/50-EA	heating	88.7 ± 4.1	25.0 ± 0.6	17.6	55.0	19.2	56.2	21.2	57.8	44.5 ± 2.0	89.0 ± 4.1	35.8 ± 0.8	32.0 ± 0.7
	cooling	88.1 ± 1.8	25.7 ± 0.5	16.1	40.9	16.4	38.7	14.0	36.0				
C_{16}/PCL-70/30-EA	heating	113.2 ± 7.2	24.1 ± 1.1	17.5	55.0	19.5	56.2	22.7	58.4	56.8 ± 3.7	81.1 ± 5.2	57.7 ± 2.8	40.0 ± 1.9
	cooling	111.7 ± 5.1	25.9 ± 1.8	16.1	40.8	16.4	38.8	13.6	35.8				
Neat-PCL-Chl	heating		59.6 ± 2.0		55.6		57.6		59.8				
	cooling		57.2 ± 1.9		41.5		37.9		34.4				
C_{16}/PCL-30/70-Chl	heating	35.6 ± 0.7	31.6 ± 1.6	15.9	54.9	18.1	56.2	19.1	57.8	17.8 ± 0.4	59.4 ± 1.2	32.4 ± 1.6	27.6 ± 1.4
	cooling	35.3 ± 1.0	33.2 ± 1.6	13.6	41.2	12.8	39.0	11.9	36.1				
C_{16}/PCL-50/50-Chl	heating	72.4 ± 0.6	25.0 ± 0.3	17.2	55.0	19.2	56.3	21.0	58.0	36.3 ± 0.3	72.6 ± 0.6	35.8 ± 0.4	28.1 ± 0.1
	cooling	71.1 ± 0.4	26.0 ± 0.5	15.8	41.1	14.8	39.4	12.4	36.6				
C_{16}/PCL-70/30-Chl	heating	99.4 ± 5.7	17.0 ± 1.5	17.5	55.0	19.5	56.2	21.0	57.7	49.9 ± 2.8	71.2 ± 4.1	40.5 ± 2.7	24.2 ± 2.2
	cooling	96.9 ± 4.7	15.8 ± 0.4	15.7	41.0	15.5	38.8	13.8	35.6				

Table 4-2 Thermal properties of n-eicosane, neat PCL microspheres and a series of n-eicosane/PCL microcapsules obtained from ethyl acetate and chloroform solutions at three weight ratios between n-eicosane and PCL.

Sample Label		Latent Heat ($J \cdot g^{-1}$)		T_{onset} (°C)		T_m or T_c (°C)		T_{end} (°C)		*LC* (%)	*EE* (%)	$X_{c(th)}$ (%)	$X_{c(m)}$ (%)
n-eicosane (C_{20})	heating	205.3 ± 1.7		34.3		36.9		39.2					
	cooling	204.2 ± 1.9		35.7		30.7		28.7					
Neat-PCL-EA	heating		57.0 ± 1.1		54.9		56.4		58.5				
	cooling		54.7 ± 1.3		41.2		39.5		37.2				
C_{20}/PCL-(30/70)-EA	heating	42.3 ± 2.0	32.1 ± 1.1	32.8	55.3	35.5	57.0	36.6	59.0	20.6 ± 1.0	68.6 ± 3.2	32.9 ± 1.1	29.0 ± 1.0
	cooling	41.2 ± 3.1	31.3 ± 2.7	34.2	41.4	28.1	40.3	27.3	38.5				
C_{20}/PCL-(50/50)-EA	heating	72.4 ± 7.3	21.2 ± 1.2	33.2	55.5	36.3	57.0	37.8	58.7	35.3 ± 3.4	70.6 ± 7.2	30.5 ± 1.7	23.5 ± 1.3
	cooling	72.1 ± 7.1	21.6 ± 1.6	34.8	42.0	29.4	40.6	28.2	39.0				
C_{20}/PCL-(70/30)-EA	heating	107.2 ± 2.4	17.8 ± 0.5	33.9	55.8	36.4	57.1	38.4	58.6	52.3 ± 1.1	74.7 ± 1.6	42.5 ± 1.3	26.7 ± 0.9
	cooling	106.9 ± 2.6	17.7 ± 0.7	35.4	42.9	31.5	41.2	30.0	39.6				
Neat-PCL-Chl	heating		59.6 ± 2.0		55.6		57.6		59.8				
	cooling		57.2 ± 1.9		41.5		37.9		34.4				
C_{20}/PCL-(30/70)-Chl	heating	60.2 ± 0.2	37.3 ± 2.4	34.0	55.4	36.0	56.7	37.1	58.1	29.3 ± 0.1	97.8 ± 0.4	38.2 ± 2.4	37.9 ± 2.4
	cooling	59.9 ± 1.3	38.0 ± 5.5	35.2	41.6	30.9	40.6	30.2	39.0				
C_{20}/PCL-(50/50)-Chl	heating	94.3 ± 0.8	28.1 ± 2.5	34.2	55.4	36.3	56.7	37.7	58.6	45.9 ± 0.4	91.9 ± 0.8	40.3 ± 3.5	37.2 ± 5.4
	cooling	93.1 ± 3.3	29.8 ± 4.1	34.5	41.9	32.1	40.6	30.9	39.0				
C_{20}/PCL-(70/30)-Chl	heating	121.1 ± 1.9	17.4 ± 0.6	34.3	55.6	36.7	57.0	39.6	58.3	59.0 ± 0.9	84.3 ± 0.7	41.6 ± 1.3	30.4 ± 1.0
	cooling	117.4 ± 1.2	17.2 ± 0.5	35.5	43.4	31.2	41.5	29.7	39.9				

Differential Scanning Calorimetry was also used to determine the effect of solvent and core compounds on the thermal properties of PCL microparticles. All data were determined from the second run, and the first run was used to clear the thermal history. The DSC thermograms (Figures 4-3 and 4-4) show single melting peaks with maximum melting start and end temperatures of 54.9 and 56.4 °C for ethyl acetate solution, which increase slightly to 55.6 and 57.6 °C for chloroform. The latent heat of fusion associated with these transitions is approximately 57.0 and 59.5 $J \cdot g^{-1}$, which corresponds to a crystallinity degree of 40.8 and 42.7%, respectively. The presence of n-alkanes in the microparticles does not affect the melting temperatures of the PCL, but at high n-hexadecane content, there is a slight decrease in crystallization temperatures, while n-eicosane acts as a nucleating agent of the PCL, and therefore the crystallization temperatures increase. However, n-alkanes play a significant role in the formation of the crystalline phase of PCL. The increase in the n-alkane content leads to a decrease in the crystalline phase. This trend is quite similar, regardless of the solvent and n-alkane used.

In addition, the calculated crystallinity index of PCL matrix in the mPCMs is influenced by the solvent/n-alkane pair used, which is correlated with the crystallization rate during the electrospraying process. When the measured crystallinity index values ($X_{c(m)}$) are compared with the calculated (theoretical) values ($X_{c(th)}$), they are lower, except low weight ratio, where they are close. Thus, the presence of n-alkanes in the microparticles, reduces the PCL chain mobility, which gives rise to a lower crystallinity index in both the selected solvent and the n-alkane systems.

Thus, the presence of n-alkanes leads to a decrease in the crystallinity index. In the early stages of the electrospray process, the droplets contain solvent, PCL macromolecular chains and PCMs molecules. Depending on the solubility of PCMs and PCL in each solvent system, the PCMs molecules are dispersed together to form a mixed solution in which the macromolecular PCL chains have an intermolecular interaction or are entangled in the PCMs chains when the solvent evaporates. The presence of PCMs molecules reduces the mobility of PCL macromolecular chains and thus limits their availability for crystallization. This results in a more amorphous matrix (Dubernet, 1995; Jenquin, & McGinity, 1994; Mochane, & Luyt, 2012; Valo et al., 2009). In addition, the solvent used also affects the crystallinity index, PCL and n-alkanes are more soluble in Chl than in EA, which leads to the preparation of the most homogeneous working solutions.

The rapid evaporation rate of Chl, during the early stages of the process, induces a higher phase separation between PCL and PCM, and therefore, a higher crystallinity index in the case of n-eicosane compared to the use

of EA. The low evaporation rate of EA during the process leads to a higher degree of entanglement of the PCL macromolecular chains and PCM molecules, and therefore to a more amorphous matrix. Considering that n-hexadecane is liquid state during the process, the molecules diffuse into the inner nucleus of the droplets during the slow evaporation of EA, allowing the PCL macromolecular chains to organize themselves to build the shell. On the other hand, the crystallinity index of PCL was found to decrease with increasing PCM content when Chl was used as a solvent. This observation suggests that the organization of the macromolecular chains is limited.

However, the difference between the theoretical content and the determined content of n-alkanes in the microparticles also suggests the presence of a PCM chain dispersed in the PCL matrix. Thus, the microparticles contain in the inner nucleus the n-alkanes, surrounded by a mixture of PCL/PCM chains, entrapped in a PCL shell.

4.4 Thermal stability of electro-sprayed n-alkanes/PCL mPCMs

The thermal stability of the raw PCMs, the neat PCL electrosprayed microparticles and mPCMs were analyzed by TGA. TG and DTG curves of PCL microparticles, n-hexadecane (or n-eicosane) and n-hexadecane (or n-eicosane) based microparticles from chloroform and ethyl acetate are shown in Figure 4-5 (or Figure 4-6). The thermal behavior of n-hexadecane and n-eicosane displays single step degradation under N_2 atmosphere. The decomposition of n-alkanes, characterized by the onset temperature at 5% weight loss, starts at 151.6 and 178.8 °C for n-hexadecane, and n-eicosane, respectively. The main decomposition peaks of n-hexadecane and n-eicosane corresponding to the n-alkanes backbone decomposition take place at 246 °C and 269 °C, and the maximum rates of decomposition are about 2.2, and 2.6% $°C^{-1}$, respectively. Furthermore, there is no residue for these compounds at over 280 °C. Under an inert atmosphere, PCL electro-sprayed microparticles display a single step degradation between 350 to 500 °C, corresponding to polymer pyrolysis with a maximum of degradation temperature at 411 or 413 °C, according to the solvent used in the electrospraying process. The initial degradation temperatures (T_{onset}) were found to occur at 359 and 369 °C for samples prepared from ethyl acetate and chloroform, respectively. Furthermore, it seems that the solvent used has a few influences on the temperatures and maximum rate degradation (Table 4-3).

n-alkanes based microparticles exhibit a two-step degradation. The first one, located from about 100 to 350 °C is ascribed to the PCM degradation, whereas the second one to the PCL matrix between 350 to 500 °C. The presence of PCL does not have an effect on the initial degradation temperature in the case of n-hexadecane,

but a shift from 10 to 18 °C is observed for samples containing n-eicosane (Table 4-4). In the first degradation step, two types of phenomena occur, the first one corresponds to the degradation of n-alkane at the surface of the sample until 250 °C. When the temperature reaches 60–62 °C, PCL melts, and then all the microparticles samples are in a liquid state. Due to its lower density, a part of n-alkane chains can diffuse at the crucible surface and starts its degradation. The second phenomenon, between 250 to 300 °C, is related to the entrapped n-alkane chains in the PCL matrix and their entanglements, which required more thermal energy to be degraded since PCL acts as a barrier to prevent the degradation. In addition, with the increasing of n-alkane content, the maximum degradation rate in the first stage increases gradually; on the other hand, the second step is similar to that of the PCL.

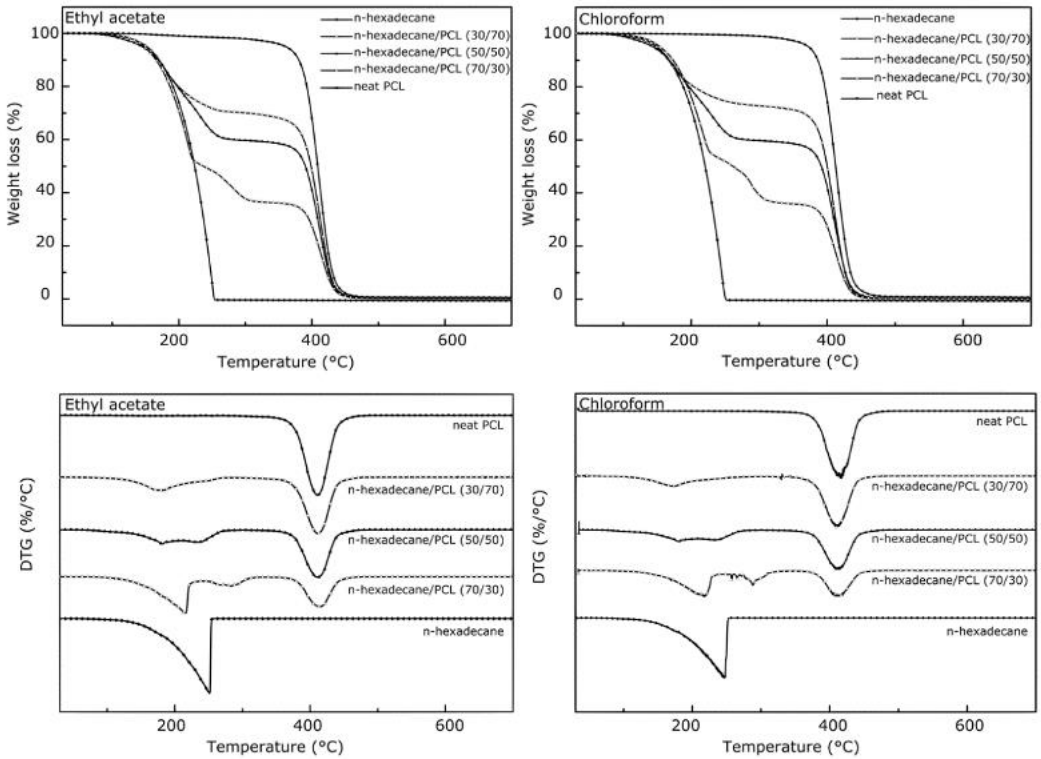

Figure 4-5 TG and DTG curves of n-hexadecane, neat PCL and the microencapsulated n-hexadecane.

On the one hand, even if the initial degradation temperatures are close to the n-hexadecane, the maximum degradation temperatures in the first stage are significantly lower than the raw compound, increase with the increase in the loading content, and are not very dependent on the solvent used. On the other hand, when n-eicosane was used as a core compound, the initial thermal degradation temperatures are 10 to 18 °C higher than that of the raw compound one and decrease with the increase in the loading content. The maximum degradation temperatures in the first stage are 30 °C lower than n-eicosane one for low loading content and increase up to the

n-alkane one at higher loading content. Furthermore, chloroform based microparticles have better thermal stability than the ethyl acetate-based one. This stability is related to the affinity between PCL and n-alkanes chains in the solvent solutions, which can favorize the entanglement during the electrospraying process.

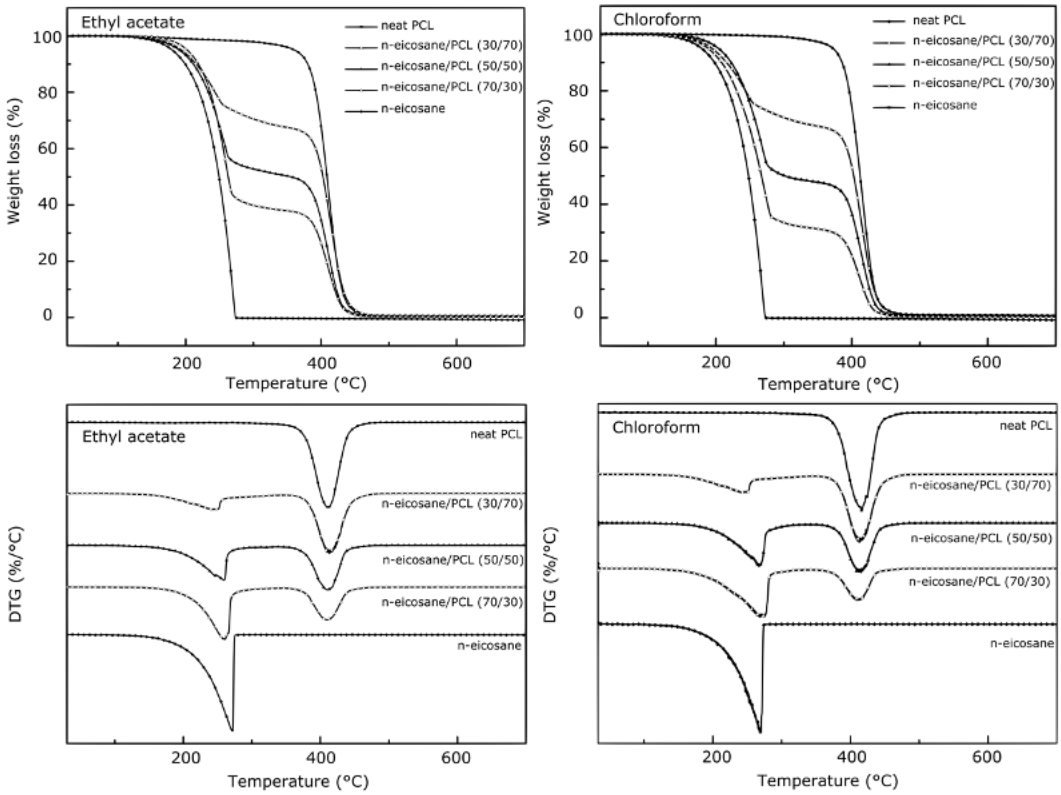

Figure 4-6 TG and DTG curves of n-eicosane, neat PCL and the microencapsulated n-eicosane.

Table 4-3 Thermogravimetric data for of n-hexadecane, neat PCL microsphere and n-hexadecane microcapsules in inert atmosphere at a heating rate of 10 °C.min^{-1}.

Sample	Initial Degradation Temperature (°C)	First Step			Second step		
		Weight Loss (100–350 °C) (%)	Maximum Degradation Temperature (°C)	Maximum Degradation Rate (%/°C)	Weight Loss (350–500 °C) (%)	Maximum Degradation Temperature (°C)	Maximum Degradation Rate (%.°C^{-1})
Neat-PCL-EA	358.9 ± 3.1	4.2 ± 0.9	-	-	95.0 ± 1.1	411.4 ± 0.4	2.2 ± 0.1
Neat-PCL-Chl	369.2 ± 3.6	3.0 ± 0.4	-	-	96.1 ± 0.4	413.4 ± 1.6	2.3 ± 0.02
Raw *n*-hexadecane (C_{16})	151.6 ± 1.1	99.4 ± 0.1	246.6 ± 0.7	2.2 ± 0.1	-	-	-
C_{16}/PCL-30/70-EA	150.8 ± 1.9	29.6 ± 1.7	174.3 ± 9.1	0.3 ± 0.1	69.6 ± 1.9	412.9 ± 3.4	2.0 ± 0.9
C_{16}/PCL-50/50-EA	145.8 ± 2.3	39.5 ± 5.7	183.5 ± 10.3	0.5 ± 0.2	59.3 ± 6.3	411.9 ± 2.4	1.4 ± 0.2
C_{16}/PCL-70/30-EA	149.5 ± 5.8	59.2 ± 4.3	214.9 ± 5.9	0.9 ± 0.2	39.9 ± 8.5	413.3 ± 1.4	1.0 ± 0.2
C_{16}/PCL-30/70-Chl	150.1 ± 3.1	27.3 ± 0.9	173.5 ± 2.7	0.3 ± 0.03	72.0 ± 1.0	413.7 ± 0.3	1.8 ± 0.02
C_{16}/PCL-50/50-Chl	147.3 ± 4.6	37.4 ± 2.4	177.5 ± 1.6	0.4 ± 0.04	61.8 ± 2.8	412.5 ± 1.5	1.5 ± 0.1
C_{16}/PCL-70/30-Chl	151.8 ± 6.1	60.4 ± 4.0	217.0 ± 1.0	0.9 ± 0.1	38.9 ± 7.3	414.7 ± 2.4	0.9 ± 0.1

Table 4-4 Thermogravimetric data for of *n*-eicosanee, neat PCL microsphere and *n*-eicosane microcapsules in inert atmosphere at a heating rate of 10 °C.min^{-1}.

Sample	Initial Degradation Temperature (°C)	First Step			Second Step		
		Weight Loss (100–350 °C) (%)	Maximum Degradation Temperature (°C)	Maximum Degradation Rate (%/°C)	Weight Loss (350–500 °C) (%)	Maximum Degradation Temperature (°C)	Maximum Degradation Rate (%/°C)
Neat-PCL-EA	358.9 ±3.1	4.2 ± 0.9	-	-	95.0 ± 1.1	411.4 ± 0.4	2.2 ± 0.1
Neat-PCL-Chl	369.2 ± 3.6	3.0 ± 0.4	-	-	96.1 ± 0.4	413.4 ± 1.6	2.3 ± 0.02
raw *n*-eicosane (C_{20})	178.8 ± 1.3	99.9 ± 0.1	269.1 ± 0.01	2.6 ± 0.1	-	-	-
C_{20}/PCL-30/70-EA	196.4 ± 9.7	26.9 ± 3.0	236.1 ± 6.1	0.4 ± 0.1	72.4 ± 5.4	414.9 ± 0.6	1.7 ± 0.1
C_{20}/PCL-50/50-EA	194.0 ± 13.6	44.1 ± 4.9	254.8 ± 3.5	0.9 ± 0.04	55.3 ± 5.4	413.6 ± 2.3	1.3 ± 0.2
C_{20}/PCL-70/30-EA	188.8 ± 14.0	58.1 ± 6.8	248.2 ± 12.9	1.2 ± 0.2	41.6 ± 6.8	407.0 ± 5.1	1.0 ± 0.3
C_{20}/PCL-30/70-Chl	194.3 ± 11.8	30.6 ± 4.4	237.3 ± 4.9	0.4 ± 0.1	68.8 ± 4.3	414.4 ± 1.8	1.6 ± 0.1
C_{20}/PCL-50/50-Chl	195.9 ± 7.8	49.5 ± 4.0	268.1 ± 1.0	1.0 ± 0.1	49.8 ± 3.7	414.1 ± 2.2	1.2 ± 0.1
C_{20}/PCL-70/30-Chl	186.8 ± 10.5	69.3 ± 1.1	269.5 ± 5.6	1.3 ± 0.2	30.2 ± 0.8	413.2 ± 3.5	0.7 ± 0.04

4.5 Structural stability of the electro-sprayed n-alkanes/PCL mPCMs

The shape stabilization of the electro-sprayed microparticles shape was investigated by SEM analyses after the heating and cooling process from −30 to 50 °C and 50 to −30 °C (Figure 4-7). After the thermal treatment, the shape and the particle morphology present any changes. The observed particles are spherical shape, smooth, and compact surface morphology. The absence of n-hexadecane on the SEM micrographs indicated that the PCL shell protects the PCM core from the leakage. Therefore, the entrapment of PCM in the PCL matrix with this electrospraying process allows obtaining suitable stability.

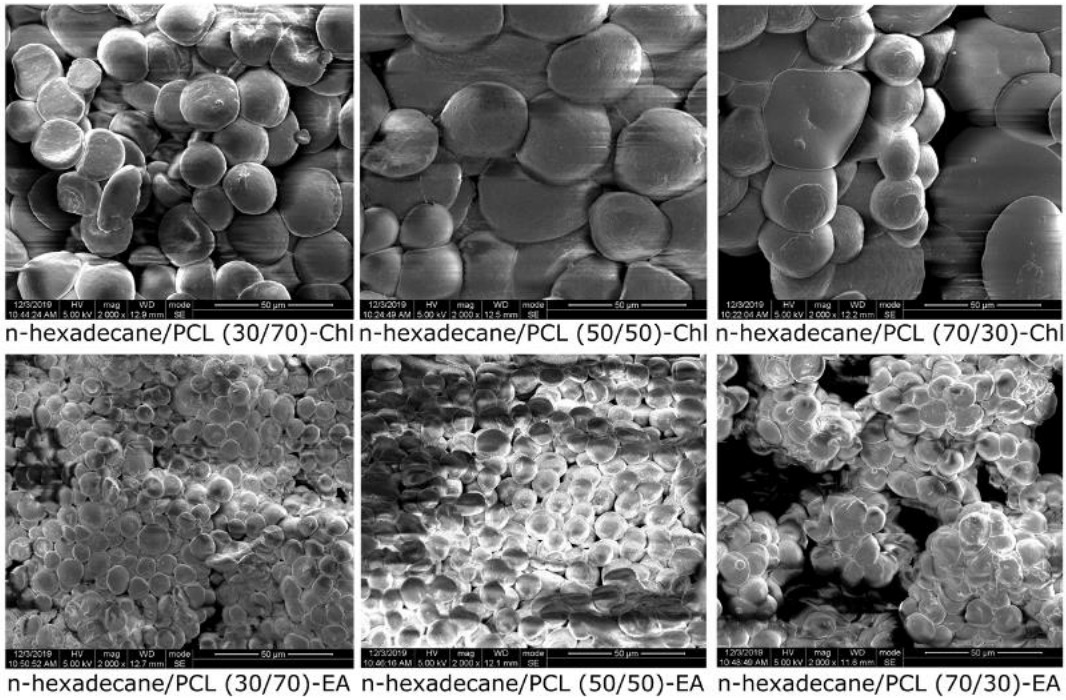

Figure 4-7 SEM micrographs of n-hexadecane/PCL microparticles after thermal treatment.

4.6 Conclusions

The microencapsulated phase change materials in the PCL matrix were successfully manufactured by an electrospray process, using two types of solvents, ethyl acetate and chloroform, and three loading contents (30, 50, and 70% by weight). The process not only produces particles with a mono-dispersed particle size distribution, an average micrometric diameter, a non-porous morphology, but also a high encapsulation efficiency. The microparticles have a latent heat correlated to the theoretical load and good thermal stability. The break up process

in the early stages of the electroplating method mainly determines the particle size of the mPCMs. Thus, depending on the choice of n-alkane, n-hexadecane, or n-eicosane, two phenomena occur. On the one hand, in the case of n-hexadecane, which is in a liquid state at room temperature, the break-up of the charged droplets takes place throughout the flight process, from the nozzle to the collector, which allows the solvent to evaporate entirely and thus obtain a low mean diameter. On the other hand, the droplets loaded with n-eicosane break-up only in the earliest stages of the flight process, as the evaporation of the solvent leads to the n-alkane crystallization, which stops the process, resulting in higher mean diameters and broad size distribution. The surface morphology of the electro-sprayed mPCM is either smooth, and dense or rough and wrinkled when n-hexadecane, and n-eicosane are used, respectively. Besides, n-eicosane tends to be on the surface of particles as its loading content increases. Also, the choice of solvent affects the particle size and morphology of the particles, which may be related to changes in the physico-chemical properties of solutions, such as surface tension, vapor pressure, and viscosity. The loading content depends mainly on the diffusion of n-alkane chains during the process, which is also influenced by solvent evaporation or phase separation, the interactions between PCL macromolecular chains, and n-alkane chains, and the evolution of the physical state of PCM. Thus, the encapsulation efficiency and charge content of an n-alkane liquid at room temperature are respectively higher and lower than those of a solid n-alkane in ethyl acetate, but in chloroform, it is the opposite.

References

Bordes, C., Fréville, V., Ruffin, E., Marote, P., Gauvrit, J. Y., Briançon, S., & Lantéri, P. (2010). Determination of poly(ε-caprolactone) solubility parameters: Application to solvent substitution in a microencapsulation process. *International Journal of Pharmaceutics*, *383*(1–2), 236–243. https://doi.org/10.1016/j.ijpharm.2009.09.023

Dubernet, C. (1995). Thermoanalysis of microspheres. *Thermochimica Acta*, *248*(C), 259–269. https://doi.org/10.1016/0040-6031(94)01947-F

Entekhabi, E., Haghbin Nazarpak, M., Moztarzadeh, F., & Sadeghi, A. (2016). Design and manufacture of neural tissue engineering scaffolds using hyaluronic acid and polycaprolactone nanofibers with controlled porosity. *Materials Science and Engineering C*, *69*, 380–387. https://doi.org/10.1016/j.msec.2016.06.078

Jenquin, M. R., & McGinity, J. W. (1994). Characterization of acrylic resin matrix films and mechanisms of drug-polymer interactions. *International Journal of Pharmaceutics*, *101*(1–2), 23–34.

https://doi.org/10.1016/0378-5173(94)90072-8

Mochane, M. J., & Luyt, A. S. (2012). Preparation and properties of polystyrene encapsulated paraffin wax as possible phase change material in a polypropylene matrix. *Thermochimica Acta*, *544*, 63–70. https://doi.org/10.1016/j.tca.2012.06.017

Pereira, C. N., & Vebber, G. C. (2019). A Relationship Between the Heat of Vaporization, Surface Tension, and the Solubility Parameters, Which Includes the Ratio of the Coordination Numbers, Based on Stefan's Rule. *Polymer Engineering and Science*, *59*(1950), E312–E321. https://doi.org/10.1002/pen.24956

Valo, H., Peltonen, L., Vehviläinen, S., Karjalainen, M., Kostiainen, R., Laaksonen, T., & Hirvonen, J. (2009). Electrospray encapsulation of hydrophilic and hydrophobic drugs in poly(L-lactic acid) nanoparticles. *Small*, *5*(15), 1791–1798. https://doi.org/10.1002/smll.200801907

Xie, J., Marijnissen, J. C. M., & Wang, C. H. (2006). Microparticles developed by electrohydrodynamic atomization for the local delivery of anticancer drug to treat C6 glioma in vitro. *Biomaterials*, *27*(17), 3321–3332. https://doi.org/10.1016/j.biomaterials.2006.01.034

Zhang, S., Campagne, C., & Salaün, F. (2019). Preparation of Electrosprayed Poly(caprolactone) Microparticles Based on Green Solvents and Related Investigations on the Effects of Solution Properties as Well as Operating Parameters. *Coatings*, *9*(2), 84. https://doi.org/10.3390/coatings9020084

Chapter 5 Preparation of n-Hexadecane/Poly (lactic acid) Microparticles via Single Nozzle Electrospraying and Related Characterizations

The formation of mPCMs during electrospraing process is influenced by the shell material. The solidification rate of shell material and the flexibility of macromolecular chains influence the diffusion of PCMs during the evaporation of solvent, which result in a decrease of the encapsulation efficiency. Meanwhile, the physical, chemical, thermal, and mechanical properties of the microcapsules depend on the choice of the coating material during the microencapsulation process. In general, shell materials should present enough physical strength, high thermal stability and chemical stability, and barrier performance. These characteristics allow not only mPCMs to withstand high external stress (including pressure, shear and friction), but also improve the stability, as well as the durability of mPCMs in harsh environment (e.g. high temperature or corrosion). When PCL is used as shell matrix to encapsulate PCMs, the thermal and mechanical properties of PCL, its low melting point of about 60 °C, its glass transition temperature of about -60 °C, and poor physical hardness limit the fields of application of these microcapsules.

In order to seek a substitute to PCL for encapsulating PCMs, and investigate the effects of different shell materials on the structures, morphologies and properties of electrosprayed mPCMs, poly(lactic acid) (PLA) as a non-toxic, bio-compatible and bio-degradable polyester, owing to its physical, thermal and mechanical properties comparable to conventional commodity polymers, was selected as shell matrix to encapsulate n-hexadecane. In this chapter, a series of n-hexadecane/PLA solutions with different PLA concentrations (3 wt % or 5 wt %) in chloroform and different weight ratios between n-hexadecane/PLA (30/70, 50/50 and 70/30) were used to prepare electrosprayed mPCMs. The structures, morphologies, and thermal properties of the mPCMs were characterized by optical microscopy (OM), scanning electron microscopy (SEM), differential scanning calorimeter (DSC) and thermogravimetric analysis (TGA).

5.1 Size and morphology of electrosprayed n-hexadecane/PLA mPCMs

The effects of the PLA concentrations and the weight ratio n-hexadecane/PLA on the mean diameter, particle size distribution, and morphology, are illustrated in Figure 5-1 and Table 5-1. The solution concentration does not change the mean diameter and particle size distribution for all the ratios, excepted for the 70/30 one. An increase in concentration leads to an increase in viscosity, and a decrease in electrical conductivity makes the cone jet unstable, resulting from an increase in the size distribution and the mean diameter. For all these ratios, monodispersed distributions are obtained. The increase of the n-hexadecane content leads to an increase in the mean diameter from 10 to 22 µm and 11 to 27 µm, for 3 and 5 w/v%, respectively. Furthermore, the broadening of particle size distribution is also observed. With the increase of n-hexadecane decreases the solution conductivity, restraining the polarization of n-hexadecane/PLA electrosprayed droplets under electrostatic force and leads to the instability of the break-up process, increasing the mean diameter and the particle size distribution (Zhang, Campagne, & Salaün, 2019b).

The SEM analysis confirms that the particles are nearly monodispersed in size and solid with a surface state or morphology depending on the PLA concentration and n-hexadecane to PLA weight ratio. With the increase of PLA concentration from 3 wt% to 5 wt%, the surface morphology of neat PLA particles changed from rough and flat to spherical and smooth. With the increase of n-hexadecane, the particles are less porous, more smooth and more spherical. High content in n-hexadecane decreases the chloroform evaporation rate, allows maintaining the spherical shape of the droplets during the flying process, more especially for 5 w/v%. n-hexadecane acts as a non-solvent during the polymer phase separation (Zhang et al., 2020).

Thus, PLA concentration of 5 w/v %, and n-hexadecane to PLA weight ratio of 50/50 and 70/30 is most suitable for obtaining a uniform particle with a relatively smooth surface with fewer defect structures. Furthermore, from the SEM and OM micrographs, they are no n-hexadecane detected on the particles' surface, suggesting the complete entrapment of the PCM in the PLA shell.

Table 5-1 The mean diameter and size distribution of obtained microparticles.

PLA solution concentration	C_{16}/PLA-00/100	C_{16}/PLA-30/70	C_{16}/PLA-50/50	C_{16}/PLA-70/30
3 wt%	10.5 ±1.4 µm	14.5 ±2.4 µm	16.8 ±4.3 µm	22.7 ±3.3 µm
5 wt%	11.5 ±1.4 µm	14.5 ±2.7 µm	16.6 ±3.4 µm	27.1 ±5.4 µm

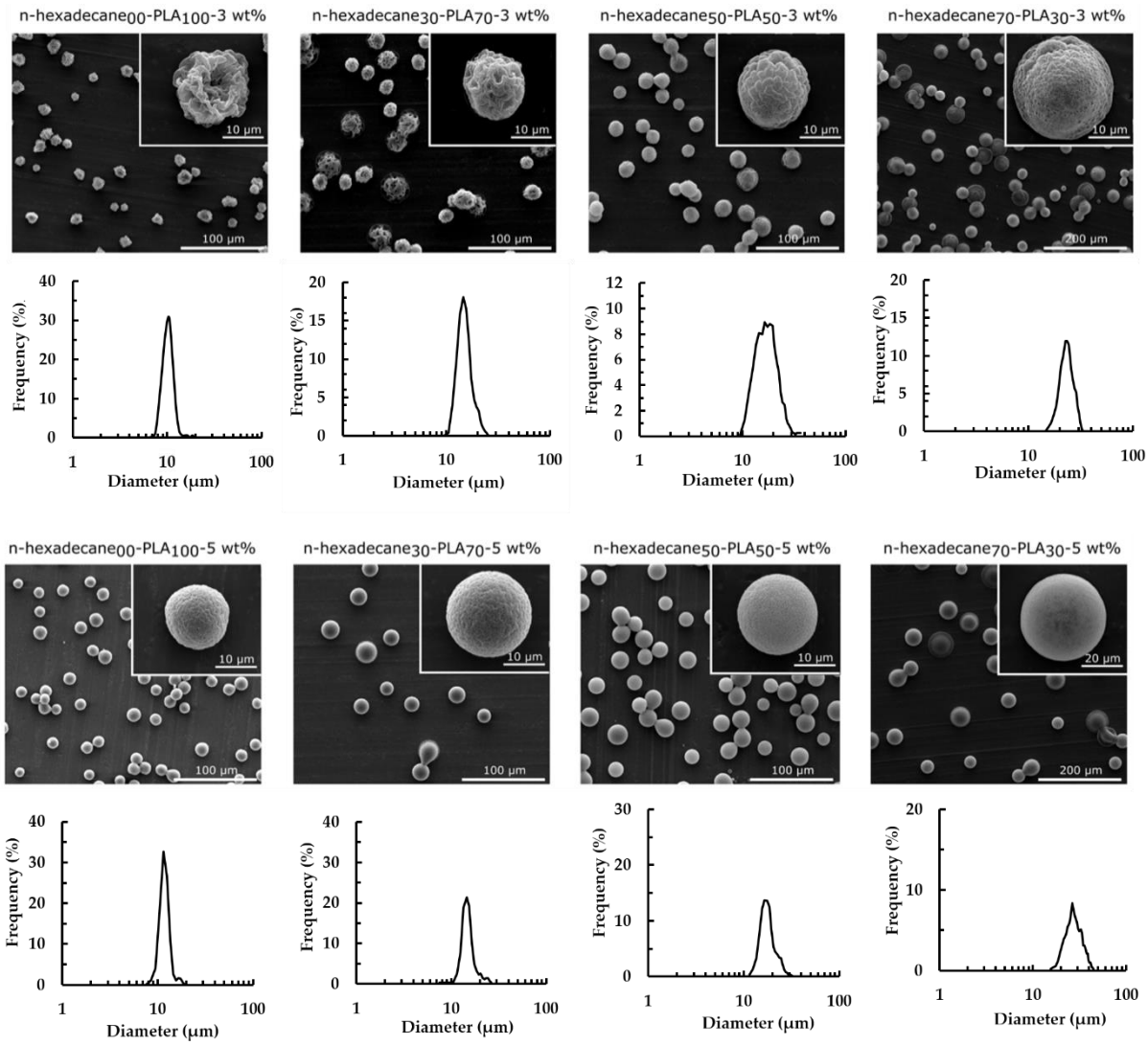

Figure 5-1 The scanning electron microscopy (SEM) images and size distribution of neat PLA microparticles and a series of n-hexadecane/PLA electrosprayed mPCMs obtained from different conditions and their particle size distributions.

5.2 Phase change properties of electro-sprayed n-hexadecane/PLA mPCMs

The phase transition behaviors of raw n-hexadecane, PLA microparticles and a series of n-hexadecane/PLA microparticles during cycles of heating or cooling process are measured by DSC (Figure 5-2 and 5-3). All the related thermal parameters are listed in Table 5-2 and 5-3. For raw n-hexadecane, its phase transition enthalpy was about 199 J/g, and its melting point at 17.9 °C and crystallized at 16.2 °C. For n-hexadecane/PLA-30/70 microparticles, the onset temperature for melting or crystallizing decreased to 15.6 °C or 13.8 °C for 3 wt% PLA,

and 15.8 °C or 11.2 °C for 5 wt% PLA. It is explained by the improvement in the thermal conductivity and heat exchange efficiency of encapsulated n-hexadecane compared to the raw n-hexadecane. As the increase in the specific surface area of n-hexadecane/PLA microparticles, the heat exchange efficiency between PCMs and heat flow is improved. Therefore, the energy required for the melting of the encapsulated n-hexadecane decreased and the temperature for carrying out its crystallization also decreased. The decrease in the specific surface area of mPCMs caused by the increase of the mean diameter depress the heat exchange efficiency between mPCMs and heat transfer medium. Therefore, the onset temperature of encapsulated n-hexadecane for melting or crystallizing increased gradually with the increase of n-hexadecane content in mPCMs.

The encapsulation of n-hexadecane into PLA shell also leads to an enlargement of its melting peak or crystalline peak compared with raw n-hexadecane, and two or multiple crystalline peaks are obtained. The presence of multiple crystalline peaks is related with the existence of multiple n-hexadecane crystalline phases when n-hexadecane was microencapsulated into PLA matrix. For n-hexadecane/PLA electrosprayed mPCMs, due to the variation in the viscosity and surface tension between PLA phase and n-hexadecane phase, n-hexadecane is dispersed in PLA matrix randomly. Some n-hexadecane is located in the center of microparticles or in the holes of PLA matrix. Due to the differences in volume or specific surface area of each part of n-hexadecane existed in PLA matrix, each part of encapsulated n-hexadecane has different surface free energy. Combining with the existence of PLA matrix as nucleating agent, the crystallization or melting process of encapsulated n-hexadecane is broadened and different n-hexadecane crystalline phases or intermediate RI phase are obtained.

With the increase of the weight ratio between n-hexadecane and PLA in electrospraying solutions from 30/70 to 70/30, the phase change enthalpy of n-hexadecane in mPCMs increased from 48 J/g to 95 J/g in 3 wt% PLA systems, and from 58 J/g to 119 J/g in 5 wt% PLA systems, respectively. The loading content of n-hexadecane in mPCMs increased from 24.2 % to 48.2 %, and from 28.7 % to 59.7 % for 3 and 5 wt% PLA, respectively. It can find that the actual loading content (LC) of n-hexadecane in mPCMs was lower than the theoretical addition of n-hexadecane. And the actual loading contents of n-hexadecane in electrosprayed mPCMs fabricated from 5 wt% PLA are higher than these results obtained from 3 wt% PLA, and are close to the theoretical values. Thus, during the electrospraying process, some n-hexadecane molecular escape from mixed droplets to air with the evaporation of solvent. For a higher PLA concentration, the loss of n-hexadecane is prevented due to the higher viscoelastic forces in mixed droplets and the stronger intermolecular entanglements among n-hexadecane and PLA chains

(Zhang, Campagne, & Salaün, 2020). It also explains that the encapsulation efficiency of n-hexadecane from 5 wt% PLA solution is higher than the situation from 3 wt% PLA solution based on the same n-hexadecane addition. The encapsulation efficiency of n-hexadecane both decreased under two concentrations of PLA (3 wt% and 5 wt%) when the weight ratio between n-hexadecane and PLA reached 70/30 in electrospraying solution. In this condition, it is difficult for limited PLA matrix to capture completely excessive n-hexadecane during electrospraying process.

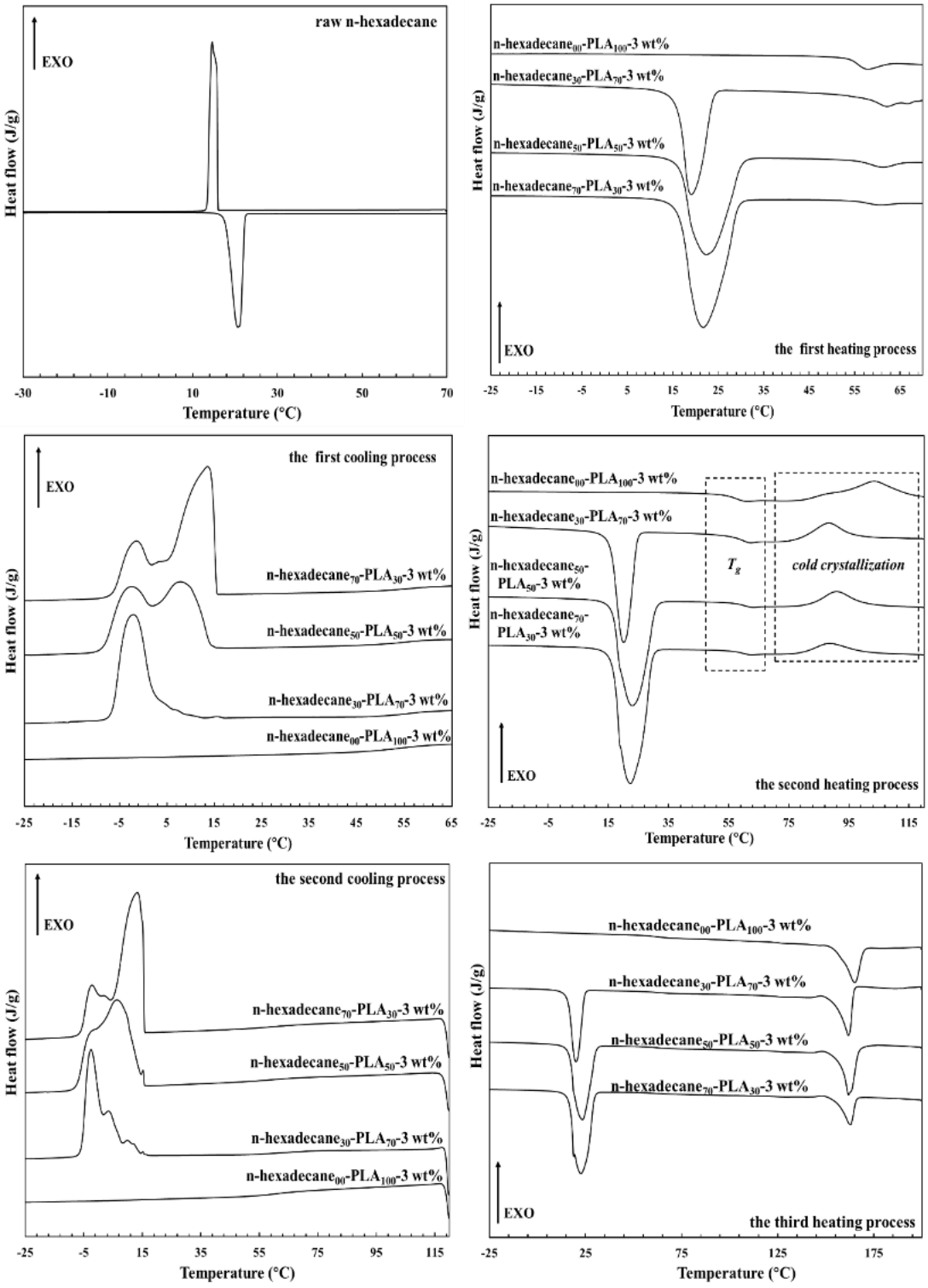

Figure 5-2 DSC curves of raw n-hexadecane, neat PLA microparticles and a series of n-hexadecane/PLA microcapsules obtained from PLA concentrations at 3 w/v % with different loading ratios between n-hexadecane and PLA.

Table 5-2 The thermal parameters of raw n-hexadecane, neat PLA microparticles and a series of n-hexadecane/PLA microcapsules obtained from 3 wt% PLA concentrations at three loading ratios between n-hexadecane and PLA

Sample lable		ΔH_m or ΔH_c (J/g)		T_{onset} (℃)		T_m or T_c (℃)		T_{end} (℃)		T_g (℃)	ΔH_{cc} (J/g)	$\Delta H_{cc(r)}$ (J/g)	$T_{onset(cc)}$ (℃)	T_{cc} (℃)	$T_{end(cc)}$ (℃)	LC (%)	EE (%)	$X_{c(th)}$ (%)	$X_{c(m)}$ (%)
n-hexadecane (C_{16})	heating	199.4		17.9		20.7		23.7		-			-	-	-	-	-	-	-
	cooling	195.9		16.2		16.0		13.0		-			-	-	-	-	-	-	-
C_{16}/PLA-00/100-3	heating		39.0		157.4		165.0		168.5	57.2	22.9	22.9	82.3	104.0	113.8	-	-	41.9	41.9
wt%	cooling		-		-		-		-	-	-		-	-	-	-	-	-	-
C_{16}/PLA-30/70-3	heating	48.1	35.2	15.6	154.5	20.0	161.7	24.7	164.5	59.2	15.2	20.1	78.2	88.3	97.4	24.2	80.6	54.1	49.9
wt%	cooling	47.9	-	13.8	-	-2.1	-	-8.3	-	-	-		-	-	-	-	-	-	-
C_{16}/PLA-50/50-3	heating	80.0	24.4	16.4	159.0	22.8	162.5	30.8	166.1	60.1	13.5	22.6	81.9	90.9	100.8	40.2	80.4	52.5	43.9
wt%	cooling	77.4	-	15.2	-	7.8	-	-9.6	-	-	-		-	-	-	-	-	-	-
C_{16}/PLA-70/30-3	heating	95.9	21.4	16.7	155.9	22.1	162.8	29.6	165.8	60.0	11.1	21.4	79.0	88.6	101.4	48.2	68.8	76.7	44.4
wt%	cooling	93.7	-	15.8	-	13.7	-	-8.5	-		-		-	-	-	-	-	-	-

Table 5-3 The thermal parameters of raw n-hexadecane, neat PLA microparticles and a series of n-hexadecane/PLA microcapsules obtained from 5 wt% PLA concentrations at three loading ratios between n-hexadecane and PLA

Sample lable		ΔH_m or ΔH_c (J/g)		T_{onset} (℃)		T_m or T_c (℃)		T_{end} (℃)		T_g (℃)	ΔH_{cc} (J/g)	$\Delta H_{cc(r)}$ (J/g)	$T_{onset(cc)}$ (℃)	T_{cc} (℃)	$T_{end(cc)}$(℃)	LC (%)	EE (%)	$X_{c(th)}$ (%)	$X_{c(m)}$ (%)
n-hexadecane (C_{16})	heating	199.4		17.9		20.7		23.7		-			-	-	-	-	-	-	-
	cooling	195.9		16.2		16.0		13.0		-			-	-	-	-	-	-	-
C_{16}/PLA-00/100-5	heating		41.3		156.7		165.0		169.6	58.2	24.2	24.2	82.4	104.0	114.1	-	-	44.4	44.4
wt%	cooling		-		-		-		-	-	-		-	-	-	-	-	-	-
C_{16}/PLA-30/70-5	heating	57.1	32.9	15.8	156.8	19.4	162.6	26.7	167.0	59.2	17.3	24.3	78.7	87.2	96.1	28.7	95.6	50.5	49.6
wt%	cooling	58.7	-	11.2	-	-2.9	-	-10.8	-	-	-		-	-	-	-	-	-	-
C_{16}/PLA-50/50-5	heating	99.5	25.6	16.6	159.0	22.3	162.5	30.0	166.1	60.6	14.5	28.9	79.7	89.0	100.1	49.9	99.8	55.1	54.9
wt%	cooling	97.8	-	15.8	-	9.0	-	-9.0	-	-	-		-	-	-	-	-	-	-
C_{16}/PLA-70/30-5	heating	119.0	19.2	16.1	156.1	23.4	162.0	32.2	166.3	60.0	11.5	28.5	79.7	90.1	101.3	59.7	85.3	68.8	51.2
wt%	cooling	116.7	-	15.9	-	11.5	-	-7.1	-		-		-	-	-	-	-	-	-

In 3 wt% PLA systems, the encapsulation efficiency of n-hexadecane reaches 80 % in C_{16}/PLA-30/70-3 wt% or C_{16}/PLA-50/50-3 wt% sample. And in 5 wt% PLA systems, 95.6 % of encapsulation efficiency for C_{16}/PLA-30/70-5 wt% sample and 99.8 % of encapsulation efficiency for C_{16}/PLA-50/50-3 wt% are achieved. When the weight ratio between n-hexadecane and PLA in electrospraying solution reached 70/30, the encapsulation efficiency of n-hexadecane in corresponding mPCMs decreased to 68.8 % or 85.3 % for 3 wt% PLA or 5 wt% PLA, respectively.

PCL was used as shell matrix for achieving the microencapsulation of n-hexadecane (Zhang, Campagne, & Salaün, 2020; Zhang et al., 2020). Some drawbacks and limitations from PCL material including low mechanical properties, low melting point and low thermal mechanical property still restrain the application of n-hexadecane/PCL mPCMs. When PLA matrix with enough physical strength and high thermal mechanical property was considered as a suitable substitution for PCL matrix, it is necessary to carry out a comparison between PLA and PCL based on the loading content of n-hexadecane in corresponding mPCMs as well as encapsulation efficiency. In Figure 5-4, when different weight ratios between n-hexadecane and polymer matrix were added into chloroform for preparing a series of electrospraying solutions, the encapsulation efficiency and actual loading content of n-hexadecane in corresponding electrosprayed mPCMs prepared from PLA solution were higher than these results obtained from PCL solution. In the case of 50/50 weight ratio between n-hexadecane and polymer matrix in electrospraying solution, the encapsulation efficiency of 99.8% can be achieved from 5 wt% PLA solution, 80.4 % from 3 wt% PLA solution and 72.6 % from 10 wt% PCL solution. With further increasing the weight ratio between n-hexadecane and polymer matrix to 70/30, the actual loading content of n-hexadecane in mPCMs can reach 59.7 wt% from 5 wt% PLA solution, 48.2 wt% from 3 wt% PLA solution and 49.9 wt% from 10 wt% PCL solution. These results indicate that PLA matrix had a stronger ability to entrap more n-hexadecane during electrospraying process compared to PCL matrix. Due to the great difference in glass transition temperature between PLA (about 60 °C) and PCL (about -60 °C), PCL chains exhibited elastic state, and had strong flexibility and mobility under room temperature. On the contrary, PLA chains are in glass state, and exhibite rigidity and immovability. Therefore, PLA chains have stronger ability to fix n-hexadecane molecular in the inner of mPCMs compared to PCL chains. PLA chains had enough rigidity to depress the movement or diffusion of n-hexadecane during electrospraying process. In addition, the solubility of PCL in chloroform is higher than that of PLA in chloroform (Agrawal et al., 2004; Zhang, Campagne, & Salaün, 2019a). And a low polymer solubility in organic

solvent and fast solidification of polymeric matrix also resulted in a high encapsulation efficiency to core material. Therefore, it can confirm that PLA matrix is a suitable substitution for PCL matrix for achieving higher encapsulation efficiency and high actual loading content of n-hexadecane in electrosprayed mPCMs.

In addition, the presence of n-hexadecane influences the crystallization process, as well as the thermal properties of the PLA matrix. For PLA microparticles, the cold crystallization enthalpy was about 22.9 J/g and 24.2 J/g for the samples fabricated from 3 wt% and 5 wt%, respectively. With the variation of PLA concentration, the onset and peak temperatures of cold crystallization does not change, and kept at 82.0 °C and 104 °C, respectively. Meanwhile, the glass transition temperature was 57.2 °C for 3 wt% PLA, and 58.2 °C for 5 wt% PLA. And blank PLA microparticles melted at 157.4 °C for 3 wt% PLA with a melting enthalpy of 39.0 J/g, melted at 156.7 °C for 5 wt% PLA with a melting enthalpy of 41.3 J/g. Correspondingly, the crystallization degree reached about 41.9 % for 3 wt% PLA and 44.4 % for 5 wt% PLA, respectively. With the increase of n-hexadecane content in PLA matrix, the cold crystallization enthalpy of PLA matrix decreases gradually regardless of the concentration of PLA solution. Thus, the weight fraction of PLA in mPCMs decreases gradually with the increase of n-hexadecane content. In order to analyze the effects of n-hexadecane on the cold crystallization ability of PLA matrix, it is necessary to compare the cold crystallization enthalpy of PLA matrix based on the same weight fraction of PLA matrix. Therefore, a parameters named relative cold crystallization enthalpy ($\Delta H_{(cc(r))}$) was introduced in our investigation. The value of $\Delta H_{(cc(r))}$ was calculated via converting the weight fraction of PLA matrix into 100 wt% PLA matrix as shown in Equation (2-10). In Table 5-2, the $\Delta H_{(cc(r))}$ values of electrosprayed mPCMs obtained from 3 wt% PLA system does not change obviously with the variation of the weight ratio between n-hexadecane and PLA, and kept at 20~22 J/g. However, from Table 5-3, these ΔH(cc(r)) values obtained from 5 wt% PLA system increased from 24.2 J/g to 29.0 J/g in the case of 50/50 or 70/30 weight ratio between n-hexadecane and PLA in electrospraying solution. Thus, after introducing n-hexadecane in PLA matrix, n-hexadecane chains diffuse into PLA chains, then the intermolecular entanglements among PLA chains decrease (Ali et al., 2009; Quero et al., 2012). Therefore, the mobility of PLA chains is enhanced during the heating or cooling process. With the further increase of n-hexadecane content in PLA matrix, more intermolecular entanglements between n-hexadecane chains and PLA chains and less entanglements among PLA chains is obtained. Due to the increase in the mobility of PLA chains, more PLA chains participate in the cold crystallization process, and the cold crystallization temperatures (onset, peak and end) also decreased with the increase of n-

hexadecane content in PLA matrix compared with neat PLA matrix. It can conclude that the cold crystallization process of PLA matrix is accelerated via adding n-hexadecane. Meanwhile, due to the acceleration of cold crystallization of PLA matrix and the enhancement of PLA chains mobility, the crystallization degree of PLA matrix also increases after adding n-hexadecane.

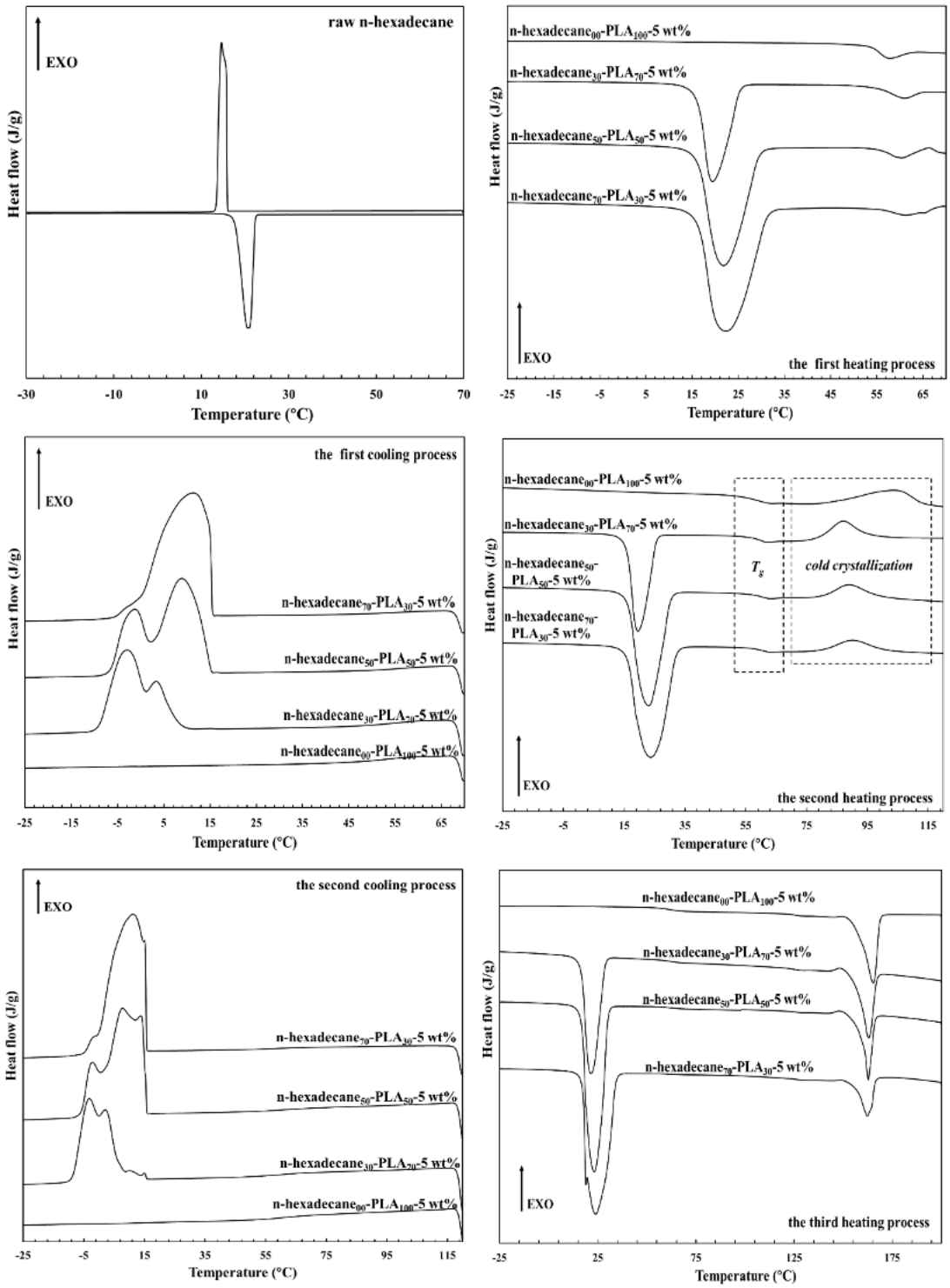

Figure 5-3 DSC curves of raw n-hexadecane, neat PLA microparticles and a series of n-hexadecane/PLA microcapsules obtained from PLA concentrations at 5 w/v % with different loading ratios between n-hexadecane and PLA.

And the improvement in the crystallization degree of PLA matrix is more obviously in 5 wt% PLA systems compared with 3 wt% PLA systems as listed in Table 5-2 and Table 5-3. When the weight ratios between n-

hexadecane and PLA in 5 wt% PLA solution reached 50/50, the crystallization degree of PLA matrix increased to 54.9 %. Compared with PLA particles, the melting temperature of PLA matrix containing n-hexadecane decreased from 165 °C to 162 °C regardless of the concentration of PLA and as well as the content of n-hexadecane.

This phenomenon was different from the situation obtained from n-hexadecane/PCL single nozzle electrospraying (Zhang, Campagne, & Salaün, 2020). The crystallization degree of PCL matrix reduced gradually after adding n-hexadecane compared with blank PCL matrix. Thus, under room temperature, the mobility of PCL chains (soft and elastic) is stronger than PLA chains (rigidity). Introducing n-hexadecane chains increase the intermolecular entanglements among PCL chains and n-hexadecane chains. Therefore, the mobility of PCL chains is restrained and lower crystallization degree of PCL matrix is obtained after adding n-hexadecane. On the contrary, as rigid chains under room temperature, the intermolecular entanglements among PLA chains is reduced via introducing n-hexadecane chains. Therefore, the mobility of PLA chains and the crystallization ability of PLA matrix is improved after adding n-hexadecane.

In addition, the glass transition temperature of PLA matrix was also affected by the addition of n-hexadecane. With the increasing of the weight ratio between n-hexadecane and PLA in electrospraying solution from 0/100 to 70/30, the glass transition temperatures of resulted PLA matrix increased from 57.2 °C to 60.1 °C for 3 wt% PLA solution, from 58.2 °C to 60.0 °C for 5 wt% PLA solution. The increase in the glass transition temperature of PLA matrix after adding n-hexadecane might be related with the improvement in the crystallization degree of PLA matrix. According to Solarski, Ferreira & Devaux (2005), with the increasing of PLA matrix crystallization degree, the energy for moving PLA chains in amorphous phase also increased gradually. As a consequence, the temperature for PLA chains to pass from a glassy state to a rubbery state is higher.

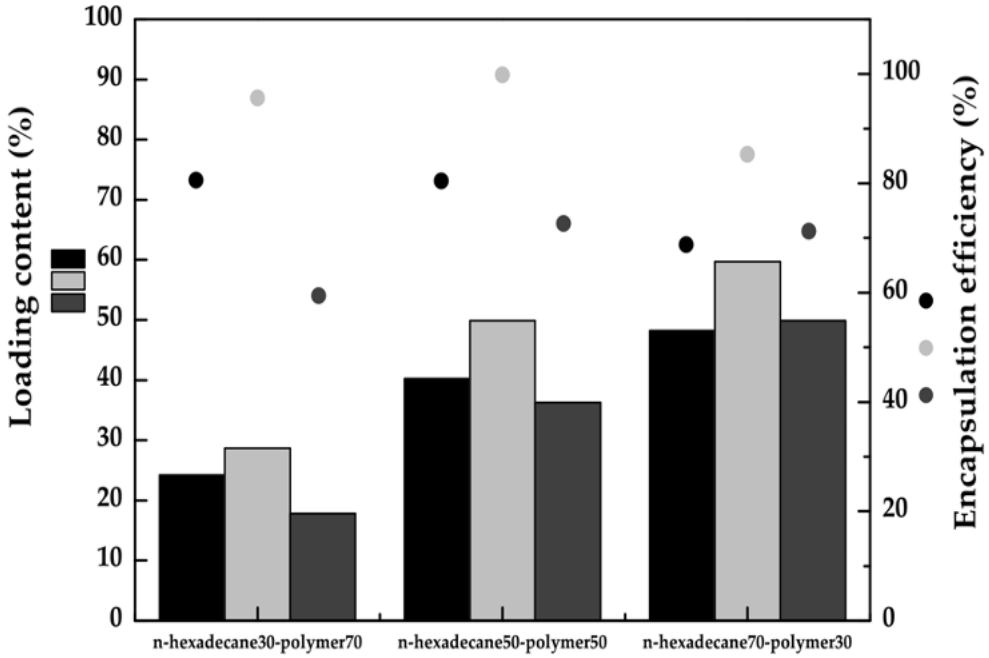

Figure 5-4 Influence of the different polyesters and the concentration of the PLA solution on the loading content and encapsulation efficiency of n-hexadecane (black-PLA-3 w/v %; light grey-PLA-5 w/v %; dark grey-PCL-10 w/v %).

5.3 Thermal stability of electrosprayed n-hexadecane/PLA mPCMs

The thermal degradation processes of raw n-hexadecane, blank PLA microparticles and a series of n-hexadecane/PLA mPCMs were analyzed via TGA, and the related thermograms and DTG curves obtained from different PLA concentrations were presented in Figure 5-5 and Figure 5-6, respectively. The related degradation data for each step from corresponding PLA concentration was listed in Table 5-4 and Table 5-5, respectively. For raw n-hexadecane, a single step degradation was observed from 100 °C to 250 °C. The initial degradation temperature (onset temperature at 5% weight loss (T5%)) of raw n-hexadecane was 149.3 °C, and maximum degradation temperature for carrying out its backbone decomposition was 247.2 °C with a maximum degradation rate of 2.8 %/°C. After 280 °C, the thermal degradation of n-hexadecane completed, and the weight of the residue was close to 0 wt%. For n-hexadecane-free PLA microparticles, a single step degradation was also observed from 300 °C to 400 °C. The initial degradation temperature for 3 wt% and 5 wt% PLA was 304.0 °C and 309.7 °C, respectively. And the maximum degradation temperature for 3 wt% PLA was 367.7 °C with a maximum degradation rate of 2.8 %/°C. When PLA concentration increased to 5 wt%, related maximum degradation

temperature with a 2.6 %/°C degradation rate increased to 370.3 °C.

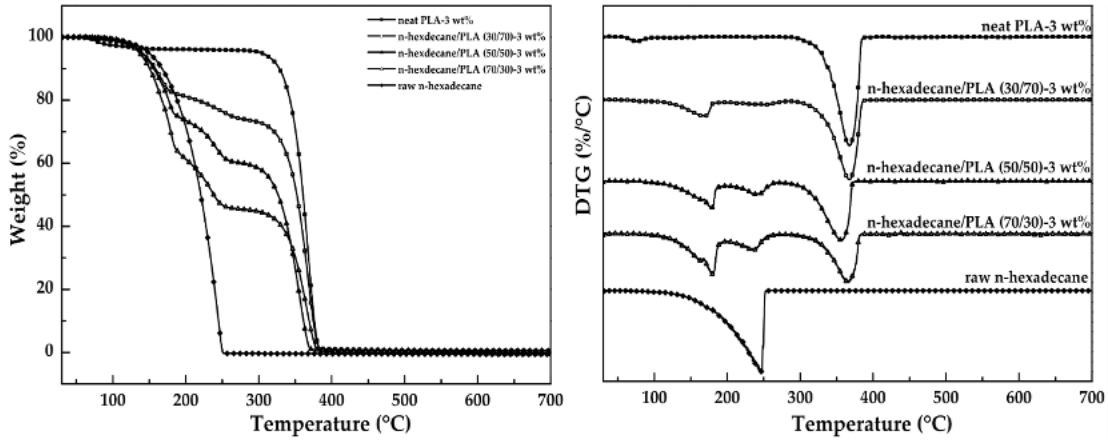

Figure 5-5 TG and DTG curves of raw n-hexadecane, blank PLA microparticles and a series of n-hexadecane/PLA microcapsules obtained from 3 wt% PLA systems.

When n-hexadecane is encapsulated into PLA matrix, the thermal degradation process of n-hexadecane/PLA microparticles occurs into two steps. The first step from 100 °C to 300 °C was attributed to the thermal degradation of n-hexadecane, and the second step from 300 °C to 400 °C is related with the thermal degradation of PLA matrix. Meanwhile, the thermal degradation of encapsulated n-hexadecane is divided into two steps. From 100 °C to 176-200 °C depending on the addition of n-hexadecane as well as PLA concentration, it belongs to the evaporation of some n-hexadecane that existed in the surface pores of PLA matrix or formed weak intermolecular interactions with PLA chains. The next degradation step from about 200 °C to 300 °C is attributed to the leaving of n-hexadecane in PLA matrix. Furthermore, compared with raw n-hexadecane, the initial degradation temperature of encapsulated n-hexadecane decreases. After single nozzle electrospraying process, bulk n-hexadecane is dispersed into small volume units and is distributed in PLA matrix randomly. It means that some n-hexadecane units exist in the surface pores of mPCMs, and some n-hexadecane unit are surrounded by PLA matrix. Due to the increase in the surface specific area of the n-hexadecane that existed in the surface pores of PLA matrix, the heat transfer efficiency is enhanced, and the evaporation temperature for this n-hexadecane reduced. When the addition of n-hexadecane increases from 30 wt% to 70 wt%, the initial degradation temperature of encapsulated n-hexadecane decreases gradually, and the maximum degradation temperature increases. This phenomen is related to the fact that more n-hexadecane are located in the surface pores of the mPCMs. Furthermore, when temperature increases to 170 °C, PLA matrix melted into liquid state, and the n-hexadecane located in the inner of PLA matrix diffuse out. With the increase of n-hexadecane content in mPCMs, the surface specific area of inner n-hexadecane

decreases. Therefore, the maximum degradation temperature increases.

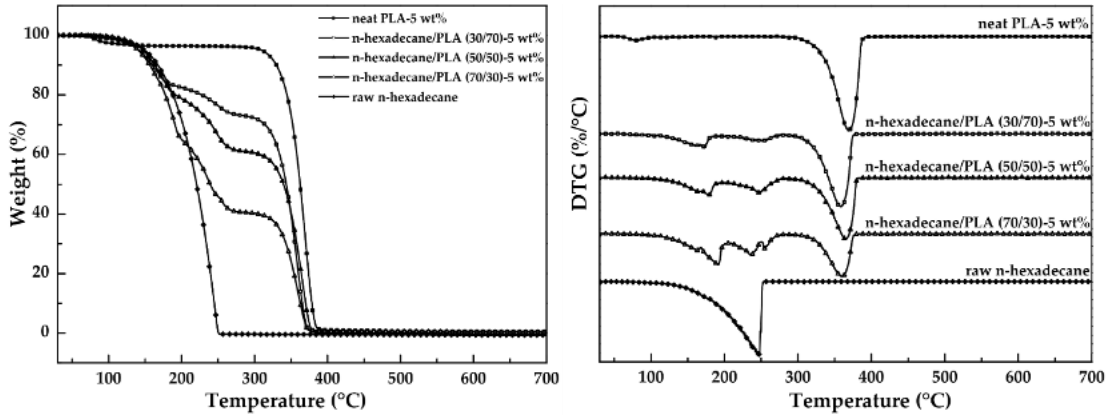

Figure 5-6 TG and DTG curves of raw n-hexadecane, blank PLA microparticles and a series of n-hexadecane/PLA microcapsules obtained from 5 wt% PLA systems.

Table 5-4 Thermogravimetric data of raw n-hexadecane, neat PLA microparticles and a series of n-hexadecane/PLA microcapsules obtained from 3 wt% PCL concentrations with different loading ratios between n-hexadecane and PLA

Sample	Initial degradation temperature-$T_{5\%}$ (℃)	First step			Second step		
		Weight loss (100-300 ℃) (%)	Maximum degradation temperature (℃)	Maximum degradation rate (%/℃)	Weight loss (300-400 ℃) (%)	Maximum degradation temperature (℃)	Maximum degradation rate (%/℃)
C_{16}/PLA-00/100-3 wt%	304.0	4.8	-	-	95.2	367.7	2.8
n-hexadecane (C_{16})	149.3	99.3	247.2	2.1	-	-	-
C_{16}/PLA-30/70-3 wt%	140.3	25.9	170.0	0.4	72.9	368.2	2.0
C_{16}/PLA-50/50-3 wt%	140.3	41.0	178.7	0.7	58.4	357.8	1.5
C_{16}/PLA-70/30-3 wt%	136.5	54.7	180.2	1.0	44.7	367.0	1.2

Table 5-5 Thermogravimetric data of raw n-hexadecane, neat PLA microparticles and a series of n-hexadecane/PLA microcapsules obtained from 5 wt% PCL concentrations with different loading ratios between n-hexadecane and PLA

Sample	Initial degradation temperature-$T_{5\%}$ (°C)	First step			Second step		
		Weight loss (100-300 °C) (%)	Maximum degradation temperature (°C)	Maximum degradation rate (%/°C)	Weight loss (300-400°C) (%)	Maximum degradation temperature (°C)	Maximum degradation rate (%/°C)
C_{16}/PLA-00/100-5 wt%	309.7	4.4	-	-	95.6	370.3	2.6
n-hexadecane (C_{16})	149.3	99.3	247.2	2.1	-	-	-
C_{16}/PLA-30/70-5 wt%	141.2	27.0	172.3	0.4	72.2	358.8	2.1
C_{16}/PLA-50/50-5 wt%	147.0	39.0	178.8	0.5	60.5	364.3	1.7
C_{16}/PLA-70/30-5 wt%	140.7	59.3	192.3	0.9	40.2	359.7	1.2

In addition, higher initial degradation temperature and higher maximum degradation temperature of encapsulated n-hexadecane is obtained in the higher PLA concentration systems. It indicated that more n-hexadecane is located in the inner of PLA matrix and the evaporation of n-hexadecane is further depressed by the physical barrier effect of PLA matrix. With the increase of n-hexadecane content in mPCMs, the weight loss in first step increases, and the corresponding maximum degradation rate also increases too. On the contrary, the weight loss in second step related with the degradation of PLA matrix as well as the maximum degradation rate decreases. For 3 wt% PLA systems, after adding n-hexadecane, the maximum degradation temperature of PLA matrix does not change obviously compared to PLA microparticles, excepted for the sample with 50 wt% n-hexadecane for which the temperature decreases to 357.8 °C. For 5 wt% PLA systems, after adding n-hexadecane, the maximum degradation temperature of PLA matrix decreases compared to PLA particles.

5.4 Conclusions

In this chapter, a series of n-hexadecane/PLA mPCMs have been successfully developped via single nozzle electrospraying. Compared to PCL systems, higher actual loading content as well as encapsulation efficiency of n-hexadecane in mPCMs are obtained.

Meanwhile, the effects of PLA concentration and n-hexadecane addition on the structures (mean diameter, size distribution and morphology) and thermal properties (phase transition enthalpy, phase change temperature, the crystallization process of PLA matrix), as well as the encapsulation efficiency and loading content of n-hexadecane in PLA matrix have been investigated. After introducing n-hexadecane, spherical electrosprayed mPCMs with mono-dispersed size distribution are obtained. With the increase of n-hexadecane addition, the mean diameter of n-hexadecane/PLA microparticles increases from about 10 μm to 22-27 μm depending on the PLA concentration, and the corresponding size distribution broadened. Furthermore, the actual loading content of n-hexadecane in mPCMs also increases with the increase of n-hexadecane content. However, corresponding encapsulation efficiency to n-hexadecane decreased for the C_{16}/PLA-70/30-3 wt% and the C_{16}/PLA-70/30-5 wt% samples. Higher PLA concentration allowed to improving the encapsulation efficiency as well as the actual loading content of n-hexadecane in mPCMs. When 70 wt% n-hexadecane was added into 5 wt% PLA solution, the encapsulation efficiency and actual loading content of n-hexadecane reached 85.3 and 59.7 %, respectively. Correspondingly, the phase transition enthalpy of encapsulated n-hexadecane reaches 119 J/g. In addition, when

n-hexadecane is encapsulated into PLA matrix, its melting process and crystalline process broadens compared to n-hexadecane. During the thermal degradation process, the initial degradation temperature and maximum degradation temperature of encapsulated n-hexadecane also decreases compared to raw n-hexadecane. The mobility of PLA chains is also improved after introducing n-hexadecane. Therefore, the cold crystallization of PLA matrix is promoted and the crystallization degree of PLA matrix also increases.

References

Agrawal, A., Saran, A. D., Rath, S. S., & Khanna, A. (2004). Constrained nonlinear optimization for solubility parameters of poly(lactic acid) and poly(glycolic acid) - Validation and comparison. *Polymer*, *45*(25), 8603–8612. https://doi.org/10.1016/j.polymer.2004.10.022

Ali, F., Chang, Y. W., Kang, S. C., & Yoon, J. Y. (2009). Thermal, mechanical and rheological properties of poly (lactic acid)/epoxidized soybean oil blends. *Polymer Bulletin*, *62*(1), 91–98. https://doi.org/10.1007/s00289-008-1012-9

Quero, E., Müller, A. J., Signori, F., Coltelli, M. B., & Bronco, S. (2012). Isothermal cold-crystallization of PLA/PBAT blends with and without the addition of acetyl tributyl citrate. *Macromolecular Chemistry and Physics*, *213*(1), 36–48. https://doi.org/10.1002/macp.201100437

Solarski, S., Ferreira, M., & Devaux, E. (2005). Characterization of the thermal properties of PLA fibers by modulated differential scanning calorimetry. *Polymer*, *46*(25), 11187–11192. https://doi.org/10.1016/j.polymer.2005.10.027

Zhang, S., Campagne, C., & Salaün, F. (2019a). Influence of solvent selection in the electrospraying process of polycaprolactone. *Applied Sciences (Switzerland)*, *9*(3). https://doi.org/10.3390/app9030402

Zhang, S., Campagne, C., & Salaün, F. (2019b). Preparation of Electrosprayed Poly(caprolactone) Microparticles Based on Green Solvents and Related Investigations on the Effects of Solution Properties as Well as Operating Parameters. *Coatings*, *9*(2), 84. https://doi.org/10.3390/coatings9020084

Zhang, S., Campagne, C., & Salaün, F. (2020). Preparation of n -Alkane / Polycaprolactone Phase-Change Microcapsules via Single Nozzle Electro-Spraying : Characterization on Their Formation , Structures and Properties. Applied Sciences, 10(2), 561-580. http://dx.doi.org/10.3390/app10020561

Zhang, S., Chen, Y., Campagne, C., & Salaün, F. (2020). Influence of a Coaxial Electrospraying System on the

n-Hexadecane / Polycaprolactone Phase Change Microcapsules Properties. Materials, 13(9), 2205-2221. http://dx.doi.org/10.3390/ma13092205

Chapter 6 Preparation of n-Hexadecane/Polycaprolactone Microparticles via Coaxial Nozzle Electrospraying and Related Characterizations

When single nozzle electrospraying was used for carrying out the microencapsulation process of n-hexadecane, some n-hexadecane molecular escape from electrosprayed droplets to air during the evaporation of solvent, which results in a reduction of encapsulation efficiency as well as the loading content of n-hexadecane. Using coaxial nozzle is a good choice to prevent the loss of n-hexadecane during electrospraying. By using a coaxial nozzle electrospray apparatus, the solutions from the core (PCMs) and polymeric shell flow independently of the inner and outer capillaries, respectively. This configuration allows a short-term limitation of the physico-chemical interactions between the core and shell compounds, which restrains the diffusion of PCMs into shell phase and induce a mono-nuclear morphology. This type of morphology makes it possible to highlight some interesting functional properties of mPCM, such as their durability, shape, and thermal stabilities. Nevertheless, adjustment of the solution properties and working parameters is required for the formation of a stable Taylor cone, and thus to induce a uniform breaking process of the charged jets, which is considered to be more difficult compared to a single-nozzle electrospraying process.

Up to now, the comprehensive comparison between single and coaxial nozzle electrospraying in the encapsulation of PCM, focusing on the structures, morphologies, and thermal properties of the microcapsules was not achieved. In this chapter, raw n-hexadecane as the core component, and 5 or 10 w/v% of polycaprolactone (PCL) solubilized in chloroform (Chl) solution for the shell material were used in a coaxial process to investigate the effect of the selected method; the core to shell weight ratios (30/70, 50/50 and 70/30); as well as the polymer concentration on the mean diameter, particle size distribution, encapsulation efficiency, loading content, morphology, and thermal properties of the mPCMs. The structures, morphologies, and thermal properties of the obtained microcapsules were characterized by scanning electron and optical microscopies (SEM and OM), differential scanning calorimetry (DSC), and thermogravimetric analysis (TGA). The results were also compared

to these obtained from a single electrospraying nozzle.

6.1 Size and morphology of n-hexadecane/PCL mPCMs from coaxial nozzle

The mean diameter, size distribution, and morphology of electrosprayed mPCMs from the different formulations were characterized by OM and SEM observations (Figures 6-1 and 6-2, Table 6-1). The polymer concentration does not influence the particle size properties of n-hexadecane-free PCL microparticles. They have a mean diameter between 7 and 9 μm and narrow size distribution. The addition of the n-hexadecane solution results in an increase in the mean diameter, which varies according to the amount of PCM and the concentration of the PCL solution. Thus, at 5 w/v % for levels of 30 and 50% n-hexadecane, the mean diameter is 22 μm, with a wide size distribution, whereas for 70%, the diameter decreases and the size distribution is relatively narrow.

The phenomenon is different for 10 w/v % in PCL since an increase of 30%–50% leads to an increase in mean diameter, which is approximately the same for 70%. These different variations are related to the low electrical conductivity of the n-hexadecane solution, which limits its polarization under the action of electrostatic forces. The formation of the Taylor cone is mainly related to the physico-chemical properties of the PCL solution. It allows the realization of the cone-jet mode at the tip of the coaxial nozzle, due to the stabilization of the n-hexadecane solution by the viscoelastic forces and the interfacial interactions of this solution. Nevertheless, obtaining a broader size distribution is one of the consequences of the instability of the breaking process of the charged droplets, due to the unstable coulombic repulsions. Indeed, they lead to different encapsulated quantities of n-hexadecane within the particles.

Some PCL droplets entrapped more n-hexadecane to form bigger microparticles, while others trapped less n-hexadecane to form smaller ones. A higher amount of n-hexadecane leads to a progressive narrowing of the size distribution of the microcapsules, which is linked to a decrease in the quantity of the small ones and an increase of the large ones. Besides, the increase in the PCL solutions (or PCL concentration) allows stabilizing the n-hexadecane core solution during the Taylor cone formation and the breakup process. Therefore, it leads to the obtention of a mono-dispersed distribution, especially when the core to shell proportion is higher than 30:70.

A higher amount of n-hexadecane leads to a progressive narrowing of the size distribution of the microcapsules, which is linked to a decrease in the quantity of the small particles and an increase of the large particles. Besides, the increase in the PCL solutions (or PCL concentration) allows stabilizing the n-hexadecane

core solution during the Taylor cone formation and the breakup process. Therefore, it leads to the obtention of a mono-dispersed distribution, especially when the core to shell proportion is about 30:70. For single nozzle electrospraying, microcapsules with a mono-disperse distribution are obtained regardless of the amount of n-hexadecane used (Zhang, Campagne, & Salaün, 2020). Indeed, the presence of the solvent increases the electrical conductivity, which leads to better stabilization of the Taylor cone and facilitates the breaking process. This phenomenon is only achieved for the higher core flow rates or higher PCL concentrations when the coaxial system is used.

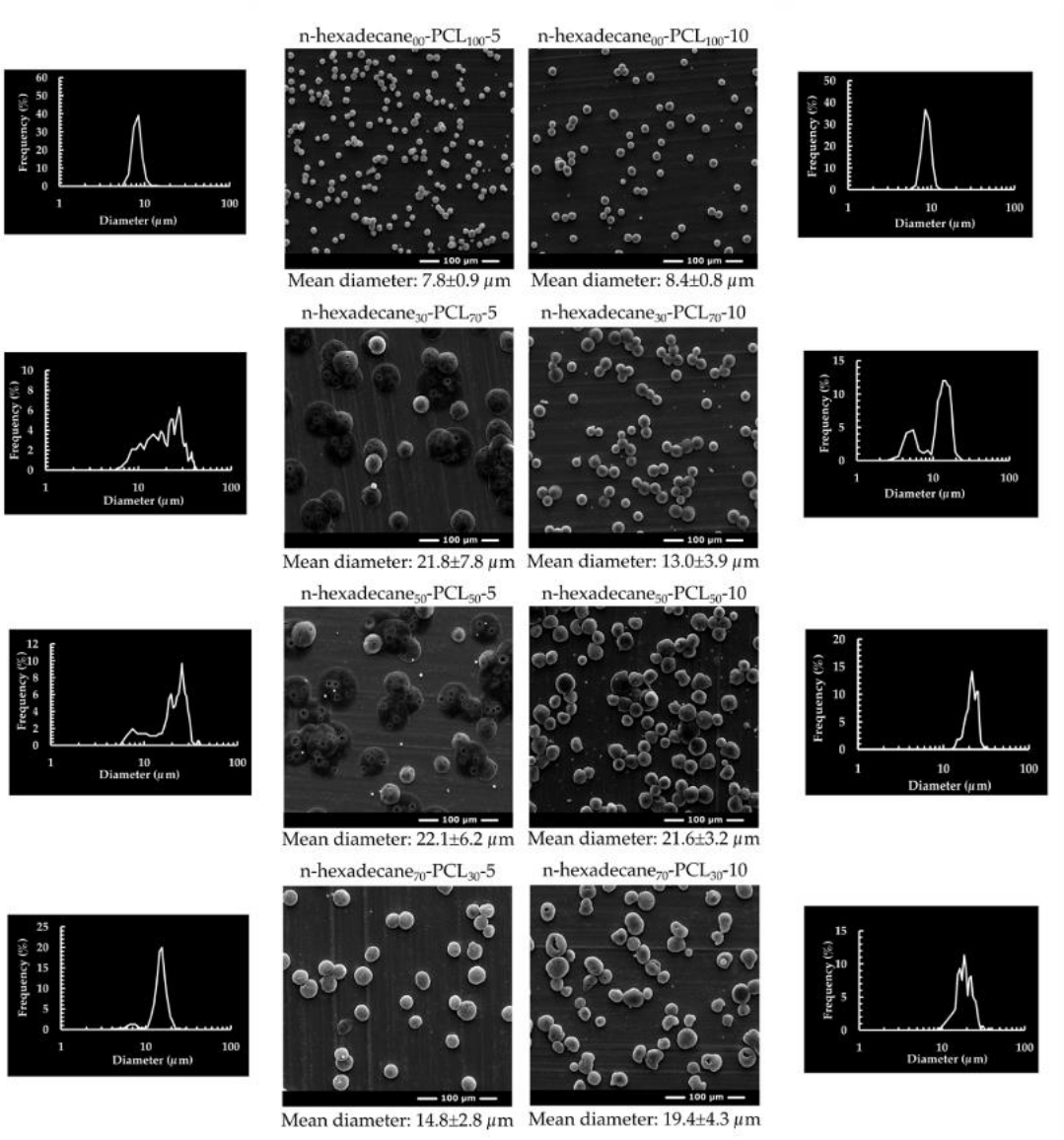

Figure 6-1 Scanning electron microscopy (SEM) images of the various microparticles and their particle size distribution.

Table 6-1 The mean diameter and size distribution of obtained microparticles.

Shell Liquid Concentration	C_{16}/PCL-00/100	C_{16}/PCL-30/70	C_{16}/PCL-50/50	C_{16}/PCL-70/30
5 wt %	7.8±0.9 μm	21.8±7.8 μm	22.1±6.2 μm	14.8±2.8 μm
10 wt %	8.4±0.8 μm	13.0±3.9 μm	21.6±3.2 μm	19.4±4.3 μm

6.2 Surface state of the n-hexadecane/PCL mPCMs from coaxial nozzle

The PCL concentration has a direct influence on the surface state of the electrosprayed microparticles (Figure 6-2). Thus, non-porous microparticles having wrinkled and smooth surface states are obtained with 5 and 10 w/v % of PCL solutions (samples C_{16}/PCL-00/100-5 and C_{16}/PCL-00/100-10), respectively. The deformation of the electrosprayed droplets is mainly related to the physico-chemical properties of the solvent used. In the case of chloroform, its high vapor pressure induces quick evaporation during the flying process of the electrosprayed droplets from the nozzle to the collector. A higher PCL concentration leads to a higher solution viscosity, and the macromolecular chain entanglements act as a barrier to the solvent evaporation process. Thus, 10 w/v % of the PCL solution allows for obtaining spherical microparticles with a smooth surface state (Moghaddam, & Mortazavi, 2015).

The presence of n-hexadecane in the internal capillary of the coaxial nozzle induces some changes in the formation of microparticles at low concentrations of PCL. They appear to be porous with a smooth outer polymer film. In the first step of the process, the solvent diffuses into the core substance, resulting in the rapid solidification of the outer PCL matrix. During the flight process, the chloroform trapped in the inner core of the microparticles diffuses through the macromolecular chain network of the PCLs and causes tiny holes on the surface of the particles. This phenomenon is less pronounced when the amount of core substance increases or the content of the outer phase decreases. Thus, the core substance acts as a barrier to solvent evaporation in the coaxial configuration. The use of a higher concentration of PCL leads to the formation of smooth and spherical microparticles for a small amount of n-hexadecane (C_{16}/PCL-30/70-10 and C_{16}/PCL-50/50-10). On the other hand, when the amount of n-hexadecane increases or the PCL decreases, more specially for the sample C_{16}/PCL-70/30-10, the formation of a porous structure is observed, due to the competition between the formation of the solid polymer shell, the evaporation of the solvent, and the break-up process. In addition, the spherical form takes on an ovoid shape.

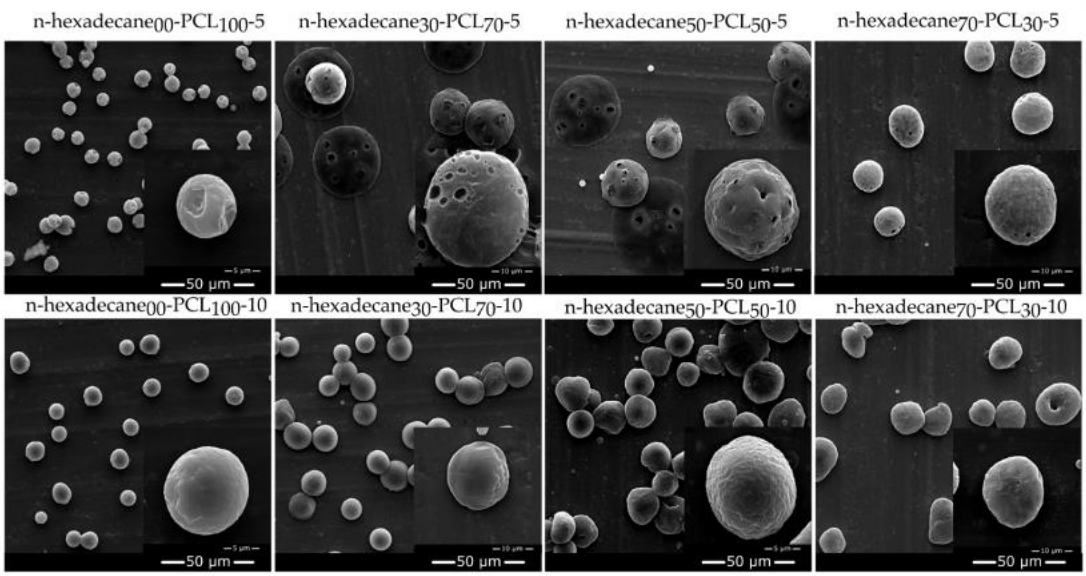

Figure 6-2 Surface state and morphologies of PCL, and n-hexadecane/PCL microparticles obtained from SEM analyses.

6.3 Phase change properties of n-hexadecane/PCL mPCMs

Phase change properties of the electrosprayed neat PCL microparticles, raw n-hexadecane, and n-hexadecane/PCL particles, such as phase change temperatures and their related latent heats, have been determined by DSC measurements and are summarized in Table 6-2. The latent heat of melting and crystallization, and their related temperatures for the raw n-hexadecane were found at about 199 J.g-1, 17.9 °C, and 16.2 °C respectively. Those of PCL microparticles, namely C_{16}/PCL-00/100-5 and C_{16}/PCL-00/100-10, have been measured at 61.6 J.g-1 (58.0 J.g-1), 55.6 °C, and 41.4 °C (41.8 °C) respectively. Thus, the concentration of PCL in the shell solution used changes the crystallinity index to some extent, since it is about 44.2% and 41.6% for the samples prepared from 5% and 10% by weight, respectively. Furthermore, the onset melting and crystallization temperatures change little (0.5 °C) or not at all depending on the concentration used. DSC thermograms of microencapsulated n-hexadecane show the thermal transitions of the PCM and PCL (Figure 6-3).

During the microencapsulation process, due to the variation in viscous forces and surface tension between the two phases, n-hexadecane molecules were dispersed in the pores of the PCL matrix and also located in the inner core of the particles. Therefore, the PCM co-exist in two “states”, the bulk n-hexadecane state and the confined n-hexadecane state. The difference in the free energy of these two phases leads to the presence of an intermediate RI phase, which is not present in the raw state of this molecular solid (Fu et al., 2011). Thus, the

crystallization of the confined and bulk n-hexadecane in the microparticles occurs in two independent transformation steps, which is observed by the presence of two differential scanning calorimetry transformation peaks (Illeková et al., 2012).

Increasing n-hexadecane to PCL by 30 to 70 wt. % in the working solution results in an increase in the enthalpy of fusion (and crystallization) of 52 to 115 $J.g^{-1}$, and 46 to 134 $J.g^{-1}$, for 5 and 10 wt. % PCL, respectively. These values also correspond to an increase in the loading content of n-hexadecane in mPCMs from 26.2% to 58.0%, and from 23.4% to 67.4%, which is lower than the theoretical content. The variations are relatively lower for the 10% PCL solution by weight, suggesting that the viscosity of the solution acts as a key parameter in the encapsulation process, in relation to the encapsulation efficiency values (EE %). The lower encapsulation efficiency, or "phase change efficiency", determined for the samples C_{16}/PCL-30/70-5 and C_{16}/PCL-30/70-10, can be related either to the unstable breakup process of the mixed droplets, or to the trapping of n-hexadecane molecule chains in the PCL macromolecular, such as a plasticizing agent. In this configuration, the PCM chains are not able to organize themselves and they cannot have a phase change transition. The increase of n-hexadecane in the system allows preventing the diffusion of the molecular chains in the PCL matrix, which allows the n-hexadecane molecular chains to organize themselves and therefore induces phase change transitions. The loading content in n-hexadecane in the electrosprayed microparticles when the 10 w/v % was used in the coaxial nozzle system is close to the theoretical ones. Furthermore, the latent heat of phase change reached 134 $J.g^{-1}$, for the sample labeled C_{16}/PCL-70/30-10, which shows that more than 96% of n-hexadecane was entrapped in the PCL matrix and may undergo a phase change transition with the temperature changes. Thus, apart from the value for 30% n-hexadecane, the encapsulation efficiency values are always higher for processes prepared from a 10% PCL solution rather than a 5% PCL solution. Also, for all systems, the encapsulation efficiency reaches a maximum value for an n-hexadecane charge amount of 50% by weight at 92.5% and 98.7% for 5% and 10% by weight PCL solutions, respectively. Besides, the loading content has no significant effect on the onset phase change transition temperatures, which are slightly lower (0.2 or 0.3 °C) than the raw n-hexadecane ones.

One of the main interests in the use of a coaxial nozzle system to encapsulate phase change material is related to the increase in the efficiency of the system. Thus, with regard to our previous study (Zhang et al., 2020), it is noticed that the encapsulation efficiency as well as the loading content of n-hexadecane in mPCMs depend on the type of nozzle and the solutions used. The encapsulation efficiency and loading content of n-hexadecane in

mPCMs obtained from a coaxial nozzle electrospraying system are found to be higher than with a single nozzle one at 10 w/v % PCL solution. Furthermore, the data gathered in Figure 6-4 illustrate that the values obtained with a single nozzle at 10 w/v % are lower than at 5 w/v % with a coaxial system. The use of the coaxial system allows reaching a loading content of about 58.0% or 67.4% for 5% and 10 w/v % of PCL compared to 49.9% for the single nozzle. The encapsulation efficiency corresponding to these values increased to 10 or 25 points compared to that obtained for the single system.

The loss of n-hexadecane is related to the evaporation of the solvent during the flying process in the electrospray system. In the single nozzle configuration, n-hexadecane and PCL are mixed in the same solvent solution before being used in the experiment, resulting in chemical interactions between the three compounds, depending on the solubility parameters. On the one hand, during the flight process from the nozzle to the collector, n-hexadecane molecules present in the solvent phase diffuse directly into the air if the concentration of PCL in the charged droplets is too low. On the other hand, in the coaxial configuration, the n-hexadecane-solvent is the inner solution and the PCL/solvent is the outer one. Thus, during the process, the solvent of the inner solution can diffuse at the droplet/air interface, and the presence of PCL macromolecular chains prevents diffusion of n-hexadecane due to molecular interactions. As a result, the n-hexadecane molecules are completely entrapped by the PCL chains, leading to the formation of a core/shell structure due to PCL stiffening, and if the concentration of the PCL solution is sufficient, smooth, non-porous particles are obtained. The morphology of the microparticles also depends on the type of nozzle used.

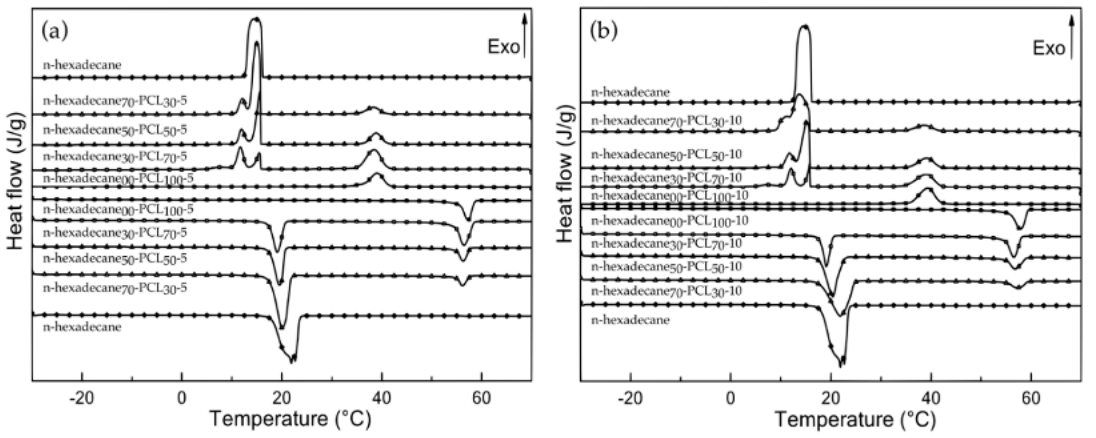

Figure 6-3 DSC thermograms of raw n-hexadecane, neat PCL microparticles and a series of n-hexadecane/PCL microcapsules obtained from PCL concentrations at 5 (a) and 10 (b) w/v % with different loading ratios between n-hexadecane and PCL.

Table 6-2 Thermal properties of n-hexadecane, neat PCL microparticles and a series of n-hexadecane/PCL microcapsules obtained from different PCL concentrations at three loading ratios between n-hexadecane and PCL.

Sample Label		Latent Heat (J/g)		T_{onset} (°C)		LC (%)	EE (%)	$X_{c(th)}$ (%)	$X_{c(m)}$ (%)
n-hexadecane (C_{16})	heating	199.4		17.9					
	cooling	195.9		16.2					
C_{16}/PCL-00/100-5	heating		61.6		55.6			44.2	
	cooling		59.1		41.4				
C_{16}/PCL-30/70-5	heating	52.2	56.9	17.5	54.7	26.2	87.3	58.5	55.5
	cooling	51.1	56.7	15.9	41.0				
C_{16}/PCL-50/50-5	heating	92.0	35.0	17.6	54.8	46.2	92.5	50.4	46.8
	cooling	90.4	35.7	15.9	41.0				
C_{16}/PCL-70/30-5	heating	115.5	15.8	17.6	54.9	58.0	82.9	37.9	27.1
	cooling	112.9	18.2	15.9	40.6				
C_{16}/PCL-00/100-10	heating		58.0		55.6			41.6	
	cooling		56.0		41.8				
C_{16}/PCL-30/70-10	heating	46.5	49.7	17.8	54.7	23.4	77.9	50.9	46.5
	cooling	45.5	50.0	16.0	41.9				
C_{16}/PCL-50/50-10	heating	98.3	32.7	17.7	54.8	49.4	98.7	46.9	46.1
	cooling	97.5	33.2	16.0	41.8				
C_{16}/PCL-70/30-10	heating	134.1	20.5	17.7	54.9	67.4	96.3	49.0	45.1
	cooling	130.3	21.1	16.0	42.0				

The electrospraying process also affects the crystallinity of the PCL matrix. The calculated crystallinity index of PCL in the mPCM is influenced by the PCL concentration and n-hexadecane content used, which is correlated with the crystallization rate during the electrospraying process. For each sample, the measured crystallinity index values (Xc(m)) are lower than the calculated (theoretical) values (Xc(th)), which is similar to the use of a single nozzle (Zhang et al., 2020). The variation in the crystallinity index is related to the physico-chemical phenomena occurring in the earlier stage of the electrospraying process. Furthermore, an increase of the PCL concentration leads to a decrease of the crystallinity index from 44.2% to 41.6% due to quick stiffening during the flying process, which limits the organization of the macromolecular chains (Table 6-2). In a coaxial system, the n-hexadecane and PCL molecular chains are not mixed; therefore, the PCM chains are less entangled in the PCL ones during the solvent evaporation. Nevertheless, the presence of PCM molecules reduce the mobility of PCL macromolecular chains and thus limits their availability for crystallization. It results in a more amorphous matrix. The presence of n-hexadecane in the particles leads to a decrease in the onset melting temperature of about 1°C, whereas this influence is less marked for the crystallization phenomenon. On the one hand, it is noticed that the phase change enthalpy of the PCL is correlated to the amount or loading content of n-hexadecane, and therefore, decreases with the increase of PCM in the solution. On the other hand, at low PCL concentration when the n-hexadecane content

increases, the amorphous phase of the obtained particles also increases, whereas at 10 w/v % no changes are observed. Furthermore, the crystallinity index of the mPCM is higher than the blank PCL particles one.

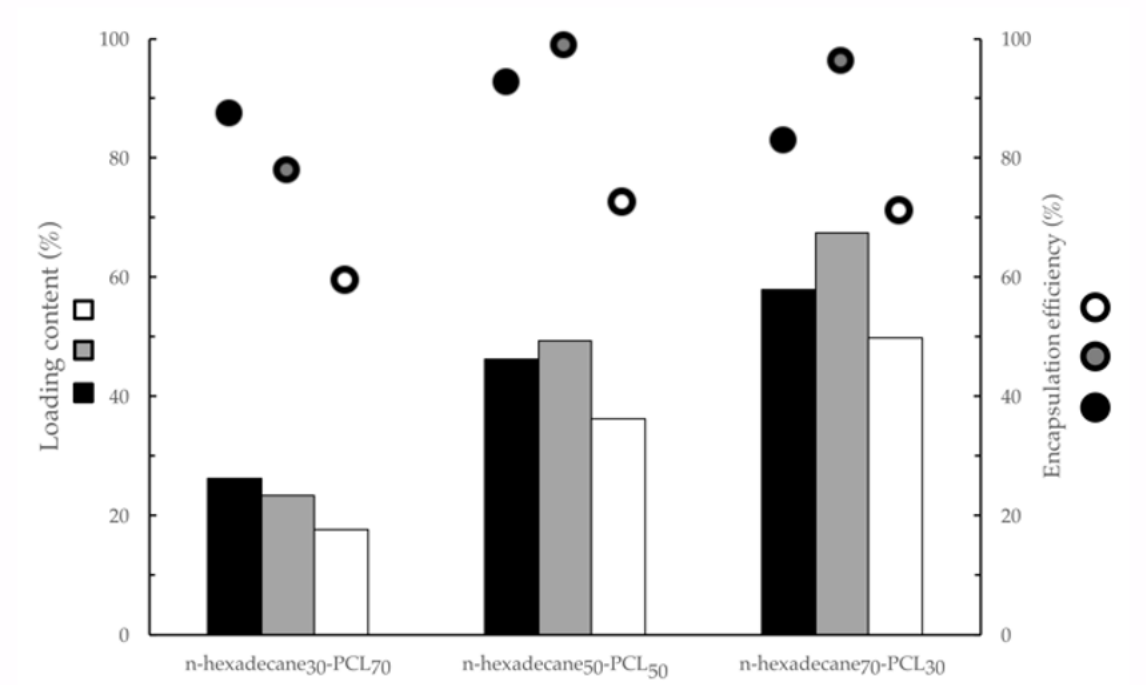

Figure 6-4 Influence of the nozzle system and the concentration of the PCL solution on the loading content and encapsulation efficiency (black—coaxial nozzle—5 w/v % PCL; grey—coaxial nozzle—10 w/v % PCL; white—single nozzle—10 w/v % PCL).

6.4 Thermal stability of n-hexadecane/PCL mPCMs

The thermal stability of raw n-hexadecane, neat PCL microparticles, and mPCMs was analyzed by TGA. The various thermograms, as well as the calculated DTG curves, are shown in Figure 6-5, and most of the primary data are summarized in Table 6-3. The thermal behavior of n-hexadecane displays single step degradation under N2 atmosphere and is characterized by an onset temperature at 5% weight loss (T5%), which starts at 149.3 °C; the maximum decomposition step of the n-alkane backbone takes place at 247.3 °C; and the maximum rate of decomposition is about 2.1 %·°C^{-1}. At over 280 °C, no residue was observed. The degradation of blank PCL microparticles, regardless of the concentration of the initial solution, occurs in a single step degradation between 360 and 460 °C, with a maximum degradation rate of about 2.1% or 2.2%·°C^{-1} at 413 °C. The concentration in PCL in the initial solution has little influence on these thermal properties.

n-hexadecane-based microparticles exhibit a two-stage degradation, i.e. (i) from 150 to 300°C, attributed to

the degradation of n-hexadecane, and (ii) from 350 to 500°C corresponding to that of the PCL matrix. The first stage can be divided into two main steps, i.e. (i) evaporation of the leakage core materials from 150 to 200–250 °C depending on the n-hexadecane/PCL weight ratio, and (ii) the last step has been attributed to n-hexadecane from within the microparticles or trapped in the macromolecular chains of the PCL, which evaporate completely at about 280–300°C. The increase in the onset temperature of the first stage indicated the protective effect of the shells, which enhanced the thermal stability of the core materials. The shape of the TGA (and DTG) curve is related to the different phenomena that occur during the test due to the change in the physical state of the materials. The increase in temperature up to 62 °C causes the melting of the PCL; therefore, from this point on, all compounds are in a liquid state. The lower density of n-hexadecane allows it to diffuse to the surface of the crucible and thus initiate its degradation or evaporation from 150 °C onwards. However, as the loading content of n-hexadecane increases, these molecules become trapped in the liquid matrix of the PCL, and most of the chains become entangled. Thus, the diffusion of molecular chains has been delayed or shifted to higher temperatures since the presence of PCL acts as a physical barrier to the thermal degradation of n-hexadecane. Besides, the decrease in the PCL content leads to an increase and a decrease in the maximum rate of degradation in the first step and in the second step, respectively.

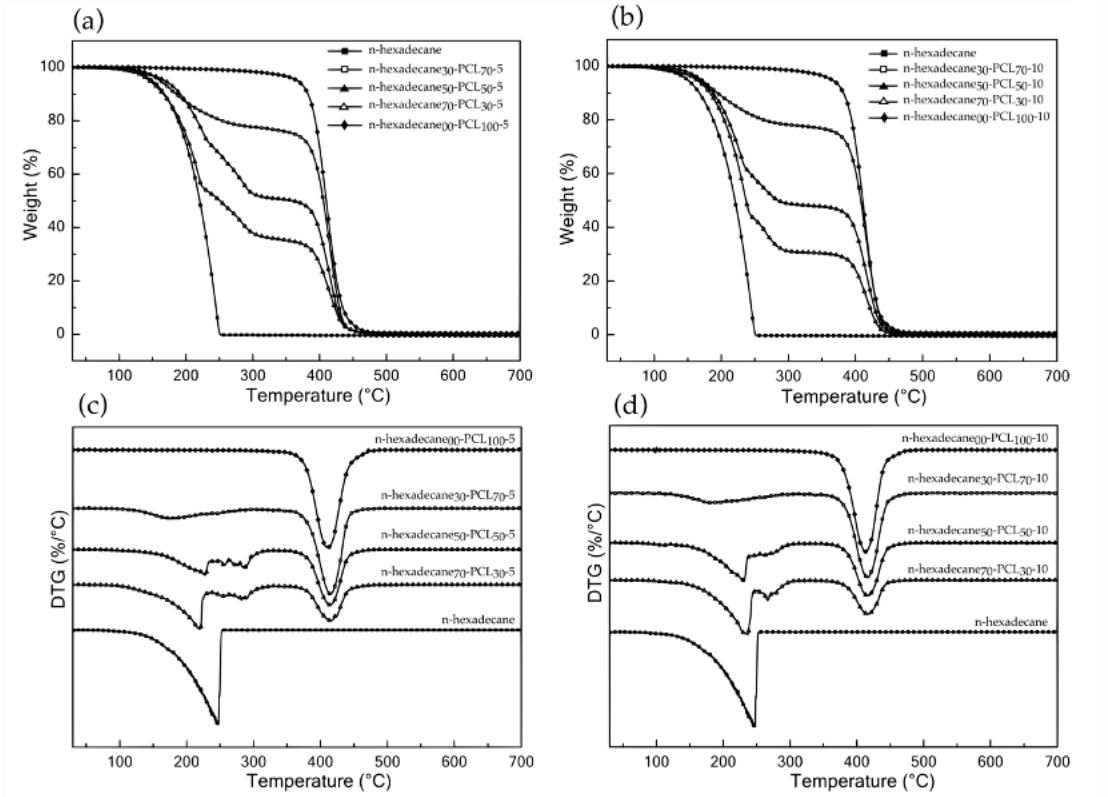

Figure 6-5 TG and DTG curves of raw n-hexadecane, neat PCL microparticles and a series of n-hexadecane/PCL microcapsules obtained from two PCL concentrations with different loading ratios between n-hexadecane and PCL.

Table 6-3 Thermogravimetric data of raw n-hexadecane, neat PCL microparticles and a series of n-hexadecane/PCL microcapsules obtained from two PCL concentrations with different loading ratios between n-hexadecane and PCL.

Sample	Initial Degradation Temperature – $T_{5\%}$ (°C)	First Step			Second Step		
		Weight Loss (100-350 °C) (%)	Maximum Degradation Temperature (°C)	Maximum Degradation Rate (%/°C)	Weight Loss (350-500°C) (%)	Maximum Degradation Temperature (°C)	Maximum Degradation Rate (%/°C)
C_{16}/PCL-00/100-5	366.8	3.4	-	-	96.1	412.7	2.1
C_{16}/PCL-00/100-10	364.7	3.6	-	-	95.8	413.8	2.2
n-hexadecane (C_{16})	149.3	99.3	247.3	2.1	-	-	-
C_{16}/PCL-30/70-5	161.5	24.0	177.7	0.2	75.5	416.3	1.9
C_{16}/PCL-50/50-5	168.5	49.3	227.0	0.6	50.0	414.7	1.2
C_{16}/PCL-70/30-5	145.5	64.4	218.3	1.0	34.8	415.0	0.8
C_{16}/PCL-30/70-10	170.0	23.1	180.5	0.2	76.4	415.7	1.8
C_{16}/PCL-50/50-10	166.3	51.8	231.1	0.8	47.6	416.5	1.2
C_{16}/PCL-70/30-10	163.3	69.3	236.8	1.2	30.1	416.5	0.7

The variations of the onset degradation temperature are another example of the effect of the electrospraying system on the properties of the microparticles (Figure 6-6). On the one hand, mPCMs obtained from a single nozzle have an onset degradation temperature close to the raw-hexadecane ones, whatever the n-hexadecane to PCL ratio used. On the other hand, the measured T5% is higher for microparticles obtained from a coaxial nozzle, except for the sample labeled n C_{16}/PCL-70/30-5. This difference is related to the change in the particle morphology. It was postulated that the use of a single nozzle leads to the formation of a material structure, in which tiny droplets of n-hexadecane are dispersed in the PCL matrix. The use of the 10 w/v % of PCL solution from coaxial nozzle electrospraying allows for obtaining higher onset degradation temperatures, which tends to decrease with the increase of the n-hexadecane to PCL weight ratio. For the sample C_{16}/PCL-70/30-10, T5% was found 14 °C higher than this of raw n-hexadecane, underlining the protective barrier of the PCL during the degradation process, which prevents the diffusion of the PCM molecule. Thus, based on the TGA and DSC results, the use of the 10 w/v% PCL solution leads to the formation of a core-shell structure, such as a microcapsule. The decrease of the T5% value with the increase of n-hexadecane content is related to the decrease of the thickness of the PCL shell (Moghaddam & Mortazavi, 2015). The use of the 5 w/v% PCL solution in a coaxial system induces the formation of a morphology intermediate of the two other cases, such as a salami-like structure. At higher PCL content, the n-hexadecane core materials are entirely confined in the polymeric matrix. The increase of core content leads to the formation of a porous structure due to the mixing of both solutions and the solvent evaporation during the flying process. When the ratio n-hexadecane/PCL reaches 70/30, the thermal stability of the blend PCM and PCL macromolecular chains constituting a part of the matrix structure is too weak to protect the dispersed n-hexadecane from its thermal degradation.

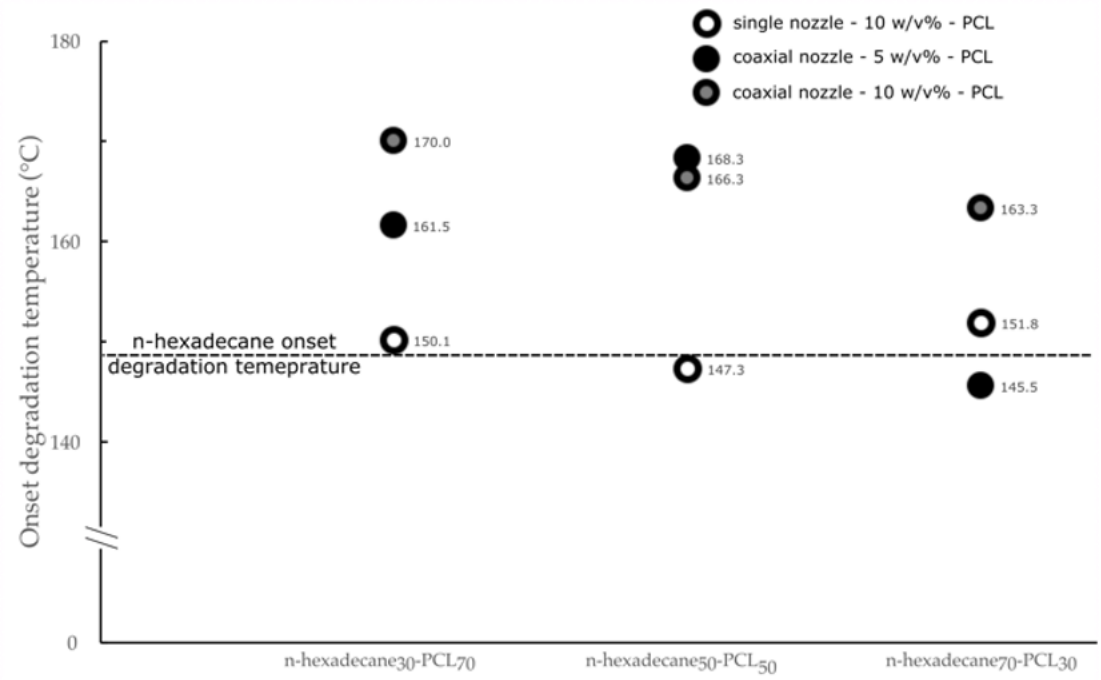

Figure 6-6 Influence of the electrospraying process on the thermal degradation of the mPCMs.

6.5 Conclusions

n-hexadecane was successfully encapsulated in a PCL matrix with a coaxial nozzle electrospraying system. The use of a 10 w/v % PCL solution allows forming a Taylor cone to stabilize the breakup process of double-component liquid, and therefore, monodispersed microcapsules with a mean diameter of about 20 µm are obtained for an initial loading content of n-hexadecane of about 50% or 70%. The concentration of the PCL solution and/or the initial content of n-hexadecane also affect the surface morphology of the obtained microparticles. Thus, the increase from 5 to 10 w/v % of the PCL solution, as well as the n-hexadecane when a 5 wt % of PCL was used, changed a porous surface state to a non-porous one. The use of a coaxial system also allows increasing a higher encapsulation efficiency compared to a single nozzle process. Furthermore, higher loading content of n-hexadecane was also achieved. Thus, when 70% n-hexadecane was introduced in 10 w/v % PCL solution, the encapsulation efficiency of n-hexadecane reached 96.3%, and correspondingly, the active loading content of n-hexadecane reached 67.4 %. This content allows storing more than 130 $J.g^{-1}$ of latent heat via its liquid-solid phase transition. The presence of PCL surrounding the n-hexadecane phase enhances its thermal stability. Furthermore, the morphology of the microparticles can be adjusted depending on the initial PCL and n-hexadecane contents in

the formulation, as expected from the TGA and DSC tests. Thus, a lower n-hexadecane to PCL ratio leads to a matrix morphology, whereas the higher amount in n-hexadecane allows obtaining either a salami-like or a core/shell structure. The use of a coaxial system allows for improving the encapsulation efficiency and loading content of n-hexadecane compared to a single nozzle electrospraying. Stable cone-jet mode and stable breakup process of charged droplets are more comfortable to control for a single nozzle than for a coaxial electrospraying, where the outer physico-chemical properties play a crucial role. The formation of microparticles from an electrospraying process is an excellent alternative to other physical or chemical microencapsulation methods and is a high-efficiency choice for energy storage and thermal regulation system.

References

Fu, D., Su, Y., Xie, B., Zhu, H., Liu, G., & Wang, D. (2011). Phase change materials of n-alkane-containing microcapsules: Observation of coexistence of ordered and rotator phases. *Physical Chemistry Chemical Physics*, *13*(6), 2021–2026. https://doi.org/10.1039/c0cp01173h

Illeková, E., Miklošovičová, M., Šauša, O., & Berek, D. (2012). Solidification and melting of cetane confined in the nanopores of silica gel. *Journal of Thermal Analysis and Calorimetry*, *108*(2), 497–503. https://doi.org/10.1007/s10973-011-2113-5

Moghaddam, K. M., & Mortazavi, S. M. (2015). Preparation, characterisation and thermal properties of calcium alginate/n-nonadecane microcapsules fabricated by electro-coextrusion for thermo-regulating textiles. *Journal of Microencapsulation*, *32*(8), 737–744. https://doi.org/10.3109/02652048.2015.1073388

Zhang, S., Campagne, C., & Salaün, F. (2020). Preparation of n -Alkane / Polycaprolactone Phase-Change Microcapsules via Single Nozzle Electro-Spraying : Characterization on Their Formation , Structures and Properties. Applied Sciences, 10(2), 561-580. http://dx.doi.org/10.3390/app10020561

Chapter 7 Preparation of n-Hexadecane/Poly (lactic acid)/Poly(caprolactone) Phase Change Microcapsules with Double-Layered Shells and Related Characterizations

When phase change microcapsules (mPCMs) were used for fabricating thermal regulation textiles, high loading content of phase change material (PCM), good physical strength and high thermo-mechanical properties and good interfacial adhesion between mPCMs and textiles are necessary. For electrosprayed microcapsules with single-layered shell, for example n-hexadecane/PCL microcapsules or n-hexadecane/PLA microcapsules, it is difficult for them to meet all requirements in the preparation of thermal regulation textiles. Owing to low glass transition temperature as well as low melting point, PCL can offer good interfacial adhesion with textiles via simple heat treatment, but the physical strength and thermal stability of PCL is limited. And PLA matrix can offer good thermos-mechanical properties and physical strength, but it interfacial interactions with textiles is bad. Therefore, electrosprayed mPCMs with double-layered shell consisted of PLA and PCL can not only obtain good thermos-mechanical properties and physical strength, but also achieve strong bonding with textiles.

In general, electrosprayed mPCMs with double-layered shell can be fabricated via using coaxial nozzle electrospraying. Meanwhile, when coaxial nozzle electrospraying was used for carrying out the microencapsulation of phase change materials, high encapsulation efficiency and high loading content of PCMs can be easily achieved. Therefore, in this chapter, PCL was used as outer shell and PLA was used as inner shell to encapsulate n-hexadecane based on coaxial nozzle electrospraying. The effects of different n-hexadecane additions, different weight ratios between PCL and PLA on the structures, morphologies and properties of obtained mPCMs were investigated in details. The structures, morphologies, and thermal properties of the mPCMs were characterized by optical microscopy (OM), scanning electron microscopy (SEM), differential scanning calorimeter (DSC) and thermogravimetric analysis (TGA).

7.1 Size and morphology of n-hexadecane/PLA/PCL mPCMs

The mean diameter, size distribution and surface morphology of PLA50/PCL50 electrosprayed microparticles (reference sample) and a series of n-hexadecane/PLA/PCL electrosprayed mPCMs were presented in Figure 7-1 and Figure 7-2, and the mean diameters of corresponding particles were also listed in Table 7-1 and Table 7-2. Firstly, for PLA50/PCL50 microparticles, they not only have a mono-dispersed size distribution, but also a spherical and smooth morphology. The mean diameter of these microparticles is 6.6 μm with a standard deviation of 0.7 μm. Compared with the single-layered PCL or PLA microparticles obtained from single or coaxial nozzle electrospraying, the mean diameter of PLA/PCL double-component microparticles obtained from coaxial nozzle electrospraying is less. It is related with the differences in the viscosity of working solutions and the differences in the working window of applied voltage for different systems. For neat PCL microparticles obtained from single nozzle electrospraying, the PCL (mean molecular weight: 37,000 g/mol) concentration of working solution was fixed at 10 wt%, and applied voltage was fixed at 4.0 kV. For neat PLA microparticles obtained from single nozzle electrospraying, the PLA (mean molecular weight: 58300 g/mol) concentration of working solution was fixed at 3 wt% or 5 wt%, and applied voltage was set at 7.25 kV. For neat PCL microparticles obtained from coaxial nozzle electrospraying, the PCL concentration of working solution was fixed at 5 wt% or 10 wt%, and applied voltage was set at 8.25 kV. For PLA/PCL double-component microparticles obtained from coaxial nozzle electrospraying, the PLA and PCL concentrations in working solutions were both fixed at 5 wt%, and applied voltage was set at 9.25 kV. Owing to lower viscosity of working solution and higher applied voltage, the breakup process of PLA/PCL charged droplets was stronger (Bock, Dargaville, & Woodruff, 2012; Zhang et al., 2012). Therefore, smaller PLA/PCL electrosprayed microparticles can be obtained.

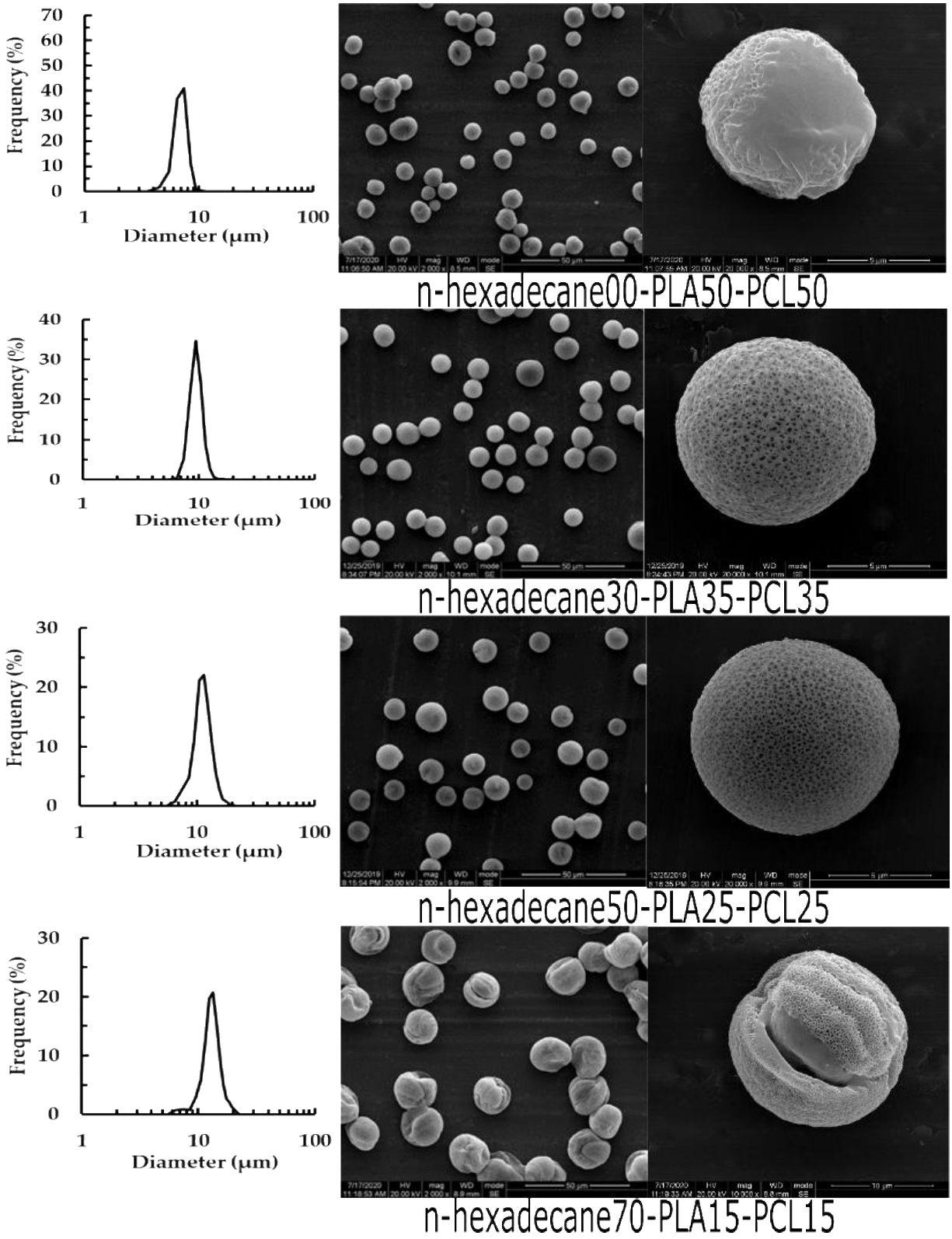

Figure 7-1 The SEM images and size distribution of PLA/PCL microparticles and a series of n-hexadecane/PLA/PCL electrosprayed mPCMs with different n-hexadecane additions.

Table 7-1 The size of PLA/PCL microparticles and a series of n-hexadecane/PLA/PCL electrosprayed mPCMs with different n-hexadecane additions.

Sample	n-hexadecane00-PLA50-PCL50	n-hexadecane30-PLA35-PCL35	n-hexadecane50-PLA25-PCL25	n-hexadecane70-PLA15-PCL15
Mean diameter	6.6±0.7 μm	9.2±1.2 μm	11.1±2.0 μm	12.9±2.3 μm

The effects of n-hexadecane additions on the mean diameter, size distribution and surface morphologies of n-hexadecane/PLA/PCL microcapsules were also presented in Figure 7-1, and the related mean diameters of various samples were also listed in Table 7-1. With the increasing of n-hexadecane additions in PLA/PCL microparticles, the mean diameter of obtained microcapsules increased gradually. N-hexadecane as low electrical conductivity liquid, when it was added into PLA/chloroform electrospraying solution (inner liquid), the electrical conductivity of working solution decreases and the viscosity of working solution increases (Zhang, Campagne, & Salaün, 2019). The variations in the electrical conductivity and the viscosity of working solution with different n-hexadecane additions will depress the breakup process of charged droplets, and finally result in a larger mean diameter. Meanwhile, due to the existence of n-hexadecane in electrosprayed droplets, the breakup process of charged droplets also became unstable, which will result electrosprayed particles of different sizes. Therefore, with the increasing of n-hexadecane addition in PLA/PCL microparticles, although the mono-dispersed size distributions are still obtained, the standard deviation of corresponding mean diameter increased gradually and the peak of size distribution also broadened. In addition, the gradual increase in the mean diameter of n-hexadecaane/PLA/PCL microparticles after adding n-hexadecane is also related to the increase in loading content of n-hexadecane in particles.

For the effects of n-hexadecane addition on the surface state of obtained particles, when n-hexadecane was introduced into microparticles, some tiny pores appeared on the surface of microparticles. The appearance of porous structure on the surface of n-hexadecane/PLA/PCL microparticles was mainly related with the phase separation between PCL phase and chloroform phase. During the flight process of charged droplets from the tip of nozzle to collector, chloroform will evaporate from n-hexadecane/PLA/PCL droplets to air. With the leaving of chloroform, some n-hexadecane will diffuse from PLA phase to PCL phase. N-hexadecane as non-solvent for PCL phase, when it enters PCL phase, some chloroform existed in PCL phase will move into n-hexadecane phase. The mild phase separation between PCL and chloroform resulted from the diffusion of n-hexadecane will lead to the appearance of porous structure on the surface of n-hexadecane/PLA/PCL microparticles. Thus, with the migration

of chloroform from PCL phase to n-hexadecane phase during the solidification of PCL phase, the position where the diffused chloroform originally occupied in the PCL phase will form some vacancies, finally left some pores after the complete solidification of PCL phase (Wu, & Clark, 2007).

When the theoretical addition of n-hexadecane in whole microparticles increased from 30 % to 50 %, the shape, morphology and porous structure of obtained microparticles didn't not change obviously. With the further increase of the theoretical addition of n-hexadecane to 70 %, the shape of microparticles became irregular, and rough as well as groove morphology can be observed on the surface of microparticles. It was related with the weight fraction among n-hexadecane, PLA and PCL in electrospraying solution. When the theoretical addition of n-hexadecane in n-hexadecane/PLA/PCL system reach 70 %, the breakup process of charged droplets will become unstable owing to the existence of excessive n-hexadecane (low electrical conductivity liquid) in electrosprayed droplets. It will bring some structural defects or unevenness on the surface morphology of obtained microparticles. Meanwhile, owing to the intermolecular interactions between n-hexadecane and chloroform, the evaporation rate of chloroform in electrosprayed droplets will be slowed down after introducing excessive n-hexadecane.

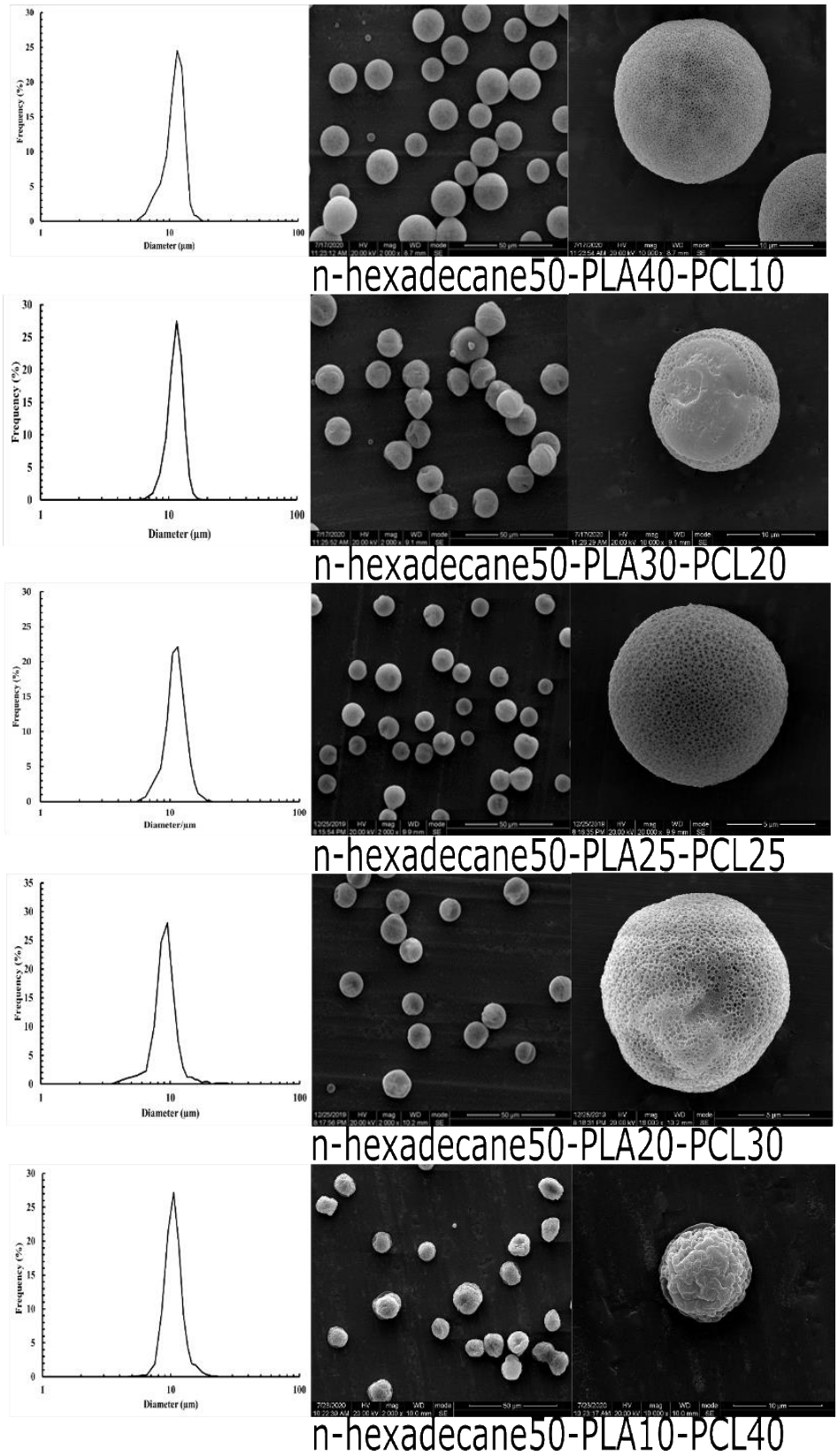

Figure 7-2 The SEM images and size distribution of a series of n-hexadecane/PLA/PCL electrosprayed mPCMs with different weight fractions between PLA and PCL.

Table 7-2 The size of a series of n-hexadecane/PLA/PCL electrosprayed mPCMs with different weight fractions between PLA and PCL.

sample	n-hexadecane50-PLA40-PCL10	n-hexadecane50-PLA30-PCL20	n-hexadecane50-PLA25-PCL25	n-hexadecane50-PLA20-PCL30	n-hexadecane50-PLA10-PCL40
Mean diameter	10.9±0.7 μm	11.0±1.4 μm	11.1±2.0 μm	9.2±2.4 μm	10.4±1.9 μm

Therefore, the balance between the condensation of polymeric chains and the leaving of solvent in electrosprayed droplets will be broken. After the complete condensation of polymeric chains, the leaving of chloroform will leave gully morphology or porous morphology on the microparticles surface.

In order to investigate the effects of different weight fractions between PLA component and PCL component on the structure and morphology of obtained mPCMs, the theoretical addition of n-hexadecane was fixed at 50 wt% and a series of n-hexadecane/PLA/PCL microparticles with different weight fractions between PLA component and PCL component (50/40/10, 50/30/20, 50/25/25, 50/20/30 and 50/10/40) were prepared. The size, size distribution and morphology of corresponding microparticles were presented in Figure 7-2, and related mean diameters were listed in Table 7-2. With the variations of the weight ratio between PLA component and PCL component from 4/1 to 1/4, the mean diameter of corresponding microparticles didn't change obviously. Meanwhile, their size distributions still kept mono-dispersed under different weight ratios between PLA component and PCL components. With the decreasing of PLA component, the standard deviation of mean diameter of obtained microparticles increased gradually. It means that the size distribution of corresponding microparticles broadened gradually. It indicated that the existence of PLA component can stabilize the formation of Taylor cone as well as the breakup process of charged droplets. Thus, n-hexadecane as a non-polar liquid existed in PLA/chloroform solution (inner solution) will influence the formation of Taylor cone as well as the stabilization of the whole electrospraying process (Gañán-Calvo, 1994).

In addition, with the variations of weight ratio between PLA component and PCL component, the changes of the surface morphology of obtained microparticles were also be studied. When the weight ratio between PLA component and PCL component decreased from 4/1 to 2/3, the shape and surface morphology didn't change obviously, still kept spherical, smooth and porous. However, when the weight ratio between PLA component and PCL component further deceased to 1/4, the shape of obtained microparticles became irregular, and corresponding surface morphology became rough and rugged, and the number of porous structure also decreased. This

phenomenon is caused by two reasons. On the one hand, n-hexadecane as a low electrical conductivity liquid, its existence in PLA/chloroform solution will destroy the stability of cone-jet mode and the uniformity of breakup process. Meanwhile, PLA component in inner liquid can make up for the instability and unevenness caused by the existence of n-hexadecane. With the decreasing of PLA component to 10 wt%, the limited PLA component in inner liquid can't stabilize the electrospraying process. Therefore, the shape of obtained microparticles became irregular. On the other hand, with the increasing of PCL component to 40 wt% in n-hexadecane/PLA/PCL system, the phase separation between PCL phase and chloroform phase caused by the diffusion of n-hexadecane will be depressed. Therefore, the porous structure on the surface of obtained microparticles decreased, and the surface morphology also changed from smooth to rugged.

7.2 Phase transition behaviors of n-hexadecane/PLA/PCL mPCMs

The phase transition behaviors and the thermal properties of raw n-hexadecane, PLA50/PCL50 microparticles and a series of n-hexadecane/PLA/PCL microcapsules with different n-hexadecane additions were characterized by DSC (Figure 7-3), and related thermal parameters of encapsulated n-hexadecane, PLA component and PCL component were also listed in Table 7-3, Table 7-4 and Table 7-5, respectively.

Table 7-3 Thermal properties of raw n-hexadecane and encapsulated n-hexadecane in a series of n-hexadecane/PLA/PCL microcapsules with different n-hexadecane additions

Sample label		ΔHm or ΔHc (J/g)	Tonset (°C)	Tm or Tc (°C)	Tend (°C)	LC (%)	EE (%)
n-hexadecane	heating	199.4±2.2	17.9	20.7	23.7	-	-
	cooling	195.9±4.7	16.2	16.0	13.0	-	-
n-hexadecane00-PLA50-PCL50	heating	-	-	-	-	-	-
	cooling	-	-	-	-	-	-
n-hexadecane30-PLA35-PCL35	heating	50.4	17.7	24.3	31.2	25.3	84.3
	cooling	50.2	15.8	7.2	-9.3		
n-hexadecane50-PLA25-PCL25	heating	98.9	17.8	27.6	34.2	49.6	99.2
	cooling	97.6	15.8	9.6	-7.3		
n-hexadecane70-PLA15-PCL15	heating	113.6	17.9	19.4	35.8	57.0	81.4
	cooling	109.8	16.0	14.8	-4.8		

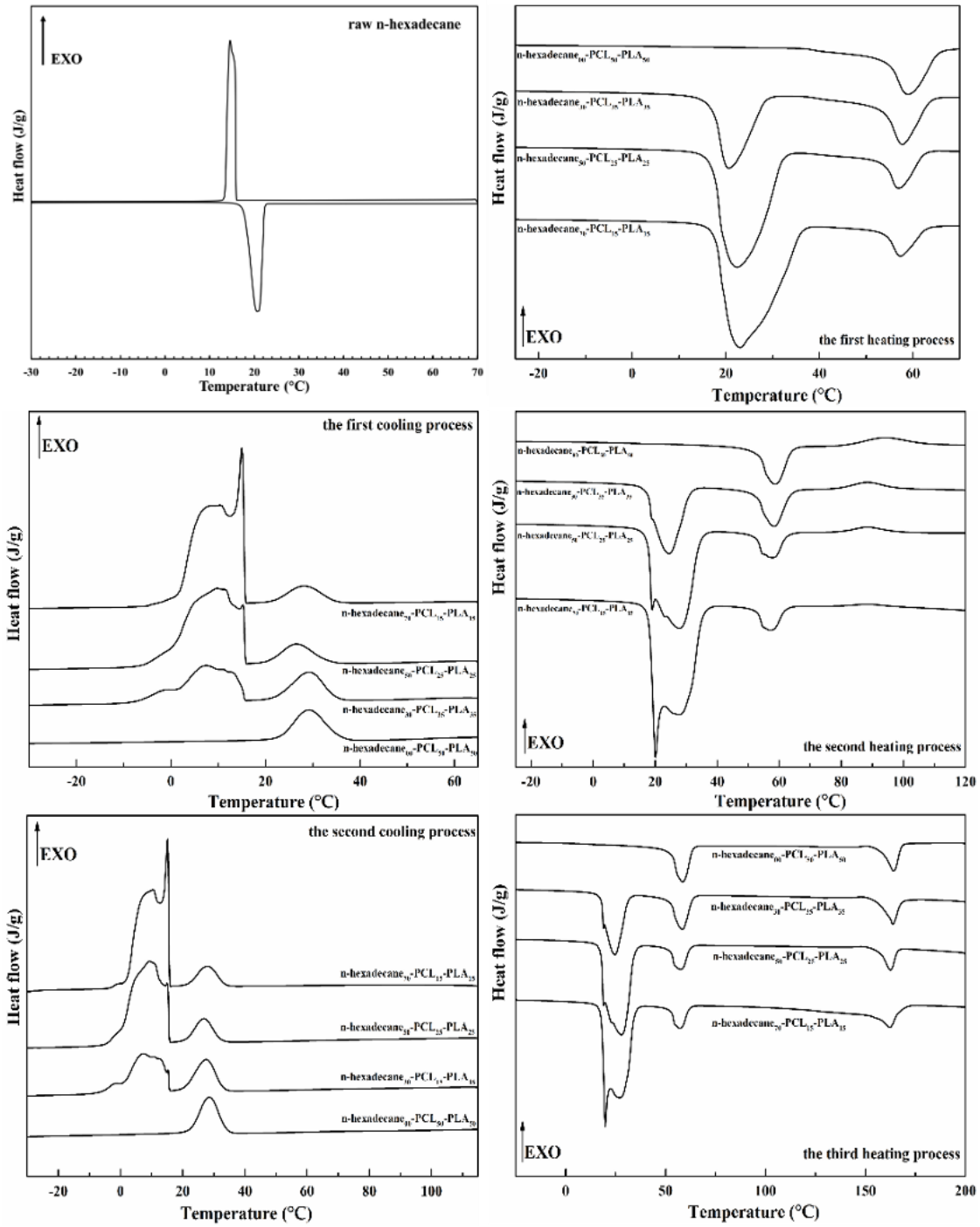

Figure 7-3 The DSC curves of raw n-hexadecane, PLA50/PCL50 microparticles and a series of n-hexadecane/PLA/PCL microcapsules with different n-hexadecane additions.

Table 7-4 Thermal properties of PLA component in PLA50/PCL50 and in a series of n-hexadecane/PLA/PCL microcapsules with different n-hexadecane additions

Sample label		ΔHm or ΔHc (J/g)	Tonset (°C)	Tm or Tc (°C)	Tend (°C)	ΔHcc or ΔHcc(r)-th (J/g)	Tonset (°C)	Tcc (°C)	Tend (°C)	Xc(th)-PLA (%)	Xc(m)-PLA (%)
n-hexadecane00-PLA50-PCL50	heating	16.9	157.3	164.0	167.9	11.8/23.6	80.8	93.8	108.9	36.3	-
	cooling										
n-hexadecane30-PLA35-PCL35	heating	17.5	158.5	163.4	167.8	7.7/22.0	78.1	88.3	98.9	53.8	50.0
	cooling										
n-hexadecane50-PLA25-PCL25	heating	12.7	156.7	162.2	166.0	5.3/21.2	79.3	88.4	98.4	54.6	54.0
	cooling										
n-hexadecane70-PLA15-PCL15	heating	9.5	156.0	161.9	166.8	2.8/18.7	74.5	88.8	103.5	67.9	47.3
	cooling										

Table 7-5 Thermal properties of PCL component in PLA50/PCL50 and in a series of n-hexadecane/PLA/PCL microcapsules with different n-hexadecane additions

Sample label		ΔHm or ΔHc (J/g)	Tonset (°C)	Tm or Tc (°C)	Tend (°C)	Xc(th)-PCL (%)	Xc(m)-PCL (%)
n-hexadecane00-PLA50-PCL50	heating	28.7	52.7	58.3	63.5	41.1	-
	cooling	26.9	34.1	28.6	22.6	-	-
n-hexadecane30-PLA35-PCL35	heating	24.2	52.0	58.1	63.5	49.6	46.4
	cooling	22.9	33.0	27.7	20.7		
n-hexadecane50-PLA25-PCL25	heating	15.7	52.2	57.4	45.1	44.6	44.6
	cooling	16.5	32.2	26.9	21.1		
n-hexadecane70-PLA15-PCL15	heating	14.2	52.5	56.8	61.7	67.9	47.3
	cooling	15.0	32.4	28.1	20.7		

In Table 7-3, for raw n-hexadecane, it melts at 17.9 °C with a latent heat of 199.4 J/g and solidifies at 16.2 °C with a latent heat of 195.9 J/g. And the peak temperature of its melting or crystallization process is 20.7 °C and 16.0 °C, respectively. For PLA50/PCL50 double-component microparticles, their DSC curves not only present the phase transition behaviors of PCL component, but also the phase transition behaviors of PLA component. PLA component melts at 157.3 °C with a melting enthalpy of 16.9 J/g. And the peak temperature of the melting process of PLA component is 164.0 °C. Based on the the theoreticl content of PLA component in PLA/PCL double-component microparticles, the theoretical crystallization degree of PLA component is 36.3 %. Compared with the neat PLA microparticles obtained from single-nozzle electrospraying, although the melting temperatures (including onset temperature, peak temperaturue and end temperature) of PLA component in PLA50/PCL50 microparticles didn't change obviously, the cold crystallization temperatures (including onset temperature, peak temperature and end tempsrature) of PLA component in PLA50/PCL50 microparticles decreased to 80.8 °C, 93.8 °C and 108.9 °C, respectively. The reduction in cold crystallization temperature was related with the improvement in the movement activity of PLA chains. During the formation process of PLA50/PCL50 electrosprayed droplets, some PLA chains will diffuse into PCL phase and some PCL chains will also move into PLA phase with the evaporation of chloroform. Owing to the newly formed intermolecular interactions between PLA chains and PCL chains, the original intermolecular interactions among PLA chains will reduce. Combining with the flexibility of PCL chains, the movement activity of PLA chains in PLA50/PCL50 microparticles will be enhanced compared with the situation in neat PLA microparticles. Therefore, the temperature for carrying out the cold crystallization process of PLA component in PLA50/PCL50 microparticles decreased. Meanwhile, compared with neat PLA microparticles obtained from single nozzle electrospraying, the crystallization degree of PLA component in PLA50/PCL50 microparticles decreased from 44.4 % to 36.6 %. Thus, the ordered arrangement of PLA chains will be destoried by the intermolecular interactions between PLA chains and PCL chains, which will cause the reduction of the crystallization degree of PLA component.

For the PCL component in PLA50/PCL50 microparticles, it melts at 52.7 °C with a melting enthalpy of 28.7 J/g and solidifies at 34.1 °C with a crystallization enthalpy of 26.9 J/g. And the related peak temperature of the melting or crystallization process is 58.3 °C or 28.6 °C, respectively. Based on the theoretical content of PCL component in PLA/PCL double-component microparticles, the theoretical crystallization degree of PCL component reaches 41.1 %. Compared with neat PCL microparticles obtained from single nozzle electrospraying

or coaxial nozzle electrospraying, not only the melting or crystallization temperature of PCL component in PLA50/PCL50 microparticles decreased, but also the crystallization degree of PCL component. The decrease of melting or crystallization temperature of PCL component in PLA50/PCL50 microparticles might be related with the decrease of particles size. Compared with neat PCL microparticles obtained from single nozzle electrospraying and coaxial nozzle electrospraying, the size of PLA50/PCL50 microparticles decreased, which will cause an increase in the specific surface area of PLA50/PCL50 microparticles. Then, the thermal conductivity and heat exchange efficiency of PLA50/PCL50 microparticles also enhanced owing to the increase in contact area with heat flow. Therefore, the temperature for achieving the melting or crystallization of PCL component in PLA50/PCL50 microparticles also decrease.

When n-hexadecane was encapsulated into PLA/PCL double-layered microcapsules, the latent heat of encapsulated n-hexadecane was related with the addition of n-hexadecane. With the increase of n-hexadecane addition from 30 wt% to 70 wt%, the latent heat of encapsulated n-hexadecane in PLA/PCL double-layered microcapsules increased from 50.4 J/g to 113.6 J/g. Correspondingly, the loading content of n-hexadecane in PLA/PCL double-layered microcapsules increased from 25.3 % to 57.8 %, and the encapsulation efficiency of n-hexadecane increased from 84.3 % to 99.2 % with the increase of n-hexadecane addition from 30 wt% to 50 wt%, then decreased to 81.4 % with the further increase of n-hexadecane addition to 70 wt%. When the addition of n-hexadecane is 30 wt%, the limited n-hexadecane chains are not able to organize themselves and they cannot have a phase change transition. Meanwhile, it is difficult for limited n-hexadecane to be captured completely by PLA chains and PCL chains, and some of them will diffuse to air with the leaving of solvent. That is why the latent heat of n-hexadecane30/PLA35/PCL35 is low. When the addition of n-hexadecane increased to 50 wt%, the increase of n-hexadecane in the system not only improves the chance of being caught by PLA chains or PCL chains, but also allows preventing the diffusion of the n-hexadecane molecular chains to air, which allows the n-hexadecane molecular chains to organize themselves and therefore induces phase change transitions. Therefore, a loading content of 49.6 % and an encapsulation efficiency of 99.2 % can be obtained when 50 wt% n-hexadecane was introduced in microcapsule system. It also indicated that double-layered structure and coaxial nozzle electrospraying are good method to achieve a high encapsulation efficiency of PCM in electrosprayed microcapsules. When n-hexadecane addition further increased to 70 wt%, it is difficult for limited PLA component and limited PCL component to capture excessive n-hexadecane completely. Owing to the existence of chloroform

in inner liquid and outer liquid, limited PLA chains and limited PCL chains can't prevent the diffusion of n-hexadecane induced by the leaving of solvent. Therefore, some n-hexadecane will escape to air during the flight process of electrosprayed droplets, which causes a reduction in the loading content as well as encapsulation efficiency of n-hexadecane in final microcapsules.

In addition, although the onset temperature of the melting or freezing of encapsulated n-hexadecane didn't change obviously compared with raw n-hexadecane, the melting or crystallization process (temperature range) of encapsulated n-hexadecane broadened. Thus, when n-hexadecane was encapsulated into PLA/PCL matrix, more crystalline phases of n-hexadecane can be obtained due to the existence of PLA/PCL shell as nucleating agent and the increase of the specific surface area of encapsulated n-hexadecane.

When n-hexadecane was encapsulated into PLA/PCL matrix, the thermal parameters of PLA component in n-hexadecane/PLA/PCL microcapsules were also influenced. In Table 7-4, the melting enthalpy of PLA component decreased gradually from 16.9 J/g to 9.5 J/g with the increasing of n-hexadecane addition. Based on the theoretical addition of PLA component and measured content of n-hexadecane in n-hexadecane/PLA/PCL system, the calculated crystallization degree of PLA component increased after adding n-hexadecane. It is related with the improvement in the movement activity of PLA chains after introducing n-hexadecane. Before coaxial nozzle electrospraying of n-hexadecane/PLA/PCL systems, n-hexadecane was mixed with PLA/chloroform solution completely. Therefore, the intermolecular interactions between PLA chains and n-hexadecane chains will destroy the original entanglements among PLA chains. It can enhance the movement activity of PLA chains, which causes an increase in the crystallization degree of PLA component after adding n-hexadecane. The improvement in the movement activity of PLA chains also accelerated the cold crystallization process of PLA component. Therefore, the temperatures (including onset temperature, peak temperature and end temperature) for carrying out the cold crystallization of PLA component also decreased compared with n-hexadecane-free microparticles. For the melting temperatures (including onset temperature, peak temperature and end temperature) of PLA component in n-hexadecane/PLA/PCL systems, it didn't change obviously compared with the situation in PLA/PCL system. In addition, the relative cold crystallization enthalpy of PLA component in n-hexadecane/PLA/PCL system decreased mildly compared with that of PLA component in PLA/PCL system.

For the PCL component in n-hexadecane/PLA/PCL system, its thermal parameters were also influenced by the introducing of n-hexadecane. In Table 7-5, the melting (or crystalline) enthalpy of PCL component decreased

gradually from28.7 (or 26.9) J/g to 14.2 (15.0) J/g with the increasing of n-hexadecane addition. Based on the theoretical addition of PCL component and measured content of n-hexadecane in n-hexadecane/PLA/PCL system, the calculated crystallization degree of PCL component increased after adding n-hexadecane. When the n-hexadecane addition in n-hexadecane/PLA/PCL system reached 70 wt%, the crystallization degree of PCL component can reach 47.3 %. During the fight process of n-hexadecane/PLA/PCL electrosprayed droplets, some PLA chains and n-hexadecane chains will diffuse into PLA phase with the evaporation of solvent. On the one hand, n-hexadecane chains can form new intermolecular interactions with PCL chains, which can destroy original entanglements among PCL chains. Therefore, the movement activity of PCL chains can be enhanced after adding n-hexadecane. On the other hand, PLA chains as rigid chains, when they diffused into PCL phase, they can play a role of nucleating agent to accelerate the crystallization of PCL chains. Therefore, the crystallization degree of PCL component in n-hexadecane/PLA/PCL microcapsules increased compared with the situation in PLA/PCL microparticles. In addition, the adding of n-hexadecane didn't influence the melting or crystallization temperatures of PCL component in n-hexadecane/PLA/PCL systems (Matta, Rao, Suman, & Rambabu, 2014).

The effects of different weight fractions between PLA component and PCL component on the thermal behaviors of a series of n-hexadecane/PLA/PCL electrosprayed microcapsules were also investigated via DSC (Figure 7-4). For the encapsulated n-hexadecane in electrosprayed microcapsules, when the weight fractions between PLA component and PCL component were higher than 1:1 (including 4:1, 3:2 and 1:1), the melting (or crystallization) enthalpy of encapsulated n-hexadecane can reach 95-100 J/g. Correspondingly, the loading content of n-hexadecane in obtained microcapsules reached more than 47.4 %, and the encapsulation efficiency of n-hexadecane can reach more than 95 %.

Table 7-6 Thermal properties of encapsulated n-hexadecane in a series of n-hexadecane/PLA/PCL microcapsules with different weight fractions between PLA component and PCL component.

Sample label		ΔHm or ΔHc (J/g)	Tonset (°C)	Tm or Tc (°C)	Tend (°C)	LC (%)	EE (%)
n-hexadecane50-PLA40-PCL10	heating	99.6	17.3	24.3	34.0	49.9	99.9
	cooling	97.2	15.7	10.5	-7.3		
n-hexadecane50-PLA30-PCL20	heating	94.5	17.2	25.9	33.9	47.4	94.8
	cooling	91.4	15.8	7.4	-6.8		
n-hexadecane50-PLA25-PCL25	heating	98.9	17.8	27.6	34.2	49.6	99.2
	cooling	97.6	15.8	9.6	-7.3		
n-hexadecane50-PLA20-PCL30	heating	72.3	16.0	27.5	35.1	36.3	72.5
	cooling	71.4	15.3	5.1	-6.7		
n-hexadecane50-PLA10-PCL40	heating	71.4	17.6	19.1	25.6	35.8	71.6
	cooling	70.1	15.6	15.3	-0.8		

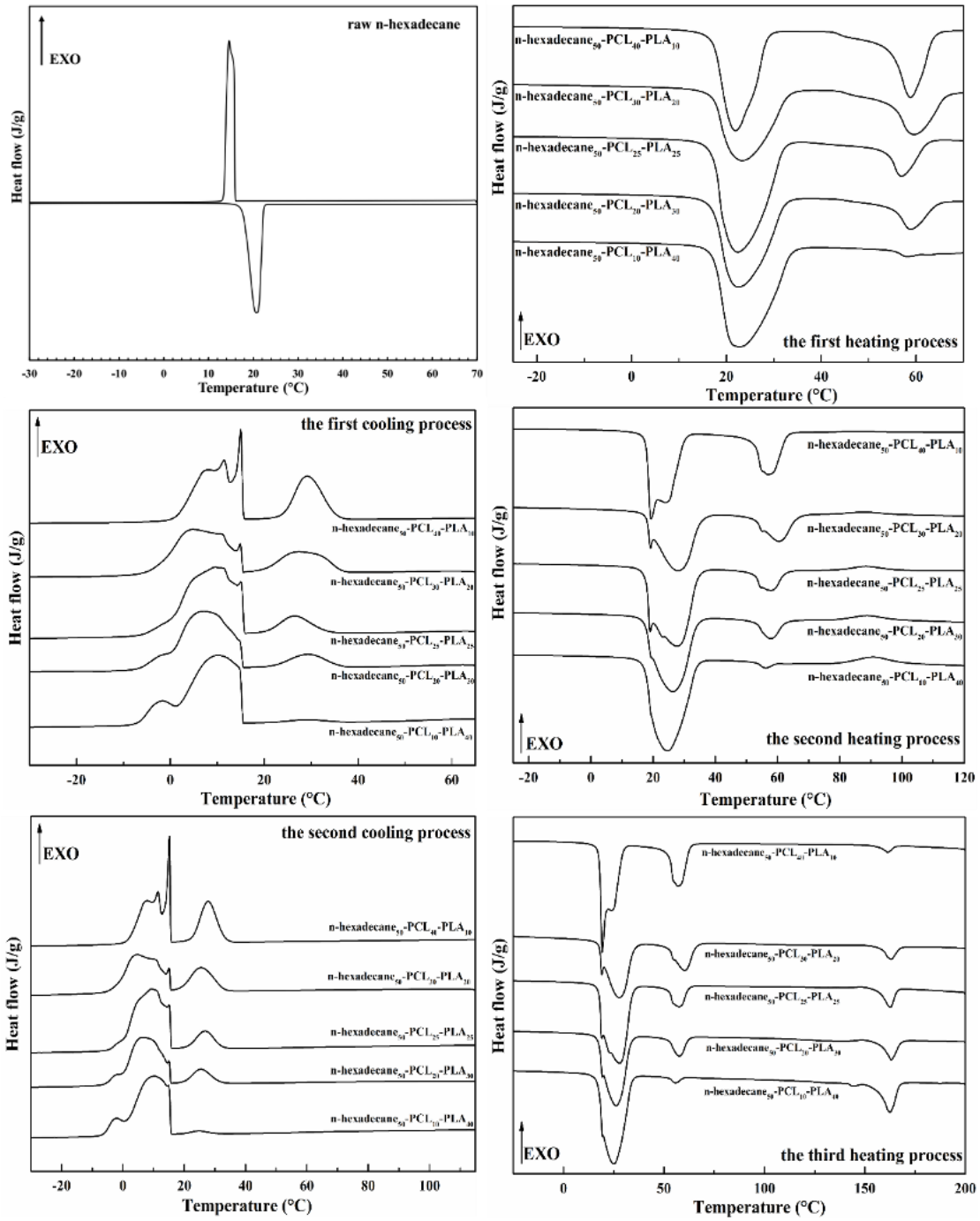

Figure 7-4 The DSC curves of raw n-hexadecane and a series of n-hexadecane/PLA/PCL microcapsules with different weight fractions between PLA component and PCL component.

However, when the weight fractions between PLA component and PCL component were less than 1:1 (including 2:3 and 1:4), the latent heat of encapsulated n-hexadecane decreased to 70 J/g. Correspondingly, the loading content of n-hexadecane in obtained microcapsules decreased to 36 %, and the encapsulation efficiency of n-hexadecane also decreased to 72 %. It indicated that the existence of PLA component in inner liquid can

prevent the diffusion of n-hexadecane caused by the leaving of solvent. And enough PLA component can capture n-hexadecane chains and fix them in PLA phase during coaxial nozzle electrospraying. Therefore, high encapsulation efficiency of n-hexadecane in obtained microcapsules can be achieved when more PLA component was designed in n-hexadecane/PLA/PCL system. With the decrease of PLA component, some n-hexadecane chains can't be fixed by limited PLA component, and they will diffuse into PCL phase with the evaporation of solvent. Finally, these n-hexadecane chains will escape to air with the leaving of solvent. It is why the loading content and encapsulation efficiency of n-hexadecane in obtained microcapsules decreased when the weight fraction between PLA component and PCL component is 2:3 or 1:4. In addition, apart from n-hexadecane50-PLA20-PCL30 sample, the onset temperatures of encapsulated n-hexadecane to melt or freeze didn't change obviously with the variations of the weight fractions between PLA component and PCL component (Vogel & Siesler, 2008).

The thermal parameters of PLA component in n-hexadecane/PLA/PCL microcapsules were also influenced by the variations of the weight fractions between PLA component and PCL component. In Table 7-7, with the decrease of PLA component in n-hexadecane/PLA/PCL systems, the melting enthalpy of PLA component also decreased gradually from 23.5 J/g to 3.8 J/g. Correspondingly, based on the measured loading content of n-hexadecane and theoretical addition of PLA component in n-hexadecane/PLA/PCL systems, the measured crystallization degree of PLA component in obtained microcapsules also decreased from 62.7 % to 31.7 %. This phenomenon is related with the changes of aggregate structure of PLA component under different weight fractions between PLA component and PCL component. During the evaporation process of chloroform, some PLA chains will diffuse into PCL phase and some PCL chains will also diffuse into PLA phase. Therefore, when the weight fraction between PLA component and PCL component is 4:1, most of PLA component as continuous phase existed in n-hexadecane/PLA/PCL microcapsules and a small amount of PLA as dispersed phase existed. And most of PCL component as dispersed phase existed in n-hexadecane/PLA/PCL microcapsules and a small amount of PCL as continuous phase. In general, polymeric chains existed in continuous phase tended to form crystalline structure, and polymeric chains existed in dispersed phase tended to form amorphous structure. Therefore, PLA component with high crystallization degree can be obtained in n-hexadecane/PLA/PCL microcapsules when the weight fraction between PLA component and PCL component is 4:1. With the decrease of the PLA component in n-hexadecane/PLA/PCL microcapsules, the content of PLA continuous phase decrease gradually, correspondingly,

the content of PLA dispersed phase increase gradually. Therefore, the crystallization degree of PLA component in n-hexadecane/PLA/PCL microcapsules decreased with the decreasing of PLA weight fraction. It is also why the crystallization degree of PCL component in n-hexadecane/PLA/PCL microcapsules increased gradually with the increasing of PCL weight fraction as shown in Table 7-8

Table 7-7 Thermal properties of PLA component in a series of n-hexadecane/PLA/PCL microcapsules with different weight fractions between PLA component and PCL component.

Sample label		ΔHm or ΔHc (J/g)	Tonset (°C)	Tm or Tc (°C)	Tend (°C)	ΔHcc or ΔHcc(r)-th (J/g)	Tonset (°C)	Tcc (°C)	Tend (°C)	Xc(th)-PLA (%)	Xc(m)-PLA (%)
n-hexadecane50-PLA40-PCL10	heating	23.5	156.5	162.2	167.0	9.5/23.8	79.5	90.8	101.7	62.8	62.7
	cooling										
n-hexadecane50-PLA30-PCL20	heating	14.5	157.5	162.8	167.7	6.6/20.9	78.5	88.7	98.9	51.6	49.2
	cooling										
n-hexadecane50-PLA25-PCL25	heating	11.9	156.7	162.2	166.0	5.3/21.2	79.3	88.4	98.4	50.9	50.4
	cooling										
n-hexadecane50-PLA20-PCL30	heating	8.4	158.2	162.9	167.4	3.1/12.2	77.8	87.7	97.9	44.9	35.3
	cooling										
n-hexadecane50-PLA10-PCL40	heating	3.8	156.8	161.2	165.0	1.2/9.3	75.6	85.1	95.9	40.6	31.7
	cooling										

Table 7-8 Thermal properties of PCL component in a series of n-hexadecane/PLA/PCL microcapsules with different weight fractions between PLA component and PCL component.

Sample label		ΔHm or ΔHc (J/g)	Tonset (°C)	Tm or Tc (°C)	Tend (°C)	Xc(th)-PCL (%)	Xc(m)-PCL (%)
n-hexadecane50-PLA40-PCL10	heating	2.6	53.3	56.1	59.7	18.6	18.7
	cooling	2.7	36.3	29.1	21.6	-	-
n-hexadecane50-PLA30-PCL20	heating	14.5	52.6	57.6	62.4	52.0	49.3
	cooling	14.5	36.3	29.5	21.9		
n-hexadecane50-PLA25-PCL25	heating	16.6	52.3	57.7	62.4	47.6	47.2
	cooling	16.2	33.4	26.6	20.6		
n-hexadecane50-PLA20-PCL30	heating	26.3	52.4	60.3	66.0	62.8	49.3
	cooling	27.2	36.7	27.5	20.0		
n-hexadecane50-PLA10-PCL40	heating	36.3	52.3	56.8	63.0	65.1	50.7
	cooling	36.2	35.4	29.3	24.2		

In addition, the change of the aggregate structure of PLA component with the variations of PLA weight fraction in n-hexadecane/PLA/PCL microcapsules also influenced the cold crystallization behaviors of PLA component. With the decreasing of PLA weight fraction in n-hexadecane/PLA/PCL microcapsules, the relative cold crystallization enthalpy of PLA component also decreased gradually. It indicated that the cold crystallization behavior of PLA component was also depressed with the increasing of PLA dispersed phase. Meanwhile, the temperatures (including onset temperature, peak temperature and end temperature) for carrying out the cold crystallization of PLA component also decreased with the decreasing of PLA weight fraction. However, the temperatures (including onset temperature, peak temperature and end temperature) for carrying out the melting process of PLA component didn't change obviously under different weight fractions of PLA component in a series of n-hexadecane/PLA/PCL microcapsules.

For PCL component in a series of n-hexadecane/PLA/PCL microcapsules with different weight fractions between PLA component and PCL component, its thermal behavior was also influenced by the variations in the weight fractions between PLA component and PCL component. The melting or crystallization enthalpy of PCL component in n-hexadecane/PLA/PCL microcapsules increased with the increasing of PCL weight fraction. Correspondingly, based on the measured loading content of n-hexadecane and theoretical addition of PCL component, the measured crystallization degree of PCL component in n-hexadecane/PLA/PCL microcapsules can be calculated and increased gradually with the increasing of PCL weight fraction. For the temperatures (including onset temperature and peak temperature) for carrying out the melting process or crystallization process of PCL component didn't change obviously with the variations of weight fraction between PLA component and PCL component.

7.3 Thermal stability of n-hexadecane/PLA/PCL mPCMs

The thermal stability of raw n-hexadecane, PLA50/PCL50 microparticles and a series of n-hexadecane/PLA/PCL microcapsules with different n-hexadecane additions were investigated via TGA analyze (Figure 7-5), and related thermogravimetric data were also listed in Table 7-9.

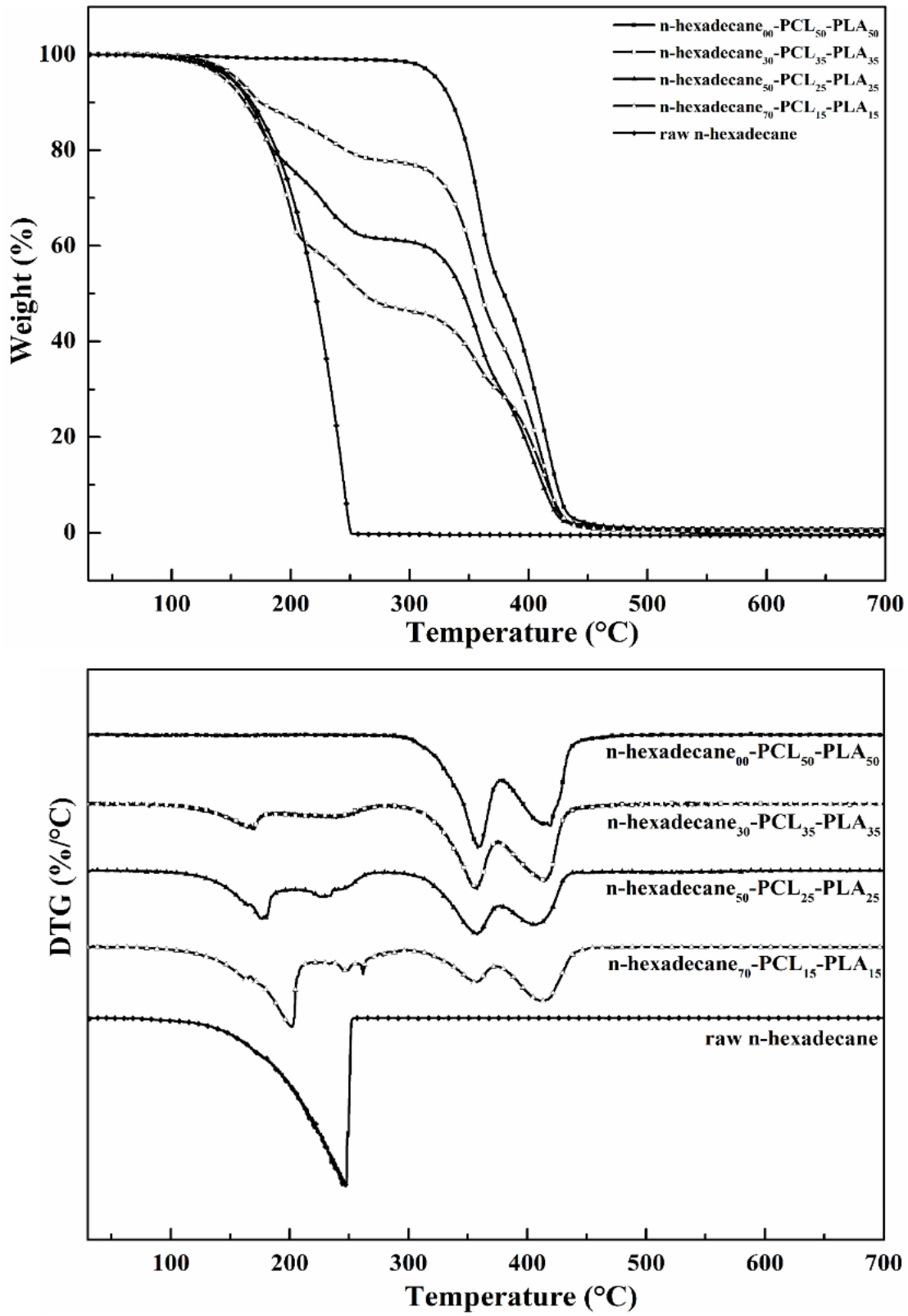

Figure 7-5 The TGA and DTG curves of raw n-hexadecane, PLA50/PCL50 micropaarticles and a series of n-hexadecane/PLA/PCL microcapsules with different n-hexadecane additions.

Table 7-9 The thermogravimetric data of raw n-hexadecane, PLA50/PCL50 microparticles and a series of n-hexadecane/PLA/PCL microcapsules with different n-hexadecane additions.

Sample label	Initial degradation temperature-$T_{5\%}$ (°C)	The first step			The second step			The third step		
		Weight loss (100-300 °C) (%)	Maximum degradation temperature (°C)	Maximum degradation rate (%/°C)	Weight loss (300-378 °C) (%)	Maximum degradation temperature (°C)	Maximum degradation rate (%/°C)	Weight loss (378-500 °C) (%)	Maximum degradation temperature (°C)	Maximum degradation rate (%/°C)
Raw n-hexadecane	149.3	99.3	246.2	2.1	-	-	-	-	-	-
n-hexadecane00-PLA50-PCL50	323.0	1.4	-	-	48.0	358.7	1.4	50.1	418.3	1.1
n-hexadecane30-PLA35-PCL35	155.0	22.6	170.3	0.3	38.2	357.7	1.0	39.0	415.2	0.9
n-hexadecane50-PLA25-PCL25	150.3	38.9	176.8	0.6	31.4	357.2	0.8	29.2	407.2	0.7
n-hexadecane70-PLA15-PCL15	144.3	53.6	201.7	1.0	17.1	355.8	0.4	28.7	411.8	0.7

Table 7-10. the thermogravimetric data of a series of n-hexadecane/PLA/PCL microcapsules with different weight fractions between PLA component and PCL component

Sample label	Initial degradation temperature-$T_{5\%}$ (°C)	The first step			The second step			The third step		
		Weight loss (100-300 °C) (%)	Maximum degradation temperature (°C)	Maximum degradation rate (%/°C)	Weight loss (300-378 °C) (%)	Maximum degradation temperature (°C)	Maximum degradation rate (%/°C)	Weight loss (378-500 °C) (%)	Maximum degradation temperature (°C)	Maximum degradation rate (%/°C)
n-hexadecane50-PLA40-PCL10	137.8	46.3	197.2	0.6	44.8	366.8	1.3	8.8	395.8	0.2
n-hexadecane50-PLA30-PCL20	152.5	35.4	188.8	0.3	38.8	355.5	1.1	25.5	410.3	0.6
n-hexadecane50-PLA25-PCL25	150.5	39.2	176.8	0.6	32.2	357.7	0.8	28.6	404.0	0.7
n-hexadecane50-PLA20-PCL30	156.2	30.2	170.8	0.4	23.1	350.8	0.6	46.3	417.3	1.1
n-hexadecane50-PLA10-PCL40	161.5	33.3	182.3	0.3	12.3	339.8	0.2	54.4	418.3	1.4

For raw n-hexadecane, its thermal degradation behavior displays single step degradation under N2 atmossphere and its initial degradation temperature starts at 149.3 °C. Meanwhile, the maximum decomposition step of the n-alkane backbone takes place at 246.2 °C with a maximum degradation rate of 2.1 %·°C-1. At over 280 °C, no residue was observed. For PLA50/PCL50 microparticle, its thermal degradation behavior displays two steps degradation, and the first step occurred from 300 °C to 378 °C is attributed to the thermal degradation of most PLA component and a small amount of PCL component in PLA50/PCL50 microparticles, and the second step occurred from 378 °C to 500 °C is attributed to the thermal degradation of most PCL component and a small amount of PLA component. During the electrospraying process of PLA50/PCL50 mixed droplets, some PLA chains diffused into PCL phase and some PCL chains also diffused into PLA phase with the evaporation of solvent. Therefore, after the solidification of electrosprayed droplets, the phase structure of PLA50/PCL50 microparticles can be divided into three parts including neat PLA phase, PLA and PCL mixed phase and neat PCL phase. The initial degradation temperature of PLA50/PCL50 microparticle starts at 323.0 °C, which is related with the initial degradation of the PLA component in n-hexadecane/PLA/PCL microcapsules. Compared with neat PLA microparticles obtained from single nozzle electrospraying, the initial degradation temperature of PLA component increased from 309.0 °C to 323.0 °C. With the incresing of the surrouding temperature in TGA analyze, PCL phase melts into liqud phase at about 56 °C and PLA phase melts into liquid phase at about 165 °C. Therefore, when the surrounding temperature in TGA analyze reaches above 300 °C, both PLA phase and PCL phase become liquid state. Because the density of PCL (1.15 g/cm3) is lower than that of PLA (1.21~1.43 g/cm3), most of the PCL phase is located in the upper layer of the mixed liquid and most of the PLA phase is located in the lower layer of the mixed liquid. In other words, PLA layer is covered by PCL layer in the mixed liquid. Due to the physical barrier effect of PCL layer in PLA/PCL mixed liquid, the heat exchange efficiency between PLA layer and heat flow will be depressed. Therefore, the thermal degradation process of PLA component in PLA50/PCL50 microparticles will be delayed, and the initial degradation temperature of PLA component also increased. In addition, the weight loss in the first step degradation process reaches 48 %, and the maximum degradation temperature in the first step degradation process is 358.7 °C with a maximun degradation rate of 1.4 %·°C-1. And the weight loss in the second step degradation process reaches 50.1 %, the maximum degradation temperature in the second step is 418.3 °C with a maximum degradation rate of 1.1 %·°C-1. Compared with neat PLA microparticles obtained from single nozzle electrospraying, the maximum degradation temperature in first step

degradation process of PLA50/PCL50 microparticles decreased from 378.3 °C to 358.7 °C. Compared with neat PCL microparticles obtained from single nozzle electrospraying or coaxial nozzle electrospraying, the maximum degradation temperature in second step degradation process of PLA50/PCL50 microparticles increased from 412.0 °C to 418.3 °C. On the one hand, the thermal degradation of some PCL chains in first step process will result in the decrease of the maximum degradation temperature. On the other hand, the thermal degradation products from the thermal degradation of PLA component also delayed the thermal degradation of PCL component in the second step degradation.

When n-hexadecane is encapsulated into PLA/PCL matrix, the thermal degradation process of n-hexadecane/PLA/PCL microcapsules can be divided into three steps. The first step from 100 °C to 300 °C is mainly related with the thermal degradation of encapsualted n-hexadecane, the second step from 300 °C to 378 °C is attributed to the thermal degradation of most PLA component and a small amount of PCL component, and the third step from 378 °C to 500 °C is attributed to the thermal degradation of most PCL component and a small amount of PLA component. When the theoretical addition of n-hexadecane in n-hexadecane/PLA/PCL system reaches 30 wt%, the initial degradation temperature of obtained microcapsules is 155.0 °C. Compared with raw n-hexadecane, the initial degradation temperature of encapsulated n-hexadecane increased from 149.3 °C to 155.0 °C. The increase in the initial degradation temperature of the first stage indicated the protective effect of the shells (PLA matrix and PCL matrix), which enhanced the thermal stability of the core materials. With the increasing of n-hexadecane addition to 50 wt% in n-hexadecane/PLA/PCL system, the initial thermal degradation temperature of encapsulated n-hexadecane decreased to 150.3 °C. It was related with the location of n-hexadecane in obtained microcapsules. When n-hexadecane addition is 30 wt% in n-hexadecane/PLA/PCL system, PLA inner matrix and PCL outer matrix can prevent the diffusion of n-hexadecane with the evaporation of solvent and fix them on the inner area of obtained microcapsule. Therefore, PLA matrix and PCL matrix can play the roles of physical barrier and proctive layer to delay the thermal degradation of n-hexadecane. When the addition of n-hexadecane increased to 50 wt%, the ability of PLA matrix as well as PCL matrix to prevent the diffusion of n-hexadecane is weakened. Some n-hexadecane will move to PCL layer or even near the surface of the microcapsule with the evaporation of solvent during the solidification process of electrosprayed droplets. Therefore, the initail degradation temperature of n-hexadecane decreased gradually due to the weaken of the physical barrier as well as protective ability of polymeric matrix. When n-hexadecane addition further increased to 70 wt%, it was difficult

for limited PLA matrix and PCL matrix to capture completely excessive n-hexadecane and fix them in the inner area of obtained microcapsules. More and more n-hexadecane diffused to to the near surface area of fianl microcapsules with the increasing of n-hexadecane addition. Meanwhile, compared with bulk raw n-hexadecane, encapsulated n-hexadecane were dispersed into PCL liquid and PLA solid when TGA analyze temperature increase to over 140 °C. Due to the increase in the specific surface area of encapsulated n-hexadecane, the heat transfer efficiency between n-hexadecane and heat flow was improved. Therefore, the initial degradation temperature of encapsulated n-hexadecane is lower than that of raw n-hexadecane under 70 wt% n-hexadecane addition.

In addition, with the increasing of n-hexadecane addition in obtained microcapsules, the weight loss in the first degradation process increased gradually. However, the values of weight loss in the first step degradation process were all lower than the actual loading content of n-hexadecane in obtained microcapsules under different n-hexadecane additions. There are two reasons to explain this phenomenon. On the one hand, most n-hexadecane was surrounded completely PLA matrix and PCL matrix. The physical barrier and protection effects of shell matrix will delay the thermal degradation of some n-hexadecane to the second step process. On the other hand, the intermolecular interaction among PLA chains, PCL chains and n-hexadecane chains also prevent the evaporation process of n-hexadecane with the increasing of surrounding temperature. Compared with raw n-hexadecane, the maximum degradation temperature of n-hexadecane30/PLA35/PCL35 microcapsules in first step process decreased from 246.2 °C to 170.3 °C. It is mainly related with the changes of the specific surface area of encapsulated n-hexadecane. Compared with bulk raw n-hexadecane, the specific surface area of encapsulated n-hexadecane increased obviously. Therefore, the heat exchange efficiency between dispersed n-hexadecane and heat flow enhanced obviously, which will result in a decrease in the maximum thermal degradation temperature. With the increasing of n-hexadecane addition in n-hexadecane/PLA/PCL system, the specific surface area of n-hexadecane in obtained microcapsules decreased gradually. Therefore, the maximum thermal degradation temperature of encapsulated n-hexadecane increased gradually. In addition, with the increasing of the n-hexadecane addition in obtained microcapsules, the maximum degradation rate also increased gradually.

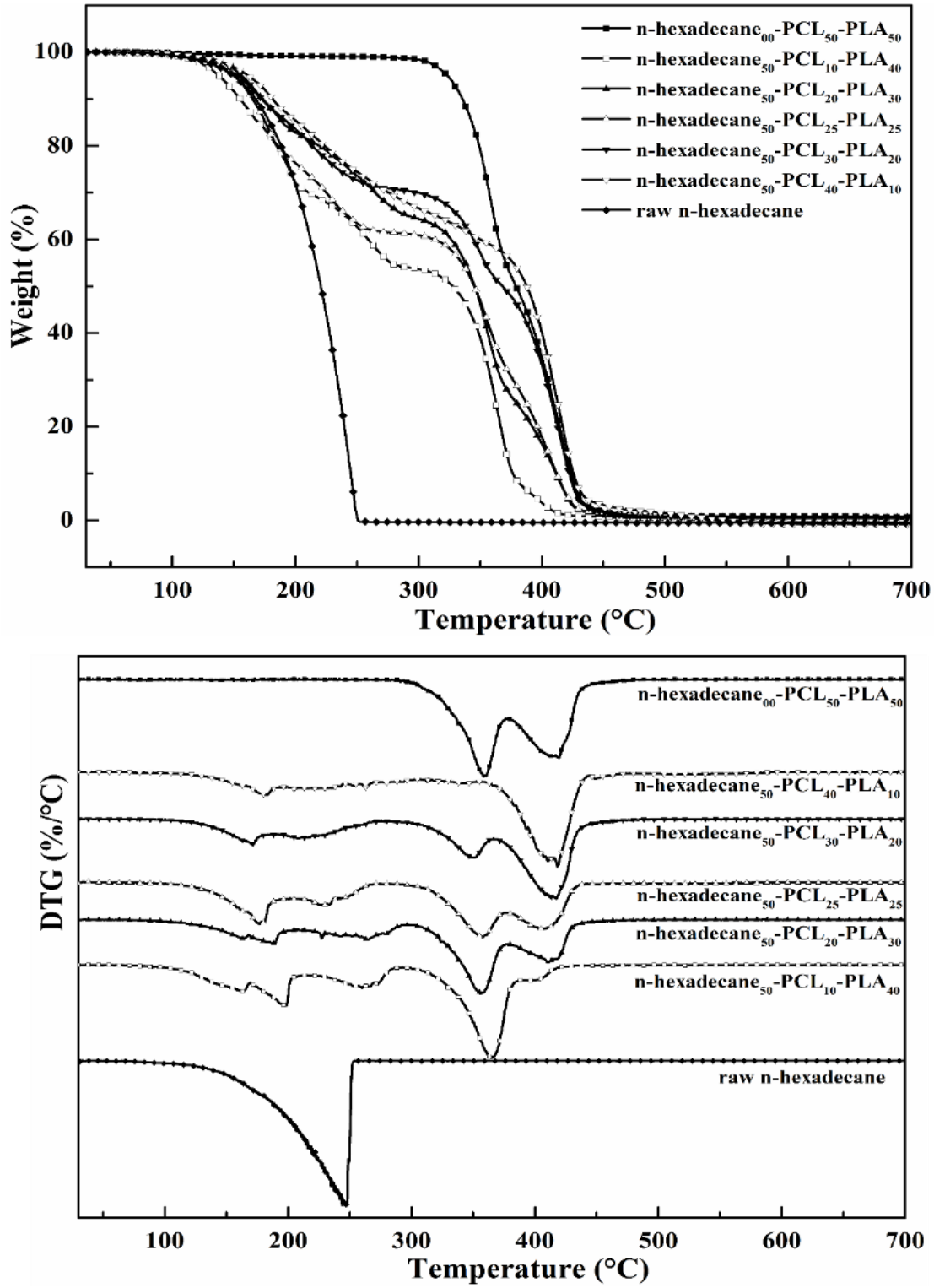

Figure 7-6 The TGA and DTG curves of raw n-hexadecane, a series of n-hexadecane/PLA/PCL microcapsules with different weight fractions between PLA component and PCL component.

For the weigh loss in the second step degradation process and the third step degradation process, the value decreased gradually with the increasing of n-hexadecane addition in n-hexadecane/PLA/PCL system. Meanwhile,

the maximum degradation temperature and the maximum degradation rate in the second step process also decreased from 358.7 °C to 355.8 °C, and from 1.4 %·°C^{-1} to 0.4 %·°C^{-1}, respectively. In addition, the maximum degradation temperature and the maximum degradation rate in the third step process also decreased from 418.3 °C to 411.8 °C, and from 1.1 %·°C^{-1} to 0.7 %·°C^{-1}, respectively.

The effects of different weight fractions between PLA component and PCL component on the thermal stability of final n-hexadecane/PLA/PCL microcapsules were also investigated via TG analyze (Figure 7-6), and the related thermogravimetric data were also listed in Table 7-10. Compared with raw n-hexadecane, when the weight fraction between PLA component and PCL component is 4:1, the initial degradation temperature of encapsulated n-hexadecane in first step process decreased from 149.3 °C to 137.8 °C. During the flight process of n-hexadecane/PLA/PCL electrosprayed droplets, n-hexadecane tended to migrate from PLA phase (inner shell) to PCL phase (outer shell) with the evaporation of solvent. Meanwhile, PCL layer as outer shell, can play the role of protection and physical barrier to prevent the loss of n-hexadecane. For the thermal stability of encapsulated n-hexadecane, the existence of PCL layer can also delay the thermal degradation process of encapsulated n-hexadecane. However, for low weight fraction of PCL component in n-hexadecane/PLA/PCL system, it is difficult for limited PCL matrix to prevent the heat exchange between n-hexadecane and heat flow. Meanwhile, because encapsulated n-hexadecane is dispersed in PLA matrix and PCL matrix, the heat exchange efficiency between dispersed n-hexadecane and heat flow enhanced obviously compared with bulk raw n-hexadecane. Therefore, the initial degradation temperature of encapsulated n-hexadecane with 10 wt% PCL content in n-hexadecane/PLA/PCL system is lower than raw n-hexadecane. With the increasing of PCL content in n-hexadecane/PLA/PCL system, the initial degradation temperature of encapsulated n-hexadecane increased gradually. It indicated that the physical barrier and protection effects from shell matrix will be improved with the increasing of PCL content.

The values of weight loss in first step degradation process decreased with the decreasing of PLA content in obtained microcapsules. It is related with the loss of n-hexadecane during the formation process of n-hexadecane/PLA/PCL microcapsules. PLA matrix as inner shell matrix, can prevent the diffusion of n-hexadecane during the evaporation of solvent, and fix n-hexadecane in the inner area of obtained microcapsules. With the decreasing of PLA content in electrosprayed droplets, more n-hexadecane escaped into air with the leaving of solvent. Therefore, the weight loss in the first step degradation process also decreased with the decreasing of PLA

content. Meanwhile, with the decreasing of PLA content in electrosprayed droplets, more and more n-hexadecane migrated to the PCL phase or to the near surface area of the microcapsules. Therefore, the maximum degradation temperature in the first step process also decreased with the decreasing of PLA content.

In addition, with the decreasing of PLA content in final microcapsules, the weight loss, the maximum degradation temperature and maximum degradation rate in second step degradation process all decreased gradually. On the contrary, with the increasing of PCL content in final microcapsules, the weight loss, the maximum degradation temperature and maximum degradation rate in third step degradation process all increased gradually.

7.4 Conclusions

n-hexadecane/PLA/PCL electrosprayed microcapsules with double-layered shells based on PLA as inner shell and PCL as outer shell were fabricated successfully from coaxial nozzle electrospraying. The effects of different n-hexadecane additions and different weight fractions between PLA component and PCL component on the structure, morphology and properties of obtained microcapsules were investigated in details. Firstly, double-component microparticles named PLA50/PCL50 with spherical shape, smooth surface and mono-dispersed size distribution were prepared from coaxial nozzle electrospraying. And the mean diameter of PLA50/PCL50 microparticles is 6.6 μm. With the increasing of n-hexadecane addition, the mean diameter of n-hexadecane/PLA/PCL microcapsules increased from 6.6 μm to 12.9 μm, and the size distribution always kept mono-dispersed distribution. Meanwhile, although the shape of final microcapsules kept spherical under different n-hexadecane additions, the surface morphology of final microcapsules changed from non-porous to porous with the increasing of n-hexadecane addition. When the n-hexadecane addition increased to 70 wt%, grooved and rugged structure can be found on the surface of obtained microcapsules. Furthermore, with the variation of weight fraction between PLA component and PCL component from 4/1 to 1/4, the mean diameter of n-hexadecane/PLA/PCL microcapsules didn't change obviously. And the standard deviation of mean diameter of obtained microparticles increased gradually with the decreasing of PLA content. It indicated that the existence of PLA component can stabilize the formation of Taylor cone as well as the breakup process of mixed droplets. Finally, on the one hand, with the decreasing of the weight fraction between PLA component and PCL component from 4/1 to 2/3, the porous structure and morphology of n-hexadecane/PLA/PCL microcapsules did'n change

obviously. On the other hand, the morphology became irregular, rough and rugged and the number of porous structure also decreased when the weight fraction between PLA component and PCL component reached 1/4.

The double-layered shell structure also offers high loading content of n-hexadecane and high encapsulation efficiency of n-hexadecane for final electrosprayed microcapsules. When the addition of n-hexadecane is 50 wt% and the weight fraction between PLA component and PCL component is 1/1, the actual loading content and encapsulation efficiency of n-hexadecane can reach 49.6 % and 99.2 %, respectively. And the corresponding latent heat obtained from the phase transition of n-hexadecane reached 98.9 J/g. With the further increasing of n-hexadecane addition to 70 wt%, although the actual loading content of n-hexadecane and the corresponding latent heat increased to 57.0 % and 113.6 J/g, respectively, the encapsulation efficiency of n-hexadecane decreased to 81.4 %. It indicated that it is very difficult for limited PLA matrix and PCL matrix to prevent the diffusion (even loss) of excessive n-hexadecane caused by the evaporation of solvent. In addition, with the adding of n-hexadecane, not only the cold crystallization process of PLA matrix can be accelerated, but also the crystallization degree of PLA matrix increased.

With the decreasing of the weight fraction between PLA component and PCL component from 4/1 to 1/4, the actual loading content of n-hexadecane, the encapsulation efficiency of n-hexadecane and corresponding latent heat of n-hexadecane all decreased gradually. It indicated that PLA component as inner shell matrix not only can prevent the migration of n-hexadecane during the evaporation process of solvent, but also fix n-hexadecane in the inner area of obtained microcapsules. With the decreasing of PLA content in electrosprayed droplets, more and more n-hexadecane diffused into PCL phase or even the surface of final microcapsules. In addition, with the decreasing of the weight fraction between PLA component and PCL component, the crystallization degrees of PLA matrix and PCL matrix decreased and increased, respectively.

Finally, double-layered shell structure can also better thermal stability for encapsulated n-hexadecane. Under low n-hexadecane addition (30 wt% or 50 wt%) in electrospraying solutions, the initial degradation temperature of emcapsualted n-hexadecane in obtained microcapsules is higher than that of raw n-hexadecane. Meanwhile, the existence of PCL matrix can play the role of physical barrier and protection to improve the thermal stability of encapsulated n-hexadecane. With the increasing of PCL content in final microcapsules, the initial degradation temperature of encapsulated n-hexadecane increased gradually. Combining with the DSC results and TGA results, it can conclude that some n-hexadecane chains and PLA chains will move into PCL phase with the evaporation

of solvent during electrospraying process. And some PCL chains also diffused into PLA phase. Therefore, the shell structures in n-hexadecane/PLA/PCL microcapsules can be divided into PLA layer, PLA and PCL mixed layer and PCL layer. Strong intermolecular interactions between PLA phase and PCL phase can be confirmed. N-hexadecane/PLA/PCL microcapsules with double-layered shells not only can offer much advantages and potential in fabricating mPCMs with desired structures and properties (including core-shell structure, high encapsulation efficiency, high latent heat and thermal stability), but also offer a new strategy to carry out the functional coating of textiles with good interfacial adhesion, durability and lowest damage to the original structure and properties of the textiles.

References

Bock, N., Dargaville, T. R., & Woodruff, M. A. (2012). Electrospraying of polymers with therapeutic molecules: State of the art. *Progress in Polymer Science*, *37*(11), 1510–1551. https://doi.org/10.1016/j.progpolymsci.2012.03.002

Gañán-Calvo, A. M. (1994). the Size and Charge of Droplets in the Electrospraying of Polar liquids in cone-jet mode, and the minimum droplet size. *Journal of Aerosol Science*, *25*(X), 309–310.

Matta, A. K., Rao, R. U., Suman, K. N. S., & Rambabu, V. (2014). Preparation and Characterization of Biodegradable PLA / PCL Polymeric Blends. *Procedia Materials Science*, *6*(Icmpc), 1266–1270. https://doi.org/10.1016/j.mspro.2014.07.201

Vogel, C., & Siesler, H. W. (2008). *Thermal Degradation of Poly (e -caprolactone), Poly (L-lactic acid) and their Blends with Poly (3-hydroxy-butyrate) Studied by TGA / FT-IR Spectroscopy*. 183–194. https://doi.org/10.1002/masy.200850520

Wu, Y. Q., & Clark, R. L. (2007). Controllable porous polymer particles generated by electrospraying. *Journal of Colloid and Interface Science*, *310*(2), 529–535. https://doi.org/10.1016/j.jcis.2007.02.023

Zhang, L., Huang, J., Si, T., & Xu, R. X. (2012). Coaxial electrospray of microparticles and nanoparticles for biomedical applications. *Expert Review of Medical Devices*, *9*(6), 595–612. https://doi.org/10.1586/erd.12.58

Zhang, S., Campagne, C., & Salaün, F. (2019). Influence of solvent selection in the electrospraying process of polycaprolactone. *Applied Sciences (Switzerland)*, *9*(3). https://doi.org/10.3390/app9030402

General Conclusions and Prospects

Electrospraying technology has been proved to be a green, feasible and high-efficiency method to fabricate phase change microcapsules (mPCMs). Not only mono-dispersed size distribution, high loading content of PCMs and high encapsulation efficiency of PCMs can be achieved during electrosporaying process, but also the design of the size, core-shell structure, surface morphology and properties of targeted microcapsules. Meanwhile, electrospraying technology is also expected to be a coating method to carry out the functionalization of textiles by electrosprayed mPCMs for obtaining thermal-regulated textiles. Furthermore, electrosprayed mPCMs with double-layered shells can present more improved structures and properties compared with electrosprayed mPCMs with sinlge-layered shell. And electrosprayed mPCMs with double-layered shells also make the functional coating of textiles easier and more effective. In addition, because a series of mPCMs were fabricated successfully based on PCL and PLA as shell materials, n-alkanes as core materials and a series of green solvents as carriers, a green, non-toxic and high-efficiency mPCMs production process can be achieved during electrospraying.

The purpose of this thesis is to design the electrosprayed mPCMs with double-layered shells and further applied them for carrying out the functional coating of textiles to obtain thermal-regulated textiles. The detailed protocol is divided into fifth steps: (1) the selection of suitable solvent system for carrying out the electrospraying process of PCL microparticles and PLA microparticles and investigating the effects of solution properties and operating parameters on the the formation of Taylor cone and the structure and morphology of final electrosprayed microparticles (2) the preparation of n-alkane/PCL microparticles with single-layered shell and investigating the microencapsulation of n-alkanes during electrospraying process and clarifying the effects of different solvent systems, different n-alkanes and different n-alkane additions on the structures, morphologies and properties of obtained microcapsules (3) the preparation of n-hexadecane/PLA microparticles with single-layered shell and investigating the effects of different shell materials, the concentration of shell solution and the addition of n-hexadecanee on the structures, morphologies and properties of obtained microcapsules (4) the design of n-hexadecane/PCL microcapsules with core-shell structure from coaxial nozzle electrospraying and investigating the effects of different nozzle geometries on the structures, morphologies and properties of obtained microcapsules (5) the fabrication of n-hexadecane/PLA/PCL with double-layered shell from coaxial nozzle electrospraying and

investigating the effects of the double-layered shell, the addition of n-hexadecane and the different weight fractions between PLA component and PCL component on the structures, morphologies and properties of obtained microcapsules.

In Chapter III, among five green solvents including ethyl acetate, acetone, chloroform, acetic acid and anisole, chloroform and ethyl acetate were proved to be suitable solvents for the formation of stable Taylor cone and fabricating PCL microparticles with mono-dispersed size distribution and desired surface morphology. And the effects of solution properties and operating parameters on the formation of electrosprayed PCL microparticles had been clarified. The applied voltage range for cone-jet mainly depends on the electrical conductivity of electrospraying solution. Solution with higher electrical conductivity needs higher applied voltage to achieve cone-jet during electrospraying. Meanwhile, ideal cone-jet mode is easier to obtain under high viscosity and low surface tension. With the increasing of viscosity, the stability of ideal Taylor cone also improved gradually. Furthermore, the shape of Taylor cone also influences the size and distribution of PCL electrosprayed microparticles. In generally, under short distance from nozzle to tip of Taylor cone and thin charged jet, small and homogeneous microparticles can be prepared.

For electrospraying liquids with mild electrical conductivity, mono-dispersed microparticles can be fabricated. Their sizes closely correlate to their surface tensions and viscosities. For chloroform and ethyl acetate, small mean diameter about several microns can be obtained from 1 wt% PCL concentration, and particle size increases with the increasing of PCL concentration. For anisole, large mean diameter about hundreds microns can be obtained from 1 wt% PCL concentration, and particle size decreases with the increasing of PCL concentration. For electrospraying liquid with high electrical conductivity, microparticles with poly-dispersed distribution can be obtained at low PCL concentration. With the increasing of PCL concentration, size distribution of microparticles narrows gradually. At 10 wt% PCL, mono-dispersed microparticles with about 15 μm mean diameter can be prepared from glacial acetic acid or acetone. Furthermore, for all electrospraying liquids, mono-dispersed microparticles are easier to fabricate under long working distance. During the solidification of electrosprayed droplets, insufficient condensation of polymer chains or remaining solvent in collected particles both introduce large mean diameter. Only the sufficient condensation of polymer chains and the complete evaporation of solvent carry out simultaneously, tiny electrosprayed particles can be prepared. In addition, the mean diameter of all PCL microparticles decreases with the increasing of applied voltage or dripping time.

Meanwhile, their size distributions also narrow gradually. For the morphology of electrosprayed PCL microparticles, the slowness of solvent evaporation or complete phase separation between solvent and PCL is good for obtaining nonporous and smooth morphology. When the evaporation rate of solvent is faster than the rate of phase separation, particles with porous and wrinkle morphology can be obtained.

In Chapter IV, the microencapsulated phase change materials in the PCL matrix were successfully manufactured by an electrospray process, using two types of solvents, ethyl acetate and chloroform, and three loading contents (30, 50, and 70% by weight). The process not only produces particles with a mono-dispersed particle size distribution, an average micrometric diameter, a non-porous morphology, but also a high encapsulation efficiency. The microparticles have a latent heat correlated to the theoretical load and good thermal stability. The break up process in the early stages of the electroplating method mainly determines the particle size of the mPCMs. Thus, depending on the choice of n-alkane, n-hexadecane, or n-eicosane, two phenomena occur. On the one hand, in the case of n-hexadecane, which is in a liquid state at room temperature, the break-up of the charged droplets takes place throughout the flight process, from the nozzle to the collector, which allows the solvent to evaporate entirely and thus obtain a low mean diameter. On the other hand, the droplets loaded with n-eicosane break-up only in the earliest stages of the flight process, as the evaporation of the solvent leads to the n-alkane crystallization, which stops the process, resulting in higher mean diameters and broad size distribution. The surface morphology of the electro-sprayed mPCM is either smooth, and dense or rough and wrinkled when n-hexadecane, and n-eicosane are used, respectively. Besides, n-eicosane tends to be on the surface of particles as its loading content increases. Also, the choice of solvent affects the particle size and morphology of the particles, which may be related to changes in the physico-chemical properties of solutions, such as surface tension, vapor pressure, and viscosity. The loading content depends mainly on the diffusion of n-alkane chains during the process, which is also influenced by solvent evaporation or phase separation, the interactions between PCL macromolecular chains, and n-alkane chains, and the evolution of the physical state of PCM. Thus, the encapsulation efficiency and charge content of an n-alkane liquid at room temperature are respectively higher and lower than those of a solid n-alkane in ethyl acetate, but in chloroform, it is the opposite.

In chapter V, a series of n-hexadecane/PLA mPCMs can be developped successfully via single nozzle electrospraying. Compared with PCL shell matrix, not only enough physical strength and higher thermal stability can be obtained from PLA shell material, but also higher actual loading content as well as encapsulation efficiency

of n-hexadecane in mPCMs. Meanwhile, the effects of PLA concentration and n-hexadecane addition on the structures (mean diameter, size distribution and morphology) and thermal properties (phase transition enthalpy, phase change temperature, the crystallization process of PLA matrix) as well as the encapsulation efficiency and loading content of n-hexadecane in PLA matrix were also investigated. After introducing n-hexadecane, spherical electrosprayed mPCMs with mono-dispersed size distribution can be obtained. With the increasing of n-hexadecane addition, the mean diameter of n-hexadecane/PLA microparticles increased gradually from about 10 μm to 22-27 μm depending on PLA concentration, and the corresponding size distribution broadened gradually. Furthermore, the actual loading content of n-hexadecane in mPCMs also increased gradually with the increasing of n-hexadecane addition, however, corresponding encapsulation efficiency to n-hexadecane decreased under 70 wt% n-hexadecane addition. Higher PLA concentration allowed to improving the encapsulation efficiency as well as the actual loading content of n-hexadecane in mPCMs. When 70 wt% n-hexadecane was added into 5 wt% PLA solution, the encapsulation efficiency and actual loading content of n-hexadecane reached 85.3 and 59.7 %, respectively. Correspondingly, the phase transition enthalpy of encapsulated n-hexadecane can reach 119 J/g. In addition, when n-hexadecane was encapsulated into PLA matrix, its melting process and crystalline process broadened compared with raw n-hexadecane. And during the thermal degradation process, the initial degradation temperature and maximum degradation temperature of encapsulated n-hexadecane also decreased compared with raw n-hexadecane. The mobility of PLA chains was also improved after introducing n-hexadecane. Therefore, the cold crystallization of PLA matrix can be accelerated and the crystallization degree of PLA matrix also increased after entrapping n-hexadecane.

In Chapter VI, n-hexadecane was successfully encapsulated in a PCL matrix with a coaxial nozzle electrospraying system. The use of a 10 w/v % PCL solution allows forming a Taylor cone to stabilize the breakup process of double-component liquid, and therefore, monodispersed microcapsules with a mean diameter of about 20 μm are obtained for an initial loading content of n-hexadecane of about 50% or 70%. The concentration of the PCL solution and/or the initial content of n-hexadecane also affect the surface morphology of the obtained microparticles. Thus, the increase from 5 to 10 w/v % of the PCL solution, as well as the n-hexadecane when a 5 wt % of PCL was used, changed a porous surface state to a non-porous one. The use of a coaxial system also allows increasing a higher encapsulation efficiency compared to a single nozzle process. Furthermore, higher loading content of n-hexadecane was also achieved. Thus, when 70% n-hexadecane was introduced in 10 w/v %

PCL solution, the encapsulation efficiency of n-hexadecane reached 96.3%, and correspondingly, the active loading content of n-hexadecane reached 67.4%. This content allows storing more than 130 J.g-1 of latent heat via its liquid-solid phase transition. The presence of PCL surrounding the n-hexadecane phase enhances its thermal stability. Furthermore, the morphology of the microparticles can be adjusted depending on the initial PCL and n-hexadecane contents in the formulation, as expected from the TGA and DSC tests. Thus, a lower n-hexadecane to PCL ratio leads to a matrix morphology, whereas the higher amount in n-hexadecane allows obtaining either a salami-like or a core/shell structure. The use of a coaxial system allows for improving the encapsulation efficiency and loading content of n-hexadecane compared to a single nozzle electrospraying. Stable cone-jet mode and stable breakup process of charged droplets are more comfortable to control for a single nozzle than for a coaxial electrospraying, where the outer physico-chemical properties play a crucial role. The formation of microparticles from an electrospraying process is an excellent alternative to other physical or chemical microencapsulation methods and is a high-efficiency choice for energy storage and thermal regulation system.

In chapter VII, N-hexadecane/PLA/PCL electrosprayed microcapsules with double-layered shells based on PLA as inner shell and PCL as outer shell were fabricated successfully from coaxial nozzle electrospraying. The effects of different n-hexadecane additions and different weight fractions between PLA component and PCL component on the structure, morphology and properties of obtained microcapsules were investigated in details. Firstly, double-component microparticles named PLA50/PCL50 with spherical shape, smooth surface and mono-dispersed size distribution were prepared from coaxial nozzle electrospraying. And the mean diameter of PLA50/PCL50 microparticles is 6.6 μm. With the increasing of n-hexadecane addition, the mean diameter of n-hexadecane/PLA/PCL microcapsules increased from 6.6 μm to 12.9 μm, and the size distribution always kept mono-dispersed distribution. Meanwhile, although the shape of final microcapsules kept spherical under different n-hexadecane additions, the surface morphology of final microcapsules changed from non-porous to porous with the increasing of n-hexadecane addition. When the n-hexadencane addition increased to 70 wt%, grooved and rugged structure can be found on the surface of obtained microcapsules. Furthermore, with the variation of weight fraction between PLA component and PCL component from 4/1 to 1/4, the mean diameter of n-hexadecane/PLA/PCL microcapsules didn't change obviously. And the standard deviation of mean diameter of obtained microparticles increased gradually with the decreasing of PLA content. It indicated that the existence of PLA component can stabilize the formation of Taylor cone as well as the breakup process of mixed droplets.

Finally, on the one hand, with the decreasing of the weight fraction between PLA component and PCL component from 4/1 to 2/3, the porous structure and morphology of n-hexadecane/PLA/PCL microcapsules did'n change obviously. On the other hand, the morphology became irregular, rough and rugged and the number of porous structure also decreased when the weight fraction between PLA component and PCL component reached 1/4.

The double-layered shell structure also offers high loading content of n-hexadecane and high encapsulation efficiency of n-hexadecane for final electrosprayed microcapsules. When the addition of n-hexadecane is 50 wt% and the weight fraction between PLA component and PCL component is 1/1, the actual loading content and encapsulation efficiency of n-hexadecane can reach 49.6 % and 99.2 %, respectively. And the corresponding latent heat obtained from the phase transition of n-hexadecane reached 98.9 J/g. With the further increasing of n-hexadencane addition to 70 wt%, although the actual loading content of n-hexadecane and the corresponding latent heat increased to 57.0 % and 113.6 J/g, respectively, the encapsulation efficiency of n-hexadecane decreased to 81.4 %. It indicated that it is very difficult for limited PLA matrix and PCL matrix to prevent the diffusion (even loss) of excessive n-hexadecane caused by the evaporation of solvent. In addition, with the adding of n-hexadencane, not only the cold crystallization process of PLA matrix can be accelerated, but also the crystallization degree of PLA matrix increased.

With the decreasing of the weight fraction between PLA component and PCL component from 4/1 to 1/4, the actual loading content of n-hexadecane, the encapsulation efficiency of n-hexadecane and corresponding latent heat of n-hexadecane all decreased gradually. It indicated that PLA component as inner shell matrix not only can prevent the migration of n-hexadecane during the evaporation process of solvent, buut also fix n-hexadecane in the inner area of obtained microcapsules. With the decreasing of PLA content in electrosprayed droplets, more and more n-hexadecane diffused into PCL phase or even the surface of final microcapsules. In addition, with the decreasing of the weight fraction between PLA component and PCL component, the crystallization degrees of PLA matrix and PCL matrix decreased and increased, respectively.

Finally, double-layered shell structure can also better thermal stability for encapsulated n-hexadecane. Under low n-hexadecane addition (30 wt% or 50 wt%) in electrospraying solutions, the initial degradation temperature of emcapsualted n-hexadecane in obtained microcapsules is higher than that of raw n-hexadecane. Meanwhile, the existence of PCL matrix can play the role of physical barrier and protection to improve the thermal stability of encapsulated n-hexadecane. With the increasing of PCL content in final microcapsules, the initial degradation

temperature of encapsulated n-hexadecane increased gradually. Combining with the DSC results and TGA results, it can conclude that some n-hexadecane chains and PLA chains will move into PCL phase with the evaporation of solvent during electrospraying process. And some PCL chains also diffused into PLA phase. Therefore, the shell structures in n-hexadecane/PLA/PCL microcapsules can be divided into PLA layer, PLA and PCL mixed layer and PCL layer. Strong intermoleculat interactions between PLA phase and PCL phase can be confirmed. N-hexadecane/PLA/PCL microcapsules with double-layered shells not only can offer much advantages and potential in fabricating mPCMs with desired structures and properties (including core-shell structure, high encapsulation efficiency, high latent heat and thermal stability), but also offer a new strategy to carry out the functional coating of textiles with good interfacial adhesion, durability and lowest damage to the original structure and properties of the textiles.

Prospects

Based on the practical experience in the completed research, there are some suggestions for further developing this topic, which can be taken into consideration in the future work. It can be divided into four aspects, introducing nanoparticles, replacing shell materials, designing multi-layered shell structure and the functional coating of textiles or other matrix materials.

- **Introducing nanoparticles:**

(1) Graphene, graphene oxide and reduced graphene oxide as novel two-dimensional carbon nanomaterials have prominent mechanical strength, electrical conductivity, thermal conductivity and physical barrier effects. When they were added into electrospraying solution for preparing mPCMs, the thermal conducticity and mechanical properties of final mPCMs can be enhanced obvioulys. Meanwhile, due to the physical barrier effect of these carbon nanomaterials, the diffusion of PCMs caused by the evaporation of solvent can be prevented effectively. Therefore, the loading content and encapsulation efficiency of PCMs can also be improved. In addition, the effects of carbon nanomaterials addition on the structures, morphologies and properties of obtained microcapsules can also be clarified.

(2) Some metal nanoparticles, metal oxide nanoparticles and inorganic nanoparticles were also regarded as effective nanofillers to improve the thermal conductivity of electrosprayed mPCMs. Meanwhile, the effects of the shape and the addition of nanoparticles on the structures, morphologies and properties of

obtained microcapsules can also be investigated.

(3) When nanoparticles with prominent properties (for example, flame-retardant, antibacterial, electrical conductivity and magnetic) were introduced into electrosprayed mPCMs, electrosprayed mPCMs with multiple functions can be prepared.

- **Replacing shell materials**

(1) Apart from polycaprolactone (PCL) and poly(lactic acid) (PLA), some natural polymers (e.g. agar, arabic gum and gelatine) and some high performance engineering plastics (including polyamide, polycarbonate, polyformaldehyde, poly(butylene terephthalate) and poly(phenylene oxide)) can be considered as shell matrix to capture PCMs to fabricate mPCMs. Some better performances and advantages obtained from various shell materials can be offered to electrosprayed mPCMs.

(2) Multi-component blending materials can also be used as shell matrix to encapsulate PCMs during the process of electrospraying. Sometimes, blending composites shell has more advantages and better performances than single material shell, for example, higher mechanical strength, thermal stability, toughness and physical barrier. In addition, the surface porous of mPCMs can be designed and controlled via removing one component of the multi-component blend shell.

- **Designing multi-layered shell structure**

(1) The electrosprayed mPCMs with multi-layered shell structure can be desighed via applying coaxial nozzle with multiple capillaries. Meanwhile, on the one hand, higher loading content of PCMs and higher encapsulation efficicency can be obtained when multi-layered shell structure was designed for electrosprayed mPCMs. On the other hand, electrosprayed mPCMs with multi-layered shell structure can present more functions owing to different functions endowed from different shell materials.

(2) Different core materials with different functions can be introduced into different layer shell materials for endowing more functions to final electrosprayed PCMs. For example, when different PCMs with different phase change temperatures were added into different layer shell materials, the thermal regulation range of electrosprayed mPCMs can be further extended. In addition, when different core materials were added into different layer shell materials, the interactions or mutual contact among different core materials can be isolated and restricted to the greatest extent. And the stability and

durability of each core materials can be improved obviously.

- **the functional coating of textiles or other matrix materials**

(1) Electrosprayed mPCMs with double-layered shell structure can be used directly for the functional coating of textiles to fabricate thermal-regulated textiles. The effects of different additions of PCMs, different weight fractions between two-component shells, different heat treatment times and temperatures, different electrospraying times on the structures, morphologies and properties of final thermal-regulated textiles can also be investigated.

(2) Apart from textiles, electrosprayed mPCMs can also be used to other matrix materials to endow the thermal-regulated functions. For example, electrosprayed mPCMs can be sprayed directly on the surface of precision electronic devices to reduce their heating problems during use.

Appendix 1: Phase change materials

When human life and social production activities enter the 21st century, energy consumption and environmental pollution have become two major problems that plague us. Seeking and applying green and renewable energy has become one of the solutions to people's troubles (Sharma, Tyagi, Chen, & Buddhi, 2009; Zalba, Marín, Cabeza, & Mehling, 2003). Until now, the scientists all over the world have been attracted by energy storage device, which are as important as developing green and renewable energy. In general, common energy storage devices mainly include mechanical energy storage, electrical storage, thermal energy storage, thermochemical energy storage and solar energy storage (Chen et al., 2009; Hasnain, 1998; Kenisarin, & Mahkamov, 2007; Steinmann, 2017). For example, mechanical power from tides or wind can be converted into electrical energy via hydroelectric or wind power station, then the resulting electrical energy can be stored or released. Meanwhile, thermal energy can be stored or released via the phase transition process of phase change materials (PCMs). In addition, in the batteries, the stored chemical energy from electrode active material is converted into electrical energy via oxidation and reduction reaction (Sharma, Ganesan, Tyagi, Metselaar, & Sandaran, 2015).

Among these energy storage devices, due to their relatively higher thermal capacity and storage density, enabling a compact energy storage system at nearly isothermal conditions, high latent heat release or storage, thermal and chemical stability, non-toxicity and low cost, PCMs as a thermal storage device had presented more advantages and potential compared with other energy storage devices (Pielichowska, & Pielichowski, 2014). A large amount of heat energy can be released or stored, when PCMs changed from one phase state (liquid, solid or gas) to another phase state with the variation of surrounding temperature. Although PCMs was first studied by M. Telkes and E. Raymond in 1949 (Mourid, El Alami, & Kuznik, 2018), it had not received wide attention until the 1970s. In 1971, in order to protect astronauts from the extreme temperature fluctuation in space, National Aeronautics and Space Administration (NASA) triggered the application of PCMs in the field of thermal regulation fields for the first time (Hale, Hoover, & Neill, 1971). Then, in the next 50 years, PCMs had been widely investigated and applied in the fields of space equipment, thermal regulation textiles, industrial waste heat recovery, energy conservation in buildings, electric appliances with thermostatic regulator, energy-storage kitchen utensil and solar energy use (Farid, Khudhair, Razack, & Al-Hallaj, 2004). PCMs have been regarded as the main

candidates for delaying the increase in energy consumption and for satisfying the growing demand for thermal management.

1. Mechanism

PCMs can be defined as smart materials due to their ability to release or absorb heat energy with the variation of surrounding temperature. When the surrounding temperature reached to a certain value, the phase state of PCMs (gas, liquid or solid) changed into another phase state (gas, liquid or solid) (Figure A1-1). During the process of phase transition, a large amount of latent heat can be released or absorbed to prevent or delay the changes of surrounding temperature. The storage heat capacity of PCMs latent heat system can be calculated by followed Equation (1) (Sharma et al., 2009).

$$Q = \int_{T_i}^{T_m} mC_p \mathrm{d}T + ma_m \Delta h_m + \int_{T_m}^{T_f} mC_p \mathrm{d}T \qquad \text{Equation (A1-1)}$$

Where, Q was the quantity of heat storage (J), T_m, T_i *and* T_f were the melting temperature (°C), initial temperature (°C) and final temperature (°C), respectively; m was the weight of PCMs, C_p was special heat capacity (J/(g·K)), a_m was the fraction melted, Δh_m was the heat of fusion per unit weight (J/g), C_{sp} was the average specific heat between T_i and T_m (J/(g·K)) and C_{lp} was average specific heat between T_m and T_f (J/(g·K)).

Among these three phase transition processes, the transition from solid state to liquid state (or from liquid state to solid state) is a safe, high-efficiency and economic process for using in thermal storage system. On the one hand, a large amount of latent heat was released or stored via the solid-liquid transition process. On the other hand, during the solid-liquid transition process, the change in the volume of PCMs medium is small (10 % or less) (Sharma et al., 2009). Apart from solid-liquid transition process, higher latent heat was released or stored via the solid-gas transition process or liquid-gas transition process. However, the larger change in the volumeof PCMs during solid-gas (or liquid-gas) phase transition process increased their difficulties of use as well as technical requirements and further restricted their developments in the fields of energy storage and thermal regulation (Abhat, 1983).

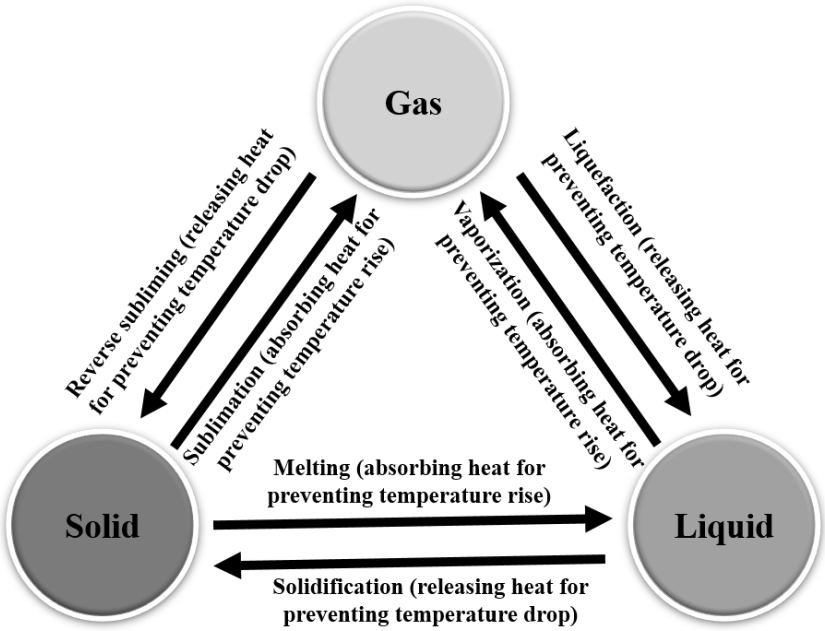

Figure A1 - 1 Schematic representation of phase change process.

In general, the solid-solid transition of PCMs can be carried out via the mutual transformation among different crystalline phases (Pillai, & Brinkworth, 1976). The solid-solid transition generally has smaller latent heat and smaller volume change during phase transition process compared with previous three phase transition processes. Based on the insignificant volume changes before and after solid-solid transition process, less stringent container requirements and greater design flexibility are obtained. In general, the latent heat thermal storage system consists of a suitable PCMs with a desired phase transition temperature range, a separate heat transfer medium and a container compatible with the PCMs. The change in the volume of PCMs during phase transition process affects the special volume design of container to PCMs as well as the whole thermal storage system. The container used for PCMs should have the ability to withstand the volume change during phase transition process and should be compatible with the PCMs used. Meanwhile, considering the low thermal conductivity of PCMs, a heat exchanger medium is also necessary to accelerate the heat transfer between PCMs and surroundings. Phase change microcapsules (mPCMs) consisted of PCMs and shell material are regarded as the efficient and practical thermal storage systems. On the one hand, the existence of shell material plays the role of container for achieving the preservation of PCMs. On the other hand, shell material is also regarded as the heat exchanger medium for improving the heat transfer efficiency of PCMs. When inorganic materials (ceramic, metal or metal oxide) were used as shell materials for mPCMs, the heat exchange efficiency between PCMs and external medium can be

further enhanced.

2. Properties

When PCMs were applied in the fields of energy storage and thermal regulation, some properties and characteristics, including thermal, physical, kinetic, chemical and economics, are necessary (Abhat, 1983; Sharma et al., 2009).

For the thermal properties, firstly, PCMs should have suitable phase-transition temperature. In general, when PCMs were used for a particular application, their phase-transition temperatures should match to the operating temperature of the heating or cooling. Secondly, the latent heat released or stored from the phase transition of PCMs should be as high as possible. The more latent heat released or stored from the phase transition process of PCMs, the stronger the heat regulation ability provided by the thermal storage system. Finally, PCMs are expected to have high thermal conductivity for carrying out high heat exchange efficiency between PCMs and external medium.

For the physical properties, a favorable phase equilibrium of PCMs is necessary. In other words, the phase transition process of PCMs should be stable, and the phase separation phenomenon should be avoided. It would help towards setting heat storage or release. Meanwhile, PCMs with high density can reduce the size of related container, then decrease the cost as well as the design difficulty of the whole thermal storage system. Furthermore, the small volume changes before and after the phase transition of PCMs also allowed to reduce the design difficulties of thermal storage devices. Finally, low vapor pressure of PCMs waas also desired for easy incorporation and design in thermal storage system.

For the kinetic properties, the supercooling phenomenon should be avoided during the crystalline processes of PCMs. Supercooling liquid is in a metastable state, and is unstable. Supercooling of more than a few degrees reduced the ability of PCMs to release latent heat as the ambient temperature decreases. Meanwhile, 5-10 °C supercooling prevented completely the release of latent heat from the cooling process of PCMs. In addition, the high crystallization rate is also desired to the application of PCMs in the fields of energy storage as well as thermal regulation.

For chemical properties, firstly, PCMs should have long-term chemical stability for improving their durability and safety in various use environments. Secondly, a good compatibility between PCMs and container

or some matrix materials is also necessary. In addition, PCMs should be non-explosive, non-flammable and non-toxic for safe use.

For economics properties, the sources of PCMs are also very extensive and available, mainly including petroleum derivations (paraffin waxes), some chemical synthetic products (esters, fatty acids, alcohols and glycols), some inorganics (salt hydrate and metallics). Meanwhile, low price is also one of the economic characteristics of PCMs.

3. Classification

As mentioned above, there are a large amount of substances that can be used as PCMs for the fields of energy storage and thermal regulation. According to the differences in the chemical composition of various PCMs, PCMs can be divided into three groups, i.e., (a) organic compounds, (b) inorganic compounds and (c) inorganic eutectics or eutectic mixtures (Figure A1-2). Due to the differences in the composition and structure of various PCMs, different types of PCMs have different properties and characteristics. For their very different thermal and chemical behavior, the properties of each subcategory which affects the design of latent heat thermal energy storage systems.

3.1 Organic PCMs

In general, based on their congruent melting behaviors during heating process, organic PCMs melt and freeze repeatedly without the consequent degradation of their latent heat of fusion as well as the phase separation phenomenon. Meanwhile, the self-nucleation ability of organic PCMs results in the crystallization process of PCMs without supercooling phenomenon. In addition, non-corrosiveness is also one of the advantages of organic compounds. According to their differences in chemical structure, organic compounds can be divided into paraffins and non-paraffins.

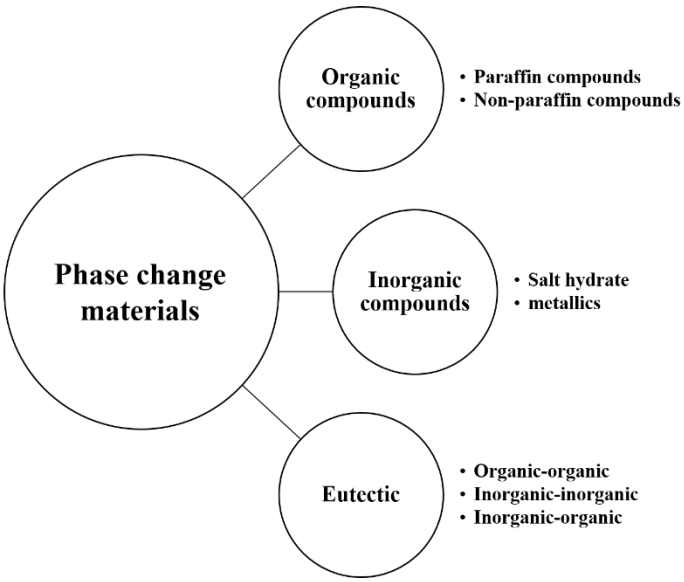

Figure A1 - 2 Classification of PCMs.

Paraffin compounds

N-alkanes mixture (CH_3-$(CH_2)_n$-CH_3) with 14-34 carbon atoms are defined as paraffin waxes. In general, they are consisted of 80-95 wt% straight chain alkanes and 20 wt% or less branched alkanes and monocyclic cycloalkanes with long side chains (Gulfam, Zhang, & Meng, 2019). Paraffin wax is derived from the lubricating oil obtained by the distillation petroleum. The lubricating oil fraction is solvent-refined, solvent-dewaxed or wax-freeze crystallized, pressed and dewaxed to obtain wax paste, and then de-oiled and supplemented to obtain paraffin wax. During the melting or freezing process of paraffin wax, a large amount of latent heat is absorbed or released. The latent heat of paraffin waxes is range from 170 J/g to 269 J/g as the variation of the number of carbon atom (Sharma et al., 2009). Meanwhile, the melting point of paraffin waxes increases gradually with the increasing of the number of carbon atom. For thermal regulation clothes, the textiles coated with paraffin waxes is expected to protect the wearer from the change of surrounding temperature. Therefore, the phase transition temperatures of paraffin waxes used in thermal regulation textiles should be closed to the body comfortable temperature (14-35 °C). When surrounding temperature is lower than 14 °C or higher than 35 °C, the human body will feel cold or hot. Among a series of paraffin waxes, n-hexadecane (melting point: ~16.7 °C) and n-eicosane (melting point: ~35 °C) are suitable for designing thermal storage systems used in thermal regulation textiles.

As n-alkanes with long straight carbon backbone, paraffin waxes show chemical inertness and good thermal stability below 500 °C. Meanwhile, paraffin waxes are non-toxic, non-corrosive and less expensive. Therefore, paraffin waxes are regarded as green, safe, reliable and economics PCMs for the fabrication of thermal storage

system. Furthermore, little volume changes and low vapor pressure during the phase transition process are also the advantages of paraffin waxes. In addition, the congruent melting behavior also ensures that there is no the phase separation phenomenon and the consequent degradation of their latent heat of fusion in the phase transition process of paraffin waxes. Apart from these favorable characteristics of paraffin waxes, some disadvantages or drawbacks also limit the development and application of paraffin waxes. For example, the thermal conductivity of paraffin waxes is low, and paraffin waxes are flammable. Therefore, microencapsulation technology is regarded as an effective method to overcome these drawbacks from paraffin waxes. Due to the increasing of specific surface area, the heat exchange efficiency between paraffin waxes and external medium can be enhanced effectively. Meanwhile, the existence of shell matrix also depresses the flammability of paraffin waxes.

Non-paraffin organic PCMs

Apart from paraffin waxes, major of organic PCMs are composed of non-paraffin compounds. Due to their many categories and large quantity, non-paraffin organic PCMs are regarded as the largest category of candidate's materials for phase change storage. According to Abhat et al and Buddhi et al, non-paraffin organic PCMs can be further subdivided into four groups, i.e., (a) fatty acids, (b) alcohols, (c) glycols and (d) esters based on their differences in their chemical composition and chemical structure (Sharma et al., 2009). Therefore, unlike paraffin waxes which have very similar properties, the properties of non-paraffin organic PCMs are variable and different among different categories. Each of categories non-paraffin organic PCMs will have its own properties. Among these four types of non-paraffin organic PCMs, fatty acids are the most investigated and applied by scientific researchers and related industries. According to the length of carbon backbone, fatty acids are divided into short chain fatty acids (the number of carbon atom is less than 6), medium chain fatty acids (the number of carbon atom is range from 6 to 12) and long chain fatty acids (the number of carbon atom is more than 12). According to the unsaturation degree of hydrocarbon chain, fatty acids are also divided into saturated fatty acid, monounsaturated fatty acid and polyunsaturated fatty acid. Common fatty acids used as PCMs with their melting points and latent heat of fusion are listed in Table A1-1 (Sharma et al., 2009).

Being similar to paraffin waxes, a reproducible melting or freezing process without the degradation of the latent heat of fusion and the phase separation phenomenon is also obtained from fatty acids. Meanwhile, there is also no supercooling phenomenon during the freezing process of fatty acids (Rozanna, Chuah, Salmiah, Choong,

& Sa'ari, 2005; Yuan, Zhang, Tao, Cao, & He, 2014). The disadvantages of fatty acids are their unsafety, high cost and low thermal conductivity. The flash point of fatty acids is low. Therefore, fatty acids are flammable, and are unstable at high temperature. And, fatty acids can't be exposed to excessively high temperature, flames or oxidizing agents. In addition, different fatty acids have varying level of toxicity as well as corrosive. For the high cost, the price of fatty acids is 2-2.5 times higher than that of technical grade paraffin waxes.

3.2 Inorganic PCMs

The inorganic PCMs are divided into salt hydrate and metallics. For salt hydrate, the latent heat of fusion comes from the solid-liquid phase transition based on the dehydration of hydration of the salt. For metallic, the latent heat of fusion is obtained from the solid-liquid transition of metals or metal eutectics with low melting point. As inorganic compounds, their biggest advantage is high thermal conductivity. In addition, with repeated cycles of phase transition process, the latent heat of fusion of inorganic PCMs still kept stable.

Table A1 - 1 Melting point and latent heat of fusion of non-paraffin organic PCMs.

Materials	Melting point (°C)	Latent heat (J/g)
Formic acid	7.8	247
Caprilic acid	16.3	149
Glycerin	17.9	198.7
D-Lattic acid	26.0	184
Methyl palmitate	29.0	205
Camphenilone	39.0	205
Docasyl bromide	40.0	201
Caprylone	40.0	259
Phenol	41.0	120
Heptadecanone	41.0	201
4-Heptadacanone	41.0	197
p-Joluidine	43.3	167
Cyanamide	44.0	209
Methyl eicosanate	45.0	230
3-Heptadecanone	48.0	218
2-Heptadecanone	48.0	218
Hydrocinnamic acid	48.0	118
Cetyl alcohol	49.3	141
α-Nepthylamine	50.0	93
Camphene	50.0	238
O-Nitroaniline	50.0	93
9-Heptadecanone	51.0	213
Thymol	51.5	115
Methyl behenate	52.0	234
Diphenyl amine	52.9	107
p-Dichlorobenzene	53.1	121
Oxolate	54.3	178
Hypophosphoric acid	55.0	213
O-Xylene dichloride	55.0	121
β-Chloroacetic acid	56.0	147
Chloroacetic acid	56.0	130
Nitro naphthalene	56.7	103
Heptaudecanoic acid	60.6	189
α-Chloroacetic acid	61.2	130
β-Bromophenol	63.5	86
Azobenzene	67.1	121
Dinto toluent (2,4)	70.0	111
Phenylacetic acid	76.7	102
Thiosinamine	77.0	140
Bromcamphor	77.0	174
Durene	79.3	156
Benzylamine	78.0	174
Methyl brombrenzoate	81.0	126
Alpha napthol	96.0	163
Glautaric acid	97.5	156
p-Xylene dichloride	100.0	138.7
Catechol	104.3	207
Quinone	115.0	171
Acetanilide	118.9	222
Succinic anhydride	119.0	204
Benzoic acid	121.7	142.8
Stibene	124.0	167
Benzamide	127.2	169.4

Salt hydrates

In general, salt hydrate with a general formula AB·nH2O is a typical crystalline alloy consisted of inorganic salts and water. During their solid-liquid phase transition processes, some water molecular break away from salt hydrates via dehydration reaction as shown in Equation 2 or Equation 3 (Xie et al., 2017).

$$\mathrm{AB} \cdot nH_2O \rightarrow \mathrm{AB} \cdot m\mathrm{H_2O} + (n-m)\mathrm{H_2O} \qquad \text{Equation (A1-2)}$$

$$\mathrm{AB} \cdot nH_2O \rightarrow \mathrm{AB} + n\mathrm{H_2O} \qquad \text{Equation (A1-3)}$$

When temperature reaches their melting points, the solid-liquid phase transition of salt hydrates as well as the dehydration reaction occur simultaneously. Finally, salt hydrates breakup into lower salt hydrates with fewer crystal water or anhydrous salt as well as all free water. The free water released promotes the dissolution of solid phase salt hydrate during the solid-liquid phase transition. According to Sharma et al, the melting behavior of salt hydrates can be divided into congruent melting, incongruent melting and semi-congruent melting. For congruent melting, the whole anhydrous salt can be completely dissolved in free water released during the solid-liquid transition process, and the repeated solid-liquid phase transition process is stable. And there is no phase separation phenomenon during the phase transition process. For incongruent melting, salt hydrates solid can't be completely dissolved in free water released from dehydration reaction during the melting process. Therefore, there is a phase separation phenomenon during the incongruent melting process. For semi-congruent melting, an equilibrium between solid phase and liquid phase can be obtained during the solid-liquid phase transition of salt hydrates due to the conversion of the hydrate salt to a lower-hydrated salt through loss of water. For most salt hydrates, since the amount of free water released from dehydration reaction is not sufficient to dissolve all solid salt hydrate, their melting processes are regarded as incongruent melting. Due to the phase separation phenomenon resulted from incongruent melting process, the phase transition process of salt hydrate is unstable, and the storage or release of energy is also influenced. Meanwhile, combining the incongruent melting behavior with the density differences among undissolved salt hydrates (including lower salt hydrated and anhydrous salt), some salt hydrates solid deposites on the bottom of container, which will also influence the heat transfer efficiency of heat storage system as well as its durability. Thus, the deposited salt solid is unfavorable the recombination between anhydrous salts and water during the reverse process of freezing. It also results in a gradual decrease in the quality of the salt hydrates participated into each solid-liquid phase transition cycle. In order to reduce the effects of incongruent melting behavior as well as phase separation phenomenon on the ability of salt hydrates to store or release energy,

some methods can be considered. Firstly, the solubility of anhydrous salts in free water released is improved effectively via mechanical stirring. Meanwhile, the blocked anhydrous salts solid can also be stirred and further dissolved into free water released. With the improvement of the solubility of anhydrous salts, the phase separation phenomenon between solid phase and liquid phase can be effectively alleviated. Secondly, the phase separation phenomenon can also be depressed via microencapsulating salt hydrates into shell matrix. Thirdly, the solidification of anhydrous salts can be prevented effectively via adding some thickening agent in the suspension liquid. Furthermore, adding excessive water can accelerate the dissolution of anhydrous salts solid during the solid-liquid phase transition process. Finally, adding some chemical agents for enhancing the solubility of salt hydrates in water or modifying the chemical composition of salt hydrates system for turning incongruent melting into congruent melting is also considerable means.

Apart from incongruent melting behavior, poor nucleation ability is also one of the disadvantages of salt hydrates (Porisini, 1988). Poor nucleation ability results in a slow nucleation rate of salt hydrates during the cooling process of salt hydrates, as well as a supercooling phenomenon also occurs. Thus, when temperature drops to the crystallization temperature of salt hydrates, the nucleation rate is too slow to trigger the crystallization process. Therefore, salt hydrates still keep liquid state at their crystallization temperatures, and their crystallization processes are postponed to below the crystallization process. Due to the supercooling phenomenon, the ability of the salt hydrates to release heat during the cooling process is weakened. In order to improve the disadvantage of poor crystallization ability, two effective methods are considered. On the one hand, adding nucleation agent can increase the nucleation rate of salt hydrates. On the other hand, retaining some crystals in a small cold region to serve as nuclei can also increase their nucleation rate.

Salt hydrates as the most important group of PCMs used in latent heat thermal energy storage systems, they also have many attractive properties and characteristics. Firstly, they have high latent heat of fusion per unit volume during their phase transition processes. Secondly, they have relatively high thermal conductivities. Generally, their thermal conductivities are twice higher than that of paraffin wax products. Thirdly, the volume changes of salt hydrates in the solid-liquid phase transition process is small. In addition, most salt hydrates are relatively low in cost, toxicity and corrosiveness for the use in energy storage and thermal regulation. Common salt hydrates used as PCMs with their melting points and latent heat of fusion are listed in Table A1-2 (Sharma et al., 2009).

Table A1 - 2 Melting point and latent heat of fusion of salt hydrates.

Material	Melting point (°C)	Latent heat (kJ/kg)
$K_2HPO_4·6H_2O$	14.0	109
$FeBr_3·6H_2O$	21.0	105
$Mn(NO_3)_2·6H_2O$	25.5	148
$FeBr_3·6H_2O$	27.0	105
$CaCl_2·12H_2O$	29.8	174
$LiNO_3·2H_2O$	30.0	296
$LiNO_3·3H_2O$	30.0	189
$Na_2CO_3·10H_2O$	32.0	267
$Na_2SO_4·10H_2O$	32.4	241
$KFe(SO_4)_2·12H_2O$	33.0	173
$CaBr_2·6H_2O$	34.0	138
$LiBr_2·2H_2O$	34.0	124
$Zn(NO_3)_2·6H_2O$	36.1	134
$FeCl_3·6H_2O$	37.0	223
$Mn(NO_3)_2·4H_2O$	37.1	115
$Na_2HPO_4·12H_2O$	40.0	279
$CoSO_4·7H_2O$	40.7	170
$KF·2H_2O$	42.0	162
$MgI_2·8H_2O$	42.0	133
$CaI_2·6H_2O$	42.0	162
$K_2HPO_4·7H_2O$	45.0	145
$Zn(NO_3)_2·4H_2O$	45.0	110
$Mg(NO_3)·4H_2O$	47.0	142
$Ca(NO_3)·4H_2O$	47.0	153
$Fe(NO_3)_3·9H_2O$	47.0	155
$Na_2SiO_3·4H_2O$	48.0	168
$K_2HPO_4·3H_2O$	48.0	99
$Na_2S_2O_3·5H_2O$	48.5	210
$MgSO_4·7H_2O$	48.5	202
$Ca(NO_3)_2·3H_2O$	51.0	104
$Zn(NO_3)_2·2H_2O$	55.0	68
$FeCl_3·2H_2O$	56.0	90
$Ni(NO_3)_2·6H_2O$	57.0	169
$MnCl_2·4H_2O$	58.0	151
$MgCl_2·4H_2O$	58.0	178
$CH_3COONa·3H_2O$	58.0	265
$Fe(NO_3)_2·6H_2O$	60.5	126
$NaAl(SO_4)_2·10H_2O$	61.0	181
$NaOH·H_2O$	64.3	273
$Na_3PO_4·12H_2O$	65.0	190
$Ba(OH)_2·8H_2O$	78.0	265
$Mg(NO_3)_2·6H_2O$	89.9	167
$KAl(SO_4)_2·12H_2O$	91.0	184
$MgCl_2·6H_2O$	117.0	167

Metallics

In general, the metallics used for PCMs in the fields of energy storage and thermal regulation consists of some metals or metal mixtures with low melting point. The advantages of metallics are high thermal conductivity, high latent heat of fusion per unit volume and relatively vapor pressure. In general, the thermal conductivity of

metallics is higher than that of other PCMs. The disadvantages of metallics are low latent heat of fusion per unit weigh and low specific heat.

3.3 Eutectics

In general, eutectics used for PCMs in the fields of energy storage and thermal regulation consists of two or more components with low melting point (Rathod, & Banerjee, 2013; Raud, Jacob, Bruno, Will, & Steinberg, 2017). For these components, they melt or freeze congruently to obtain the mixture of component liquid or component crystals during their phase transition processes. Meanwhile, there is no phase separation phenomenon in the process of solid-liquid transition. For these PCMs components, the weight ratio among different ingredients also influences their phase transition properties including their congruent melting or freezing behavior. Some common eutectics used as PCMs with their melting points and latent heat of fusion are listed in Table A1-3 (Sharma et al., 2009).

Table A1 - 3 Melting point and latent heat of fusion of common organic and inorganic eutectics

Material	Composition (wt%)	Melting point (°C)	Latent heat (kJ/kg)
$CaCl_2 \cdot 6H_2O+CaBr_2 \cdot 6H_2O$	45+55	14.7	140
Triethylolethane+water+urea	38.5+31.5+30	13.4	160
$C_{14}H_{28}O_2+C_{10}H_{20}O_2$	34+66	24.0	147.7
$CaCl_2+MgCl_2 \cdot 6H_2O$	50+50	25.0	95
$CH_3CONH_2+NH_2CONH_2$	50+50	27.0	163
Triethylolethane+urea	62.5+37.5	29.8	218
$Ca(NO_3) \cdot 4H_2O+Mg(NO_3)_3 \cdot 6H_2O$	47+53	30.0	136
$CH_3COONa \cdot 3H_2O+NH_2CONH_2$	40+60	30.0	200.5
$NH_2CONH_2+NH_4NO_3$	53+47	46.0	95
$Mg(NO_3)_3 \cdot 6H_2O+NH_4NO_3$	61.5+38.5	52.0	125.5
$Mg(NO_3)_3 \cdot 6H_2O+MgCl_2 \cdot 6H_2O$	58.7+41.3	59.0	132.2
$Mg(NO_3)_3 \cdot 6H_2O+MgCl_2 \cdot 6H_2O$	50+50	59.1	144
$Mg(NO_3)_3 \cdot 6H_2O+Al(NO_3)_2 \cdot 9H_2O$	53+47	61.0	148
$CH_3CONH_2+C_{17}H_{35}COOH$	50+50	65.0	218
$Mg(NO_3)_2 \cdot 6H2O+MgBr_2 \cdot 6H_2O$	59+41	66.0	168
Napthalene+benzoic acid	67.1+32.9	67.0	123.4
$NH_2CONH_2+NH_4Br$	66.6+33.4	76.0	151
$LiNO_3+NH_4NO_3+NaNO_3$	25+65+10	80.5	113
$LiNO_3+NH_4NO_3+KNO_3$	26.4+58.7+14.9	81.5	116
$LiNO_3+NH_4NO_3+NH_4Cl$	27+68+5	81.6	108

4. Applications

There are a large amount of inorganic and organic materials that can be used as PCMs in the fields of energy storage and thermal regulation. From 1971 year, when the benefits of PCMs were presented by NASA via incorporating PCMs with space equipment for achieving the insulation and thermal regulation in harsh space

environment, the investigations and development of PCMs as well as some productions incorporated with PCMs had attracted more and more attention. Thus, the investigation, development and application of PCMs can improve human living standard and promote the progress of social production. On the one hand, PCMs offer tremendous potential to fulfill the growing energy needs for cooling and heating applications across various industries, including aerospace industry, energy conservation in buildings, thermal-regulated textiles, industrial waste heat recovery and solar energy use. On the other hand, the use of different PCM technologies in various fields can reduce environmental pollution, damage to human health, required cost and the dependence on traditional fossil fuels (oil and coal) during thermal energy storage or release and utilization. Therefore, these application values promotes the growth and development of the global PCMs market (Sarier, & Onder, 2012). The global PCMs market was estimated at $1.9 billion in 2019 and is slated to exceed $4.4 billion by 2026, registering a Compound Annual Growth Rate (CAGR) of 17.04% from 2020 to 2026 (related information from: https://www.gminsights.com/pressrelease/phase-change-material-market). In terms of product, eutectics, paraffin, and non-paraffin segment are considered as the highest revenue generating segments of the phase change materials market. In fact, in 2019, the paraffin product segment is the key revenue generator for the overall market, the segment further is anticipated to grow at a CAGR of 18.3% through the forecast timeframe. In terms of application fields, building and construction industries presently are the largest application market of organic PCMs due to the globally increasing requirement for cooling buildings, which in turn has arisen in consequence of the shift from heavy thermal mass design to lightweight architecture. Meanwhile, textiles incorporated with PCMs have also been used in numerous products and application from apparel, outdoor wear (parkas, vests, thermals, snowsuit and trousers), underwear, socks, accessories and shoes to bedding, sleeping bags, blankets, duvets, mattresses and pillowcases for achieving thermal regulation function. Moreover, in recent decades, more and more scientific researchers have put in a lot of effort to develop thermal-regulated textiles via introducing PCMs. And the proportion of paraffin waxes used in the field of thermal-regulated textiles has also increased year by year, second only to their applications in the building and construction industries. In addition, PCMs can even be found in some specialty productions, such as antiballistic vests, automotive, medical or special industrial applications. And some industry participants including BASF, Honeywell, Outlast Technologies, Devan Chemicals and Samsung had started to collaborate with universities to conduct research and development on advanced PCMs in an attempt to increase market penetration of the PCM products as well as accelerate the

application of PCMs in various fields (related information from: https://www.marketsandmarkets.com/Market-Reports/pcm-market-250.html).

4.1 Aerospace industry

When people began to explore outer space, due to the extremely harsh ambient temperature (too high or too low temperature) in outer space, ensuring the use temperature of precision electronic instruments and maintaining the body surface temperature of astronauts are two problems that confuse scientific researchers. In order to solve these problems, NASA firstly incorporated PCMs into the design of electronic instruments as well as spacesuits. Facing with the dramatic changes of outside temperature in space, the surrounding temperature of electronic instruments was kept within a certain range for ensuring the normal operations of these machines based on the absorption or release of heat derived from the phase transition of PCMs. Meanwhile, the body temperature of astronauts was also kept within a comfortable range (about 18-23 °C) in outer space via introducing n-hexadecane into the design of spacesuits. According Wu et al, compared with conventional thermal control system, the spacecraft equipped with a shape-stabilized PCMs (a novel thermal regulation system) had stronger ability to resist the impact of sudden temperature changes (Wu, Liu, Cheng, & Liu, 2013).

4.2 Energy conservation in building

For a long time, temperature regulation of the indoor environment where humans live and work is one of the sources of conventional fossil energy consumption and greenhouse gas emissions. So far, the heating or cooling measures for buildings in different seasons mainly rely on the combustion of fossil energy and the use of air conditioning. In order to reduce the emission of greenhouse gas and the consumption of conventional energy, it is necessary to seek a new thermal adjustment system to replace the use of air condition as well as fossil fuel. PCMs as a high thermal capacity and storage density, high latent heat release or storage, non-toxicity and low cost materials, were used as new thermal adjustment system in building design (Baetens, Jelle, & Gustavsen, 2010). On the one hand, new building materials with heat storage and temperature regulation functions will be prepared when traditional building materials are incorporated with PCMs. These new building materials not only improve the thermal comfort of the indoor environment effectively, but also reduce the building energy consumption and costs for heating and cooling. On the other hand, when PCMs are introduced into the design of building, the

related environmental pollution issues will also be solved to a certain extent. Until now, there are many ways to introduce PCMs into traditional building materials, including direct blending, direct immersion, carrier encapsulation, melting blending, porous adsorption method and microencapsulation method. (Morovat, Athienitis, Candanedo, & Dermardiros, 2019) (Liu, Wang, & Qian, 2017) (Cabeza et al., 2007). Furthermore, some different possible building applications for PCMs have been studied, especially trying to improve the performances of technical installations such as hot water heat stores, cool thermal energy storage, pipe insulation, and latent heat thermal storage systems. In addition, the improvement of double facades with PCMs has been studied to achieve a better control of the cavity temperature.

4.3 Thermal-regulated textiles

Recently, the incorporation of PCMs in textiles by coating or encapsulation to obtain thermo-regulated smart textiles has grown interest to the researcher. These thermal-regulated textiles which have automatic acclimatising properties not only can be used in clothing industry to improve people's clothing comfort, but also can be used in bedding and accessories, medical applications, shoes and accessories, automobile textiles and some special fields for achieving thermal regulation functions.

4.4 Industrial waste heat recovery

In industry activities, most of energy is obtained from the burning of fossil fuels. Meanwhile, a lot of waste heat and greenhouse gas were obtained from the process of industrial production. Achieving the recycling of industrial waste heat not only can effectively alleviate the problem of energy shortage, but also reduce the environmental pollution caused by industrial activities. By applying the heat recovered from cooling media, hot exhausted gases and hot equipment surfaces during industrial process to various fields such as space comfort and electricity generation, this technology can provide an attractive opportunity to reduce the costs of energy and mitigate environmental effects. However, some limitations and difficulties still delay the realization of industrial waste heat recycling (Li, Wang, Ding, Yao, & Huang, 2019; Merlin, Soto, Delaunay, & Traonvouez, 2016). The industrial waste heat supply is discontinuous, and there is always a long distance between the heat source and heat demand. Therefore, it is necessary to seek a thermal storage system for storing industries waste heat, then releasing the stored waste heat according to needs. PCMs as high-efficiency thermal storage systems, due to their relatively

higher thermal capacity and storage density and good operating reliability, were used for storing or releasing industries waste heat via their phase transition behaviors. Such ability possessed by this system not only allows the possibility of bridging the temporal and geographical gaps between the heat supply and demand but also helps to extend the utilization of industrial waste heat. During the past years, the PCMs-assisted thermal energy storage systems for industrial waste heat storage have received an extensive amount of attention. As summarized by Miró et al, desirable PCMs for industrial waste heat storage should have suitable phase change temperature (usually lower than 300 °C) to meet the application requirements, high enthalpy to make sure a large heat storage capacity and good thermal and chemical stability for long-term use. Cost effective and good compatibility with commonly used container materials are favored considering the budget for waste heat storage systems (Miró, Gasia, & Cabeza, 2016).

4.5 Solar energy use

Solar water heaters are becoming popular nowadays and are alternatives to gas or electric hot water systems. One single solar water heater can reduce ~50 tons of CO_2 emissions to the atmosphere in a 20-year period (Kee, Munusamy, & Ong, 2018). However, efficient thermal energy storage systems are important for storing solar thermal energy for water heating purposes. Solar-thermal energy can be stored in the form of latent heat by using a suitable PCM. Integration of solar thermal heating systems with solid-liquid PCMs based thermal energy storage technology would enhance the efficiency of existing solar-thermal water heating systems. The amount of heat that a water tank installed with PCMs absorbs is much higher than that of a normal water tank filled with only water. Fewer fluctuations in the temperature of the stored water are another key advantage of the latent heat storage systems based on PCMs. Paraffin wax (melting point: 54 °C) is a very commonly used latent heat storage PCM for solar water heating. Hasan et al. also studied some fatty acids as potential candidates for PCM latent heat storage for domestic water heating and recommended that myristic acid, palmitic acid, and stearic acid, with melting temperatures between 50 and 70 °C are the most promising PCMs for solar water heating (Hasan, & Sayigh, 1994). Tayeb et al. developed a hot water heating system using $Na2SO_4 \cdot 10H_2O$ as the PCMs and compared it with the simulation model that gives the optimum flow rate of the inlet water supply required to maintain the constant temperature of the water at the outlet (El Qarnia, 2009).

In addition, PCMs can also be incorporated into thermophotovoltaics (TPV) technology for accelerating the

conversion of heat radiation into electrical energy (Datas, & Martí, 2017; Veeraragavan, Montgomery, & Datas, 2014). In general, thermal radiation is directly converted to electrical power by photovoltaic cells. The operating temperature range is >1000 °C, TPV has advantages over concentrating solar power as it does not involve any mechanically moving part and thus low maintenance cost. The solar energy that can be harvested during insolation period can be stored in thermal energy storage systems comprising of PCMs and used efficiently at night for power generation applications by coupling thermal energy storage system with TPV. A heat-to-electricity efficiency greater than 50% is reported in the literature, which makes the system more versatile. Veeraragavan et al. conducted a night-time performance analysis of a PCM-based TES integrated with a solar TPV system and found average night power density up to 30.8 W·m-2 with a storage duration of 7.3 h. Silicon as a PCM having 1800 kJ/kg latent heat is an attractive option for this application, but larger storage tanks have the disadvantage of low power output. The need for heat transfer enhancement in the design of the PCM storage tank is highly recommended for efficient systems (Datas, Chubb, & Veeraragavan, 2013).

4.6 Thermal management of the batteries

Demand for rechargeable batteries, most importantly for lithium-ion batteries (LIBs), grows rapidly due to their high energy densities for use in portable electronics, battery powered tools, and electric vehicles. The main barriers in using these batteries for large fleets of vehicles on public roads are the safety, costs related to cycle and calendar life, and performance. These challenges are coupled with thermal effects in batteries. For a better battery pack, the rate of heat dissipation should be fast enough so that the battery pack never reaches the thermal runaway temperatures (Khan, Swierczynski, & Kær, 2017). However, larger power demands and increasing energy density of lithium-ion battery packs result in higher operating temperatures. Most of the commercial LIB chemistries tend to degrade or age at or above 60 °C, which leads to rapid loss of capacity over subsequent charge/discharge cycles as well as reduced overall power output. In order to address these concerns, numerous studies into both active and passive thermal management systems for batteries have been undertaken for many applications that use LIBs. Thermal management systems rely on the transfer of heat away from the cell surface, thereby inhibiting core temperature rise and limiting material degradation. PCMs are very commonly used to effectively mitigate large temperature escalation during discharging as well as charging, thereby relieving performance degradation over the life of the battery and increasing the safety of the battery system (Ling et al., 2014). Passive thermal

management using PCMs for LIBs in all-electric vehicles (EV) and hybrid electric vehicles (HEV) have been studied by Said et al. at the Illinois Institute of Technology (Al-Hallaj et al., 2005).

References

A. Hasan, & A. A. Sayigh. (1994). Some fatty acids as PCM energy storage materials. *Renewable Energy*, *4*(I), 69–76.

Abhat, A. (1983). Low temperature latent heat thermal energy storage: Heat storage materials. *Solar Energy*, *30*(4), 313–332. https://doi.org/10.1016/0038-092X(83)90186-X

Al-Hallaj, S., Kizilel, R., Lateef, A., Sabbah, R., Farid, M., & Rob Selman, J. (2005). Passive thermal management using phase change material (PCM) for EV and HEV Li-ion batteries. *2005 IEEE Vehicle Power and Propulsion Conference, VPPC*, *2005*, 376–380. https://doi.org/10.1109/VPPC.2005.1554585

Baetens, R., Jelle, B. P., & Gustavsen, A. (2010). Phase change materials for building applications: A state-of-the-art review. *Energy and Buildings*, *42*(9), 1361–1368. https://doi.org/10.1016/j.enbuild.2010.03.026

Cabeza, L. F., Castellón, C., Nogués, M., Medrano, M., Leppers, R., & Zubillaga, O. (2007). Use of microencapsulated PCM in concrete walls for energy savings. *Energy and Buildings*, *39*(2), 113–119. https://doi.org/10.1016/j.enbuild.2006.03.030

Chen, H., Cong, T. N., Yang, W., Tan, C., Li, Y., & Ding, Y. (2009). Progress in electrical energy storage system: A critical review. *Progress in Natural Science*, *19*(3), 291–312. https://doi.org/10.1016/j.pnsc.2008.07.014

Datas, A., Chubb, D. L., & Veeraragavan, A. (2013). Steady state analysis of a storage integrated solar thermophotovoltaic (SISTPV) system. *Solar Energy*, *96*, 33–45. https://doi.org/10.1016/j.solener.2013.07.002

Datas, A., & Martí, A. (2017). Thermophotovoltaic energy in space applications: Review and future potential. *Solar Energy Materials and Solar Cells*, *161*(October 2016), 285–296. https://doi.org/10.1016/j.solmat.2016.12.007

El Qarnia, H. (2009). Numerical analysis of a coupled solar collector latent heat storage unit using various phase change materials for heating the water. *Energy Conversion and Management*, *50*(2), 247–254. https://doi.org/10.1016/j.enconman.2008.09.038

Farid, M. M., Khudhair, A. M., Razack, S. A. K., & Al-Hallaj, S. (2004). A review on phase change energy storage: Materials and applications. *Energy Conversion and Management*, *45*(9–10), 1597–1615. https://doi.org/10.1016/j.enconman.2003.09.015

Gulfam, R., Zhang, P., & Meng, Z. (2019). Advanced thermal systems driven by paraffin-based phase change materials – A review. *Applied Energy*, *238*(January), 582–611. https://doi.org/10.1016/j.apenergy.2019.01.114

Hale, D. V, Hoover, M. J., & Neill, M. J. O. (1971). *PHASE CHANGE MATERIALS HANDBOOK by NASA Contractor Report NASA CR-51363*. 232. Retrieved from http://hdl.handle.net/2060/19720012306

Hasnain, S. M. (1998). Review on sustainable thermal energy storage technologies, part I: Heat storage materials and techniques. *Energy Conversion and Management*, *39*(11), 1127–1138.

Kee, S. Y., Munusamy, Y., & Ong, K. S. (2018). Review of solar water heaters incorporating solid-liquid organic phase change materials as thermal storage. *Applied Thermal Engineering*, *131*, 455–471. https://doi.org/10.1016/j.applthermaleng.2017.12.032

Kenisarin, M., & Mahkamov, K. (2007). Solar energy storage using phase change materials. *Renewable and Sustainable Energy Reviews*, *11*(9), 1913–1965. https://doi.org/10.1016/j.rser.2006.05.005

Khan, M. R., Swierczynski, M. J., & Kær, S. K. (2017). Towards an ultimate battery thermal management system: A review. *Batteries*, *3*(1). https://doi.org/10.3390/batteries3010009

Li, D., Wang, J., Ding, Y., Yao, H., & Huang, Y. (2019). Dynamic thermal management for industrial waste heat recovery based on phase change material thermal storage. *Applied Energy*, *236*(1), 1168–1182. https://doi.org/10.1016/j.apenergy.2018.12.040

Ling, Z., Zhang, Z., Shi, G., Fang, X., Wang, L., Gao, X., … Liu, X. (2014). Review on thermal management systems using phase change materials for electronic components, Li-ion batteries and photovoltaic modules. *Renewable and Sustainable Energy Reviews*, *31*, 427–438. https://doi.org/10.1016/j.rser.2013.12.017

Liu, F., Wang, J., & Qian, X. (2017). Integrating phase change materials into concrete through microencapsulation using cenospheres. *Cement and Concrete Composites*, *80*, 317–325. https://doi.org/10.1016/j.cemconcomp.2017.04.001

Merlin, K., Soto, J., Delaunay, D., & Traonvouez, L. (2016). Industrial waste heat recovery using an enhanced

conductivity latent heat thermal energy storage. *Applied Energy*, *183*, 491–503. https://doi.org/10.1016/j.apenergy.2016.09.007

Miró, L., Gasia, J., & Cabeza, L. F. (2016). Thermal energy storage (TES) for industrial waste heat (IWH) recovery: A review. *Applied Energy*, *179*, 284–301. https://doi.org/10.1016/j.apenergy.2016.06.147

Morovat, N., Athienitis, A. K., Candanedo, J. A., & Dermardiros, V. (2019). Simulation and performance analysis of an active PCM-heat exchanger intended for building operation optimization. *Energy and Buildings*, *199*, 47–61. https://doi.org/10.1016/j.enbuild.2019.06.022

Mourid, A., El Alami, M., & Kuznik, F. (2018). Experimental investigation on thermal behavior and reduction of energy consumption in a real scale building by using phase change materials on its envelope. *Sustainable Cities and Society*, *41*, 35–43. https://doi.org/10.1016/j.scs.2018.04.031

Pielichowska, K., & Pielichowski, K. (2014). Phase change materials for thermal energy storage. *Progress in Materials Science*, *65*, 67–123. https://doi.org/10.1016/j.pmatsci.2014.03.005

Pillai, K. K., & Brinkworth, B. J. (1976). The storage of low grade thermal energy using phase change materials. *Applied Energy*, *2*(3), 205–216. https://doi.org/10.1016/0306-2619(76)90025-8

Porisini, F. C. (1988). Salt hydrates used for latent heat storage: Corrosion of metals and reliability of thermal performance. *Solar Energy*, *41*(2), 193–197. https://doi.org/10.1016/0038-092X(88)90136-3

Rathod, M. K., & Banerjee, J. (2013). Thermal stability of phase change materials used in latent heat energy storage systems: A review. *Renewable and Sustainable Energy Reviews*, *18*, 246–258. https://doi.org/10.1016/j.rser.2012.10.022

Raud, R., Jacob, R., Bruno, F., Will, G., & Steinberg, T. A. (2017). A critical review of eutectic salt property prediction for latent heat energy storage systems. *Renewable and Sustainable Energy Reviews*, *70*(October 2016), 936–944. https://doi.org/10.1016/j.rser.2016.11.274

Rozanna, D., Chuah, T. G., Salmiah, A., Choong, T. S. Y., & Sa'ari, M. (2005). Fatty Acids as Phase Change Materials (PCMs) for Thermal Energy Storage: A Review. *International Journal of Green Energy*, *1*(4), 495–513. https://doi.org/10.1081/ge-200038722

Sarier, N., & Onder, E. (2012). Organic phase change materials and their textile applications: An overview. *Thermochimica Acta*, *540*, 7–60. https://doi.org/10.1016/j.tca.2012.04.013

Sharma, A., Tyagi, V. V., Chen, C. R., & Buddhi, D. (2009). Review on thermal energy storage with phase

change materials and applications. *Renewable and Sustainable Energy Reviews*, *13*(2), 318–345. https://doi.org/10.1016/j.rser.2007.10.005

Sharma, R. K., Ganesan, P., Tyagi, V. V., Metselaar, H. S. C., & Sandaran, S. C. (2015). Developments in organic solid-liquid phase change materials and their applications in thermal energy storage. *Energy Conversion and Management*, *95*, 193–228. https://doi.org/10.1016/j.enconman.2015.01.084

Steinmann, W. D. (2017). Thermo-mechanical concepts for bulk energy storage. *Renewable and Sustainable Energy Reviews*, *75*(October), 205–219. https://doi.org/10.1016/j.rser.2016.10.065

Veeraragavan, A., Montgomery, L., & Datas, A. (2014). Night time performance of a storage integrated solar thermophotovoltaic (SISTPV) system. *Solar Energy*, *108*, 377–389. https://doi.org/10.1016/j.solener.2014.07.005

Wu, W. F., Liu, N., Cheng, W. L., & Liu, Y. (2013). Study on the effect of shape-stabilized phase change materials on spacecraft thermal control in extreme thermal environment. *Energy Conversion and Management*, *69*, 174–180. https://doi.org/10.1016/j.enconman.2013.01.025

Xie, N., Huang, Z., Luo, Z., Gao, X., Fang, Y., & Zhang, Z. (2017). Inorganic salt hydrate for thermal energy storage. *Applied Sciences (Switzerland)*, *7*(12). https://doi.org/10.3390/app7121317

Yuan, Y., Zhang, N., Tao, W., Cao, X., & He, Y. (2014). Fatty acids as phase change materials: A review. *Renewable and Sustainable Energy Reviews*, *29*, 482–498. https://doi.org/10.1016/j.rser.2013.08.107

Zalba, B., Mar ń, J. M., Cabeza, L. F., & Mehling, H. (2003). Review on thermal energy storage with phase change: Materials, heat transfer analysis and applications. In *Applied Thermal Engineering* (Vol. 23). https://doi.org/10.1016/S1359-4311(02)00192-8

Appendix 2: Thermal-regulated textiles

Recently, the incorporation of PCMs into textiles to fabricate thermo-regulated smart textiles through coating or encapsulation has grown interest to the researcher. Textiles containing PCMs react immediately with changes in environmental temperatures, and the temperatures in different areas of the body. When a rise in surrounding temperature occurs, the PCMs change from solid state to liquid state by absorbing heat and storing this energy in the liquefied PCMs. When the surrounding temperature falls again, stored latent heat was released from liquefied PCMs and the PCMs solidify again. Owing to the absorbing or releasing heat energy automatically from the phase transition behavior of PCMs facing with the change of surrounding temperature, a thermal regulation ability was obtained when textiles were incorporated with PCMs. When the phase change temperature of selected PCMs was closed to the comfort temperature of human body (14-35 °C), textiles or clothing incorporated with these PCMs can offer satisfactory thermal comfort to wearers. According to the different application objectives, PCMs with different phase temperatures are used in different textiles to obtained various thermal-regulated textiles, which can be used in various fields. Until now, apart from clothing field, these thermal-regulated textiles have been also used in blankets, medical field, insulation, protective clothing and many others. Thermal-regulated textiles have not only become an important part of daily life, but also have played their role in some special fields. The first step for using PCMs in textiles is microencapsulation the PCMs into shell matrix to obtain phase change microcapsules (mPCMs). Then, there are lots of methods to achieve the incorporation of mPCMs with textiles for fabricating final thermal-regulated textiles, mainly including fibers forming technologies, coating and lamination (Mondal, 2008).

1. How PCMs works in textiles

In general, before using PCMs in textiles, PCMs need to be encapsulated into shell matrix to form phase change microcapsules (mPCMs). Thus, when the solid-liquid transition of PCMs occurs, liquid PCMs have fluidity and are easy to leak and lose. The existence of shell materials not only prevents the leaching behavior of PCMs, but also improves the durability of PCMs in textiles. Some external mechanical action, thermal changes and interactions with chemicals can be resisted by the shell matrix of mPCMs.

With the increasing of outside temperature, the temperature in the inner of mPCMs also increased. When the inner temperature of mPCMs reaches the melting point of PCMs, PCMs melt from solid state to liquid state via absorbing external heat, and this heat energy was stored in liquid PCMs. Due to the cooling effect caused by heat absorption of the PCMs, the textiles incorporated with PCMs also offer a cooling feeling to human body in a hot environment. On the contrary, with the decreasing of outside temperature, the temperature in the inner of PCMs also decreased. When the inner temperature of mPCMs drops to the freezing point of PCMs, PCMs solidify from liquid state to solid state. During this phase transition process, the stored heat energy in liquid PCMs is released from mPCMs. Due to the heating effect caused by heat emission of the PCMs, the textiles incorporated with PCMs can also offer a heating feeling to human body in a cold environment. Meanwhile, a thermo-regulating effect, resulting from either the heat absorption or heat emission of the PCMs which is used to keep the temperature of a surrounding substrate (textiles) nearly constant when faced with environmental temperature fluctuations. In addition, an active thermal barrier effect, resulting from either heat absorption, or heat emission of the PCM which regulates for instance, in a garment system the heat flux from the human body into the environment and adopts it to the thermal needs (i.e. activity level, ambient temperature).

Shin et al. published that the polyester knit with an ability of absorbing 4.44 J/g during a melting process was obtained via introducing 23 % n-eicosane/melamine-formaldehyde mPCMs prepared from in situ polymerization. The heat of absorption by the mPCMs delays the microclimate temperature increase of clothing. This leads to enhanced thermo-physiological comfort and prevents heat stress (Shin, Yoo, & Son, 2005). Wang et al. also investigated the impact of PCMs on smart thermal-protective clothing. By absorbing heat or releasing heat in phase transition process, the PCMs can play the role of thermal buffer material in textile matrix (Wang, Li, Hu, Tokura, & Song, 2006).

2. How to incorporate PCMs in textiles

In general, PCMs were used with fibers, textiles and foams together to fabricate corresponding thermal-regulated productions. And the common methods for achieving the incorporation of PCMs into textiles (or fibers, foams) includes coating, lamination, finishing, melt spinning, wet spinning, dry spinning, electrospinning, bi-component synthetic fiber extrusion, injection molding and foam techniques.

2.1 Microencapsulation

When PCMs were used for fabricating thermal-regulated textiles, there are still some problems to be solved. Firstly, when the solid-liquid transition of PCMs occurs, liquid PCMs have fluidity and are easy to leak and lose during their fabrication and application processes. Secondly, due to the fluidity of PCMs and the interactions (or contacts) between PCMs and external mediums (including heat source, fire source, mechanical stress and chemical reagents), the safety, durability and stability of PCMs in textiles still needs to be further improved. In addition, low density, high volatilization, low thermal conductivity and flammability characteristics also limited the application of PCMs. Microencapsulation technology is a suitable method to overcome and improve these drawbacks (Alva, Lin, Liu, & Fang, 2017; Cao, & Yang, 2014; Qiu, Li, Song, Chu, & Tang, 2012).

Firstly, microencapsulation is one of the protection or preservation techniques of PCMs via surrounding them into inorganic or polymeric shell, and leads them to a pseudo-solid compound regardless of their physical state. It can effectively limit leaching behavior coming from liquefied PCMs and prevents leakage of PCMs during phase transition as well as application process. Meanwhile, it also protects them from the surrounding environment (or external mediums). Therefore, it significantly improves the stability and durability of the PCMs. Furthermore, the increase in the surface/volume ratio of microencapsulated PCMs (mPCMs) leads to an increase in the specific contact surface area, which improves their heat transfer efficiency as well as their thermal conductivity depending on the chosen polymer shell. Depending on the selection of different shell materials, mPCMs are also endowed some new properties (Wang, Wang, Geng, & Fang, 2016; Zhang, Chen, Campagne, & Salaün, 2020). For example, when some inorganic materials with flame retardant properties (e.g. silicon materials or clay nano-particles (Clay-NPs) doped gelatin/sodium alginate)) were used for encapsulating PCMs, the flammability of PCMs was reduced obviously (Demirbağ, & Aksoy, 2016; Fang, Li, Chen, & Liu, 2010). Furthermore, the volatilization of PCMs is also avoided by the existence of shell materials.

In addition, the processability of PCMs in various fabrication and functionalization processes was improved obviously when they are microencapsulated. More importantly, when some active substances that forms interfacial interactions with textiles are used as shell materials for achieving the encapsulation process of PCMs, the durability of mPCMs-incorporated textiles will be enhanced obviously.

2.2 Fibers forming technologies

In general, textile productions are fabricated via spinning, twisting, weaving, dyeing/printing and finishing

the fibers. The common method for achieving the incorporation of mPCMs in textiles is adding mPCMs into the polymer spinning melt, polymer spinning solution, or base material. And then, mPCMs-incorporated fibers are spun according to the conventional methods such as dry spinning, wet spinning, electrospinning and melting spinning. The mPCMs-incorporated fibers can store heat over long periods, and slowly radiate heat if the surrounding temperature drops.

Jiang et al. prepared paraffin/polyvinyl alcohol (PVA) thermal-regulated composite fibers via wet spinning. In this fiber, PVA was the matrix or ‘‘sea’’ polymer to support the ‘‘island’’ paraffin, which was selected as phase change materials (PCMs) to store energy. Because of the excellent barrier ability of PVA to nonpolar substances, paraffin was remained in fiber stably. They also published that the thermal regulating fiber has the acceptable thermal stability when the content of paraffin in fiber was less than 30%. The best fiber properties of tensile strength 2.6 cN/dtex, breakage elongation 19.9%, latent heat 24.45 J/g can be achieved by manipulating the preparation process, and the latent heat of the fiber still remains 24.32 J/g after 25 times washing (Jiang, Song, Ye, & Xu, 2008). According to Li et al., an in-situ grafted/crosslinked process between polyethylene glycol (PEG200 and PEG2000) and polyvinyl alcohol (PVA) was achieved during the process of dry spinning based on butane tetracarboxylic acid (BTCA) as crosslinking agent. Based on this method, not only PEG200 (or PEG2000)/PVA composite fibers with a latent heat of 28-34 J/g were obtained, but also the PEG200 (or PEG2000) was fixed steadily in PVA fiber matrix (Li, He, Xu, & Jiang, 2015). And Hu et al. encapsulated bio-based PCMs (natural soy wax) into polyurethane (PU) ultrafine fibers via coaxial electrospinning device (Hu, & Yu, 2012). The results indicated that a uniform fiber morphology with a core-shell structure, and a homogeneous wax distribution throughout the core of the fibers can be obtained from coaxial electrospinning. When the addition of wax reached 60 wt%, the latent heat of these thermal-regulated nanofibers reached 36.47 J/g with a phase transition temperature of about 50 °C. Due to the existence of core-shell structure, these composite fibers have good thermal stability and reliability. After 100 heating-cooling test cycles, the thermal properties of these fibers were unaltered. According to Xiang et al., PEG (molecular weight: 1500 g/mol) was encapsulated by acid-etching halloysite nanotubes (A-HNTs) for preparing a novel PCMs (PEG/A-HNTs) with excellent thermal reliability and stability. Then, PEG/A-HNTs were incorporated into polyamide 66 (PA66) via melt blending extrusion (Xiang, Zhou, Zhang, Innocent, & Zhu, 2019). Finally, PEG/A-HNTs/PA66 thermal-regulated fibers were prepared from melting spinning.

2.3 Coating

Currently, there are two common concepts to define functional coating. On the one hand, a functional coating as described by Wulf et al. is a system possessing the classical properties of a coating (i.e. decoration and protection) and an additional functionality which was brought for example by thermal insulation, thermal regulation, moisture management, soil release, softening, self cleaning, insect repellent, antimicrobial, or flame retardant properties (Martin, 2019; Salaün, 2016). Thus, a functional coating is sensitive to environmental changes and responds permanently to a stimulus. On the other hand, according to Baghdachi, a smart coating corresponds to a coating being able to sense its environment and make an appropriate response to that stimulus in changing its physical or chemical properties, and preferably in a reversible way (Baghdachi, 2009). Therefore, functional or smart coating can be classified as different type depending on their functional characteristics, i.e. with optical, thermal, physic-chemical, structural and mechanical, electrical or magnetic, and hygienic properties. According the property desired, the action of the functional coating occurs either at film-substrate interface, in the bulk of the coating, or at the air-coating interfaces.

For the two last decades, the number of applications of capsules in combination with coating has grown to bring new functional properties of the substrate, which would not be possible with any other existing technology. The coating film can act not only to promote adhesion between all components and therefore their durability, to modify the properties in the bulk such as opacity, colour, diffusion etc., but also to improve mechanical resistance and surface state at the top surface. Therefore, according the location of the microparticles in the coating layer and their purposes, they can be completely embedded, or partially remained at the surface.

The first step for achieving the functional coating of textiles by mPCMs to fabricate thermal-regulated textiles is preparing coating working solution. This solution for textiles mainly consists of wetted mPCMs dispersed throughout a polymer binder, a surfactant, a dispersant, an antifoam agent and a thickener. And the common polymer binders are acrylic, vinyl acrylate, carboxylated butadiene acrylonitrile and polyurethane, etc (Shim, 2018). To prepare the coating working solution, mPCMs are wetted and dispersed in a dispersion of water solution containing a surfactant, a dispersant, an antifoam agent and a polymer binder. Then, this mixture is applied on the surface of textile substance. In general, the coating of targeted textiles by working solution is carried out by knife-over-roll, knife-over-air, pad-dry-cure, gravure coating, screen coating, transfer coating and spraying (Choi, Cho, Kim, & Cho, 2004; Salaün, Devaux, Bourbigot, & Rumeau, 2010; Shin et al., 2005; Yvonne, & David,

1996).

Knife-over-roll

Knife-over-roll coating is a common technique for achieving the functional modification of textiles. In this process, as shown in Figure A2-1, coating working solution (or coating layer) is placed on the textiles, the knife blade is suspended above a roller. The roller can be steel or rubber coated. The knife does not touch the substrate directly and there is a gap between the substrate and the knife, which controls the thickness of the coating. With the rotation of the roller, the coating working liquid is covered extensively and evenly on the textiles. The gap between the roller and the blade can be set very accurately to enable precise thickness control, but variations in substrate thickness can make the thickness of the coating nonuniform. In knife coatings, blade geometry (the shape and angle of the blade), blade flexibility, and the rheology of the coating fluid affect the amount of coating applied and the extent of penetration into the substrate (Shim, 2018).

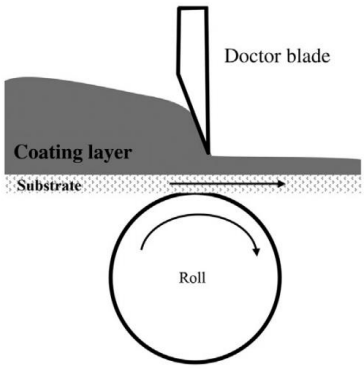

Figure A2 -1 Knife coating: knife-over-roll coating.

Kim et al. prepared a thermal-regulated textiles consisted of 100 % polyester fabrics and octadecane-containing microcapsules by a knife-over-roll coating process. Although the durability of the coated microcapsules lasts for about ten launderings, the treated fabric becomes stiffer and less smooth, soft, and full than the untreated fabric (Kim, & Cho, 2002). From DSC results, when the addition of microcapsules reached 40 %, the latent heat of treated polyester fabrics can reach 5.6 kJ/kg. Choi et al. also fabricated polyester fabrics coated with octadecane/melamine formaldehyde microcapsules via knife-over-roll method. A comparison between knife-over-roll method and screen printing method on their effects on the structures and properties of treated fabrics was also be discussed (Choi et al., 2004).

Knife-over-air

The air-knife coating process is illustrated in Figure A2-2. Instead of a knife blade, excess coating working solution is applied to the textiles and blown off by an air jet coming from the so-called air knife. Interactions between air jet and the liquid coating film is a key mechanism to control coating film thickness (Myrillas et al., 2013).

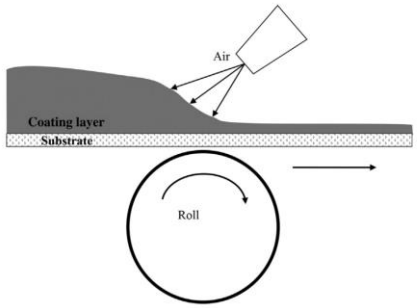

Figure A2 - 2 Knife-over-air coating.

Pad-dry-cure

According to Shin et al, melamine-formaldehyde microcapsules containing eicosane were coated on the surface of polyester knit fabrics by a conventional pad-dry-cure process to develop thermos-regulated textiles (Shin et al., 2005). With increasing the addition of eicosane/melamine-formaldehyde microcapsules, the latent heat of the mPCMs-coated textiles also increased gradually. When the addition of mPCMs reached 23 %, the heat storage capacities of thermal-regulated fabrics reached 0.91–4.44 J/g. Finally, the treated fabrics retained 40% of their heat storage capacity after five launderings.

Gravure roll coating

Gravure roll coating is the process where engraving on the roller acts as a metering device. The engraved roller is partly submerged in the coating bath and as it rotates, coating liquid fills the engraved pattern and excess coating liquid forms a film on the roller's surface (Figure A2-3). A doctor blade removes the excess surface film from the gravure roller surface and it then presses against the substrate to transfer the coating material in the engraved pattern to the substrate. This method can operate in either forward or reverse mode, but, as discussed before, the reverse mode generally provides greater stability.

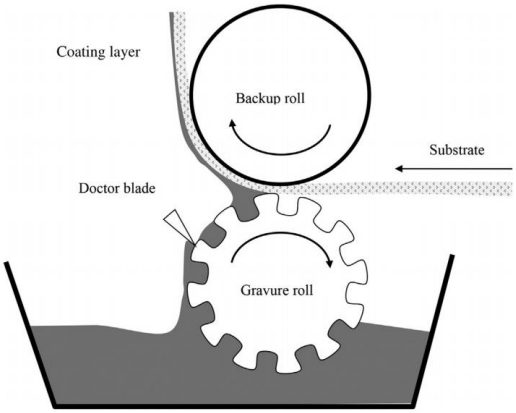

Figure A2 - 3 Gravure roll coating.

The amount of coating material delivered to the substrate is mainly controlled by the engraved patterns. Various patterns are used, examples being regular dot, irregular, quad, net structured, and rhomboid patterns (Hewson, Kapur, & Gaskell, 2006). The most important characteristics of engraved patterns that affect the amount of coating material delivered are the land area, cell openings, cell depths, cell volumes, cell angles, and cell spaces. Other parameters include viscosity of the coating material, application pressure on the substrate and type and structure of the substrate. Gravure roll coating can be used for different fluids, including hot melt adhesives. It can also produce patterned coating.

Screen coating

Screen coating is the deposition of a coating material on a substrate through a mesh screen by squeezing. The amount of coating is determined by the screen mesh number, squeeze pressure, the angle between the squeeze blade and the screen, and the viscosity of the coating fluid. It induces little or no friction or tension between the screen and the substrate, so lightweight and delicate substrates can be processed. Screen printing is also ideal for applying even coatings to substrates with uneven surfaces.

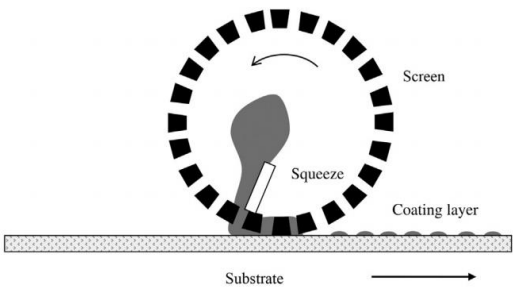

Figure A2 - 4 Screen coating.

One application of screen coating is paste dot coating. In paste dot coating, a dispersion paste consisting of

a mixture of thermo-fusible powder, a binder and water, is directly applied onto the substrate through a rotating screen (Figure A2-4). It is frequently used in interlining production for adhesive coatings on delicate fabrics. A hot melt dot coating can be done using screen coating. It is sometimes referred to as hot melt printing. Premelted hot melt resin is transferred to the substrate through the screen. This method has advantages over engraved roll coating due to the screen being cheaper, shorter exchange times, ease of controlling the amount of coating applied, and lower friction. Screen coating is also used for electrical applications, such as circuit board printing, because it provides good pattern definition with a properly masked screen and precise coating thickness control.

Transfer coating

Transfer coating is a sequential coating process where the coating material is first applied to a silicone release paper and then dried. This coated silicone release paper passes through the laminating rollers with the substrate, with the coating layer facing the substrate surface. Heat and pressure applied by rollers and ovens cause coating layer bonding with the substrate. The release paper is then peeled away, leaving a smooth or embossed, as desired, coated surface (Figure A2-5).

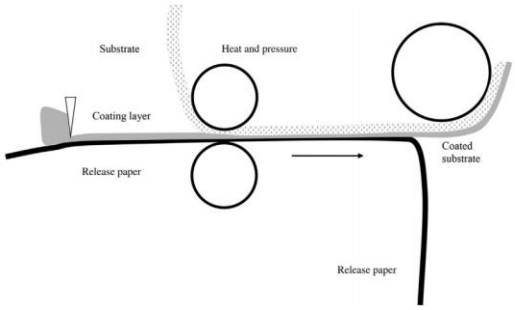

Figure A2 - 5 Transfer coating.

Despite the fact that transfer coating is more expensive than direct coating, it can be used for very delicate substrates, since little or no tension is applied during the process. Another advantage is the low degree of penetration, which reduces stiffness and generates flexible coated fabrics.

Spraying

The coating working solution can be sprayed directly onto the substrate surface. Spray coating methods include pressed air vaporization, airless pressure spray, hot flame spray, hot vapor impelled spray, electrospraying, and dry powder resin spray (Jaworek & Sobczyk, 2008; Voyer, Schulz, & Schreiber, 2008). Among these method, electrospraying has great potential and advantages for achieving the functional coating of textiles by special

microcapsules. On the one hand, the phase change microcapsules (mPCMs) with a mono-dispersed size distribution can be prepared easily from electrospraying process. Meanwhile, the mean diameter, surface morphology, core-shell structure and multi-shell structure of electrosprayed mPCMs can be designed and controlled effectively via adjusting the physico-chemical properties of electrospraying solution as well as operating parameters. On the other hand, the functional coating of textiles by electrosprayed mPCMs can be carried out directly during the fabrication process of mPCMs when targeted textiles is placed on the surface of collector as shown in Figure 2A-6. During the electrostatic coating process, electrosprayed mPCMs can be deposited directly on the surface of textiles without the use of polymeric binders, surfactant, dispersion agent and antifoam agent. Therefore, not only a green, non-toxic and high-efficiency coating process can be obtained from electrospraying, but also the original structures and morphologies of textiles matrix can be can be preserved to the greatest extent (Zhang, Campagne, & Salaün, 2020). Meanwhile, the coating thickness of mPCMs on textiles can be adjusted via changing electrospraying time. In addition, in order to enhance the interfacial adhesion between mPCMs and textiles, an outer active shell which can form interactions with textiles can be designed on mPCMs based on coaxial electrospraying (Zhang, Chen, et al., 2020). Therefore, electrostatic coating has the advantage to provide some improved properties in terms of durability and thermal comfort to textiles, while maintaining the mechanical properties, breathability and flexibility of the textiles. This is something that conventional coating methods can't achieve. Thus, the use of binders, surfactant, antifoam agent and dispersion agent from conventional methods will damage the original structure and performance of the textiles (mainly including the fabric hand, flexibility, toughness and breathability, etc.).

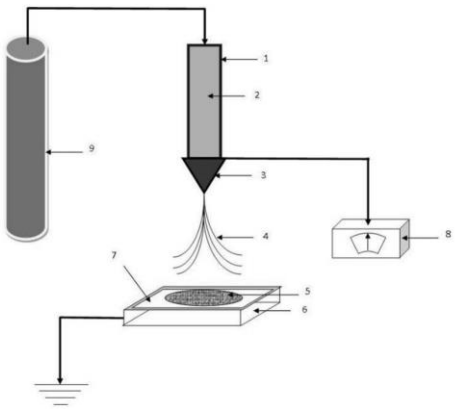

Figure A2 - 6 The schematic diagram of Electrospraying 1) Solution container, 2) Polymer solution, 3) Specially designed nozzle, 4) Electrospray, 5) Sprayed area, 6) Collector plate, 7) Fabric, 8) High voltage power supply, 9) Compressed gas cylinder.

2.4 Lamination

The second method for achieving the incorporation of mPCMs into textiles to improve the thermo-physiological wearing comfort of clothing is lamination method (Shim, 2018). In general, this method is used to improve thermo-physiological wearing comfort of protective garments. Firstly, mPCMs should be added into polymer solution to fabricate a thin polymer film blended with mPCMs. Then, this mPCMs-incorporated polymer thin film is applied to the inner side of the fabric system by lamination. The cooling or heating effect of the mPCMs can delay the temperature rise or drop when the outside temperature changes. As a result, people wearing mPCMs-incorporated protective garments can obtain a thermal comfort feeling in the face of environmental temperature changes. Meanwhile, with the increasing of moisture in the microclimate, the wearing time of the garments can be extended significantly without the occurrence of heat stress as a serious health risk. The longer wearing times will further lead to a significantly higher productivity. The more comfortable wearing conditions will also result in a reduced number of accidents and lower error rates. Beside chemical protective suits, the mPCMs can also improve the thermo-physiological wearing comfort of some protective garments made of nonwovens such as chemical protective suits, surgical gowns, uniforms, or garments worn in clean rooms.

Laminating processes are categorized according to several criteria: substrate type combinations, the number of layers, and the method used combining. Here, laminating processes are classified by bonding methods into adhesive lamination, flame lamination, and ultrasonic lamination. Adhesive lamination is further classified into three groups according to the nature of the adhesive: wet adhesive lamination, hot melt lamination, and dry heat lamination. Both economic and performance requirements need to be considered when the lamination process is selected.

3. Testing of mPCMs incorporated textiles

The structure and surface morphology of mPCMs as well as mPCMs-incorporated textiles are observed by scanning electron microscopy (SEM) as shown in Figure 2A-7 (Wang, Li, & Li, 2018). The interfacial adhesion between mPCMs and textiles and the voids on textile surface which is related with the durability and breathability of thermal-regulated textiles are also characterized by SEM. The crystal morphology and amorphous morphology of PCM during its phase transition process could be observed by polarized optical microscopy (POM) (Li, & Ding, 2007). Furthermore, the size distribution of mPCMs can also be analyzed by optical microscopy (OM).

Differential scanning calorimetry (DSC) measurement was used to determine the thermal parameters of PCM, mPCMs and mPCMs-incorporated textiles, including the thermal transitions and the associated latent heat values (melting (ΔHm) and crystallization (ΔHC) enthalpies); and the phase change temperatures such as the onset temperatures of solid-liquid and liquid-solid transitions (Tonset), end temperatures of phase transitions (Tend), and maximum temperatures of melting (Tm) and crystallization (Tc) (Alkan, Sari, Karaipekli, & Uzun, 2009). Meanwhile, the thermal stability of PCMs, mPCMs and mPCMs-incorporated textiles including initial thermal degradation temperature, maximum thermal degradation temperature and weight loss, as well as loss rate in different temperature ranges were obtained from thermogravimetric analysis (TGA) (Sari, Alkan, Karaipekli, & Uzun, 2009). For the chemical interactions between mPCMs and textiles were also characterized by infrared spectroscopy (IR) (Zhang, Campagne, et al., 2020). On the other hand, thermo-regulated properties of mPCMs containing textiles were measured by surface cooling rate measurements (Ying, Kwok, Li, Zhu, & Yeung, 2004). The indices of thermal regulating capability (Id and Δtd), static thermal insulation (Is), and the thermal psychosensory intensity (TPI) of textile incorporating phase change materials were obtained by an instrument that is called the Fabric Intelligent Hand Tester (FIHT). The index of static thermal insulation (Is) was calculated from the test data by calculating the mean heat flux at the equilibrium state. The indices of the thermal regulating capability (Id and Δtd) were measured by calculating the differences between the heat flux changes of PCM and non-PCM fabrics. The durability and bonding stanility of mPCMs-incorporated textiles were also characterized by washing treatment, sandpaper friction test and using liner abrasion (Li, Wang, & Li, 2019b, 2019a).

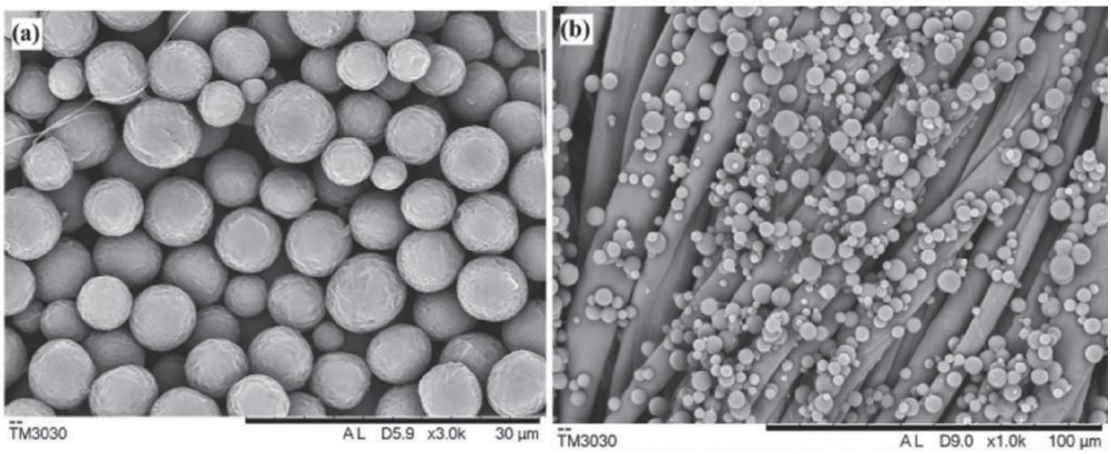

Figure A2 - 7 The SEM image of (a) mPCMs (b) mPCMs-incorporated textiles.

4. Applications of thermal-regulated textiles

4.1 Space

In 1971 year, PCMs technology was first used in space suits and gloves by NASA for protecting astronauts from the bitter cold when working in space (Hale, Hoover, & Neill, 1971). Due to the heating effect resulted from the solidification of PCMs under cold environment, astronaut obtains a thermal comfort feeling at space when he wore the space suit incorporated with PCMs.

4.2 Wearing clothes

From original applications in space suits and gloves, PCMs are nowadays used in the design and application of consumer products as well. In order to improve the thermal comfort feeling of active-wear garments, clothing textiles with thermo-regulating performances are widely used. The thermoregulating effect provided by these textiles is achieved via incorporating with PCMs. Active wear needs to provide a thermal balance between the heat generated by the body and the heat released into the environment while engaging in a sport. Snowboard gloves, underwear, active wear, ice climbing and underwear for cycling and running are some examples of applications of PCMs in sportswear.

4.3 Bedding and accessories

Incorporating mPCMs into quilts, pillows and mattress covers endows a thermal comfort feeling and thermal regulation function to these bedclothes. And people will have a good sleep when they use these bedclothes. Thus, when the body temperature rises, the additional heat energy is absorbed by the melting process of PCMs and the body cools down. When the body temperature drops, the stored energy is released from the solidification of PCMs and the body is kept warm.

4.4 Medical applications

In general, the temperature fluctuations caused by the changes of activity levels as well as external environment trigger the phase transition process of PCMs. Meanwhile, PCMs interact with the microclimate around the human body for offering a thermal comfort feeling. Therefore, the textiles incorporated with mPCMs have potential applications in surgical apparel, patient bedding materials, bandages and products to regulate patient temperatures in intensive care units. PEG-treated fabric is useful in medical and hygiene applications

where both liquid transport and antibacterial properties are desirable, such as surgical gauze, nappies and incontinence products. Heat-storage and thermo-regulated textiles keep the skin temperature within the comfort range, so they are used as a bandage and for burn and heat/cool therapy.

4.5 Shoes and accessories

Currently, mPCMs-incorporated textiles are also used in the design of footwear, especially ski boots, mountaineering boots, race car drivers' boots etc. The phase change technology reacts directly to changes in temperature of both the exterior of the garment and the body. The phase transition temperature of paraffin wax used for preparing mPCMs determines the final use of mPCMs-incorporated textiles, for example, 36.0 °C for a motor cycle helmet and 26.0 °C for gloves. Heat-storage and thermo-regulated textiles absorb, store, redistribute and release heat to prevent drastic changes in the wearer's head, body, hands and feet. In the case of ski boots, the PCMs absorbs the heat when the feet generate excess heat, and send the stored heat back to the cold spots if the feet get chilly. This keeps the feet comfortable. Ski boots, footwear and golf shoes are some of the products where PCMs can be used.

4.6 Others

PCMs are used in automobile textile such as seat cover. Automobile interior applications use paraffin waxes due to their high capacity for heat storage; lack of toxicity, corrosiveness, or hygroscopic properties; low cost; and amenability to mixing to realize the desired temperature range. The paraffin waxes are microencapsulated and applied to a textile matrix. mPCMs-incorporated textiles in headliners and seats provided superior thermal control. Helmets, fishing waders, firefighters' suits, are some other examples of application of PCMs in textiles.

References

Alkan, C., Sari, A., Karaipekli, A., & Uzun, O. (2009). Preparation, characterization, and thermal properties of microencapsulated phase change material for thermal energy storage. *Solar Energy Materials and Solar Cells*, *93*(1), 143–147. https://doi.org/10.1016/j.solmat.2008.09.009

Alva, G., Lin, Y., Liu, L., & Fang, G. (2017). Synthesis, characterization and applications of microencapsulated phase change materials in thermal energy storage: A review. *Energy and Buildings*, *144*, 276–294.

https://doi.org/10.1016/j.enbuild.2017.03.063

Baghdachi, J. (2009). Smart coatings. *ACS Symposium Series*, *1002*, 3–24. https://doi.org/10.1021/bk-2009-1002.ch001

Cao, F., & Yang, B. (2014). Supercooling suppression of microencapsulated phase change materials by optimizing shell composition and structure. *Applied Energy*, *113*, 1512–1518. https://doi.org/10.1016/j.apenergy.2013.08.048

Choi, K., Cho, G., Kim, P., & Cho, C. (2004). Thermal Storage/Release and Mechanical Properties of Phase Change Materials on Polyester Fabrics. *Textile Research Journal*, *74*(4), 292–296. https://doi.org/10.1177/004051750407400402

Demirbağ, S., & Aksoy, S. A. (2016). Encapsulation of phase change materials by complex coacervation to improve thermal performances and flame retardant properties of the cotton fabrics. *Fibers and Polymers*, *17*(3), 408–417. https://doi.org/10.1007/s12221-016-5113-z

Fang, G., Li, H., Chen, Z., & Liu, X. (2010). Preparation and characterization of flame retardant n-hexadecane/silicon dioxide composites as thermal energy storage materials. *Journal of Hazardous Materials*, *181*(1–3), 1004–1009. https://doi.org/10.1016/j.jhazmat.2010.05.114

Hale, D. V, Hoover, M. J., & Neill, M. J. O. (1971). *PHASE CHANGE MATERIALS HANDBOOK by NASA Contractor Report NASA CR-51363*. 232. Retrieved from http://hdl.handle.net/2060/19720012306

Hewson, R. W., Kapur, N., & Gaskell, P. H. (2006). A theoretical and experimental investigation of tri-helical gravure roll coating. *Chemical Engineering Science*, *61*(16), 5487–5499. https://doi.org/10.1016/j.ces.2006.04.021

Hu, W., & Yu, X. (2012). Encapsulation of bio-based PCM with coaxial electrospun ultrafine fibers. *RSC Advances*, *2*(13), 5580–5584. https://doi.org/10.1039/c2ra20532g

Jaworek, A., & Sobczyk, A. T. (2008). Electrospraying route to nanotechnology: An overview. *Journal of Electrostatics*, *66*(3–4), 197–219. https://doi.org/10.1016/j.elstat.2007.10.001

Jiang, M., Song, X., Ye, G., & Xu, J. (2008). Preparation of PVA/paraffin thermal regulating fiber by in situ microencapsulation. *Composites Science and Technology*, *68*(10–11), 2231–2237. https://doi.org/10.1016/j.compscitech.2008.04.004

Kim, J., & Cho, G. (2002). Thermal Storage/Release, Durability, and Temperature Sensing Properties of

Thermostatic Fabrics Treated with Octadecane-Containing Microcapsules. *Textile Research Journal*, *72*(12), 1093–1098. https://doi.org/10.1177/004051750207201209

Li, W. D., & Ding, E. Y. (2007). Preparation and characterization of cross-linking PEG/MDI/PE copolymer as solid-solid phase change heat storage material. *Solar Energy Materials and Solar Cells*, *91*(9), 764–768. https://doi.org/10.1016/j.solmat.2007.01.011

Li, W., Wang, H., & Li, Z. (2019a). Hierarchical structure microspheres of PCL block copolymers via electrospraying as coatings for fabric with mechanical durability and self-cleaning ability. *Polymers for Advanced Technologies*, *30*(9), 2321–2330. https://doi.org/10.1002/pat.4660

Li, W., Wang, H., & Li, Z. (2019b). Preparation of golf ball-shaped microspheres with fluorinated polycaprolactone via single-solvent electrospraying for superhydrophobic coatings. *Progress in Organic Coatings*, *131*(199), 276–284. https://doi.org/10.1016/j.porgcoat.2019.02.039

Li, Z., He, W., Xu, J., & Jiang, M. (2015). Preparation and characterization of in situ grafted/crosslinked polyethylene glycol/polyvinyl alcohol composite thermal regulating fiber. *Solar Energy Materials and Solar Cells*, *140*, 193–201. https://doi.org/10.1016/j.solmat.2015.04.014

Martin W. (2019). coating with self-cleaning properties. *Journal of Chemical Information and Modeling*, *53*(9), 1689–1699.

Mondal, S. (2008). Phase change materials for smart textiles - An overview. *Applied Thermal Engineering*, *28*(11–12), 1536–1550. https://doi.org/10.1016/j.applthermaleng.2007.08.009

Myrillas, K., Rambaud, P., Mataigne, J. M., Gardin, P., Vincent, S., & Buchlin, J. M. (2013). Numerical modeling of gas-jet wiping process. *Chemical Engineering and Processing: Process Intensification*, *68*, 26–31. https://doi.org/10.1016/j.cep.2012.10.004

Qiu, X., Li, W., Song, G., Chu, X., & Tang, G. (2012). Microencapsulated n-octadecane with different methylmethacrylate-based copolymer shells as phase change materials for thermal energy storage. *Energy*, *46*(1), 188–199. https://doi.org/10.1016/j.energy.2012.08.037

Salaün, F. (2016). Microencapsulation technology for smart textile coatings. In *Active Coatings for Smart Textiles*. https://doi.org/10.1016/B978-0-08-100263-6.00009-5

Salaün, F., Devaux, E., Bourbigot, S., & Rumeau, P. (2010). Thermoregulating response of cotton fabric containing microencapsulated phase change materials. *Thermochimica Acta*, *506*(1–2), 82–93.

https://doi.org/10.1016/j.tca.2010.04.020

Sari, A., Alkan, C., Karaipekli, A., & Uzun, O. (2009). Microencapsulated n-octacosane as phase change material for thermal energy storage. *Solar Energy*, *83*(10), 1757–1763. https://doi.org/10.1016/j.solener.2009.05.008

Shim, E. (2018). Coating and laminating processes and techniques for textiles. In *Smart Textile Coatings and Laminates*. https://doi.org/10.1016/B978-0-08-102428-7.00002-X

Shin, Y., Yoo, D. Il, & Son, K. (2005). Development of thermoregulating textile materials with microencapsulated Phase Change Materials (PCM). II. Preparation and application of PCM microcapsules. *Journal of Applied Polymer Science*, *96*(6), 2005–2010. https://doi.org/10.1002/app.21438

Voyer, J., Schulz, P., & Schreiber, M. (2008). Conducting flame-sprayed Al coatings on textile fabrics. *Journal of Thermal Spray Technology*, *17*(4), 583–588. https://doi.org/10.1007/s11666-008-9213-1

Wang, H., Li, W., & Li, Z. (2018). A Facile Strategy for Preparing PCL/PEG Block Copolymer Microspheres via Electrospraying as Coatings for Cotton Fabrics. *Macromolecular Materials and Engineering*, *303*(8), 1–12. https://doi.org/10.1002/mame.201800164

Wang, S. X., Li, Y., Hu, J. Y., Tokura, H., & Song, Q. W. (2006). Effect of phase-change material on energy consumption of intelligent thermal-protective clothing. *Polymer Testing*, *25*(5), 580–587. https://doi.org/10.1016/j.polymertesting.2006.01.018

Wang, T., Wang, S., Geng, L., & Fang, Y. (2016). Enhancement on thermal properties of paraffin/calcium carbonate phase change microcapsules with carbon network. *Applied Energy*, *179*, 601–608. https://doi.org/10.1016/j.apenergy.2016.07.026

Xiang, H., Zhou, J., Zhang, Y., Innocent, M. T., & Zhu, M. (2019). Polyethylene glycol infused acid-etched halloysite nanotubes for melt-spun polyamide-based composite phase change fibers. *Applied Clay Science*, *182*(May), 105249. https://doi.org/10.1016/j.clay.2019.105249

Ying, B. A., Kwok, Y. L., Li, Y., Zhu, Q. Y., & Yeung, C. Y. (2004). Assessing the performance of textiles incorporating phase change materials. *Polymer Testing*, *23*(5), 541–549. https://doi.org/10.1016/j.polymertesting.2003.11.002

Yvonne, G. B., & David, P. C. (1996). Moldable foam insole with reversible enhanced thermal storage properties. *United States Patent, Patent No:US005499460A*

Zhang, S., Campagne, C., & Salaün, F. (2020). Preparation of n -Alkane / Polycaprolactone Phase-Change Microcapsules via Single Nozzle Electro-Spraying : Characterization on Their Formation , Structures and Properties. Applied Sciences, 10(2), 561-580. http://dx.doi.org/10.3390/app10020561

Zhang, S., Chen, Y., Campagne, C., & Salaün, F. (2020). Influence of a Coaxial Electrospraying System on the n-Hexadecane / Polycaprolactone Phase Change Microcapsules Properties. Materials, 13(9), 2205-2221. http://dx.doi.org/10.3390/ma13092205

Appendix 3: conventional technologies for microencapsulation

The most common methods for microencapsulation include interfacial, *in-situ* and suspension polymerization methods for chemical processes and simple or complex phase coacervation for physicochemical processes; spray drying and electrospraying for the physical processes can also be used for specific applications or to obtain dried microcapsules.

1. Interfacial polymerization

Interfacial polymerization is defined as a polymerization process occurred at the interface between two immiscible phases (Kwon, Cheong, & Kim, 2010; Sari, Alkan, & Karaipekli, 2010; Shi et al., 2019). Active monomers, chemical agents and PCMs exist in the water phase and the oil phase, respectively. Most reported methods employ oil-in-water or water-in-oil systems, but oil-in-oil systems were also used to prepare microcapsules (Jiang, Gao, & Shen, 2006; Kobašlija, & McQuade, 2006; Su, Wang, & Ren, 2007; Wu et al., 2014). The formation of polymeric shell at or on a droplet or particles encloses the PCMs to obtain phase change microcapsules (mPCMs). This technology allows a wide range of core materials to be encapsulated, such as aqueous solutions, water-immiscible liquids and solid particles. In all cases, the phase containing the core substance is dispersed until it reaches the desired droplet size in a continuous phase. A key feature of the encapsulation is the diffusion of reagents to the interface to react; during wall formation, the polymeric species create a barrier to diffusion and begin to limit the reaction rate of the interfacial polymerization. The interfacial polymerization method is a widely used microencapsulation method, and one advantage of this technology is to prepare microcapsules with the mean diameter ranged from 1 to 30 μm (Salaün, 2016). In addition, this method also has some disadvantages for preparing microcapsules. Firstly, this process cannot easily produce microcapsules with high active loading content concentration. Secondly, the use of emulsifier in this method also causes a broad size distribution in resulted microcapsules. And the size distribution of final microcapsules is also influenced by type of stirrer used, the stirring speed and the concentration of emulsifier, temperature, etc. Finally, the main drawbacks of this technique are its complexity, the slowness of the reaction, the existence of parasite or secondary reactions that could disturb the system and create some unwanted reactive sides, the use of an organic solvent and, in some cases, non-biocompatible carrier materials as well as toxic chemical agents.

Liang et al. chose toluene-2,4-diisocyanate (TDI) and ethylenediamine (EDA) as monomers, butyl stearate as a core material (PCMs) to fabricate polyurea microcapsules containing PCMs based on interfacial polycondensation method. The results show that the mPCMs were synthesized successfully and that, the phase change temperature was about 29 ℃, the latent heat of fusion was about 80 J/g, the particle diameter was ranging from 20 to 35 μm (Liang, Lingling, Hongbo, & Zhibin, 2009). Zhang et al. encapsulated paraffin into shell matrix successfully to obtain mPCMs via the interfacial polymerization between isophorone diisocyanate and diethylene triamine. The particle size of the prepared microcapsules decreased and related size distribution became narrow, respectively with the increase of the emulsification time, stirring speed and emulsifier amount (Zhang, Shi, Shentu, & Weng, 2017).

2. *in-situ* polymerization

Microncapsulation carried out by an *in-situ* polymerization is based on the presence of active monomers or pre-polymers in a single phase, either in a continuous phase or in a dispersed phase. According to the solubility of monomer, pre-polymer and otained polymer in the continuous medium, Arshady and George denoted three distinct types of polymerization, i.e., (1) suspension polycondensation, when the starting monomer was insoluble in the polymerization medium; (2) precipitation polycondensation if the continuous phase was a solvent and a precipitant for the monomer and polymer, respectively, and (3) dispersion polycondensation for a system when the polymerisation medium is a good and poor solvent for the monomer and polymer, respectively. The microcapsules walls are formed from starting monomers or pre-condensates present only in the discontinuous phase or in the continuous phase (Arshady, & George, 1993).

Among various shell materials that are impermeable, amino resins, especially melamine-formaldehyde and urea-formaldehyde resins, have a main role in the encapsulation of active substances for textile applications (Sarier, & Onder, 2012; Zhang, & Wang, 2009). This process was used to produce microcapsules for various applications such as fragrance or essential oils, insect repellents, flame retardants, dyes and phase change materials (PCMs). *in-situ* polymerization not only allows the formation of microcapsules containing water-immiscible dispersed phase, but also oil-immicible dispersed phase, with improved mechanical properties and thermal stability. The use of melamine-formaldehyde resin has attracted many researchers to improve the thermal stability of the microencapsulated core compound. Furthermore, melamine-formaldehyde pre-polymers offer some advantages for the synthesis of microcapsules because of their high reactivity, and therefore short reaction time and a controlled amount of polymer is required to form

the shell with a high loading content, with good thermal and storage stabilities. Furthermore, other main advantages for using this microencapsulation method is to fabricate microcapsules with adjustable mean diameter and size distribution, and good transferability to large-scale industrial production (Su, Darkwa, & Kokogiannakis, 2015).

The first step of *in-situ* polymerization is to disperse a water-immiscible liquid or solid core materials in an aqueous phase containing monomers (i.e., melamine and formaldehyde; urea and formaldehyde; urea, melamine and formaldehyde), or commercial pre-polymers (ie, partially methylated trimethylolmelamine, dimethylolmelamine, hexamethoxy-methylolmelamine pre-condensates), surfactant and water at an acidic pH. This dispersion is the determining step to establish the size distribution of the final particles with the desired physical properties. The acidic pH value helps to reduce surface tension of the continuous phase, because the intermolecular distance between surfactant molecules is decreased, leading to an enhanced emulsification, and to create electrostatic attraction between the resin and a polyelectrolyte, such as styrene-maleic acid anhydride copolymers, polyacrylic acid, or acrylamido-propylsulfonate and methacrylic acid-acrylic acid copolymers (Fei et al., 2015; Salaün, Vroman, & Aubry, 2009)

Furthermore, the phase volume ratio was established to obtain narrow size distribution and a mean diameter within the range of 1-10 μm in most studies. In the second step of the synthesis, the amino prepolymers, which are initially soluble in the continuous phase, are activated under acidic catalyst action and undergo etherification reactions. This results in an amino pre-polymer of relatively low molecular weight in the continuous phase. In the third step, the reduction of hydroxyl content corresponding to a decrease in the water solubility of the amino resin promotes the phase separation from the continuous phase as a liquid solution relatively rich in active pre-polymer.

3. Suspension polymerization

The suspension polymerization technique leads to the formation of particles with an average diameter between 10 μm and 2 μm, close to the initial droplet. Most of the time, this process refers as bead polymerization or pearl polymerization. The dispersed phase suspended as droplet in the aqueous medium contains a water-insoluble monomer and active agent. The initiator may be solubilized in the monomer or introduced in the continuous phase. Stabilization of these droplets in the continuous medium is ensured by the use of vigorous agitation and hydrophilic polymeric stabilizers such as poly(vinyl alcohol) (PVA), cellulosic derivative or polyvinylpyrrolidone. The aqueous phase may also contain, fillers, buffers or

electrolytes. A washing step is needed after the process is completed to recover the particles. Advantages of this method, mainly used for styrene, methyl methacrylate monomers, are the heat of polymerization absorption by the continuous phase, the formation of spherical beads uniform in size and their release characteristics. Nevertheless, the coalescence of particles during the polymerization process is a main drawback (Sánchez-Silva et al., 2010; Sánchez, Sánchez, Carmona, de Lucas, & Rodríguez, 2008).

Sanchez et al. reported the development of a microencapsulation process based on the suspension polymerization technique to entrap organic PCM by a polystyrene shell (Sánchez, Sánchez, de Lucas, Carmona, & Rodríguez, 2007). They observed that the loading content and particle size distribution vary with the kind and nature of the core materials used. Furthermore, the method was more suitable for an active substance with a hydrophobic nature than with a hydrophilic one. They also noted that the reaction temperature affects the particle morphology, and it should be adjusted to between 98 °C and 113 °C to obtain spherical morphology. The particle size is closely related to the stirring rate. From the investigation of the paraffin/polymer mass ratio, they observed that encapsulation was difficult for a ratio higher than 2 (Sánchez et al., 2008). Furthermore, this encapsulation process was mainly governed by multiple simultaneous mechanisms, ie, coalescence, breakup, nucleation and diffusion of the monomer to the interface, which confers the size, structure, and surface properties of the particles. To improve these properties, they also copolymerized methyl methacrylate with styrene, which led to a decrease in the reaction time and particle size. They also observed that the use of methyl methacrylate improved the loading content because of its higher reactivity and solubility in water.

4. Phase coacervation

Phase coacervation is one of the oldest and most widely used techniques of microencapsulation and can be divided into two groups: simple coacervation, which implies the use of one colloidal solute such as gelatine, chitosan, etc.; and complex coacervation, in which the aqueous polymeric solution is prepared from the interaction of two oppositely charged colloids, such as gelatine (gum arabic or silk fibroin chitosan) (Deveci, & Basal, 2009). Coacervation can be defined as the separation of a macromolecular solution into two immiscible liquid phases: a dense coacervate phase and a dilute equilibrium one. The general outline of this method consists of four consecutive steps carried out under stirring: (1) dispersion of the active substance into a solution of a surface-active hydrocolloid; (2) precipitation of the hydrocolloid onto the dispersed droplets by lowering the solubility of the hydrocolloid (non-solvent, pH change, temperature or electrolyte); (3) addition of a second hydrocolloid to

induce the polymer-polymer complex in the case of complex coacervation; and (4) stabilization and hardening of the microcapsules by adding a cross-linking agent such as formaldehyde, glutaraldehyde or transglutaminase.

5. Solvent evaporation

The use of solvent evaporation or a solvent extraction method to prepare microcapsules has been widely used and investigated in the pharmaceutical field, and little studied for textile applications, except for the encapsulation of fragrance by polylactic acid (PLA) or thermochromic compound by ethyl cellulose. This technical involves the use of emulsification of a solution containing coating polymers and an active substance previously dissolved in a volatile solvent in a continuous medium in which they are immiscible. The gradual removal of the solvent from the dispersed phase by heating the system allows the core substance to be coated by the polymer. The general outline of this method consists of four consecutive steps carried out under stirring: (1) dissolution or dispersion of the active substance in an organic solvent containing the coating material; (2) emulsification of this organic phase in a second continuous immiscible phase; (3) extraction of the solvent from the dispersed phase by the continuous phase by heating and (4) harvesting and drying of the microcapsules. The properties of the microcapsules depend mainly on the formulation and process parameters, such as the solubility parameters of the compounds, the type and the concentration of the dispersing agent, the selected polymer/active substance ratio, and the stirring rate and the temperature (Freitas, Merkle, & Gander, 2005).

References

Arshady, R., & George, M. H. (1993). Suspension, dispersion, and interfacial polycondensation: A methodological survey. *Polymer Engineering & Science*, *33*(14), 865–876. https://doi.org/10.1002/pen.760331402

Deveci, S. S., & Basal, G. (2009). Preparation of PCM microcapsules by complex coacervation of silk fibroin and chitosan. *Colloid and Polymer Science*, *287*(12), 1455–1467. https://doi.org/10.1007/s00396-009-2115-z

Fei, X., Zhao, H., Zhang, B., Cao, L., Yu, M., Zhou, J., & Yu, L. (2015). Microencapsulation mechanism and size control of fragrance microcapsules with melamine resin shell. *Colloids and Surfaces A: Physicochemical and Engineering Aspects*, *469*, 300–306. https://doi.org/10.1016/j.colsurfa.2015.01.033

Freitas, S., Merkle, H. P., & Gander, B. (2005). Microencapsulation by solvent extraction/evaporation: Reviewing the state of the art of microsphere preparation process technology. *Journal of Controlled*

Release, *102*(2), 313–332. https://doi.org/10.1016/j.jconrel.2004.10.015

Jiang, B., Gao, C., & Shen, J. (2006). Polylactide hollow spheres fabricated by interfacial polymerization in an oil-in-water emulsion system. *Colloid and Polymer Science*, *284*(5), 513–519. https://doi.org/10.1007/s00396-005-1415-1

Kobašlija, M., & McQuade, D. T. (2006). Polyurea microcapsules from oil-in-oil emulsions via interfacial polymerization. *Macromolecules*, *39*(19), 6371–6375. https://doi.org/10.1021/ma061455x

Kwon, H. J., Cheong, I. W., & Kim, J. H. (2010). Preparation of n-octadecane nanocapsules by using interfacial redox initiation in miniemulsion polymerization. *Macromolecular Research*, *18*(9), 923–926. https://doi.org/10.1007/s13233-010-0915-0

Liang, C., Lingling, X., Hongbo, S., & Zhibin, Z. (2009). Microencapsulation of butyl stearate as a phase change material by interfacial polycondensation in a polyurea system. *Energy Conversion and Management*, *50*(3), 723–729. https://doi.org/10.1016/j.enconman.2008.09.044

Salaün, F. (2016). Microencapsulation technology for smart textile coatings. In *Active Coatings for Smart Textiles*. https://doi.org/10.1016/B978-0-08-100263-6.00009-5

Salaün, F., Vroman, I., & Aubry, C. (2009). Preparation of double layered shell microparticles containing an acid dye by a melt dispersion-coacervation technique. *Powder Technology*, *192*(3), 375–383. https://doi.org/10.1016/j.powtec.2009.01.018

Sánchez-Silva, L., Rodríguez, J. F., Romero, A., Borreguero, A. M., Carmona, M., & Sánchez, P. (2010). Microencapsulation of PCMs with a styrene-methyl methacrylate copolymer shell by suspension-like polymerisation. *Chemical Engineering Journal*, *157*(1), 216–222. https://doi.org/10.1016/j.cej.2009.12.013

Sánchez, L., Sánchez, P., Carmona, M., de Lucas, A., & Rodríguez, J. F. (2008). Influence of operation conditions on the microencapsulation of PCMs by means of suspension-like polymerization. *Colloid and Polymer Science*, *286*(8–9), 1019–1027. https://doi.org/10.1007/s00396-008-1864-4

Sánchez, L., Sánchez, P., de Lucas, A., Carmona, M., & Rodríguez, J. F. (2007). Microencapsulation of PCMs with a polystyrene shell. *Colloid and Polymer Science*, *285*(12), 1377–1385. https://doi.org/10.1007/s00396-007-1696-7

Sari, A., Alkan, C., & Karaipekli, A. (2010). Preparation, characterization and thermal properties of PMMA/n-

heptadecane microcapsules as novel solid-liquid microPCM for thermal energy storage. *Applied Energy*, *87*(5), 1529–1534. https://doi.org/10.1016/j.apenergy.2009.10.011

Sarier, N., & Onder, E. (2012). Organic phase change materials and their textile applications: An overview. *Thermochimica Acta*, *540*, 7–60. https://doi.org/10.1016/j.tca.2012.04.013

Shi, J., Wu, X., Sun, R., Ban, B., Li, J., & Chen, J. (2019). Nano-encapsulated phase change materials prepared by one-step interfacial polymerization for thermal energy storage. *Materials Chemistry and Physics*, *231*(January), 244–251. https://doi.org/10.1016/j.matchemphys.2019.04.032

Su, J. F., Wang, L. X., & Ren, L. (2007). Synthesis of polyurethane microPCMs containing n-octadecane by interfacial polycondensation: Influence of styrene-maleic anhydride as a surfactant. *Colloids and Surfaces A: Physicochemical and Engineering Aspects*, *299*(1–3), 268–275. https://doi.org/10.1016/j.colsurfa.2006.11.051

Su, W., Darkwa, J., & Kokogiannakis, G. (2015). Review of solid-liquid phase change materials and their encapsulation technologies. *Renewable and Sustainable Energy Reviews*, *48*, 373–391. https://doi.org/10.1016/j.rser.2015.04.044

Wu, C. B., Wu, G., Yang, X., Liu, Y. J., Gao, C. X., Ji, Q. H., … Chen, H. Z. (2014). Preparation of Mannitol@Silica core-shell capsules via an interfacial polymerization process from water-in-oil emulsion. *Colloids and Surfaces A: Physicochemical and Engineering Aspects*, *457*(1), 487–494. https://doi.org/10.1016/j.colsurfa.2014.06.018

Zhang, H., & Wang, X. (2009). Fabrication and performances of microencapsulated phase change materials based on n-octadecane core and resorcinol-modified melamine-formaldehyde shell. *Colloids and Surfaces A: Physicochemical and Engineering Aspects*, *332*(2–3), 129–138. https://doi.org/10.1016/j.colsurfa.2008.09.013

Zhang, H., Shi, Y., Shentu, B., & Weng, Z. (2017). Synthesis and Thermal Performance of Polyurea Microcapsulated Phase Change Materials by Interfacial Polymerization. *Polymer Science - Series B*, *59*(6), 689–696. https://doi.org/10.1134/S1560090417060124

Appendix 4. Publications

[1] **Zhang, Shengchang,** Christine Campagne, and Fabien Salaün. "Influence of solvent selection in the electrospraying process of polycaprolactone." Applied Sciences 9, no. 3 (2019): 402. doi.org/10.3390/app9030402

[2] **Zhang, Shengchang,** Christine Campagne, and Fabien Salaün. "Preparation of Electrosprayed Poly (caprolactone) Microparticles Based on Green Solvents and Related Investigations on the Effects of Solution Properties as Well as Operating Parameters." Coatings 9, no. 2 (2019): 84. doi.org/10.3390/coatings9020084

[3] **Zhang, Shengchang,** Christine Campagne, and Fabien Salaün. "Preparation of n-Alkane/Polycaprolactone Phase-Change Microcapsules via Single Nozzle Electro-Spraying: Characterization on Their Formation, Structures and Properties." Applied Sciences 10, no. 2 (2020): 561. doi.org/10.3390/app10020561

[4] **Zhang, Shengchang,** Yuan Chen, Christine Campagne, and Fabien Salaün. "Influence of a Coaxial Electrospraying System on the n-Hexadecane/Polycaprolactone Phase Change Microcapsules Properties." Materials 13, no. 9 (2020): 2205. doi.org/10.3390/ma13092205

Abstract

Phase change materials (PCMs) can store or spontaneously release a large amount of latent heat during their phase transitions induced by surrounding temperature variations. They are considered the leading candidates for thermal energy storage and meet the increasing demand for thermal management, and are also used in textiles to improve thermal comfort. In recent years, electrospraying has been widely used to manufacture microparticles and microcapsules. When textiles are placed on the collector, the functional coating of the textiles by the electrosprayed microcapsules is achieved during the electrospraying process.

This work aims at designing an appropriate electrospray method to trap the PCMs in microcapsules with a double shell layer. Poly(lactic acid) (PLA) and polycaprolactone (PCL) have been selected as fusible inner and outer shells for surface functionalization of textiles during a post-treatment by temperature rise.

PCL microparticles were produced by electrospraying using five solvents (ethyl acetate, acetone, anisole, glacial acetic acid, and chloroform) at different concentrations of PCL and adjusting the operating parameters. The effects of solution properties (surface tension, electrical conductivity, viscosity, and vapor pressure) and operating parameters (flow rate, working distance, and applied voltage) on the formation of electrosprayed particles were clarified.

Two n-alkanes (n-hexadecane and n-eicosane) with three filler contents (30%, 50%, and 70% by weight) were successfully encapsulated in a PCL matrix by single-nozzle electrospraying with ethyl acetate (EA) and chloroform (Chl) as solvents. The effects of n-alkane phase state, n-alkane additions, and solvent selection on the electro-microencapsulation process, and the structure, morphology, and properties of the resulting mPCMs were analyzed. In order to improve the efficiency of the encapsulation, a coaxial system was also used. A complete comparison between single-nozzle and coaxial electrospray in the encapsulation of MCPs, focusing on the structures, morphologies, and thermal properties of the corresponding microcapsules, was performed.

Due to certain limitations related to PCL, PLA was chosen as an alternative shell matrix to achieve the microencapsulation of PCMs. The effects of PLA concentration and n-hexadecane filler content on the structures and properties of the resulting mPCMs were analyzed. Finally, based on this work, the double membrane microcapsules were fabricated by coaxial nozzle electrospraying. In the meantime, in

order to optimize the structure, morphology, and thermal properties of the final n-hexadecane /PLA/PCL microcapsules and to better realize the functional coating of textiles, the effects of the different additions of n-hexadecane, of the different weight ratios between PCL and PLA on the structures, morphologies, and properties of the resulting mPCMs were studied in detail. Electrosprayed microcapsules with a double-layer envelope will offer great potential and advantages for the manufacture of thermally controlled textiles and a new orientation for the fields of energy storage and thermal management.

Keywords: electrospraying, microencapsulation, phase change materials, n-alkanes, PCL, PLA

Résumé

Les matériaux à changement de phase (MCP) peuvent stocker ou libérer spontanément une grande quantité de chaleur latente pendant leurs transitions de phase induite par les variations de température environnantes. Ils sont considérés comme les principaux candidats pour le stockage de l'énergie thermique et pour satisfaire la demande croissante en termes de gestion thermique, et ils sont également utilisés dans le textile pour améliorer le confort thermique. Ces dernières années, l'électro-pulvérisation a été largement utilisée pour fabriquer des microparticules et des microcapsules. En outre, lorsque les textiles sont placés sur le collecteur, le revêtement fonctionnel des textiles par les microcapsules électrosprayées est également réalisé lors du processus d' électro-pulvérisation.

Ce travail vise à concevoir une méthode d'électro-pulvérisation appropriée pour piéger les MPC dans des microcapsules à double couche d'enveloppe. Le poly(acide lactique) et le polycaprolactone ont été sélectionnés comme enveloppes interne et externe fusible pour une fonctionnalisation de surface des textiles au cours d'un post-traitement par montée de température.

Des microparticules de poly(caprolactone) (PCL) ont été produites par électro-pulvérisation en utilisant de cinq solvants (acétate d'éthyle, acétone, anisole, acide acétique glacial et chloroforme) à différentes concentrations de PCL, et en ajustant les paramètres de fonctionnement. Les effets des propriétés de la solution (tension de surface, conductivité électrique, viscosité et pression de vapeur) et des paramètres de fonctionnement (débit, distance de travail et tension appliquée) sur la formation des particules électro-pulvérisées ont été clarifiés.

Deux n-alcanes (n-hexadécane et n-eicosane) à trois teneurs de charge (30 %, 50 % et 70 % en poids) ont été encapsulés avec succès dans une matrice de polycaprolactone par électrosprayage à buse unique, avec l'acétate d'éthyle (EA) et le chloroforme (Chl) comme solvants. Les effets de l'état de phase des n-alcanes, des ajouts de n-alcanes et de la sélection des solvants sur le processus d'électro-microencapsulation ainsi que la structure, la morphologie et les propriétés des mMCP obtenues ont été analysés. Afin d'améliorer l'efficacité de l'encapsulation, un système coaxial a également été utilisé. Une comparaison complète entre l'électro-pulvérisation à buse unique et coaxiale dans l'encapsulation des MCP, en se concentrant sur les structures, les morphologies et les propriétés thermiques des microcapsules correspondantes, a été réalisée.

En raison de certaines limitations liées à la PCL, l'acide polylactique a été choisi comme autre

matrice d'enveloppe pour réaliser la microencapsulation des PCM. Les effets de la concentration de PLA et de la teneur en charge de n-hexadécane sur les structures et les propriétés des mMCP résultantes ont été analysés. Enfin, à partir de ces travaux, les microcapsules à double membrane ont été fabriquées par électro-pulvérisation à buse coaxiale. Entre-temps, afin d'optimiser la structure, la morphologie et les propriétés thermiques des microcapsules finales de n-hexadécane / PLA/PCL et de mieux réaliser le revêtement fonctionnel des textiles, les effets des différentes additions de n-hexadécane, des différents rapports de poids entre le PCL et le PLA sur les structures, les morphologies et les propriétés des mMCP obtenues ont été étudiés en détail. Les microcapsules électro-pulvérisées avec une enveloppe à double couche offriront non seulement un grand potentiel et des avantages pour la fabrication de textiles à régulation thermique, mais aussi une nouvelle orientation pour les domaines du stockage de l'énergie et de la gestion thermique.

Mots clés: électrospraying, microencapsulation, matériaux à changement de phase, n-alcanes, PCL, PLA